University of Technology, Sydney

Faculty of Engineering and Information Technology

Synchroniser analysis and shift dynamics of powertrains equipped with dual clutch transmissions

A thesis submitted for the degree of

Doctor of Philosophy

Paul David Walker

July 2011

CERTIFICATE OF ORIGINALITY

I certify that the work in this thesis has not previously been submitted for a degree nor has it been submitted as part of requirements for a degree except as fully acknowledged within the text.

I also certify that the thesis has been written by me. Any help that I have received in my research work and the preparation of the thesis itself has been acknowledged. In addition, I certify that all information sources and literature used are indicated in the thesis.

Production Note:
Signature removed prior to publication.

Paul David Walker

July 2011

ACKNOWLEDGEMENTS

I'd like to take this opportunity to thank the following people for their assistance and support during my candidature.

My supervisor Professor Nong Zhang, his knowledge and guidance has been invaluable, and together with co-supervisors Dr Jeku Jeyakumaran and Dr Jinchen Ji have guided me through this research and supported my work.

The team at NTC Powertrains – Ric Tamba and Simon Fitzgerald – whose ideas imitated this project and provided information critical to the success of this work.

My UTS colleagues whose advice, humour, and knowledge has helped me focus and provided entertainment through this journey. Salisa Abdulrahman, Yoo-shin Kim, Robert Heal, Lifu Wang, Nga Hoang, Jin Zhang, Jing Zhao and many others along the way.

Most importantly, my wife, Hoeun, who stuck with me through thick and thin, I couldn't have done this without you babe; and daughter, Abbygail, my pride and joy. My parents, Gary and Sue, for advice, and sister, Leigh, and brother, Ryan for entertainment.

Financial support for this project is provided jointly by the Australian Research Council (Linkage ID number LP0775445) and NTC Powertrains.

TABLE OF CONTENTS

LIST OF FIGURES

LIST OF TABLES

GLOSSARY OF TERMS AND NOTATION

ABBREVIATIONS USED IN THIS THESIS

DCT	–	Dual clutch transmission
MT	–	Manual transmission
AMT	–	Automated manual transmission
AT	–	Automatic transmission
CVT	–	Continuously variable transmission
TCU	–	Transmission control unit
DOF	–	Degrees of freedom
VFS	–	Variable force solenoid
NVH	–	Noise vibration and harshness
DMFW	–	Dual mass flywheel

CHAPTER 3 NOTATION

General

β	–	Bulk modulus
μ	–	Viscosity
c_r	–	Radial clearance
l	–	Sliding contact length
t	–	Time
A	–	Cross-sectional area
C_d	–	Damping coefficient
C_D	–	Discharge coefficient
D	–	Diameter
F	–	Force
K_s	–	Spring constant
M	–	Mass
P	–	Pressure
Q	–	Flow rate
V	–	Volume
X	–	Displacement
$\dot{X}$	–	Velocity

$\ddot{X}$ – Acceleration

Subscripts

0 – initial condition

syn – synchroniser

C – Cylinder

Cl – Clutch

CV## – Control volume number for fluid system

Exh – Exhaust

IN – Inlet

L – Leak

MMF – Magneto-motive force

O – Orifice

P – Piston or spool

V – Volume

CHAPTER 4 NOTATION

α – Cone angle

β – Chamfer angle

δ – Angular displacement between consecutive chamfers

θ_D – Detent contact angle

θ_H – Chamfer relative alignment

$\dot{\theta}_S$ – Cone relative speed

$\ddot{\theta}_{FW}$ – Freewheeling component acceleration

$\ddot{\theta}_R$ – Ring acceleration

μ – Transmission fluid viscosity

μ_C – Cone dynamic friction

$\mu_{C,S}$ – Cone static friction

μ_{DETENT} – Detent friction coefficient

μ_I – Chamfer friction coefficient

μ_R – Ring/sleeve sliding friction

λ – Chamfer flank contact

Π	–	Dimensionless group
Λ	–	Empirical constant that is dependent on the lubrication case ($1>\Lambda>5$)
a	–	Grooved width
b	–	Semi-width of the contact generatrix in the cone [66]
h	–	Film thickness
m_s	–	Sleeve mass
m_{S+R}	–	Sleeve and ring mass
n	–	Number of grooves
t_B	–	Unblocking time
t_S	–	Synchronisation time
x_S	–	Sleeve displacement
$\ddot{x}_S$	–	Sleeve acceleration
F_A	–	Net sleeve load
F_{DETENT}	–	Detent force
F_{FILM}	–	film squeezing force
F_{LOSS}	–	Seel drag losses
F_R	–	Radial force
I_{FW}	–	Inertia of the freewheeling components
I_R	–	Inertia of the ring
I_V	–	Vehicle inertia
K_{GR}	–	Groove coefficient
N_{CH}	–	Number of chamfers on one ring
R_C	–	Mean cone radius
R_H	–	RMS roughness of the hub
R_I	–	Pitch radius of chamfers
R_m	–	Cone mean radius
R_R	–	RMS roughness of the ring
T_B	–	Blocking torque
T_C	–	Cone torque.
T_D	–	Drag torque
T_I	–	Indexing torque
T_S	–	Synchronisation torque
T_V	–	Vehicle torque

CHAPTER 5 NOTATION

General

α	–	transverse operating pressure angle
β	–	operating helix angle
γ	–	gear ratio
ν	–	kinematic viscosity
μ	–	dynamic viscosity
ρ	–	density
ω	–	rotational velocity
ω_G	–	Gear speed
$\Delta\omega_{CL}$	–	Clutch slip speed
θ	–	Rotational displacement
b	–	Face width
d	–	Diameter
f	–	Friction
h	–	Fluid spacing
r	–	Radius (* denotes radius at critical Reynolds number)
C	–	Drag torque dimensionless coefficient
E	–	Energy
Gr	–	Turbulent flow coefficient
H	–	Sliding ratio at the start of the approach
H	–	Sliding ratio at the end of the recess
I_{FW}	–	Reflected inertia
KE	–	Kinetic energy
M	–	Mesh mechanical advantage
N	–	rotational speed (RPM)
P	–	Mesh power loss (kW)
Re	–	Reynolds number (* denotes critical Reynolds number)
Q	–	Flow rate
T	–	Torque
X	–	Profile coefficient
Z	–	module

Subscripts

o1	–	pinion outside radius
o2	–	gear outside radius
s	–	Start of approach
t	–	End of approach
w1	–	pinion operating pitch radius
w2	–	gear operating pitch radius
A	–	Tooth tip
B	–	Bearing losses
CL	–	Clutch windage
D	–	Drag
F	–	Gear friction
I	–	Inside
M	–	Mesh
O	–	Outside
P	–	Pitch point
SH	–	Inter-shaft shear
V	–	windage
W	–	Gear windage

CHAPTER 6 NOTATION*

***Any previously used terminology can be found in Chapter 4 or 5 notation**

θ_C	–	Control system rotation DOF
θ_P	–	Pinion DOF
I_C	–	Control system inertia ($_0$ for initial, Δ for change in inertia)
I_P	–	Pinion inertia
K_C	–	Control shaft stiffness
T_{CONT}	–	Control torque
T_{SYN}	–	Synchroniser torques
x_C	–	Chamfer contact displacement
Δx_S	–	Net sleeve displacement over one chamfer

CHAPTER 7 NOTATION*

***Any previously used terminology can be found in Chapter 4, 5 or 6 notation**

R	–	Cone radius

r – Chamfer pitch radius

CHAPTER 8 NOTATION

General

θ – Angular displacement

$\dot{\theta}$ – Angular velocity

$\ddot{\theta}$ – Angular acceleration

γ – Gear ratio

ω – Frequency

ϕ – Phase angle

ζ – Damping ratio

x – Displacement

$\dot{x}$ – Velocity

$\ddot{x}$ – Acceleration

T – Time

C – Damping coefficient

I – Inertia

K – Spring coefficient

M – Mass

T – Torque

X – Amplitude coefficient

Subscripts

1 – Refers to components associated with odd gears

2 – Refers to components associated to even gears

e – Engine

hys – Hysteresis

AX – Axle

C – Clutch

DIFF – Differential

F – Flywheel or Dual mass flywheel primary

DM – Clutch drum or Dual mass flywheel secondary integrated with clutch

FD – Final drive

G	–	Gear
P	–	Pinion
S	–	Synchroniser
SL	–	Synchroniser sleave
T	–	Tyre
W	–	Wheel hub

Engine models

θ	–	Crank angle
ω_e	–	Engine speed
m_T	–	Mass of gas
A_P	–	Piston area
M_P	–	Piston mass
P	–	Instantaneous piston pressure
R	–	Ideal gas constant
$\dot{S}$	–	Piston speed
T	–	Piston temperature
T_P	–	Piston torque
T_t	–	Inertia change torque
V	–	Piston volume

Clutch model

μ_D	–	Dynamic friction coefficient
μ_S	–	Static friction coefficient
$\Delta\dot{\theta}_{SL}$	–	Clutch slip speed
n	–	Number of friction surfaces
r_I	–	Inside radius
r_O	–	Outside radius
F_A	–	Axial force
T_C	–	Clutch torque
T_{avg}	–	Average torque
X	–	Piston displacement
X_0	–	Contact displacement for friction plates

Synchroniser model

Refer to Chapter 4 notation

Vehicle torque model

$\theta_{incline}$ – Angle of inclination

ρ_{air} – Air density

g – Gravity

C_D – Coefficient of drag

C_{tire} – Dimensionless tire retarding force

F_{aero} – Aerodynamic drag load

$F_{incline}$ – Incline load

F_{roll} – Aerodynamic drag load

F_R – Net resistance force

H_v – Vehicle height

M_v – Vehicle mass

R_{wheel} – Wheel radius

T_R – Net resistance torque

V_W – Linear velocity of driving wheels

W_v – Vehicle width

CHAPTER 9 NOTATION

***Any previously used terminology can be found in Chapter 8 notation**

General

Θ – Amplitude coefficient

Subscripts

C – Clutch

D – clutch drum

E – Engine

T – Transmission

V – Vehicle

1,2 – clutch or gear number

CHAPTER 11 NOTATION

***Any previously used terminology can be found in Chapter 8 notation**

General

θ –rotational degree of freedom

θ_C – Contact displacement rotation

C – Damping

I – Inertia

K – stiffness

M – Mass

r – radius

t –time

TA – throttle angle

x – gear linear degree of freedom

X_C – contact displacement length

y – pinion linear degree of freedom

Subscripts

B – Bearing

Refer to Chapter 8 subscripts

ABSTRACT

Transient dynamic investigations of dual clutch transmission equipped powertrains are conducted in this thesis through the development and application of torsional multi-body models incorporating multiple nonlinearities. Shift control studies are performed using detailed hydraulic model integrated with a 4DOF powertrain model. Results illustrate that accuracy of torque estimation, time delay in engine and clutches, and torque balance in the powertrain all influence the shift quality. Powertrain transient studies have been carried out to investigate the impact of multiple nonlinearities on powertrain dynamics and shift quality. This makes use of the clutch friction stick-slip algorithm to model nonlinearity in clutch engagements, with other nonlinearities including mean and harmonic engine torque models and dual mass flywheel with hysteresis. Comparisons between 4 and 15 DOF powertrain models are made, and the impact of using engine harmonics for the DCT powertrain identified. Results of these studies are also discussed with respect to stick-slip response clutches and the effect on post shift transient response. Finally, a backlash model is introduced for gears and synchronisers to study response under a variety of operating conditions, including synchroniser engagement, shift transients and engine tip-in/tip-out.

Investigations of synchroniser mechanism dynamics and control are undertaken with a rigid body mechanism model, and as part of the DCT powertrain using a 15 DOF multi-body model. Broad ranging parameter studies are undertaken for design and environmental variables that impact on synchroniser performance, and dimensionless torques are introduce for the study of synchroniser design parameters. Slip regeneration is identified as a significant issue in mechanism actuation, in terms of engagement repeatability and damage to chamfer friction surfaces. Alignment control methods are studied to attempt to reduce the impact of chamfer alignment and regenerated slip on engagement performance. Finally two design modifications are suggested for the mechanism to eliminate the slip issue, and provide higher synchroniser torques for a similar design envelope. Powertrain simulation results suggest that under nominal actuation, using the mean engine torque model, vibrations of the sleeve increase during indexing alignment of chamfers, indicating increased wear of friction surfaces. With the inclusion of the harmonic engine torque model, vibrations in the transmission increases significantly throughout the engagement process; however these results do not indicate that there is an increased likelihood of clash during speed synchronisation.

CHAPTER 1: INTRODUCTION

Dual clutch transmission (DCT) development has become an increasingly high priority for an array of automotive organisations as it is capable of providing transmission efficiencies on par with manual transmissions (MT) with the ride comfort of less efficient automatic transmissions (AT). Achieved through the application of different technologies from both AT and MT to the transmission; with gearing and synchronisers from MTs used in conjunction with clutches and clutch control technologies found in ATs. The major limitation of planetary automatics efficiency – the torque converter – is excluded for DCT powertrains, enabling the improved efficiency but also eliminating a significant damping component of AT powertrains. Though conceptualised in the early 1950s, shift control resulting in high quality gear change has only been achieved over the past decade with continued improvement of vehicle control technologies.

This thesis presents a detailed investigation into the transient response of a typical dual clutch transmission equipped powertrain to a variety of excitations, and the study of the application of conventional synchromesh synchronisers to the automated DCT. To date the vast majority of DCT research has focused on clutch shift and clutch launch controller development and simulation, with powertrain transient response an under-evaluated outcome of these investigations. Through these investigations many nonlinearities inherent to vehicular powertrains are ignored and their respective impact on powertrain response is neglected.

With dual clutch transmissions in early stages of design life cycle in comparison to other vehicle transmissions, such as planetary automatics, the identification and investigation of many nonlinear components of the powertrain then become very important to the maturing of DCT technology. Research conducted herein fills the gap between industry and academic knowledge in the performance of dual clutch transmissions through the application of multiple nonlinearities to the study of powertrain response under transient conditions using advanced modelling and simulation schemes for a typical DCT equipped powertrain.

The impact of nonlinearities in powertrains under different transient conditions – including hydraulic control system, synchroniser mechanism, gear mesh nonlinearities, and engine torque harmonics – are the main features of this study. Through the study of

powertrain response the most significant contributors to NVH during shifting will be identified, and provide guidance for the further development of DCT powertrains.

The synchroniser mechanism is a major component of DCTs that requires significant study. Applied to manual transmissions, engagement of synchronisers is performed with the clutch open and engine isolated from the mechanism. In DCTs, synchroniser engagement occurs prior to the shift transient with engine still driving the wheels. Additionally, with two gear trains operating in parallel in DCTs the synchroniser is now engaged in a different operating environment. Characterising the actuation of the mechanism here will identify limitations to the current mechanism design that will enable reduced actuation times, improved performance, and reliable control.

This thesis contributes significant knowledge to the engineering community through the investigation of the complex subsystems that make up DCT powertrains, and study of the impact of these subsystems to vehicle powertrains. The three most significant and novel aspects of this research are: (1) modelling and control of a DCT equipped powertrain with an integrated model of the hydraulic control system, (2) Modelling of the DCT powertrain with the integration of multiple nonlinearities, including engine harmonics, synchroniser mechanism and gear backlash as major contributors to nonlinear dynamics, and (3) the detailed study of many facets of the synchroniser dynamics and control as a component of dual clutch transmissions. These are the major features of original research, many other findings and original research contributions are detailed in both chapter summaries and the conclusion of this thesis.

1.1 PROJECT STATEMENT

The development of computationally efficient mathematical models of a powertrain equipped with a DCT for the prediction of its transient characteristics under a wide range of operating conditions, including the characterisation and analysis of the synchroniser mechanism performance as an automated component of the dual clutch transmission.

1.2 PROJECT OBJECTIVES

This thesis is focused on the investigation into synchroniser mechanism analysis and powertrain transient dynamics with multiple nonlinearities. The main objectives of this project are:

1. Model the main components of a DCT and integrate them into a vehicle powertrain model for predicting the transient characteristics during gear shifting,
2. Modelling of the fast acting synchroniser mechanism for determining dynamic characteristics of the synchronisation process,
3. Identify and study possible solutions to improve the engagement of the synchroniser mechanism as used in the DCT, and
4. Develop numerical solutions for DCT equipped powertrains to investigate dynamic coupling between multiple nonlinearities for accurate assessment of NVH characteristics.

1.3 PROJECT SCOPE

The scope of this project is limited to the following:

1. Physical modelling of the major components of DCT powertrains using conventional techniques of mechanical engineering, including Newtonian methods, lumped parameter models and fluid dynamics
2. Time domain analysis of powertrain and component transient response
3. Free and forced vibration analysis of powertrain models

Aspects of research beyond the scope of this research are:

1. The impacts of temperature on operating performance, with one exception in Chapter 4, Section 4.7.7.
2. Extensive experimental validation of simulation results
3. Launch control and launch judder of DCT powertrains
4. Investigation of electro-mechanical control of dual clutch transmissions

1.4 PRESENTATION OF THIS THESIS

DCTs and powertrains are necessarily complex mechanical systems. Detailed modelling and analysis in this thesis has required the application of fluid theories, and

rigid and flexible multi-body mechanics to sufficiently represent powertrain and component dynamics. Specific modelling and analysis methods are therefore introduced in the chapter in which they are first applied, rather than as a methodology chapter so as to aid the reader in their understanding of the procedures applied, and provide clarity and continuity of research.

To highlight this issue consider modelling the synchroniser mechanism. The detailed modelling must consider rigid body kinetics and kinematics, fluid dynamics in the form of drag torque, and fluid dynamics and mechanics of the hydraulic control system. This can be then expanded also to consider multi-body dynamics by including the powertrain. To apply a single chapter on the different methodologies for research would therefore be broad reaching, but not necessarily useful to the reader.

Figure 1.1 shows the main topics of this thesis and how each independent topic interacts with other aspects of research. It should be used to understand why this thesis is broken down into the chosen format. The arrangement of this thesis investigates several different aspects of DCTs and synchronisers before each of the subsystems are fully integrated and studied. The main topics of each chapter are introduced in the following sections.

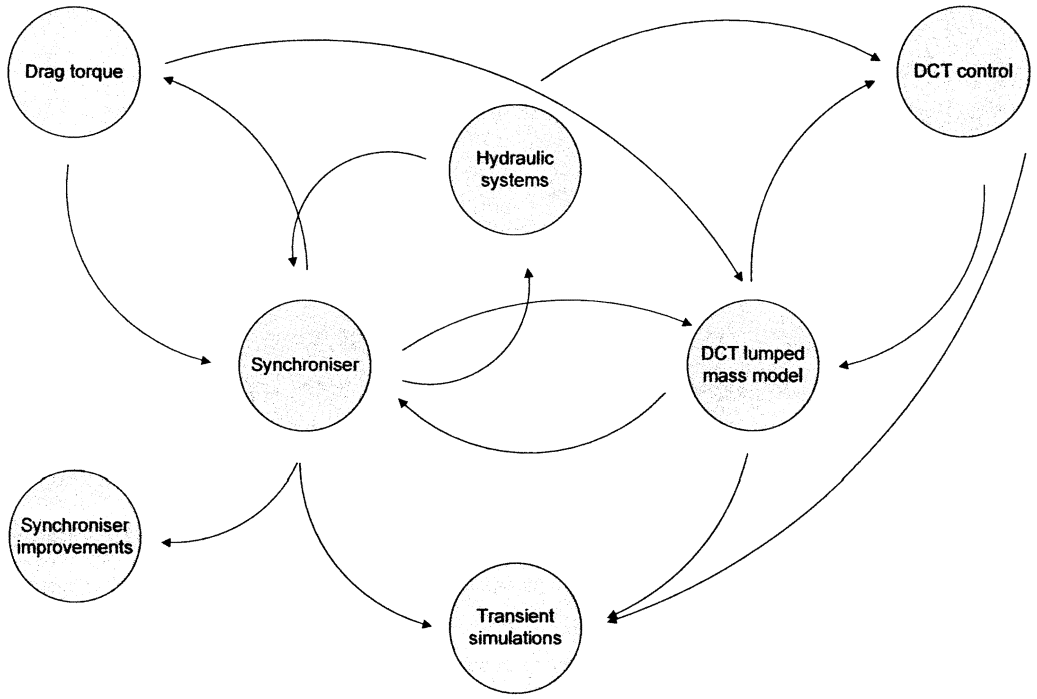

Figure 1.1: Relationship of different Chapter components of this thesis

Chapter 2

This chapter provides the framework for the research of this thesis. Initially the required background information on relevant aspects of DCT equipped powertrains is presented to introduce topics for research. This is followed by a detailed literature search into all relevant aspects of DCTs and its subsystems, identifying the state-of-the-art in DCT powertrains and major components. To complement this work brief exploration of literature is performed in each relevant chapter to identify important aspects of relevant research, as necessary.

Chapter 3

Mathematical models of the hydraulic control systems for clutch and synchroniser control are developed in this chapter using conventional theories of fluid dynamics and Newtonian mechanics. These models are applied to Matlab and Simulink environments to investigate the response to basic inputs for the characterisation of subsystem dynamics and time delay.

Chapter 4

Chapter 4 is devoted to the development of a detailed rigid body model of the mechanism with the incorporation of the previously developed hydraulic system. This chapter specifically considers the influence of DCT environment and architecture characteristics without the use of a full powertrain model, using certain simplifications acceptable for the model. Simulations are then carried out under a wide range of operating conditions, identifying several issues with the conventional design and actuation. Finally, a dimensionless torque technique is suggested for studying synchroniser design parameters.

Chapter 5

Within the DCT drag torque act in a different manner on the synchroniser than found in MTs, it's influence is the greatest unknown during synchroniser actuation. Many design and environmental variables act together and against each other to establish a net drag torque on the synchroniser mechanism. Consequently, a separate chapter is used to detail the drag torque model and identify characteristics resulting from synchroniser engagement in the DCT. The model is developed from current research into

transmission losses and integrated into the synchroniser mechanism model It is also used to approximate damping coefficients in the DCT for the lumped mass model.

Chapter 6

The synchroniser rigid body model developed in Chapter 4 is studied here, focusing primarily on the control of actuation in response to detrimental engagement conditions identified in Chapter 4. This chapter studies a popular method for engagement control of synchroniser, and identifies limitations of increased engagement delay and limited reliability of the proposed method. Alternate strategies for improving engagement performance are then presented including two excitation methods, and a suggested design modification for reducing the occurrence of regenerated slip in the cone clutch.

Chapter 7

Cone clutch torque is critical to synchroniser actuation; however for a specified design envelope limitations to this torque result from the current design and cone friction lock phenomenon. The relationship between cone and blocking torques provides a source of improvement to the synchroniser design. This Chapter presents an alternative synchroniser design with an external cone clutch that can provide increased torque capacity for the synchroniser; reducing the duration of synchronisation and improving resilience to drag torque.

Chapter 8

The thesis now moves on to the development of the DCT system model and its control. This begins with a full powertrain model of the DCT, comprising of individual models for each required powertrain state, ranging from 13 to 15 DOF. The specifics of lumped spring-inertia modelling of a DCT equipped with synchronisers are discussed here, including free vibration results. Finally the different torque models are introduced. This includes mean and harmonic engine torque models, a piecewise clutch stick-slip model, as adapted synchroniser model, and vehicle resistance torques.

Chapter 9

Chapter 9 presents a standard method for DCT shift control. A 4 DOF model of the powertrain is introduced and parameters are determined to maintain consistency with the previous DCT models. This is then integrated with the clutch hydraulic control

system presented in Chapter 3, and a combined engine and clutch control methodology is introduced that balances torque required to maintain vehicle acceleration with engine and clutch torques. Simulations are performed for alternate control strategies and investigations into delay in the clutch hydraulics and engine. Finally, the impact of the harmonic engine torque model is studied.

Chapter 10

Building on the torsional lumped inertia model in Chapter 8 and the control results in Chapter 9, Chapter 10 investigates the transient response of the DCT powertrain under a variety of operating conditions and configurations, including a range of nonlinearities. First the synchroniser mechanism engagement is studied and the impact of engine harmonics investigated. This is followed by shift transient investigations for a variety of different configurations, including application of engine harmonics, and a dual mass flywheel model. The final simulation presents the combined synchroniser and clutch shift engagements to demonstrate a complete DCT gearshift.

Chapter 11

In the final chapter the transient study of Chapter 10 is extended to include powertrain transient response with nonlinear gear mesh and synchroniser backlash. The 15 DOF powertrain model is expanded to include nonlinear backlash models in the gear mesh, with line of action displacements and bearings taken into account, and a torsional mesh nonlinearity in the synchroniser mechanism. Transient simulations for synchroniser engagement, shifting, and engine throttle tip-in/tip-out with mean and harmonic engine torque models are performed, with consideration of gear rattle and clonk, two primary concerns regarding backlash nonlinearities.

Chapter 12

The concluding chapter reviews and summaries each of these chapters, presenting important and novel results of this thesis as well as identifying the important areas for extending this research.

1.5 PUBLICATIONS

Journals

Walker, P.D., Zhang, N. & Tamba, R. 2010, "Control of gear shifts in dual clutch transmission powertrains", *Mechanical systems and signal processing,* In Press, DOI: http://dx/doi/org/10.1016/j.ymssp.2010.08.018

Walker, P.D., Zhang, N., Tamba, R. & Fitzgerald, S. 2011, "Simulation of drag torque affecting synchronisers in a dual clutch transmission", *Japan Journal of Industrial and Applied Mathematics,* In Press, DOI: 10.1007/s13160-011-0030-4

Walker, P.D. & Zhang, N. "Parameter study of a synchroniser mechanism applied to dual clutch transmissions" *International Journal of Powertrains*, Accepted for publication.

Conference proceedings

Walker, P. D., Zhang, N., Jeyakamuran, J., Tamba, R. & Fitzgerald, S. 2008, "recent advancements in dual clutch transmission modelling and simulations", *37th International Congress and Exhibition on Noise Control Engineering*, Paper No.: 0924

Walker, P. D., Zhang, N., Tamba, R. & Fitzgerald, S. 2009, "Synchroniser modelling with application specific to the dual clutch transmission, *13th Asia Pacific Vibration Conference*

Walker, P. D., Zhang, N., Tamba, R. & Fitzgerald, S. 2010, "Dynamics and simulations of shifting in a dual clutch transmission", *6th Australasian congress on applied mechanics*

CHAPTER 2: BACKGROUND INFORMATION AND LITERATURE REVIEW

2.1 INTRODUCTION

Shift control studies of DCTs has been extensively performed by Goetz [1], covering a wide range of control options focusing on the reduction of transient vibration during and after shifting. Complementing shift control is the impact of nonlinearities – i.e. hydraulic control system, backlash, engine harmonics, and torsional dampers – on the powertrains response during transient periods such as shifting. These are frequently ignored to reduce computational demand. The purpose of this survey is therefore to identify current trends in simulations and analysis of DCTs and respective components, exploring the background into each of these nonlinearities.

Furthermore the current state-of-the-art in DCT research fails to significantly cover the role of synchronisers in the transmission, and particularly the impact of employing this predictable but extensively uncontrolled mechanism in a different operating environment and architecture.

This chapter therefore covers the state-of-the-art in DCT literature, its components and applications. The initial sections of this chapter focused on introducing the DCT and its major components before undertaking research into simulations and control of the DCT, and identification of limitations in current literature. From these limitations, research is expanded into modelling of synchronisers and drag torques, control systems for clutches, studies of nonlinearities in gear meshes and splines, engine modelling and applications and other research into the current state-of-the-art for powertrain modelling and control.

2.2 BACKGROUND INTO DCT EQUIPPED POWERTRAINS

This section outlines the important characteristics of DCT equipped powertrains and its components, reviewing the system as a whole, the transmission itself, sources of nonlinearities that are relevant to this thesis, synchroniser mechanisms, drag torque, and hydraulic control systems.

2.2.1 Powertrains

Automotive powertrains, see Figure 2.1, refers to the components of a vehicle that that produce, convert, and deliver power to the road. These are torsional systems consisting of many lumped inertias, such as flywheels, gears, or differentials, and long flexible shafts. The major components are the engine, which supplies power, the transmission which converts engine torque and speed to meet driving demand, and the drivetrain that delivers the power to the road through wheels and differential.

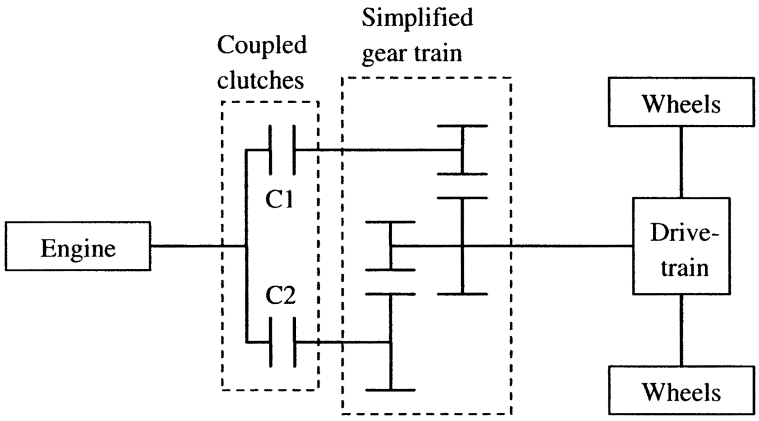

Figure 2.1: General DCT powertrain layout

Two of the major vibratory considerations for transient investigations into powertrains are excitation of the first nonzero natural frequency of the powertrain, or *shuffle* mode, and excitation of audible natural frequencies, often these referred to as *clonk*. The shuffle mode is typically 2-10Hz it is the first global powertrain mode and easily observed by the driver with respect to hard shifting. Clonk occurs at higher frequencies 500 – 4000Hz over a relatively short duration audible response, and is generally the result of nonlinear response in the powertrain.

2.2.2 Engine

The engine is a major source of nonlinear forced vibrations for DCT powertrains with torque pulses from piston firing providing highly nonlinear output torque. Unlike AT powertrains the engine is not isolated from transmission with the torque converter, rather the output shaft directly drives the transmission. For that reason two engine models are used, (1) mean torque engine model, frequently employed in DCT literature, and a (2) simple harmonic torque engine model, where cylinder-by-cylinder firings are taken into account to generate engine torque dependent on crank angle.

2.2.3 Flywheel

To compensate for engine harmonics and provide another nonlinear powertrain component alternate configurations of the flywheel are used, with both a standard flywheel and dual mass flywheel employed at different stages of investigation. Where the DFMW is used to isolate engine harmonics from the powertrain, there hysteresis is also present in the DMFW in the form of viscous and friction dependent damping. As the load on the flywheel varies friction damping transits from static to dynamic loads. Thus when using a dual mass flywheel configuration in the powertrain it can be considered a nonlinearity.

2.2.4 The dual clutch transmission

Dual lay shaft structure is generally the most popular form of dual clutch transmission, with two parallel gear sets. Shown in Figure 2.2 is a detailed line diagram of a typical DCT. It is arranged such that the two clutches having a common drum attached to the input shaft from the engine. Primary shafts, connected to independent clutch hubs, are aligned concentrically and geared such that 1^{st}, 3^{rd}, and 5^{th} are engaged with Clutch 1, and 2^{nd}, 4^{th}, 6^{th}, and reverse are engaged using Clutch 2. Thus the transmission is representative of two half size manual transmissions, and, in this sense, shifting is realised through the simultaneous shifting between these two half transmissions.

The two aspects of gear shifting are representative of manual and automatic transmissions. Prior to shifting the first requirement is to synchronise the target gear, realised using typical synchromesh synchronisers that are popular in manual transmissions with low cost and high reliability. Once complete clutch-to-clutch shifting can be performed. This applies similar methods to those performed in automatic transmissions where hydraulically actuated clutches are simultaneously released and engaged such that vibratory response is minimised in the powertrain.

The most significant change from AT to DCT clutch control is that there is no longer a torque converter to dampen any transients developed during shifting. This requires a much more precise application of clutch control to ensure shifting is completed within the minimal time with maximum quality to produce power-on gear change without loss of tractive load to the road.

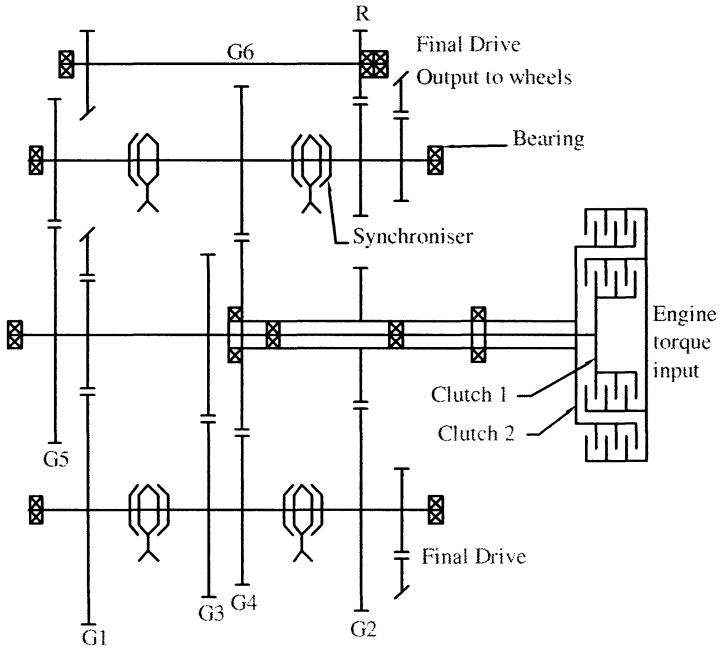

Figure 2.2: Dual lay shaft dual clutch transmission, where "C" represents clutches, "B" signifies bearing, "G" is for a gear pair, and "S" identifies synchronisers.

2.2.5 Powertrain nonlinearities

Powertrain nonlinearities arise from a diverse range of sources that will each have a different impact on the powertrain transient response.

1. Torque pulses arising from engine nonlinearity provide a substantial source of forced vibration for the vehicle powertrain.
2. Torsional vibration absorbers such as dual mass flywheels (DMFW) provide significant system damping, but also contain long travel arc springs (>90°) and friction hysteresis that impact on vehicle response.
3. Clutch and synchroniser engagement alter physical characteristics of the powertrain – particularly structure and inertia – when in different engaged states. A change in gear ratio changes the inertia, initiating a transient response.
4. Major transmission components – the gears and synchronisers – are in contact with designed clearances, or backlash. Under transient response these can contribute to NVH through clonk response during and immediately after shifting.
5. Hydraulic control system is highly nonlinear, with interaction of fluid system and spool dynamics. Hydraulic fluids with bulk modulus of the order 1~2 x 10^9

Pa, and the application of compressibility equations to these fluids results in a numerically stiff system, requiring fine time step solvers to simulate accurately.

6. Synchroniser mechanism engagement generates multiple torques; during actuation these will vary depending on sleeve location and speed in the system.

2.2.6 Synchroniser and drag torque

The synchroniser mechanism has been around in some form or other since there has been the requirement to change gears. The mechanism makes use of speed and torque variations during engagement to achieve two goals, (1) synchronise speeds between shaft and target gear, and (2) mechanically interlock gear to shaft to allow the delivery of torque through the transmission. In a real sense little has changed since the mechanism was first introduced, variations in clutch and blocking mechanism have been introduced, but the basic synchromesh type of synchroniser is the most cost effective and reliable of these designs.

Major components of the synchroniser are shown in Figure 2.3. Including: shaft and saddle as the base of the mechanism, the sleeve is controlled with hydraulic actuators in the DCT and interlocks target gear to shaft, detent and thrust piece locate the neutral position and initially move ring ahead of sleeve. The ring is externally engaged by the sleeve through chamfered splines and internally contains a cone clutch to synchronise speeds, and target gear contains cone clutch hub and chamfers to mate with the sleeve and interlock to the shaft.

Here the term chamfer refers to the dog gear, a series of chamfered splines, which play an important role in restricting the engagement process and interlocking the target gear. During actuation the cone clutch first synchronises gear and shaft speeds, sleeve chamfers unblock the ring, and then lock the gear to the shaft. The engagement of the synchroniser mechanism is highly nonlinear, and heavily reliant on torque balance for control in the DCT, whereas in a MT the driver observation will play a significant role in achieving correct engagements.

Drag torque is a major uncertainty in transmission design, particularly when selecting synchronisers, and has a significant impact on mechanism engagement in terms of success and duration. It results from speed and load dependent losses in the transmission, and, with the new architecture of the DCT, it is important to quantify how this has impacted on the development of drag in DCTs.

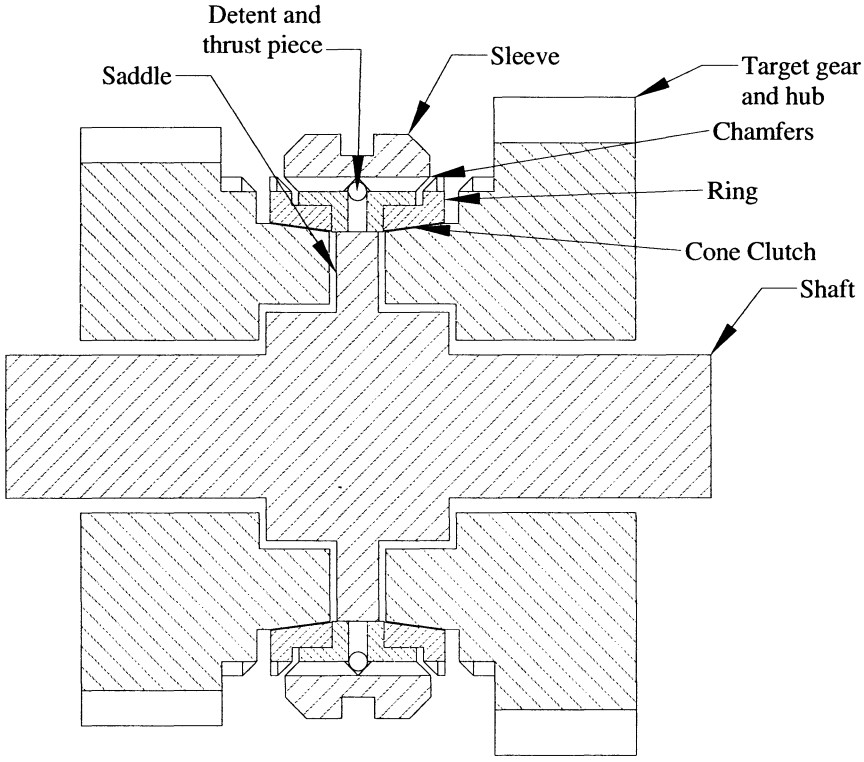

Figure 2.3: Typical synchroniser mechanism schematic

2.2.7 Control systems

The transmission control unit (TCU) is a compact, high performance hydraulic system consisting of a series of valves and solenoids to direct the engagement of clutches and synchronisers. Highly nonlinear as a result of interactions of fluid and moving parts, it must deliver precise control of the transmission under a wide range of operating conditions. Citing Holmes & Tamba [2] the hydraulic control solenoid should provide *"... precise output pressure stability control under varying temperature, source pressures, output flow demands and commanded control pressures in a contaminated hydraulic fluid media typical of automotive transmission applications. It provides fast, repeatable and stable output pressure responses. The system has low output pressure hysteresis and reduced contamination sensitivity to varying source pressure in the pressure regulating range."*

2.2.8 Drivetrain and differential

The drivetrain for a rear wheel drive powertrain consists of propeller shaft, differential, axle, wheel hubs, and tyres. Each of these are made up of some form of flexible or inertia components, and for the tyres the rolling inertia of the entire vehicle must be considered. Nonlinearities in the drivetrain are not considered in this research; nevertheless detailed models are required for a reasonable representation of the powertrain.

2.3 DCT POWERTRAINS, SIMULATIONS, MODELLING AND CONTROL

2.3.1 Designs and state-of-the-art

Dual clutch transmissions are the subject of much research and development in recent years as many automotive organisations seek to independently develop DCT technologies, an example being literature presented by LuK [3, 4]. Matthes & Geunter [5] highlight the flexibilities and capabilities of the DCT, with applications in a broad range of passenger vehicles to date. While the most popularly researched arrangement for the DCT is the dual lay shaft transmission, other researchers such as Tenberge [6] provide alternative arrangements making use multiple synchronisers in one shift state to increase the potential gear ratios. Nevertheless the current state-of-the-art in DCTs falls to a handful of transmission components that must be studied. These include type of clutch, application of control system, and various different applications of the transmission.

2.3.1.1 Wet Vs Dry clutches

Early versions of the DCT relied on multi-plate wet clutches to perform gear shifting as it is capable of absorbing the increased thermal load resulting from extended shift periods required for smooth gearshifts and launches. This however limits the capacity of the DCT to maximise fuel efficiencies as there are additional system losses in the transmission and increase transmission fluid pumping requirements. The easiest and most substantial improvement that can be made to the DCT's efficiency is the elimination of the wet clutch and associated hydraulic components. Ahlawat, *et al,* [7] provides reference for the pumping requirements for hydraulic systems with specific

application to DCTs, the particular simulations demonstrated torque requirements of less than 1Nm.

Dry clutches have significant advantage in terms of efficiency, but have limitations is torque capacity and extended slip times, both of which can be detrimental to the friction coefficient [3, 4]. Summarising Certez, *et al,* [8], application of dry clutches can yield a fuel economy improvement of 2 – 3%; however limitations to wear of the friction surfaces requires its use in lower torque applications, with some clutch envelope size limitations. While Berger, *et al,* [3] identifies the capacity to absorb high friction energy generated in constant creeping, crawling, hill starts and holding, and during general launch as a significant issue in development of dry clutch DCTs, suggesting adaptive control be utilised to overcome degradation of friction surfaces as a likely solution, implications for clutch judder are not addressed.

Rudolph, *et al*, [9] presents a comparison between the two predominant DCTs used by Volkswagen, the DQ 200, a dry clutch DCT, and the DQ 250, of wet clutch design. Much detail is given comparing the control systems developed between the two transmission systems. The primary difference between both systems being the higher efficiency of the DQ 200 at the cost of torque capacity; with the DQ 250 is capable of maintaining 100Nm higher torque load.

2.3.1.2 Electro-hydraulic or electromechanical control systems

With the implication of removing the clutch hydraulic fluid systems from the DCT comes the concept of electromechanical control of both clutch and synchroniser to completely remove hydraulics from the system, maximising the increase in system efficiency. Wagner [10] suggests the implementation of traditional electric motors for both clutch and synchroniser control through the novel application of lever mechanisms. Conversely, Wheals, *et al*, [11] makes use of compact linear actuators for the engagement of both mechanisms, with a lever arm to achieve balanced force application to the clutch. The electromechanical actuator is presented in Turner, *et al,* [12], with results demonstrating an actuator mechanism capable of providing force requirements consistent with clutch and synchroniser actuation. Both methods have been adopted for dry DCT control in some form or another with associated parent companies.

2.3.1.3 Applications

Applications of the DCT are now quiet diverse, seeing deployment in supercars and compact cars alike. Examples range from the Bugatti Veyron, with 1250Nm of torque using wet clutches, to the Volkswagen range, Polo for example, using 250Nm dry clutches. Two dual clutch transmissions that have found significant use in Volkswagen's passenger vehicle ranges are the DQ 200, a light weight dry clutch DCT with applications to low torque powertrains, and the DQ 250, a wet clutch DCT for use in higher torque applications [9].

The Chrysler ME 4-12 is a typical example of the supercar application of the DCT, development presented by Rolland, *et al,* [13]. Peak torque applied to the clutch is predicted to be 750Nm; the DCT achieves shifts in around 200ms with no loss of traction to the road. Development requirements are wide ranging including clutch and clutch control, synchroniser control, lubrication and overall control system.

The DCT also has application to hybrid vehicle systems. One example is for mild hybrid systems such as the ESG presented by Wagner & Wagner [14], where a 10 kW electric machine is used to improve vehicle efficiencies under high demand or low engine efficiency conditions. Alternative hybrid systems have been presented by Joshi, Shah & Mi [15] for a more complicated hybrid system employing two motors with the DCT used to control torque flow of the system. Such a design is capable of much broader operating modes for hybrid operation. Other examples where hybrid vehicles have been identified for use with dual clutch transmission are included in [16-18]

2.3.2 Modelling, simulations, and analysis

Generally speaking modelling of the DCT as part of a powertrain has been limited to the level required to develop a reasonable control system and simulate the results. These simulations are typically transient shift or launch simulations demonstrating the effectiveness of a particular control strategy. The choice of parameters and detail in the model will reflect on reasonableness of results, with no current validation presented.

Goetz, Levesley & Crolla has the most comprehensive work on DCTs [19-21]. Initial work develops the model, defines the shift control, and demonstrates it in simulation. The later work goes further in demonstrating its operation on upshift, downshift, and skip shift. The success of the work is primarily due to the well defined controller methodologies for each shift type. In the case presented initially in Goetz, Levesley &

Crolla [21] the complete powertrain is modelled as a series of inertial and compliant elements. Greatest precision is placed on the transmission where a parallel pair of clutches, shafts, synchronisers and gears is modelled. Additionally, drag is modelled by grounding mass elements using torsional damping elements. Similarly to Goetz, the work of Zhang, *et al,* [22], which has been built on by Kulkarni, Shim & Zhang [23], uses an arrangement of spring and inertial elements powertrain components. However, fewer degrees of freedom are used with losses lumped as a single element. This is generally considered acceptable as the focus of control is on the transmission itself, but oversimplification of the model can lead to limited accuracy of powertrain transients. Kirschstein [24] models the powertrain as a four degree of freedom system (4DOF), primarily focussing on controller gain selection for launch control of the transmission.

The most popular technique is to develop a four degree of freedom model using some variation of finite elements. Major inertia elements are sought from engine, clutch drum and plates, transmission, and vehicle, each connected by shaft stiffness. This technique is adopted by Song, Liu & Smedley [25], Kirschstein [24], Lei, Wang & Ge [26] and Liu, *et al,* [27] in addition to the previously identified authors [22, 23] for separate control strategies. These models produce sufficient responses in terms of representing the lower natural modes. A less detailed model by Xuexun, *et al,* [28] uses two degrees of freedom, one for the engine and another for the vehicle, but with no compliance elements it becomes impossible to demonstrate the vehicle transient response.

The most important aspect of developing a model is being able to reproduce results that reflect the vehicle dynamics. For shift and launch transient control the vehicle should replicate the vehicle rigid body, shuffle and lower frequency vibration modes experienced by the driver as a result of shifting. Only with such responses is it then possible to demonstrate the vehicle dynamics observed from the driver. Examples of using lumped inertia-stiffness methods see Courderc, *et al,* [29] or Crowther & Zhang [30], or distributed mass models, Bartlett & Whalley [31].

2.3.3 Control methods employed in DCTs

There are several control methods that have been applied to dual clutch transmissions, ranging from basic open loop methods through to fuzzy control techniques. To some extent the range of success of different applications is limited by the detail in the dynamic modelling presented, but the relevance of employed techniques can be assessed.

Beginning with the most detailed methods presented by Goetz, Levesley & Crolla [1, 19-21], specific control methods are presented for up, down and double shifts. Each of these papers presents similar demonstrations of shift control techniques with reasonable results. Briefly, for any shift control is split into torque and inertia phases. After shift requirement is detected pressure is reduced for the releasing clutch, and for the engaging clutch the pack is prefilled. For the torque phase slip is initiated in the released clutch and the ongoing clutch torque is matched to the required torque. On the completion of the torque phase the off going clutch is deactivated, and engine and clutch pressure for the ongoing clutch are controlled to ensure smooth lockup.

An alternate control technique presented by Lei, Wang & Ge [26] is similar to previously presented, where the ongoing clutch is controlled for slip speed, and the off going clutch is released controlling the output torque. The goal is to minimise the negative output torque resulting from clutch overlap and minimise transient responses result from the shift.

A basic method applied by Goetz in [1], Zhang, *et al,* [22] and Kulkarni, Shim & Zhang [23] is to use a predefined control signal to perform the shift. Here Zhang, *et al,* [22] and Kulkarni, Shim & Zhang [23] adopt pressure profiles to perform the shift. In this way it is somewhat similar to speed based control techniques for automatic transmissions. Liu, *et al,* [27] adopts similar methods to these authors with the introduction of PID controllers across different launch, creep and shift applications to reduce the shifting period. The drawback of these methods is the 'torque hump', or surging, as clutch torque peaks well above mean clutch torque.

Open loop control methods have be adopted by Song, Liu & Smedley [25] for heavy vehicle applications. There is demonstrative success for the capability to perform shifts, and results have similar comparison to a single clutch transmission, with reduced torque hole, as driving load is released during shift, over MTs. However, there are still significant improvements that can be made to the shift responses to improve the engagement, noting particularly the interruption of vehicle speed during shifts.

Fuzzy control techniques have been applied by Xuexun, *et al,* [28] for shift control of a DCT. Though there is demonstration of the capacity for such a method to achieve a reasonable shift in the DCT, the system variables in transmission modelling are well established, thus making the need for fuzzy based control strategies limited.

Launch control techniques are somewhat simpler. Kulkarni, Shim & Zhang [23] uses ramp inputs to perform launch control, and by modifying profiles, demonstrate the

capacity to improve ride performance with reduced gradient profiles. Kirschstein [24] progresses along an alternate method, modifying the controller gain to demonstrate the effects of poor gain selection on producing inferior launch responses, particularly results emulate clutch engagement judder as a result of poor gain selection.

Overall, control of DCTs for both shift and launch simulations focuses on the combined torque and speed control of clutches integrated with speed control of the engine. Limitations to this research lie with the lack of detailed study into different facets of shift control, such as assessment of controller accuracy or time delay. Consider principally that transient vibration minimisation results from the requirement to reduce speed, torque and inertia discontinuities during the transient. Little emphasis is placed on the variation in clutch and engine torques during the transient period.

2.3.4 Assumptions and limitations of current research

Six significant assumptions are made when investigating modelling, simulation, and control of DCTs. The first of which is critical to the simulations of control using dynamic system models, where each of the authors [19 – 24] uses different assumptions in modelling the hydraulic control systems. Though useful for developing control algorithms some of system characteristics are lost. The second regards engine models, where mean torque models are used, ignoring torque pulses present reciprocating piston engines. The third is ignoring the requirement for synchroniser engagement prior to shifting, and the fourth is modelling of nonlinear mesh in gears, where backlash during abrupt transients is ignored for the sake of model simplicity. Final assumptions include temperature and efficiency losses in the system. Each of these is detailed in the following sections of this review, studying different authors' assumptions with respect to DCTs and alternatives presented in available literature.

2.3.4.1 Hydraulic control system models

Modelling of the control systems in the DCT is quiet varied, ranging from ideal input torques [22, 23, 27] to linearised with time delay [24] and experimentally derived transfer functions [1, 19-21]. Other examples, including Song [25], use readily available software models, while Xuexun, *et al,* [28] presents a 3DOF model of clutch piston dynamics interacting with the hydraulic fluid. There are several reasons that these authors have identified for not including detailed transmission controller models.

Primarily the level of detail required in modelling hydraulic systems, and high stiffness associated with fluid bulk modulus will result in computationally intensive simulations. Kulkarni, Shim & Zhang [22, 23] use a very simple model to simulate the hydraulic components of the DCT. The hydraulic system is replaced with a lookup table to provide outputs for pressure at the clutch based on an input signal. This type of simplification fails to account for two aspects of hydraulic circuits, both the time delay experienced by the circuit and the response are ignored. Thus the system response is simplified, though it is still possible to demonstrate control of the DCT with this method. In a paper investigating clutch launch judder for DCTs, Kirschstein [24] simulates the transmission control unit (TCU) hydraulic response by linearising the system and included a time delay to represent the hydraulic delay inherent in any such system. This accounts for one aspect of the response of the hydraulics, but the high degree of nonlinearity in the system results in a varying time delay. Goetz, Levesley & Crolla [21] employ a phenomenological based model after some investigation into how to model the components, identifying computational time and contact nonlinearities as constraints to conventional modelling. This method utilised two second order transfer functions to simulate the response of the hydraulic control system, accounting for some aspects of the nonlinearities present. Methods for the development of hydraulic models for the DCT are primarily focused on the simplification of the system to provide computationally compact solutions for use in control simulations. These methods, however, can limit the range of operating conditions in which the model is applicable and are less precise when considering the high degree of nonlinearity of the hydraulic systems.

However, authors such as [32-34] have provided detailed hydraulic systems models that have proven effective for shift transient simulations in conventional planetary ATs or AMTs. Similar models for control of CVTs have also been performed by Pesgens, *et al*, [35]. By and large these rely on fundamental theory of Newtonian mechanics and fluid dynamics, with popular methods found in [36-39]. Hydraulic control systems, such as those employed in DCTs, are complicated by high nonlinearity and variable time delay, suggesting that transient simulations should use detailed hydraulic system models.

2.3.4.2 Engine torque models

The engine torque models employed in current literature fall into three groups. Kirschstein [24] linearises the engine torque based on throttle angle and speed, [22, 23, 25, 27] use engine maps with throttle and speed as references, while Goetz, Levesley & Crolla [20, 21] uses empirical mean torque models based on those presented by Moskwa & Hendrick [40]. For development and analysis of clutch shift and launch control such methods are quite reasonable, and result from current methods employed for AT shift control simulations. Kiencke & Nielson [41] or Zhang, *et al*, [42] provide typical examples for AT control modelling.

Some effort has been made by Goetz, Levesley & Crolla [21] to simulate transients through the introduction of white noise over the engine speed, but it is unclear if engine torque is affected. Crowther, *et al*, [43] uses trigonometric functions to simulate piston firing torque pulses to reproduce engine torque harmonics acting in the powertrain.

For extensive vibration studies during shift transients, engine models with harmonics torques can and probably should be deployed in DCT models. This is most important as AT systems utilise hydrodynamic torque converters to isolate engine transients from the powertrain, an assumption that cannot be entirely satisfied through the use of torsional absorbers by the likes of [1, 25] without some form of verification. Fredriksson & Karlsson [44] compares the use of mean torque and transient engine models in control applications, identifying the requirement to use transient models when considering backlash only as the powertrain damps transient vibrations. However only frequency analysis is used to identify impacts of engine transients. Consider also that lookup tables provide instantaneous changes to engine torque, while the actual engine response to throttle change is limited to the rate of piston firing, a form of time delay results.

2.3.4.3 Synchroniser

For DCTs the engagement of synchroniser occurs prior to clutch to clutch shifting, and as a consequence little study of the synchroniser engagement and the effects it may or may not have on the shift transient are researched. Goetz [1] has modelled the cone clutch for some simulations, but the complex nonlinear characteristics of interlocking gear to shaft are ignored. It is more common to treat the mechanism as either a power switch [22, 23], or ignore it entirely [24, 25, 27, 28]. The reasoning chosen by these authors is sound. Nevertheless the introduction of the synchroniser into a new operating

environment requires that some consideration for the study of synchroniser engagement and control be performed.

Rolland, *et al,* [13] provides some indication of the desired engagement times for synchronisers, referring to engagement times varying from 50 to 400ms in a high performance transmission. Using pre-selection of gears the synchroniser engagement is imperceptible to the driver [13]. However, in manual override of the transmission, the engagement must be minimised to reduce delay between shift command and actual shifting of the transmission.

2.3.4.4 Gear mesh nonlinearities

Particular to these models is the assessment of vibrations in the transmission, to which nonlinearities in the gear mesh is a significant contributor. As a typical example authors such as [22, 23] have assumed no backlash condition for gear mesh, common in control studies, eliminating the need to model nonlinear gear contacts, and significantly reducing computational demand for transient analysis. Refs [45, 46] are two typical examples of studying the impact of these nonlinearities on powertrain response, where gear lash contributes to both idle gear rattle and clonk response in the powertrain.

2.3.4.5 Temperature

Temperature effects can be quiet difficult to accurately quantify when modelling a DCT. The primary issue is that ATF properties vary significantly through different operating temperatures, and for this reason it is ignored by [22, 23], as such mechanical losses from fluid systems are constant with respect to temperature. From a design perspective, Lechner & Naunheimer [47] treats the variation in temperature by considering physical properties of ATF as a constant at 80°C, consistent with how temperature dependent variables are incorporated into system models. However, to fully understand how the temperature extremes impact on operation of synchroniser engagement in particular, the consideration of temperature extremes – particularly subzero degree centigrade cold starts – during modelling must be considered. Thus some variation of transmission fluid parameters of viscosity and density can be performed to study temperature impact on synchronisers. Furthermore Yang, *et al*, [48] investigation of wet clutch engagement shows impact on friction torque from nominal operating temperature. However, to

accurately model the variation of temperature in the transmission would require extensive application of thermodynamic theories, significantly complicating the model in a manner that is unlikely to generate information relevant to the goals of this project; therefore temperature fluctuation can be ignored.

2.3.4.6 Mechanical losses

Mechanical losses are of interest to the modelling of the DCT as the engagement of synchronisers and clutches must overcome the energy losses in addition to the energy required for engagement, as well as providing a significant source of damping in the powertrain. The handling of mechanical losses varies. Goetz, Levesley & Crolla [21] couple inertia components to the ground using dampers to simulate drag in the transmission, primarily at the gears, synchronisers, and clutch packs. Kulkarni, Shim & Zhang [23] incorporate all losses in the vehicle drag, while Zhang, *et al,* [22] treats losses as a single damping component to the ground. Kirschstein [24] ignores mechanical losses completely, as does Lei, Wang & Ge [26]. Given that the DCT design is relatively well established with only light damping in place, these sources require more consideration as part of the powertrain model.

2.3.5 A final note on DCT control and assumptions

Many authors have performed some form of research into control of the DCT and popular control techniques for combined torque and speed control of the clutch during shifting is extensively covered by authors such as [1, 19, 20, 22, 23, and 27]. Results are generally consistent with little detail beyond shift and/or launch control. It is therefore proposed that research move towards more detailed studies of DCT transient vibrations. This includes the impact of control methodologies and highly nonlinear hydraulic control systems, as well as investigation of the impact of the previously addressed assumptions, consisting of transient engine torque models and impact of vibration isolators, impact of synchroniser engagement on the powertrain, and nonlinear contact in gear mesh and synchroniser.

2.3.6 Synchroniser dynamics and modelling

In general, research into synchroniser engagement can be divided up into two groups, (1) mathematical investigation of the mechanism characteristics, and (2) numerical simulations of the engagement, each of which provide significant contributions to the understanding the process of synchroniser engagement.

2.3.6.1 Fundamental studies of synchronisers

Much of the fundamental research into the synchroniser and its actuation has been studied by ref. [49-53], covering a wide range of topics from fundamental theory through to design considerations and failure modes. Derived equations for cone and chamfer torques are consistent between these authors and are used in one form or another by many others in developing numerical models. The conclusion drawn on the synchroniser actuation is that it fundamentally relies on the correct balancing of torques – cone, chamfer, and drag – to actuate and engage normally [49-53]. Driver feel also plays a significant role in evaluating synchroniser engagements, affecting a form of closed loop control. Sykes and Szadkowski, *et al,* [54-56] present methods for evaluating shift quality observed by the driver, generally derived as a function of engagement forces. Note also that, as highlighted in Kelly & Kent [57], these forces are also affected significantly by linkages and selectors in manual transmissions.

The initial research by M'Ewen [53] develops equations relating the various torques, synchroniser time, and incorporates the inertia of the target gear in conjunction with that of the vehicle. This work is expanded to include variables such as speed dependent friction coefficient and other mechanism types. Abdel-Halim, *et al,* [50] expands on this work to include theory for multi-cone synchroniser mechanisms, particularly triple cones.

The work of Socin & Walters [49] is more expansive and includes detailed discussion of various factors that influence different stages of the synchronisation process. This includes friction surface quality, failure modes, limit stacks as examples. Of particular interest is the discussion on failure modes of the mechanism, which greatly aid understanding of certain relationships. Additionally assumptions are made to eliminate the use of vehicle inertia in the modelling process.

Razzacki [51] discusses the design of the synchromesh synchroniser in detail, specifically targeting the influence of design dimensions and tolerances. Further

research by Razzacki & Hottenstein [52] investigates the application of synchronisers for use in dual clutch transmissions, particularly developing the system drag torque model and experimentally investigating the indexing torque friction coefficient in the mechanism.

One significant consideration is for the inclusion of the synchroniser as a component of the powertrain [53] or, given that the powertrain inertia greatly exceeds that of the synchroniser and target gear, the study of the synchroniser independently of the powertrain [49], i.e. the powertrain inertia effectively acts as grounding. The reasoning behind original inclusions is associated mainly with older synchroniser designs that, with longer engagement times, are influenced by variation in vehicle speed.

Austen [58] highlights the influence of drag on manual transmissions, with it slowing the target gear for upshifts but resisting the target gear for downshifts. Rosen, *et al*, [59] disseminates knowledge on the use of synchronisers in heavy vehicles pointing out that the high drag influences the wear on friction surfaces for low gears, and the influence of low lubricant temperature on increasing drag. Both Socin & Walters [49] and M'Ewen [53] also highlight the influence of drag torque on the synchroniser, particularly with respect to the impact on mechanism failures.

2.3.6.2 Failure modes in the synchroniser

Within synchronisers there are both mechanical and material failure modes. The mechanical failure mechanisms of synchronisation primarily occur during the transition from speed synchronisation to unblocking processes, or within the indexing process itself. These failure modes are clash, partial clash, ring block out, and hub block out. These failure mechanisms arise when torque balances that control engagement are not met. Material failure modes are generally associated with damage to the cone or indexing tooth chamfers and in the case of tooth damage, arise from clash. Socin & Walters [49] provides the most comprehensive analysis of the process, understanding of the design requirements, and knowledge of failure modes. Much of this information is backed by publications by other authors who have investigated individual aspects of the mechanism.

If cone torque is less than chamfer torque during speed synchronisation, the sleeve will be able to push through the ring, and prematurely engage teeth on the hub while there is still a relative speed in between sleeve and gear hub. This is known as clash according

to Socin & Walters [49]. The result of clash is damage to the points of chamfers on sleeve and/or hub. This is generally the result of ineffective oil wiping of cone surfaces reducing the overall cone torque [47, 52, and 59]. However, it can also occur if there is torsional excitation of the powertrain which alters the blocking alignment, facilitating the translation of the sleeve [47]. Upshift grating and partial clash are essentially the same and are variants of this failure mode. These can occur when the transmission fluid is cold and the higher drag torque causes excessive relative motion when the two splines are engaging the cone dogs. Other causes are associated with damage and wear to friction and chamfer surfaces [49].

The second major failure mode occurs if drag torque exceeds chamfer or cone torque during the unblocking or indexing phase of synchronisation. This is known as block out, and can be of two forms. Either the required load will increase before the gear can be engaged, or engagement will be impossible [49]. It is generally a fault in the cone clutch where the static friction torque is low or clearance between internal and external cones is unfavourable for shifting, and can also arise from damaged chamfer surfaces, high drag during cold starts or poorly designed chamfers. When this occurs significantly more force is required for the chamfered splines to provide a rotational torque between the two friction elements [47, 59]. With respect to DCTs, the main concern is changes to drag torque are not well understood or investigated, and the resulting implications on both clash and block out during engagement. Through the evaluation of torque parameters it should be possible to design the applied load to ensure that this does not occur.

Other failures are associated with damage to the cone from thermal overload, excessive wear, or fracture of the ring developed from stress concentrations [47]. Thermal overload will have the effect of damaging the frictional surfaces and consequently reduce the frictional coefficients of said surfaces, which will reduce the efficiency of the system. Wear works in a similar manner where there will be excessive damage to frictional surfaces reducing its lifetime. Stress concentrations have largely been eliminated through good design practices but previously would damage the ring causing fundamental failure [47].

2.3.6.3 Numerical simulations of synchronisers

The three aims of modelling that have been identified are to demonstrate the shift force required by the driver in MTs, to investigate the variability in actuation of the system, and the third is focused on understanding and improving synchroniser mechanisms so as to shed light on various issues that surround the process. One popular method is optimisation of synchroniser designs [60-62] with the focus being on improved performance, reduced effort and smooth actuation. Generally speaking the focus of these works, with respect to optimisation, is the demonstration of different techniques in optimal design.

Kim, *et al*, [63] develops a synchroniser model for the purpose of investigating the required shift forces in manual transmissions. This incorporates shift forks and leavers required for the driver. As driving force must be determined Kim, *et al*, [63] use the displacement of the sleeve as the control variable. Generally speaking the results are reasonably accurate when compared to experimental work. Inaccuracies are likely to be due to the treatment of drag and lubrication, both of which will vary over the synchronisation and indexing process. Importantly, the variation in second peak load between model and experimental results indicate that the variation in indexing alignment is random and must be treated as such. By comparison Lovas, *et al,* [64] incorporate the effects of lubrication into the model and demonstrates that there are additional peaks as lubrication breakthrough progresses before synchronisation or indexing occurs.

Simulation of synchronisation performed by Hoshino [65] demonstrates several critical phases. A synchroniser model is introduced into ADAMS for the purpose investigating the process. The results illustrate that most variability in the system lies in the indexing and meshing phases of synchronisation. After meshing, as the gear is only freewheeling, the clearances and under cutting of the mesh teeth result in vibration. This should be considered backlash. The importance of considering a holistic powertrain model is demonstrated by Szadkowski [55] where the inertia and drag generated by the clutch alone are stated to be critical to the study of shift quality, the goal of most investigations into synchronisers.

The most important result presented by Hoshino [65] is achieved when increasing the sleeve speed, resulting in reduced synchronisation time. The splines make contact on the reverse edge of the synchroniser and move the sleeve backwards before completing the engagement on the back face of the splines. A similar result is achieved at lowest

speed. However the splines climb over the tooth and move down the front face of the teeth. The shortest indexing phase is when the splines make contact with the front face initially; this reduces the impact of the resiting moment on the engagement process and greatly speeds up the engagement process (Figure 2.4).

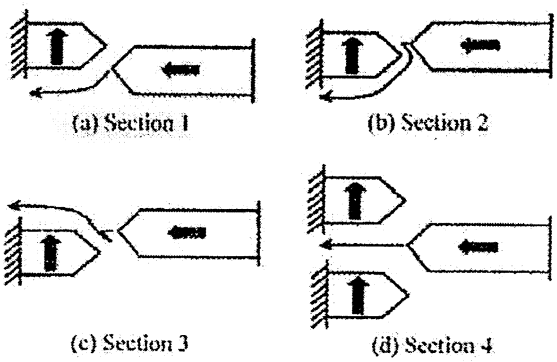

Figure 2.4: Mesh phases during indexing of the synchroniser [65]

Another investigation into synchroniser mechanisms was performed by Lovas, *et al*, [64]. A significant addition to previously discussed works is the incorporation of system drags onto the mechanism, as well as thermal effects, though the capacity of the ring to heat, expand and shrink over the cone clutch hub is a limited assumption given the speed of actuation. Also the phenomenon of stick-slip is incorporated into the model. However, again the powertrain is not included in the analysis. A significant portion of the lubricant effects studied is developed from Paffoni, *et al,* [66, 67] where the oil squeezing and hydrodynamic effects of the synchroniser cone are studied. Here theoretical and experimental studies are undertaken to develop an understanding of the influence of grooved friction surfaces on oil wiping of the synchroniser. In particular, oil squeezing forces and viscous contact friction equations are presented for application to synchroniser cones. In developing the model of the synchroniser Paffoni, Progri & Gras [66] excludes drag from bearings, gears, *et cetera*, enabling the author to normalise parameters and develop generalised solutions to the hydrodynamic model. This is not consistent with [49], drag has a significant effect on the entire engagement process, and must therefore be included in any model of synchroniser mechanisms.

With respect to stick-slip, Lovas, *et al,* [64] demonstrates that it is highly dependent on shaft stiffness, to the point that it will initiate at the cone without high stiffness values. If there is prolonged stick before synchronisation is complete then the indexing splines will start to engage the dogs and cause partial clash during indexing.

The main focus of Lovas, *et al,* [64] however is the "double bump" felt by the driver during gear engagement, and is also studied by refs. [60, 61, 65]. By including thermal effects, Lovas, *et al,* [64] demonstrates that the ring enlarges and shrinks onto the hub due to its low thermal mass. This results in the increased initial breakaway force which is applied by the indexing splines. In agreement with Hoshino [65], Lovas, *et al,* [64] demonstrates that it is easier to turn the gear against the direction of gear velocity during indexing. The presented results show that a smaller applied force is required to perform indexing. This is due to the fact that indexing no longer has to fight drag torque, but is in fact aided by the torque load. In practice the ring sticking and the initial applied force by splines make up the phenomenon of double bump. The critical variables identified by Lovas, *et al,* [64] are the tolerances in the cone, material properties, and friction coefficient for sticking bump, and the relative position of splines for indexing bump which affect the maximum forces resulting during synchronisation.

A third set of simulations was conducted by Liu & Tseng [60], again ADAMs has been used to generate a solid model to run simulations on, the focus being the controlled variables of applied load, cone friction coefficient, and indexing chamfer coefficient; as well as the uncontrolled variable of sleeve and hub spline orientation. The overall results for controlled variables are not unexpected; with the time for indexing and synchronising varying in the expected manner. The result for the uncontrolled variable is as previously discussed. The time taken can vary from 20ms for perfect alignment to 90ms seconds when chamfers are required to move up and over the backward facing chamfer. This is consistent with ref. [60, 65] (Figure 2.5). It is concluded that minor changes to this phase of the chamfer alignment has significant effect of the duration of engagement. There is no clear definition for the source of this error, some indications are considered by Hoshino [65] with respect to slip in the cone.

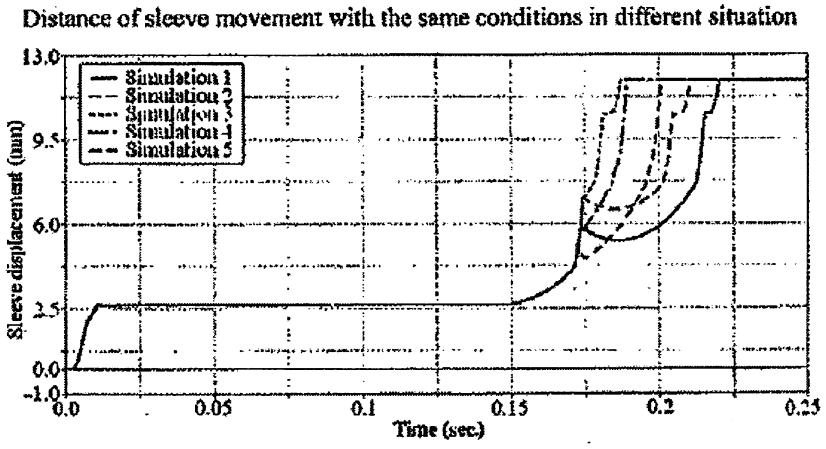

Figure 2.5: Figure of sleeve displacement with varying chamfer alignments from Liu &Tseng [60]

Abdel-Halim, *et al*, [50] demonstrated the importance of understanding the effects of lubrication on synchronisation when investigating the affect it has on the mean coefficient of friction. It was demonstrated at that there is little difference of coefficient of friction at cold start (0°C) and operating temperature (75°C) for a single cone synchroniser, but with a triple cone synchroniser under the same conditions, the coefficient of friction is almost halved. This result indicates that there is difficulty in wiping excess lubrication from the additional frictional surfaces as the cones engage.

A commonality in several of these works [63, 65] is that when modelling, to develop the random engagement of the chamfers, another layer needs to be added to the model to ensure that the engagement is random. This will have effects on modelling the double bump phenomenon.

Finally, refs. [60, 63-65] do not put forward much discussion on the influence of drag torque in developing the model. While it is identified as a significant, uncontrolled variable in other research, there is little study of its influence on the engagement of synchronisers, particularly in Hoshino [65] where relative speed after ring unblocking is identified as a potential engagement issue.

2.3.7 Drag torque

Understanding the impact of drag torque on the DCT as a whole and on the synchroniser in particular is critical to developing a precise synchroniser model that responds in a manner consistent with actuation in DCTs; it is the most significant source of losses in transmissions and contributes as an uncontrolled influence on synchroniser engagements. Identification of these drag torques and modelling the variation with

speed will provide insight into performance of the transmission and synchroniser, and how these can be influenced for improved response. Greenbaum, Kluger & Westmoreland [68] identifies major drag sources as being either load or speed dependent, depending largely on configurations chosen by transmission designers. These are further divided into windage and churning of gears and bearings, friction losses in the gears, and slipping losses in wet clutches and concentrically aligned shafts. The majority of current research is focused on only one of these drag torque sources, with the combining of different drag torques studied to a lesser extent.

2.3.7.1 Simulations of combined drag torques

Detailed studies combining different sources drag torque in transmission or gear pairs is limited, Anderson & Lowenthal [69-71] investigates losses for spur gear pairs and spur gear transmissions. Heingartner & Mba [72] investigates large power station transmission efficiencies, while Changenet, Oviedo-Marlot & Velex and Diab, *et al*, [73, 74] research targets helical gears in a manual transmission. With detailed knowledge of transmission structures and systems parameters these authors are generally capable of verifying analytical and experimental results to within 10-15%. By extending the model to include local temperature variations Changenet & Velex [73] can further reduced the discrepancies to within 5%.

Both Razzacki & Hottenstein [52] and Lovas, *et al,* [64] identify the sources of losses acting on synchronisers, but the extent of detailed modelling is not well established. Lechner & Naunheimer [47] suggests as a starting point, for passenger vehicles, drag torques of 2Nm acting on the synchroniser can be expected. Briec and Hennequet [75] study of power losses in a manual transmission with different lubricants predicts losses at about 2-3 kW at 90kph depending on transmission and fluid, equating to 6-9 Nm loss of torque for the whole transmission.

2.3.7.2 Sources of drag

Research into the modelling of different sources of drag is much more extensive. The available literature is identified in this section. However rationale for application of specific methods is not presented until the chapter on drag torque. Detailed analytical methods for studying transmission losses are included in [76] for gear friction, windage, and various other losses.

The most well established bearing loss analysis is performed by Harris [77], but other models are available from bearing manufacturers, such as Malmer [78]. This can include both friction and windage losses in bearings. The methods presented by Harris [77] is manufacturer independent and therefore popularly employed.

Losses in wet clutches arise through the relative motion of friction and spacing plates through continuous submersion in transmission fluid. These are studied by refs. [48, 79-81] for constant viscosity conditions with different methods for determining reduction in wetted areas at high speeds.

Friction losses in the gear pair have been investigated in refs. [69, 76, 82-84] with investigations covering numerical and experimental research, primarily focused on friction impacts on transient vibration of the gear. Research covers either the derivation of empirical equations for time averaged friction losses, or investigations of friction loss within the variation of mesh contact, with time averages investigations being more computationally efficient. The most focus of these investigations is the application of variable friction coefficients through the mesh range of contact, typical examples being refs. [84, 85]. An observed issue by Song, Liu & Smedley [86] is that many of these friction models tend to infinity at the pitch point. Several different methods are suggested as solutions, such as a smoothed coulomb friction model. Alternatively Changenet & Velex [73] uses a time averaged friction coefficient for evaluating drag torques in a MT.

The churning losses in gears are the result of gears or gear pairs rotating through oil baths in the transmission, generally associated with dip-type lubrication. Hohn, Michaelis & Otto [87] examines the influence of immersion depth against risk of gear failure, with lower immersion increasing risk of failure. A comparison of different models is performed in refs. [88, 89], comparing popular churning models of Boness or Terekhov [90, 91] among other models. Changenet & Velex [88] provides an alternative empirical model correlated against a series of experiments. This method for model derivation is an issue with churning models in particular, where each of the models described above utilises empirical correlation to their own experimental data and use the same experimental apparatus to validate the model.

Windage, similarly to churning, of gears is the rotation through oil-air vapour mixture. Models for evaluating windage are available in refs. [69, 92]. These are evaluated by Diab, *et al*, [93] along with empirical and semi-analytical models by the same author, with reasonable results presented for the semi-analytical method. Al-Shibl, Simmons &

Eastwick [94] also investigate these windage losses, correlating data from computational fluid dynamics with experimental results. However, only Dawson [92] correctly identifies the limitation of empirical results to use for similarly designed conditions.

2.3.7.3 A final note on drag torque

Extensive literature research by Eastwick & Johnson [95] covering 41 different research papers on gear windage has found the same issue the is identified in the previous section in gear churning and windage, with models validated on the same experimental bed that the data was derived from:

> *"It is clear that all the modelling work to date is very closely allied to particular gear configurations, and this therefore makes the range of validity limited"*

This quote from Eastwick & Johnson [95] highlights a major issue with much of the experimentally derived empirical research into gear churning, windage, and friction losses. While more detailed comparison of the different drag torques is made in the Chapter 5, with only limited data available for this research, the model presented has some limitations. However, it will provide a sufficiently representative model of drag torque variation for the purposes of academic research, with limited capacity for accurate experimental validation.

2.3.8 Hydraulics

The hydraulic control system for DCTs is critical to achieving high degrees of shift quality during transient operations. The development of accurate hydraulic models for gearshift control has been performed by Jeyakumaran & Zhang [32], Watechagit & Srinivasan, [33] and Favennec, *et al,* [96] for conventional ATs, by Pesgens, *et al,* [35] for a CVT and by Lucente, Montanari & Rossi [34] for an AMT. These papers focus on the hydraulic system responses when controlling shift transients, and comparison of how these impact of the shift quality.

Numerous models for individual valves are prepared by Wang, Kraska & Ortmann [97], using transfer functions, or refs. [98-100] using conventional techniques. Procedure for modelling is consistent with methods suggested in refs. [36, 37], applying conventional Newtonian Mechanics and fluid dynamic equations for compressible systems. A common issue identified being the high stiffness inherent in hydraulic systems, Ferreira,

et al, [101] suggests the use of semi-empirical models, in this case applied in dSPACE, for hardware-in-the-loop simulations, increasing the model time-step significantly. Alternatively Valdes, *et al*, [102] uses incompressible flow and computational fluid dynamics to attempt to reduce the order of conventional hydraulic system models.

Yu, *et al*, [103] studies the variation in hydraulic fluid effective bulk modulus. Sources of variation include air content, oil pressure, oil temperature, and pipe and seal rigidity. Simulation and experimentation demonstrated that the use of variable bulk modulus produces a more accurate result. Another aspect considered is modelling of the electromechanical solenoid. Kajima & Kawamura [104] study various factors affecting solenoid designs, providing a detailed methodology for mathematical modelling of electromagnetic systems, while Topcu, Kamis & Yuksel [105] suggests that the rapid response of solenoids means that models can be replaced by look up tables.

In summary, it is common practice to model hydraulic systems for numerical studies of vehicle transmission or the hydraulic system itself, though this has not been performed for DCTs. This is most frequently achieved using conventional fluid theory and Newtonian mechanics. Generally, consideration is given on how to treat the magneto-motive force generated in the solenoid, either as a lookup table or by modelling the electromagnetic process in the windings, again applying well established theory.

2.3.9 Engine models

The applications of engine models for the DCT are critical to transient studies. With no torque converter, engine harmonics are no longer isolated from the powertrain; furthermore precise engine control is now required to achieve best quality results for shifting. The methods for engine modelling identified in current literature are empirical engine models [1], engine maps and lookup tables [22], and linearised models [24]. Empirical engine models such as [40, 106] provide the most flexibility for control with the capability to modify variables such as spark advance, exhaust gas recirculation and air fuel ratio, while the use of maps generally only consider throttle angle and engine speed for control purposes. Each of these models provides precise mean torque values and utilise control without consideration of the delays associated with piston firing on output engine torque.

Neglected from each of these models is the transient engine torque. Only mean values are used. This is reasonable for control applications with conventional ATs, but as the

DCT requires precise control, and to evaluate the influence of engine dynamics on shifting, the use of transient engine models is required. Taylor [107] provides methods for determining instantaneous torque from individual pistons based on piston head pressure and variable inertia of piston and connecting rods. An example of torsional finite element model for an engine is presented in Larmi [108], though the size of the engine, a marine diesel, is significantly larger that the engine used here, results however show the variation of output torque through rotation of the crankshaft.

In this research two separate engine models will be used. For initial control and ideal transient simulations, a mean torque map will be used for transient simulations. However, a lumped mass model of an engine will also be employed to study the effects of transient torque and limitations to engine control.

2.3.10 Dual Mass Flywheel

The isolation of engine transient vibration and reduction of lockup transients are probably two of the most significant issues affecting DCT in terms of NVH. While the focus of shift transient reduction is mainly focused on the minimisation of transient vibration during lockup events, isolation of engine transients is more associated with the use of torsional dampers and dual mass flywheels (DMFW). For example the DQ250 uses conventional torsional dampers to isolate engine from transmission.

Significant industrial research is provided by LuK with literature published in regular symposiums. Research is presented as early as 1986 in [109] where development and initial models are discussed. Much of the LuK research covers development of different DMFW models for vibration isolation, demonstrating model parameters and research into effects of hysteresis [109-113]. Most recent research by Reik [110] suggests that improved efficiencies of powertrain may require introduction of pendulum absorbers in addition to the DMFW (see ref. [114] for formulation of pendulum absorber model). Yamamoto, *et al,* [115] provides a comparative study for development of a DMFW, similarly to previous a long travel arc spring is used to isolate high frequency forced vibrations of the engine from the drivetrain.

Gaillard & Singh [116] offer several different models for studying the use of torsional dampers on gear rattle, suggesting that the nonlinear model requires application of visco-elastic and dry friction elements for accurate representation of hysteresis. Simulations indicate that some models more capable of minimising vibrations under

certain resonances. Kim [117] studies the use of different torsional absorbers on improving launch performance. The DMFW is demonstrated to have the best launch performance through the isolating rapid accelerations in the engine from the powertrain, reducing impulsive speed changes and improving driver feel. Theodossiades, *et al*, [118] experimentally studies the capacity for DMFW to partially suppress clonk through attenuation of specific modes associated with its transmission through the powertrain.

2.3.11 Powertrain modelling methods

Application of finite element and lumped mass models is one of the more popular methods for studying the behaviour of powertrains in transient conditions. Comparing Goetz, Levesley & Crolla [1] using a 12DOF model to Kulkarni, Shim & Zhang [23] using a 4DOF model, impacts of the different DOF are reasonably perceptible in terms of peak-to-peak vibrations and overall response, though damping appears similar. Examples of different studies using finite elements are available for MT [29] and ATs [119]. For such models, nonlinear studies of gear mesh, shift transients, and tip-in tip-out transients are investigated. Alternative methods include rigid body simulations, similar to those of Zhang, Chen & Xi [42]. However transient dynamics are compromised with lower degrees of freedom limiting the response, these models more applicable to control studies. Bartlett & Whalley [31] demonstrate a hybridised lumped-distributed mass model applying transfer matrices to a simple geartrain.

An extensive finite element study of an AT is performed in Refs. [30, 43, 119-121], where a series of lumped spring-inertia models are produced to study shift transients in the AT, including the influence of mesh nonlinearities, speed dependent friction and judder, using modified versions of the same model, with degrees of freedom varying between 4 and 24 depending on the model requirements. System responses are studied and validated on a powertrain test rig.

The general result of the application of different lumped spring-inertia models influence of chosen DOF on the response of the powertrain. This is largely dependent on the target of investigations and the preferences of the author. One issue in DCT powertrain modelling is that the focus has so far been on shift and launch control studies. The impact of nonlinearities in the powertrain and response of the synchroniser are not studied. The behaviour of the DCT powertrain, particularly as considered an underdamped system, is likely to be significant.

2.3.12 Powertrain control

The control of shifting in powertrains is divided into two components, clutch control and engine control; these are frequently decoupled to simplify the control process [41]. Similar methods are adopted in Serrarens, Dassen & Steinbuch [122] for developing shift control models for dry clutches and in Luchente, Montanari & Rossi [34] for AMT control simulations. To highlight some of the issues in transmission control of shift transients consider Sun & Hebbale [123]. Consideration must be made for accurate prefilling of the clutch piston, with under or over filling resulting in poor shift quality. It is noted that in friction launch transmissions such as the DCT - an undamped powertrain - transient events can initiate transient response of the driveline, and emulating torque converter response is considered a major challenge.

Haj-Fraj & Pfeiffer [124] highlights the integration of engine speed control in the powertrain to improve shift comfort and reduce engagement times. Ibamoto, *et al,* [125] provides an example of using torque estimation to improve the shift performance of a planetary AT.

Reviewing refs. [122, 126-128], important control aspects are highlighted. (1) Independent control of the engine to prevent stall or flaring. (2) Minimisation of lurch from overshooting torque and abrupt clutch lockup. And (3), minimisation of post lockup transients. Phillips & Bai [129] achieves high quality launches on a friction launch clutch through application of notch filtering to eliminate transients near the natural frequencies.

2.3.13 Backlash modelling

Nonlinearities in the gear, divided into nonlinear stiffness through time varying mesh stiffness or backlash in the gear mesh (ref. [130]). The state-of-the-art of nonlinear gear contacts has been studied extensively in Wang, Li & Peng [130] covering a broad range of topics with respect to backlash and nonlinear stiffness models and applications in numerical analysis.

The vibro-impact problem of backlash is studied by Singh, *et al*, [46], using torsional application of backlash to the lumped spring-inertia models. This assumes that line of action (LOA) and off line of action (OLOA) forces can be replaced by torques and uses spring stiffness as the only component of the mesh model. More extensive models have

been developed. He, *et al,* [131, 132] develops 6 and 12 degree of freedom mesh models for spur and helical gear pairs, respectively. These models include nonlinear mesh stiffness, sliding friction as damping, and DOF for LOA and OLOA forces. In Crowther, *et al*, [43] a numerical study of contact nonlinearities in automatic transmissions is expanded to include nonlinear contacts in splined shafts as well as gears. Detailed models are replaced with reduced order models to improve computational efficiency, and focus is on torsional backlash, ignoring LOA forces. Extensive clonk studies by refs. [45, 118, 133-135] on the relationship between gear nonlinearities and clonk excitation show a clear correlation of mesh excitation and the clonk response in driveshafts, with gear mesh excitation frequencies coinciding with harmonics in the driveshaft.

The influence of gear nonlinearities cannot be ignored during transient studies in the DCT when studying issues involving nonlinearities. Backlash in gears and splined shafts is particularly important to DCTs with chamfered splines or "dog gears" used in the synchroniser to engage the gear to shaft, providing what may be considered a spline backlash given the design of synchromesh dog gears.

2.4 SUMMARY AND CONCLUSION

The objectives and goals of this project are to study the transient response of dual clutch transmissions with multiple nonlinearities, and investigate the actuation of the synchroniser mechanism. The study of literature conducted in this chapter has targeted the development of the DCT in terms of an emerging technology and its study under transient control conditions as one part. The remainder of this chapter is devoted to the investigation of specific research foci, the current state-of-the-art in terms of research into relevant fields of study, and identification of applicability to the study of DCT powertrain dynamics with multiple nonlinearities.

DCT literature is divided into industrial research, demonstrating specific aspects of DCT development, and academic research, focused on shift and launch transient control. Various assumptions made in model development have highlighted the need for further study with respect to analysis of transient response. These are:

- Dynamics and control of synchronisers,
- The effects of drag torque on DCTs,
- Hydraulic control system modelling,

- Nonlinearities in the gear mesh, such as backlash and nonlinear stiffness,
- Influence of engine transients, and
- Deployment of detailed lumped inertia powertrain models with DCT

Ultimately, this chapter has provided the framework for further investigation of the DCT as a transient system. Each of these topics requires specific consideration in this thesis. Transient investigations of DCT powertrains must cover the effects of multiple nonlinearities on system response. In the following chapters each of these constituents of the DCT will be explored both individually and as part of the DCT powertrain, with focus on understanding their respective influence on the DCT, giving particular reference to transient vibration studies.

CHAPTER 3: HYDRAULIC CONTROL SYSTEM MODELLING AND ANALYSIS

3.1 INTRODUCTION

The hydraulic transmission control unit (TCU) in the dual clutch transmission performs two functions. First is the clutch-to-clutch powershifting of gears, similar in principle to conventional automatics [47], where clutches are simultaneously engaged and released to shift between gears while maintaining tractive road load. Precise control, exceeding that current in ATs, is required as a result of the lack of significant damping sources in DCT equipped powertrains. The second task is the engagement of the synchroniser mechanism. Conventionally, with the exception of AMT-type transmissions, a manual task, where human feel is used to choose and engage the gear with the synchroniser. Feedback through the shift linkage is observed by the driver and used to determine if engagement is successful [55, 57].

Given the nature of the engagement process and structure of the hydraulic TCU, where synchroniser is engaged prior to shifting, it is possible to model these two processes independently. Detailed mathematical models of both hydraulic systems are required for shift control. This is achieved through the application of Newtonian mechanics and conventional fluid dynamic principles such as orifice flow and compressibility to the hydraulic control systems. This chapter is focused on the development of models for the hydraulic control unit, including the independent modelling of both clutch and synchroniser control systems. First the background into the DCT modelling requirements are discussed, followed by explanation of applicable modelling methods that can be used for the DCT simulation, including justification for the methods selected. The second section details the specified theory and develops a general equation for application to similar hydraulic control systems. Detailed modelling of the DCT clutch hydraulic controller is then offered, showing methodology, assumptions, and results for basic simulation of clutch control systems. Finally, the procedure for synchroniser control system modelling is presented, including brief simulation results.

3.2 BACKGROUND

The DCT is, fundamentally, an automatic transmission system comprised of multiple clutch mechanisms, including two primary shifting clutches and seven coupled synchroniser mechanisms. The many similarities between wet clutch control for both ATs and DCTs provides much relevant literature on the simulation of hydraulic valve systems for automotive transmission applications. It has been cited in Chapter 2 Section 2.3.4.1 and 2.3.8 that there has not been a previous attempt to model the hydraulic system and integrate it with a DCT powertrain model.

Detailed physical modelling methods are available for the development of mathematical models specifically for hydraulic power systems. Generally speaking physical modelling requires a great amount of detail on dimensions of valves, valve tracks, and spring and magnetic force information [37]. Even with this detail there is a degree of estimation required, primarily for the friction damping which is a function of contact area, clearance, hydraulic fluid used, and operating temperature. This method is applied in the work of [32, 33] uses the well established fluid theory to describe physical phenomena. This technique is highly dependent on the information available for modelling, and can require complex representation of the interaction and feedback between different fluid control volumes.

While increased computational demands are a drawback of physical modelling, detailed hydraulic models capture the highly nonlinear nature of transmission control units that is generally not possible using second order transfer functions. As a result of this physical modelling methods will be employed in this project for modelling by clutch and synchroniser control systems, and the theory and application of these methods are discussed in the following sections.

While clutch control simulations are popular, as has been previously discussed in the literature review, there has been no focus on the synchroniser control using hydraulic systems in DCTs, however it has been performed for an AMT [34]. Typically the synchroniser is pushed forward or back, suggesting that a double acting cylinder arrangement is sufficient for control. Guan & Pan [98] present a modelling and control example for a classical double rod piston arrangement. The modelling method adopted here is typical to those found in hydraulic simulations, using physical models to represent both moving parts and fluid flow. These are again the same methods found in Stringer [37].

3.3 DEVELOPMENT OF HYDRAULIC SYSTEM MODELS: GENERAL MODEL FORMULATION

The knowledge required to develop hydraulic system physical models is well established. Typical texts such as refs [36, 37, and 39] provide detail on modelling of hydraulic systems from fundamental principles for modelling, simulation and control of different hydraulic mechanisms such as pumps, valves, and servo mechanisms. These texts are used here to derive the principle equations presented below. Any required assumptions will also be derived based on these texts.

Procedure for developing physical models of hydraulic systems is divided into two engineering fields. The model of spools and pistons in the clutch mechanism is performed through the application of Newton's Second Law. Each moving part will be considered as a second order system with external force inputs. These forces can include feedback pressure damping, electromechanical inputs, and jet action depending on the angle of the spool opening.

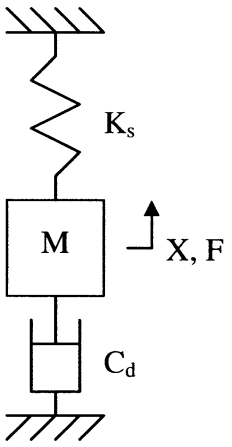

Figure 3.1: Single degree of freedom mass with damping

Consider the simple model in Figure 3.1. The second order equation of motion is:

$$\sum F = M\ddot{X} \tag{3.1}$$

where F is force, M is mass, and $\ddot{X}$ is acceleration. Equation 3.1 becomes:

$$M\ddot{X} - C_d\dot{X} - K_s X = \sum F \tag{3.2}$$

where C_d is damping coefficient, X is displacement, $\dot{X}$ is velocity, and K_s is spring constant. This provides a second order ordinary differential equation which can be used to reproduce a model in the Simulink environment for Matlab. The equation is typically

arranged in Cauchy form [136] so as to better represent the model arrangement in the Simulink environment. Equation 3.2 is arranged thus:

$$\ddot{X} = \frac{1}{M}\left(\sum F + C_d \dot{X} + K_s X\right) \tag{3.3}$$

Equation 3.3 is then integrated numerically to determine the velocity and displacement of the spool as a response to external forces.

Stiffnesses are generally derived from return springs, but also contact with hard surfaces is modelled as compliances to eliminate contact nonlinearities. For example, the spring stiffness for clutch pack in particular is highly nonlinear. The return spring is a typical coil spring of the order 10^2, but there is also compression of the friction lining once contact is achieved. This is of the order of 10^4, and clutch friction plates of order 10^5. The damping ratio is related to the frictional resistance between the spool and housing. Stringer [37] provides the following formula, Equation 3.4, for calculating the friction resistance as a function of contact length, clearance, diameter of the spool and viscosity, it is cited however that this equation can significantly underestimate the friction in the spool. The alternative method is to select a value for this damping based on experience, and re-evaluate it if necessary.

$$C_d = \frac{\mu \pi D l}{c_r} \dot{X} \tag{3.4}$$

where c_r is radial clearance, D is spool diameter, l is the sliding contact length, and μ is viscosity.

The force inputs, ΣF_x, into the model are derived from several sources. This includes feedback damping where control volumes at either ends of the spool provide pressure forces that counter the motion of the spool. For pistons this pressure force is the primary control force. The other force main being the magnetic induction derived from the coil windings in the solenoid. This force can either be calculated from magnetic flux equations, as was performed in Watechagit & Srinivasan [33], or using an experimental method, where position and current are controlled to map the response force of the solenoid based on these two variables.

The pressures in control volumes for the valve or piston must also be determined. First define the control volumes for each system. Generally, these volumes are the input, output and feedback damping volumes in valves, and for a clutch pack, the control

volume is the main fill volume in the piston. The flow rates into and out of control volumes are calculated using the sharp edged orifice flow equation (ref [37]), defined below:

$$Q_O = C_D \pi \frac{D^2}{4} \sqrt{P_2 - P_1} \tag{3.5}$$

where Q_O is flow rate through an orifice, P is pressure, and C_D is discharge coefficient. Very often the flow into a control volume includes leakage between the spool and housing. The leakage flow can be calculated in a similar manner to the orifice equation only the input area becomes the annular clearance between the spool and housing (ref [37]), and is derived thus:

$$Q_L = C_D \pi D c_r \sqrt{P_2 - P_1} \tag{3.6}$$

where Q_L is leakage flow rate. Equation 3.5 provides the area for a throttling orifice. For valve ports is somewhat different. If the port is closed the effective area is used as equation 3.6. However, for the open port the effective area is a conical surface that is made between the edge of the spool and housing for the port. This area is shown in section detail below in Figure 3.2:

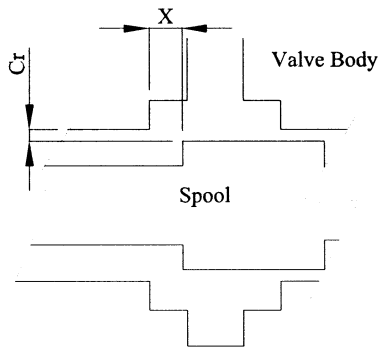

Figure 3.2: Detail of flow area for open port

To be utilised in the model the clearance in equation 3.6 can be rewritten to include valve opening area:

$$Q_P = C_D \pi D \sqrt{(X^2 + c_r^2)(P_2 - P_1)} \tag{3.7}$$

where Q_P is flow rate through port orifice. Particular to the feedback volumes and the clutch pack is the rate of change in volume with the spool or piston motion. This rate is expressed in the system as a flow rate change as fluid is forced into or out of the control volume. This is simply determined from the spool area and instantaneous velocity of the valve.

$$Q_V = A_P \dot{X} \tag{3.8}$$

where Q_V is flow rate from volume change, and A_P is the spool cross sectional area. The last source of change in flow arises from the fluid compressibility, with hydraulic systems such as the one under investigation operating under pressures in the mega-Pascal range, the compressibility of the fluid cannot be ignored. The bulk modulus can be significantly affected by the presence of air pockets in the hydraulic system. For the moment it is acceptable to ignore the effects of these as precise variation is derived experimentally. The flow resulting from compression of the hydraulic fluid is derived accordingly (ref [37]):

$$Q_C = \frac{V}{\beta} \cdot \frac{dP}{dt} \tag{3.9}$$

where Q_C is flow rate from fluid compression, P is pressure, t is time, β is bulk modulus, and V is volume. Equations 3.5-3.9 are combined to provide the net flow into or out of any control volume in a hydraulic system; through mass conservation it is assumed that:

$$\sum Q = 0 \tag{3.10}$$

Or

$$Q_O + Q_P + Q_L + Q_V + Q_C = 0 \tag{3.11}$$

Thus, for the general case of a single control volume with all applicable flows:

$$\frac{V}{\beta} \cdot \frac{dP}{dt} + A_P \dot{X} + C_D \pi D \sqrt{(X^2 + c_r^{\,2})(P_2 - P_1)} + C_D \pi D c_r \sqrt{P_2 - P_1} + C_D \pi \frac{D^2}{4} \sqrt{P_2 - P_1} = 0 \tag{3.12}$$

By re-arranging 3.12 to determine the rate of pressure change, eq. 3.12 is integrated numerically to determine the local pressure in specific control volumes:

$$P = \int \frac{\beta}{V} \left(A_P \frac{dX}{dt} + C_D \pi D \sqrt{(X^2 + c_r^{\,2})(P_2 - P_1)} + C_D \pi D c_r \sqrt{P_2 - P_1} + C_D \pi \frac{D^2}{4} \sqrt{P_2 - P_1} \right) dt \tag{3.13}$$

This results in a first order differential equation that can be used to solve for the pressure in a control volume. In the development of this specific solution there have been several assumptions that are used to simplify the equations. These are:

- Bulk modulus, β, is constant. The bulk modulus can also be assumed to be dependent on temperature and hence pressure changes, or affected by the inclusion of air content. The ideal case is assumed herein.

- The impact of pressure waves formed in opening or closing ports is negligible. For the length of any track volume and considering the sonic velocity of the hydraulic fluid it can be expected according to ref [37] that the resulting frequency response is of the order in kHz. This type of response is far higher than what will impact on the control of the system.

In developing mathematical models of the hydraulic controllers for both clutches and synchronisers, two separate ordinary differential equations have been derived. A second order ODE can be used to solve the equation for displacement of the spool or piston, and to solve the pressure changes in the system a first order ODE is employed. These equations are prepared for the following sections where specific details for the modelling of both clutch and synchroniser systems are presented.

3.4 DEVELOPMENT OF HYDRAULIC SYSTEM MODELS: SOLENOID AND CLUTCH HYDRAULICS

In hydraulic control circuits developed for conventional AT, the number of valves, solenoids and pistons can commonly exceed fifteen hydraulic components. Ultimately, the complexity results in a relatively high time delay between shift input signal and the start of actual shifting, which is undesirable for DCT control with precise control requirements. To overcome this issue, compact and direct acting solenoids are designed, (see ref [2]). Such a system must be capable of providing both precise pressure control and rapid fill time, achieved through control of pressure balances on the spool, with high pressure variation increasing the flow rate.

Figure **3.3** presents the layout for the hydraulic system for a single clutch in a dual clutch transmission, duplicated for both clutches. The system comprises of a normally low, variable force type solenoid directly feeding each clutch pack, integrated with a hydraulic damper to reduce the pressure fluctuations from shock.

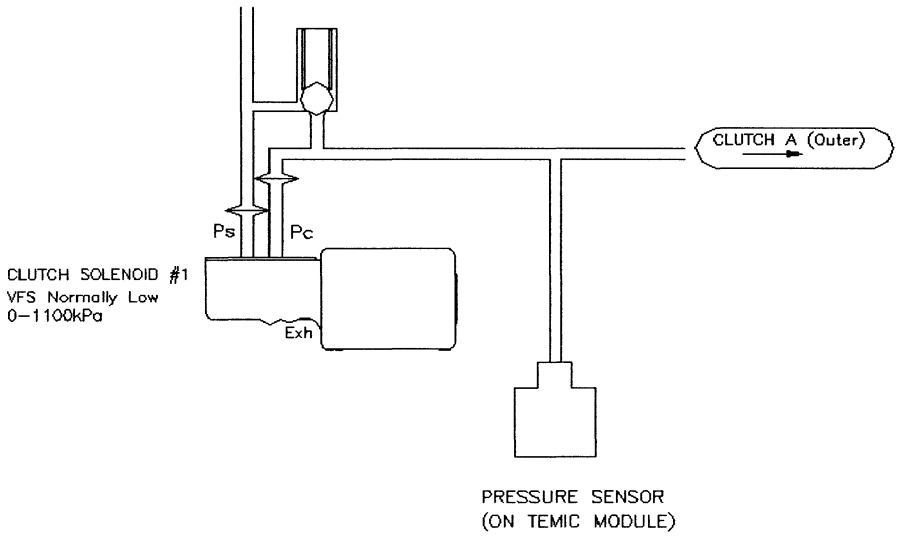

Figure 3.3: Schematic of clutch control system

Figure 3.4 shows a schematic of the solenoid and damper cross section in the idle state with output port open to the exhaust and input port closed. The input pressure line feeds both the valve spool directly and provides pressure to the hydraulic damper. In the low position the spool is closed to the high pressure line but open completely to the exhaust. Tolerance overlap is designed for the spool such that it can close both the input and exhaust ports simultaneously. When throttling pressure, input force partially closes the spool to the exhaust without opening the input port. The damping pressure at the end of the spool must equalise with the magneto-motive force for the spool position to stabilise, thus pressure throttling is achieved. However when providing high feed flow pressure the spool rapidly closes the exhaust port and opens to high pressure input until pressures equalise. The output chamber regulates the pressure for both feedback damping chambers, and provides the control pressure to the clutch pack.

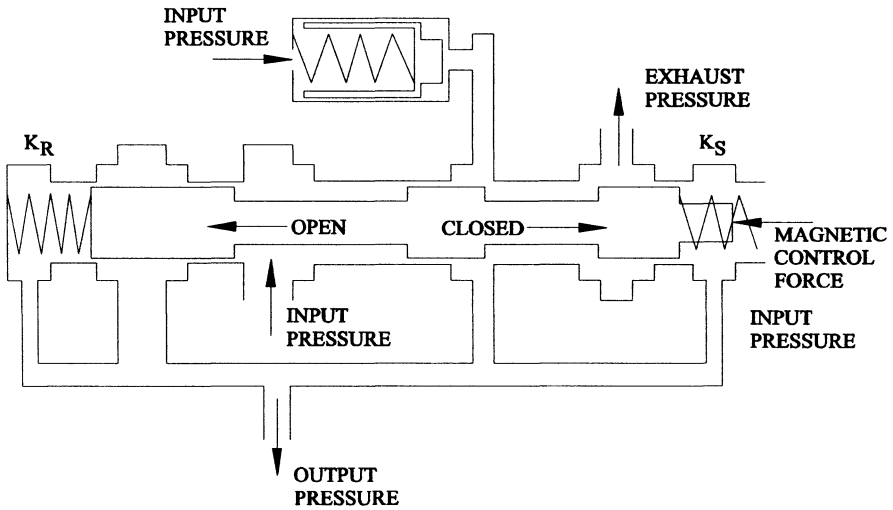

Figure 3.4: Variable force solenoid schematic with integrated damper

Each of the six control volumes shown in Figure 3.5 is characterised by different flows , these are used to determine the pressure for each volume as prescribed in Equation 3.13.

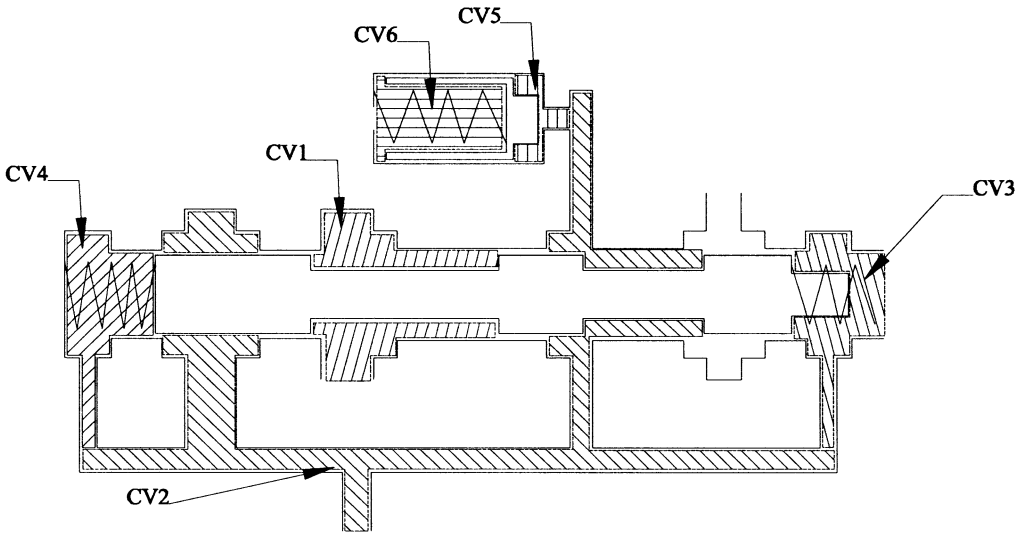

Figure 3.5: Solenoid and damper control volumes

The first control volume, designated CV1, is the input port for the valve. It accepts input flow through an orifice, and expels fluid through a port that opens to the output chamber and leakage flow to the output control volume between the spool and housing and also the output port when closed. This chamber has constant volume as it is not affected by the spool position. Its equation is defined thus:

$$P_{CV1} = \int \frac{\beta}{V} \begin{pmatrix} C_D \pi \frac{D_{CV1}^{\ 2}}{4} \sqrt{P_{IN} - P_{CV1}} - C_D \pi D_S \sqrt{(X^2 + c_r^{\ 2})(P_{CV1} - P_{CV2})} \\ - C_D \pi D_S c_r \sqrt{P_{CV1} - P_{CV2}} \end{pmatrix} dt \qquad (3.14)$$

Control volume 2 (CV2) is the control volume associated with the output pressure. It receives input flow through the port with CV1, and through the orifice with CV6, with exhaust flow also throttled. X_{IN} and X_{Exh} corresponds to valve opening to inlet and exhaust flow, respectively. Output is managed as the demand from the clutch piston, and leakage flow is received from CV1. Again this control volume is unaffected by volume changes.

$$P_{CV1} = \int \frac{\beta}{V} \begin{pmatrix} C_D \pi D_S \sqrt{(X_{IN}^2 + c_r^{\ 2})(P_{CV1} - P_{CV2})} + C_D \pi D_S c_r \sqrt{P_{CV1} - P_{CV2}} \\ + C_D \pi \frac{D_{CV5}^{\ 2}}{4} \sqrt{P_{CV5} - P_{CV2}} - C_D \pi D_S c_r \sqrt{(P_{CV2} - P_{Exh})(X_{Exh}^2 + c_r^{\ 2})} \\ - C_D \pi \frac{D_{CV3}^{\ 2}}{4} \sqrt{P_{CV3} - P_{CV2}} - C_D \pi \frac{D_{CV4}^{\ 2}}{4} \sqrt{P_{CV4} - P_{CV2}} \\ - C_D \pi \frac{D_{Output}^{\ 2}}{4} \sqrt{P_{CV4} - P_{CI}} \end{pmatrix} dt \qquad (3.15)$$

where subscripts Exh refers to exhaust, and IN for inlet. The third control volume (CV3) receives flow through an orifice port from the CV2, but also leaks flow into the exhaust port. Additionally this control volume is significantly affected by the displacement of the spool and hence volume change.

$$P_{CV3} = \int \frac{\beta}{V_0 + dV}\left(C_D \pi \frac{D_{CV3}^{\ 2}}{4}\sqrt{P_{CV2} - P_{CV3}} - A_P \dot{X} - C_D \pi D_S c_r \sqrt{P_{CV3} - P_{Exh}} \right) dt \tag{3.16}$$

Similar to the third control volume CV4 received flow from CV2 via an orifice. However there is also leakage from CV2 into this volume, as well as the control volume modified by the displacement of the spool. Similar to the previous equation it is derived as so, noting the sign changes from 3.16:

$$P_{CV4} = \int \frac{\beta}{V_0 + dV}\left(C_D \pi \frac{D_{CV4}^{\ 2}}{4}\sqrt{P_{CV2} - P_{CV4}} + A_P \dot{X} - C_D \pi D_S c_r \sqrt{P_{CV3} - P_{CV2}} \right) dt \tag{3.17}$$

Control volume 5 accepts feed from the pressure line and provides leak flow to CV6. It simulates the damper by absorbing shock pressure in the output line; therefore it is affected by the displacement of its spool. The flow equation is below:

$$P_{CV5} = \int \frac{\beta}{V_0 + dV}\left(C_D \pi \frac{D_{CV5}^{\ 2}}{4}\sqrt{P_{CV2} - P_{CV5}} - A_P \dot{X}_D + C_D \pi D_D c_{rD} \sqrt{P_{CV5} - P_{CV6}} \right) dt \tag{3.18}$$

Finally, for CV6 inputs come from leakage from CV5 and through the orifice to CV2. The direction of flow is dependent on the instantaneous pressure in CV2, and as a consequence of the high input pressure from CV5 it is generally output flow. It also is affected by the displacement of its damper spool.

$$P_{CV6} = \int \frac{\beta}{V_0 + dV}\left(C_D \pi \frac{D_{CV6}^{\ 2}}{4}\sqrt{P_{Line} - P_{CV6}} + A_P \dot{X}_D - C_D \pi D_D c_r \sqrt{P_{CV5} - P_{CV6}} \right) dt \tag{3.19}$$

The mass of the spool is the combination of the physical spool itself and the solenoid core. With this there are two spring resistances, the main spool spring and the return spring for the core, these are at opposite ends of the spool and hence provide countering forces. Similarly, with two feedback damping chambers, counterbalancing pressure forces are provided acting in opposite directions. This is characterised by the two different areas for the feedback pressures. The input force is provided from a linear solenoid acting on to the valve, with force dependent on both control current and position. Finally, frictional resistance is modelled as a constant acting against the direction of motion.

$$\ddot{X} = \frac{1}{M}\left(F_{MMF} + P_{CV3}A_{P1} - P_{CV4}A_{P2} - C_d\dot{X} - K_sX + K_RX - F_{Preload}\right) \quad (3.20)$$

Preload force is derived from the compression of the two springs during assembly of the solenoid to ensure continuous positive spring load. During simulations a lookup table using position and current defines the output magneto motive force (MMF).

The equation of motion for the damper spool combines the mass of spool and spring. It is balanced by two opposing pressures in CV5 and CV6, and has spring force and preload acting in the same direction as the pressure from CV5. As with the solenoid damping force is included as a function of the velocity.

$$\ddot{X}_D = \frac{1}{M}\left(P_{CV5}A_{P1} - P_{CV6}A_{P2} - C_d\dot{X}_D - K_DX_D - F_{Preload}\right) \quad (3.21)$$

Equations 3.16-3.21 provide the fundamental solutions to the integrated solenoid and damper system shown in Figure **3.4**. These equations demonstrate a high degree of coupling between different control volume pressures, and between spool and piston dynamics and various pressures. The development of detailed mathematical models of this system requires a good understanding of the complex feedback entailed in this type of hydraulic component. Additionally, nonlinearities such as the opening or closing of a valve port introduce additional variability into the system that, when combined with fluid bulk modulus leads to a numerically stiff model.

Figure 3.6 represents the clutch pack and hydraulic piston, made up of inner friction plates, outer spacer plates, piston head, return spring, and piston control volume. The regulated output flow from the previously developed solenoid feeds the piston. In the idle position the return spring lifts the piston off friction plates providing separation between friction and spacer plates. The piston volume, Figure **3.7**, comprises of the fill space where the feed pressure filling is counterbalanced by the preloaded return spring. Flow leakage is minimised with the use of seals, however a small leakage component is important for maintaining system flow.

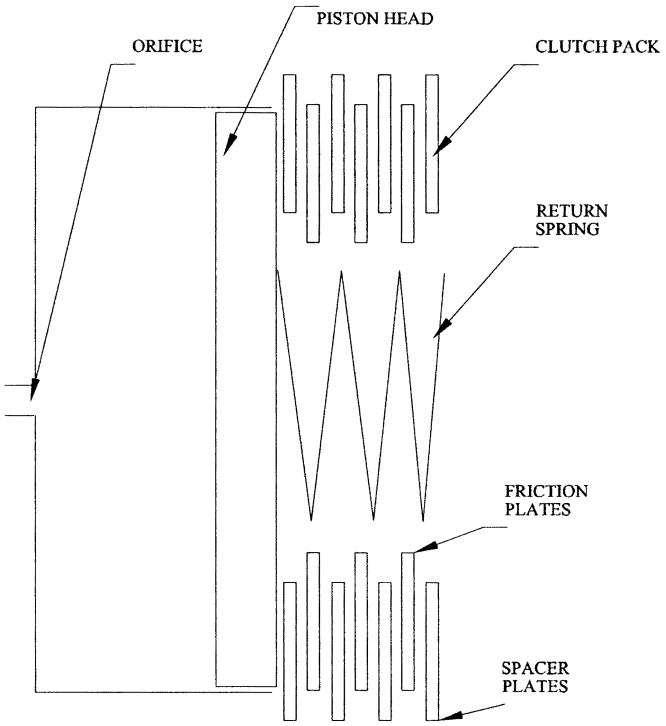

Figure 3.6: Schematic of clutch pack and piston

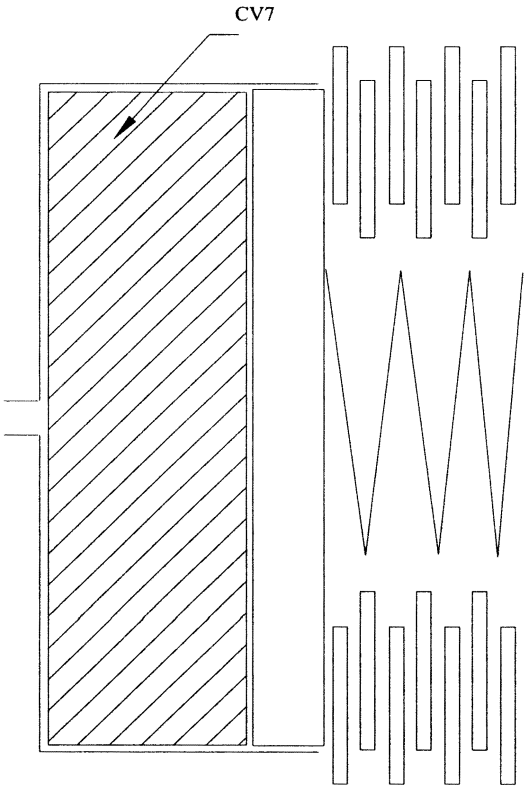

Figure 3.7: Clutch pack control volume

The piston head is the single mass that is considered in the equation of motion. It has higher frictional resistance that that of the spool as a result of its size and inclusion of seals. The spring force is nonlinear in the sense that it is initially a return spring while the piston is filling and displacing the friction plates. After the friction plates come into

contact with the spacer plates the compression of the friction lining must be taken into account. This increases a second time once the plates are fully compressed and the resistance then comes from the stopper. This spring force is an order of magnitude higher than that of the friction plates. Therefore a highly nonlinear spring force can be modelled for the clutch pack, see spring model in Figure 3.8.

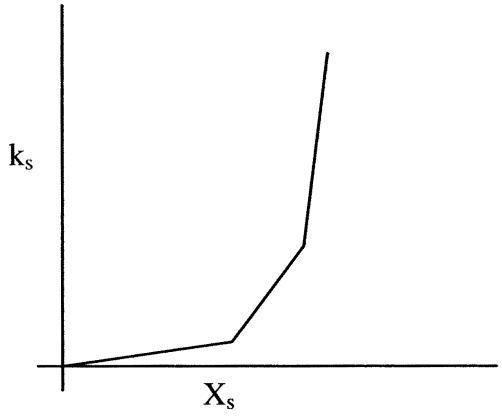

Figure 3.8: Nonlinear spring model for clutch pack

The output pressure from the solenoid becomes the controlling force in the equation of motion shown below.

$$\ddot{X}_{Cl} = \frac{1}{M_{Cl}}\left(P_{Cl}A_{Cl} - C_{Cl}\dot{X}_{Cl} - K_{Cl}X_{Cl} - F_{\mathrm{Pr}eload}\right) \tag{3.22}$$

where the subscript Cl refers to clutch. The control volume, CV 7, accepts input flow from the solenoid output through an orifice. The control volume is affected by the displacement of the piston head, and its velocity provides a flow rate change for the system. Additionally there is a small amount of leakage flow from the system around the piston to the transmission, modelled as an exhaust pressure.

$$P_{CV9} = \int \frac{\beta}{V_0 + dV}\left(C_D\pi\frac{D_{Output}^{\ 2}}{4}\sqrt{P_{CV2} - P_{Clutch}} - A_{Cl}\dot{X}_{Cl} - C_D\pi D_{Cl}c_{r,Cl}\sqrt{P_{Cl} - P_{exh}}\right)dt \tag{3.23}$$

From the equations of motion and flow rate equations (3.14 – 3.23) it is obvious that there is a high degree of coupling between the equations for solenoid and clutch piston. Furthermore, while the output pressure of the solenoid controls the clutch piston, the demand from filling the piston must feedback into the solenoid equation, coupling these two separate components. As a result of this coupling it should be recognised that there is a very intricate feedback environment involved here when modelling the hydraulic system.

3.5 SIMULINK® MODELLING AND INITIAL RESULTS

The development of mathematical models for clutch hydraulic system has been performed using the Simulink® module of Matlab®. Subsystems were built for variable force solenoid, damper and clutch, with these further broken down into subsystems based on Equations 3.13-3.23. For simulations the fourth order Runge-Kutta method has been applied using a constant time step of 10^{-7}s, with the timestep determined through iterative reduction in step size. Simulations are performed to generate characteristic curves for the valve output pressure and time delay, and provide basic results for step and ramp inputs. For the combined valve and piston results are developed for both the step and ramp inputs. Two separate results are presented for the assembly as there are two different sized clutch packs, and it is expected that there will be variation in the time delay of both assemblies. Simulation parameters for the solenoid and two clutch packs are shown in Table 3.1:

Table 3.1: Hydraulic model parameters

Parameter		*Parameter*	
Bulk modulus (MPa)	1400	**CV1 (mm^3)**	1800
Clearance (mm)	0.008	**CV2 (mm^3)**	3000
Overlap (mm)	0.05	**CV3 (mm^3)**	50
Spool diameter (mm)	7.476	**CV4 (mm^3)**	140
Damper diameter (mm)	12	**CV5 (mm^3)**	1070
Clutch 1 internal (external)	105	**CV6 (mm^3)**	117
diameter (mm)	(163)		
Clutch 2 internal (external)	139	**Clutch 1 CV (mm^3)**	12200
diameter (mm)	(193)		
Spool spring 1 rate (N/mm)	0.42	**Clutch 2 CV (mm^3)**	14080
Spool spring 2 rate (N/mm)	0.174	**Input orifice (mm)**	3.5
Damper spring rate (N/mm)	13.89	**Output orifice (mm)**	3
Clutch 1 spring rate (N/mm)	60	**Clutch 2 spring rate (N/mm)**	60
Spool 1 area (mm^2) A_{P1}	43.9	**Spool 2 area (mm^2) A_{P2}**	31.33
Damper area (mm^2) A_{S1}	113.1	-	-

The characteristic curve for a solenoid valve provides the response of the valve to step current inputs. To simulate the response accurately the model pressurises a simulated

chamber with a volume of 10^4 mm^3. This volume is comparable to clutch piston volume. The pressure responses, time delay, and spool position are presented in Figures 3.9 and 3.10.

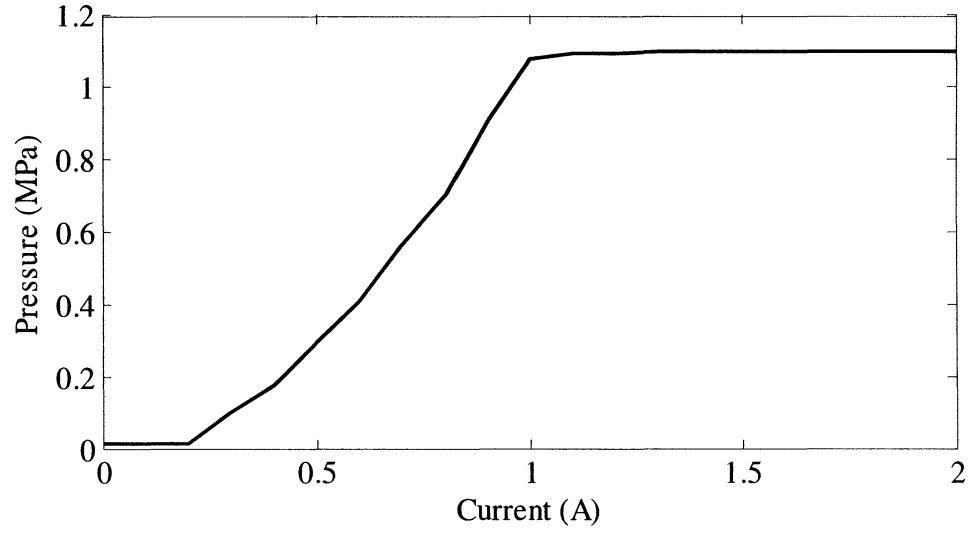

Figure 3.9: Characteristic Curve for VFS

The characteristic curve in Figure 3.9 above provides two distinct phases of operation. The input current region from 0.3 to 1 Amps provides good clutch pressure control with a reasonably linear region for the wide range of inputs. The second region is above 1 Amp, where the resulting pressure output is constant; this region is useful for achieving rapid filling of the clutch volume.

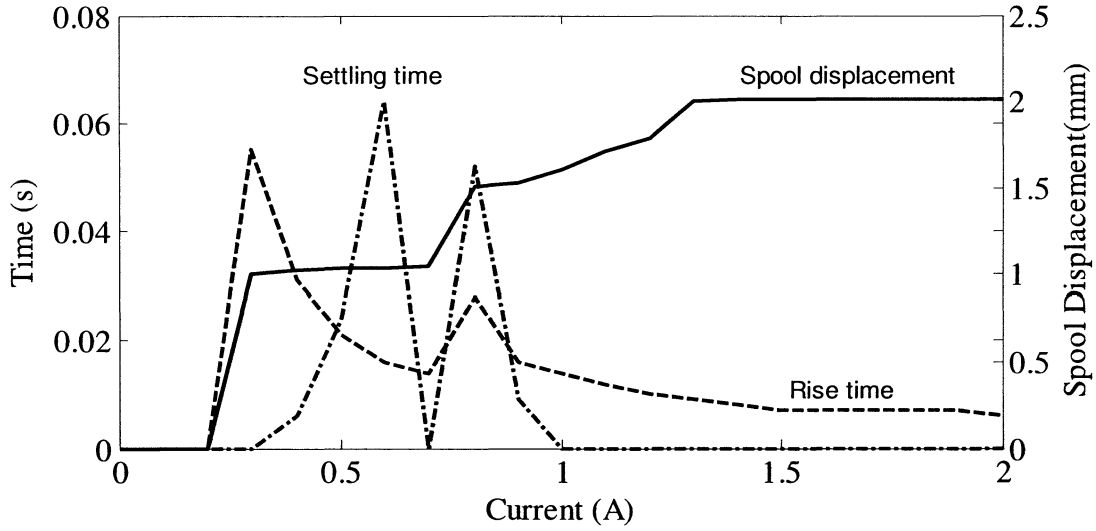

Figure 3.10: Spool displacement and time delay for VFS

Results presented in Figure 3.10 provide rise time, settling time, and spool displacement corresponding to the characteristic curve in Figure 3.9. In the pressure control region the time delay resulting from variation in rise time demonstrates the trade off required

for precise pressure control, where variable time delay resulting from targeting lower pressure provides lower forces to the solenoid, the secondary peak results from the spool pushing through the overlap region, delaying the achievement of peak pressure. Conversely, for the high response region, the results show that high force imbalance on the spool rapidly aligns to the fully open position, resulting in very low time delay. These results are backed by the spool position, where, during pressure control, there is very small difference of location for the spool. This indicates that the spool is successfully throttling the flow released to the exhaust port. The result for an input current of 0.8A is that of the spool throttling the input port pressure instead of the exhaust port as performed when the current is below 0.8A. Above 1 A the position rapidly moves to fully opened valve to the input port, resulting in the rapid achievement of the required pressure. The settling time reaches the maximum either side of the closed port region, as indicated by the spool position. A consequence of the spool moving between throttling position and overlap, and as the spool settles to a throttling position the pressure stabilises.

By using the output volume pressure to balance the MMF the most efficient pressure balancing is achieved. During the initial suction phase as the target volume is pressurised the spool is pulled to maximum open position, and only once the pressure begins to equalise force balancing occurs.

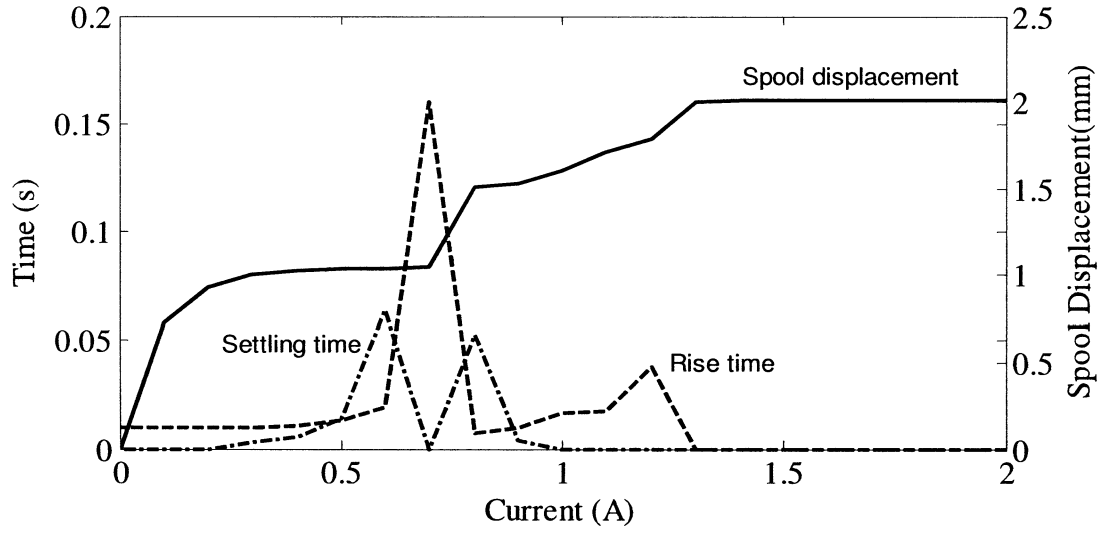

Figure 3.11: Solenoid release spool displacement and time delay curves for step down

Figure 3.11 presents the responses for the release of the solenoid from maximum current of 2 Amps, the x-axis current represents the final input current. Spool position is similar to that presented in Figure 3.10 and output pressures are the same, the real

difference occurs in the time delay present in the system. Release rise times are smaller than the comparative rise times in Figure 3.10, but the settling time is increased significantly, a result of the lower force differential is releasing pressures. This is particularly true for a 0.7A step down with equilibrium reached just the other side of the overlap, delaying engagement. Comparison of step down to step up results demonstrates the hysteric nature of time delay present in the solenoid valve.

3.5.1 Solenoid response to basic inputs: Step

The solenoid response to step inputs can be used to demonstrate the points of minimum stability according to settling time profiles, and evaluate the reaction to step up and step down control signals. The results presented in Figure 3.12 show the response of the solenoid to a step input of 0.6A, this chosen as the input as it represents the least stable input signal for the valve for the step up responses in Figure 3.10. The steady state pressure of 0.4MPa is achieved in 170ms from the initial input time. Settling at this input current is significant taking over 60ms, assuming a pressure oscillation of less than 0.02MPa as being settled. This is a result of the spool proximity to the closing of the valve port, with it moving between closed and open during settling, increasing variability of feedback forces. In conjunction with this a slight delay in the balancing of feedback pressure results in extension of settling time.

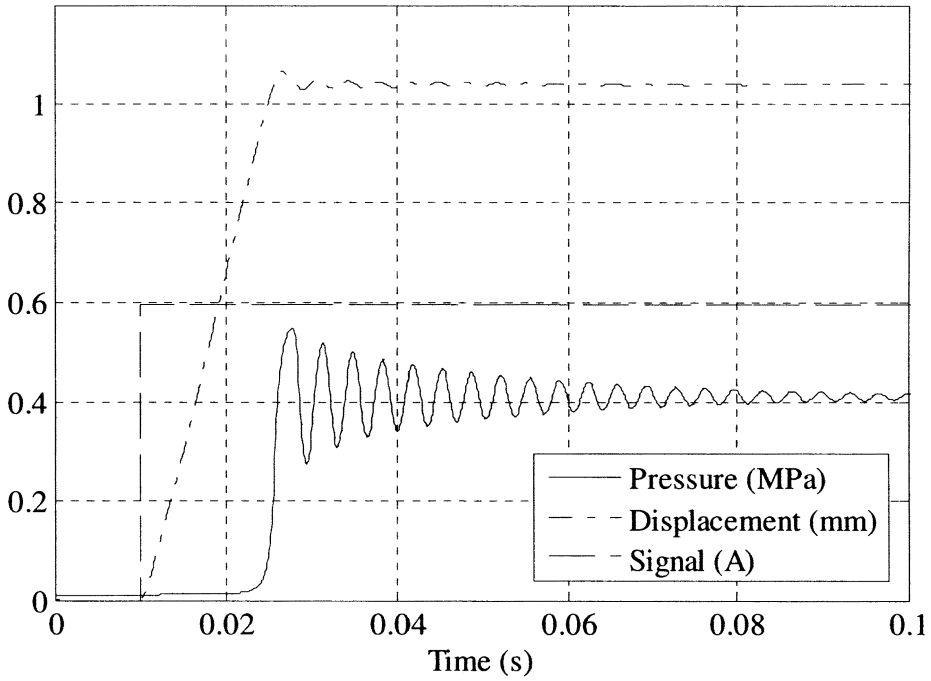

Figure 3.12: Normally low VFS response to step input

The results for Figure 3.13 show the high to low response using an initial current of 2A, down to 0.6A. This type of response is typical for high to low responses as input force is released and the return spring load and feedback forces return the spool to its initial position. During the step down the spool must move from throttling the input to throttling the exhaust, through the overlap in the valve body. Combined with the low variation in pressure between the two conditions the spool then moves slowly through the overlap; the plateau between 0.015 and 0.03 seconds. Once the steady state pressure is reached the spool experiences a similar stabilisation process as in Figure 3.12.

Comparison of the results for Figures 3.12 and 3.13 demonstrate the capacity for the valve to respond rapidly to inputs. This is desirable for control of the DCT where such responses enable rapid and precise actuation of clutch mechanisms. Figure 3.13 demonstrates an underdamped system with interference from the overlap, while Figure 3.12 demonstrates an underdamped system, resulting from the interaction of time delays in the system and balancing of multiple control volume pressures. It should be noted that the plateau between 15 and 30ms is a result of the valve being closed to both input and exhausts ports, functionally this can be minimised by decreasing the overlap.

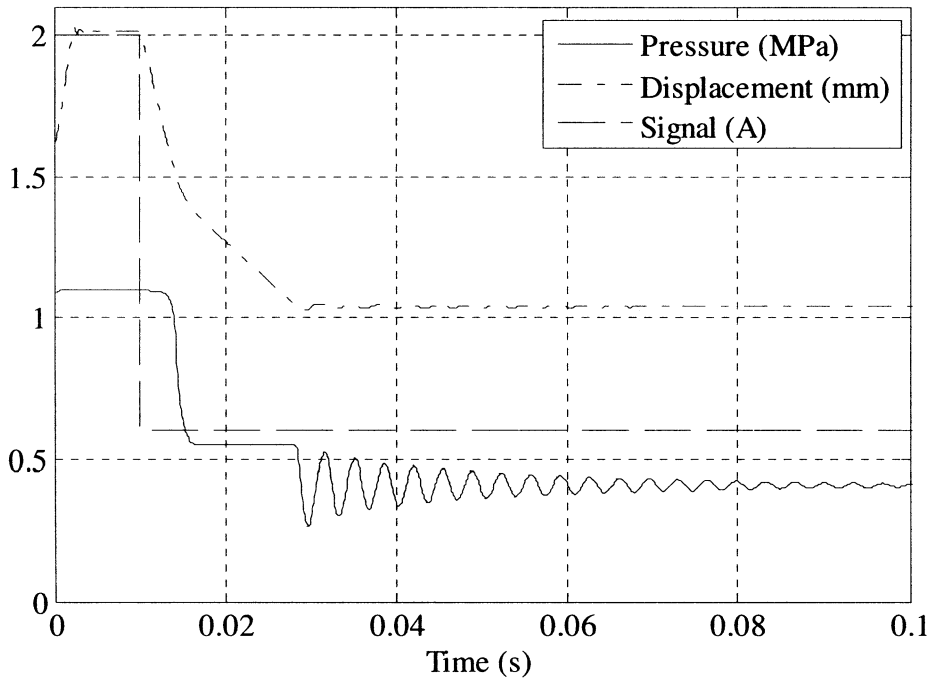

Figure 3.13: Normally high VFS response to step input

3.5.2 Solenoid response to inputs: Ramp

An alternate method for evaluation of linearity in the solenoid valve is through the application of a ramp input signal. In Figure **3.14** the solenoid response to a simple ramp input clearly demonstrating the nonlinear response of the solenoid to variable inputs. The two rapid changes in the spool displacement represent the positioning of the spool in throttling positions, first moving from idle position, then through the overlap region. With the current at less 0.3A there is insufficient load to overcome resistances, but as the current continues to increase there is a reasonably linear pressure increase once throttling is achieved. However, as overlap is reached a significant discontinuity arises, the rate of pressure change drops as both input and exhaust ports are closed. In the final throttling region the pressure must restabilise before continuing to increase. There is then a limited range of easily achieved linear control for precise clutch control. Using pressures between 0.6 and 0.8 MPa will incur significant discontinuity in pressure control.

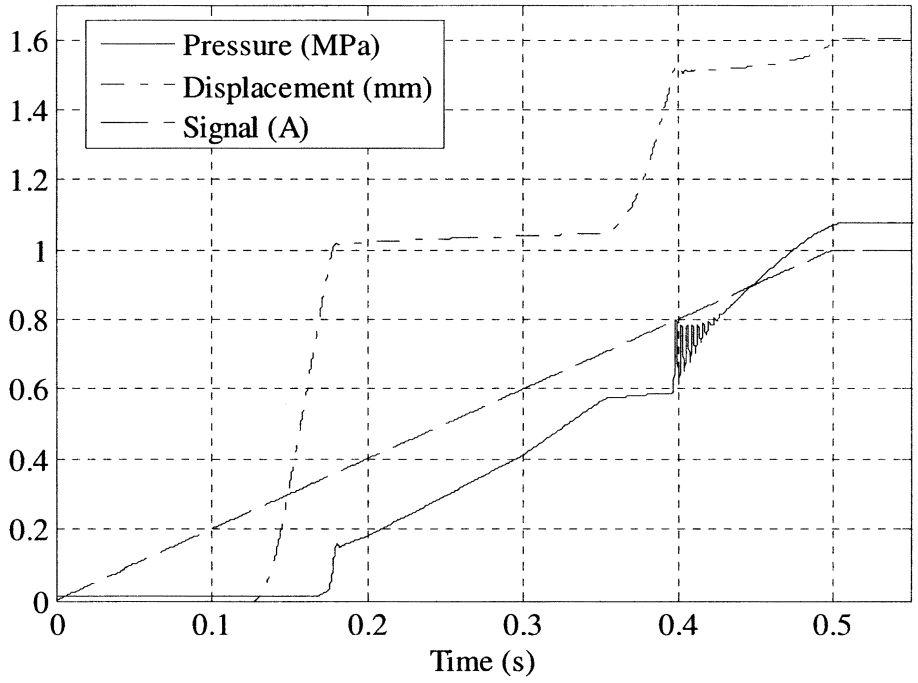

Figure 3.14: VFS response to ramp input

3.5.3 Combined system response to inputs: Step

The step input results for both combined clutch and solenoid configurations presented in this section for current inputs of 0.6 and 1.4 A. These currents have been selected as they will present mid range result indicative of the two solenoid pressure output regions. Clutch 1 is characterised by smaller contact surface area and piston fill volume as it is

the inner clutch pack in the arrangement, while clutch 2 as the outer clutch assembly has a larger area and respective control volume.

Figures 3.15 and 3.16 present the simulation results for 0.6 and 0.7 A step inputs for the clutch 1 assembly with VFS. Figure 3.15 spool responses shows that the spool is forced into fully opened position from the demand for flow from the clutch piston. This is indicated by the arrow 1. With spool at maximum displacement the VFS pressure increases rapidly, but the clutch piston is slowed by the increased resistance provided from the friction plates. As the friction plates are compressed clutch pressure rapidly increases to match VFS pressure, indicated by arrow 2. The fill duration lasts approximately 200ms as the piston moves from the neutral position to contact with the pack, and reaches pressure balance in 25ms. For an input of 1.4A, nonlinear response demonstrated in Figure 3.16 is evident, and as pressures balance an extended settling time is experienced. Shorter fill time arises from the higher input force, but as the pressures equalise, the significant settling identified in the solenoid is transferred to the clutch pressure. Lasting approximately 130ms, it is the longest experienced by the assembly. Comparing Figure 3.12 and 3.13 to 3.15 and 3.16 there is now significant damping of the valve, reducing much of the oscillations present in the solenoid responses. Thus by increasing the cylinder volume for results in Figures 3.15 and 3.16 in comparison to fill volumes in Figures 3.12 and 3.13, the system damping is increased.

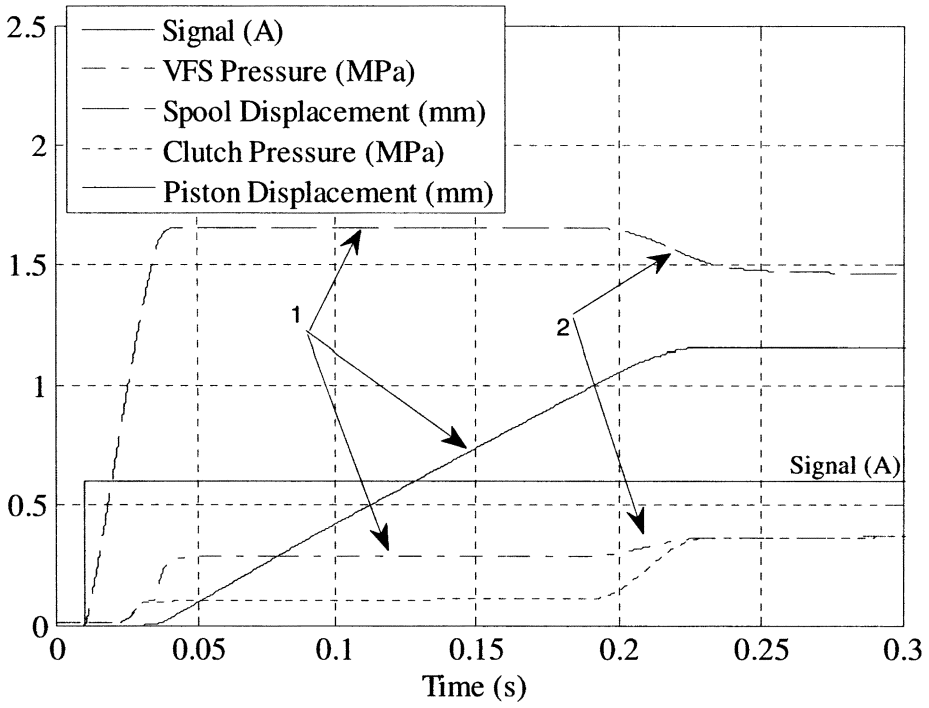

Figure 3.15: Hydraulic system response to step input for clutch 1, I=0.6A

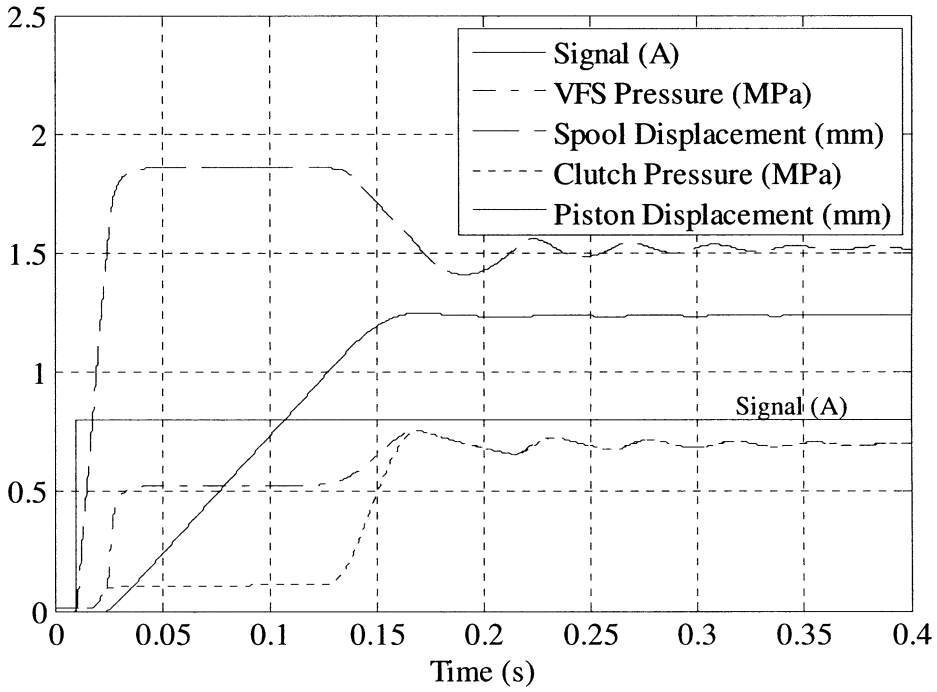

Figure 3.16: Hydraulic system response to step input for clutch 1, I=0.7A

Figures 3.17 and 3.18 present the simulation results for 0.6 and 0.7 A step inputs for the clutch 2 assembly with VFS. These results are quite similar to those presented for clutch 1 in Figures 3.15 and 3.16. However, the settling time has decreased for the 0.7 A input as a result of the increased clutch volume providing additional damping to the system, though the filling time has increased by around 20ms, suggesting that the increased clutch volume results enhances system damping at the expense of clutch increasing fill time. Moreover, this increased damping reduced peaks of the pressure response in Figure 3.18, which further reduces delay. This is also reflected in Figure 3.18, where the overall actuation time has increased, again by 20ms through increased fill time.

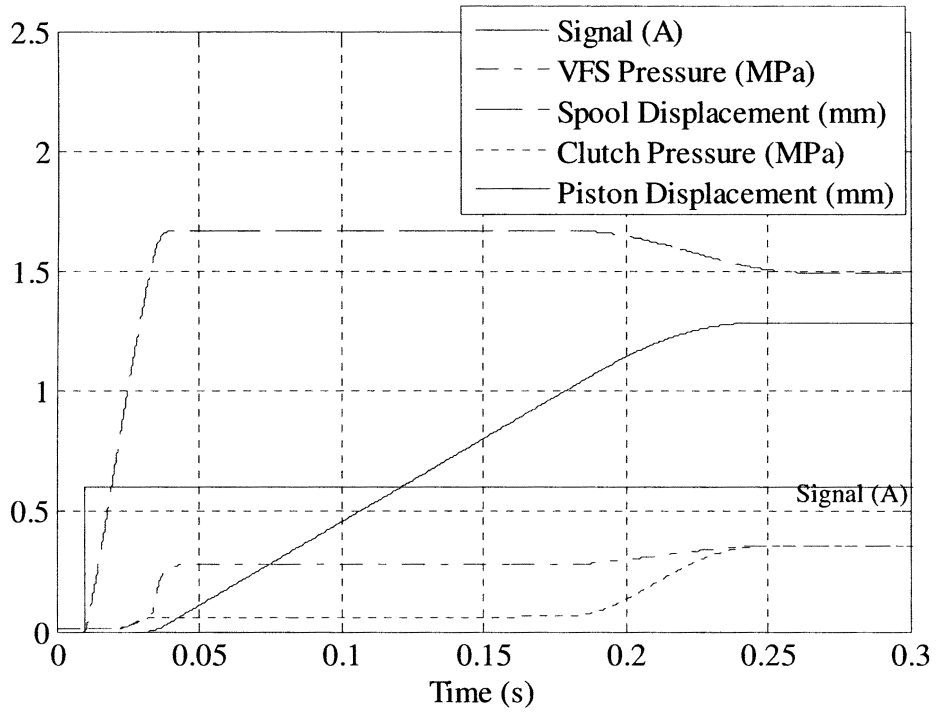

Figure 3.17: Hydraulic system response to step input for clutch 2, I=0.6A

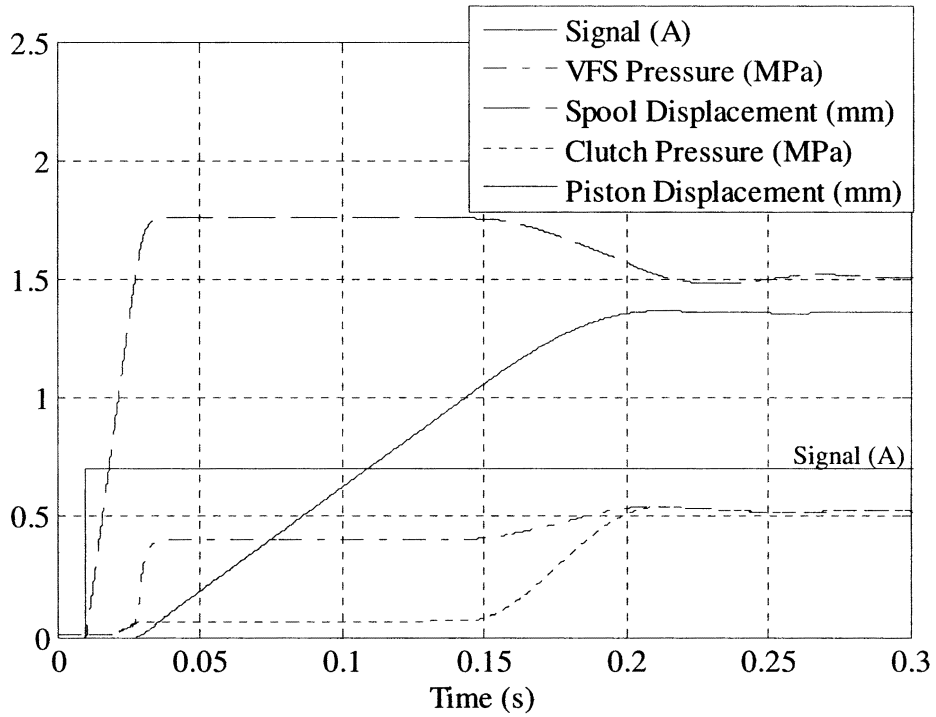

Figure 3.18: Hydraulic system response to step input for clutch 2, I=1.4A

3.5.4 Combined system response to inputs: Ramp

Demonstration of the actuation of the clutch pack with a ramp input is presented in Figure **3.19**, with the current increased from 0 to 1 A over a period of 1 second.

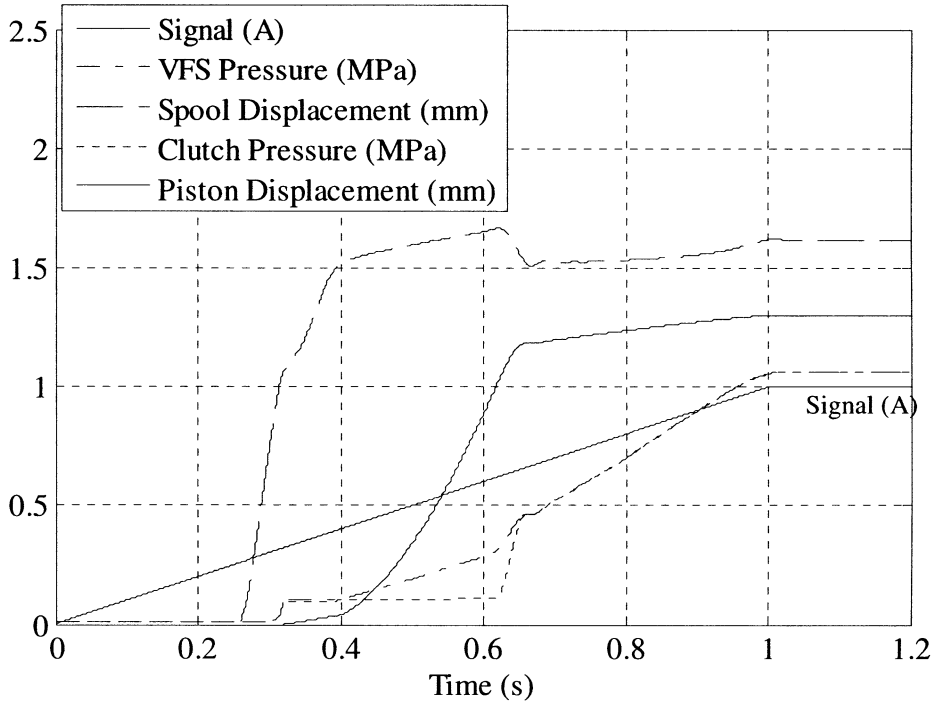

Figure 3.19: Simulation of clutch 1 and VFS combined using a ramp input

Similarly with results in Figure **3.14**, the degree of nonlinearity is again well demonstrated. Below approximately 0.6 seconds the clutch piston is filling, but once contact is achieved and the pressures equalised, the rate of pressure increase is fairly linear. This is again a significant improvement over the response of the solenoid alone, and is a result of the damping provided by the clutch pack and lower ramp rate.

The results of both VFS and clutch actuation presented in this section demonstrate the adequacy of the current model to provide both precise pressure control and rapid responses of the clutch in input signals. The solenoid is characterised by two distinct control regions, pressure throttling for lower region for precise pressure control, and rapid input flow for higher input signals. The ideal pressure curve is reasonably linear, while settling time delays seem to be the most significant drawback to this valve. The integration of the clutch pack model has the effect of significantly reducing the oscillations present using step input simulations. Thus the combined system is significantly improved for the purpose of clutch control.

3.6 DEVELOPMENT OF HYDRAULIC SYSTEM MODELS: SYNCHRONISER

The synchroniser mechanisms in the DCT are actuated through a comparatively simple hydraulic circuit as dynamic characteristics of the synchroniser allows for a simple approach to control. A consequence of the reliance on torque balancing to control mechanism motion, most notable being the generation of chamfer torques in the sleeve (discussed further in Chapter 4). In any transmission the synchroniser mechanism must be pushed either forward or backward to engage and disengage two separate gear pairs. In a conventional MT this is achieved through the use of lever mechanisms, these are described in refs [47, 63]. Through mechanical advantage input load from the driver of the order 10^1 to 10^2 N is converted to a load on the synchroniser sleeve of 10^2 to 10^3 N. As an example, Hoshino [65] generates a 3000 Newton peak output force directly at the sleeve.

The requirements of the DCT are then to apply uniform forces to move the synchroniser sleeve either backwards or forwards through a range of motion approximately 10 to 15mm. This is achieved through the application of two separate hydraulic pistons at either end of the mechanism such that motion is dependent on the cylinder actuated. The detailed hydraulic arrangement is presented diagrammatically in Figure 3.20 for synchroniser actuation in a DQ250 TCU.

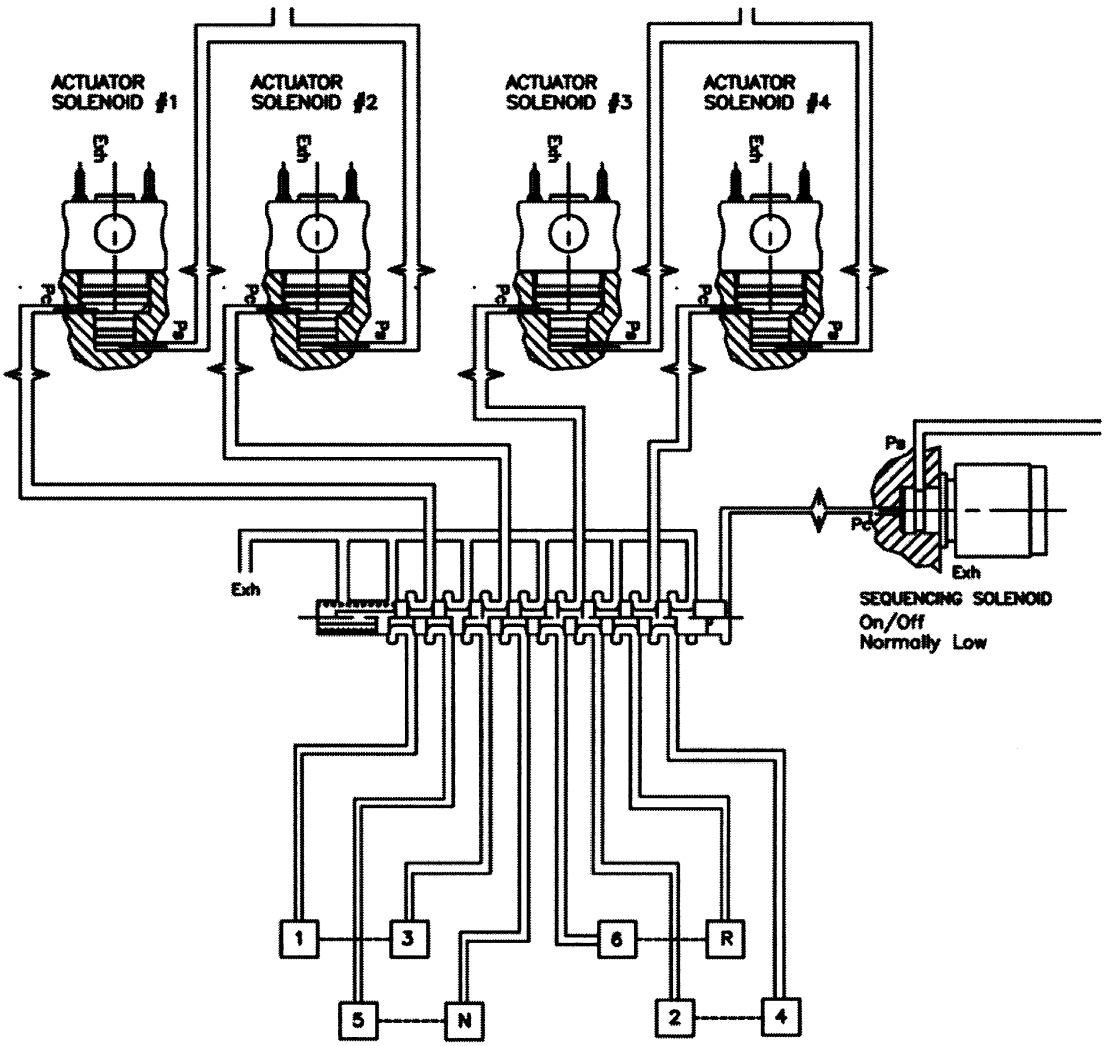

Figure 3.20: Hydraulic shift mechanisms for the DCT synchroniser control including four on/off solenoids and a sequencing solenoid

The hydraulic unit utilised in this transmission uses four actuating solenoids in the form of high flow, normally low, on/off type solenoids, as shown in Figure 3.20. However, it is immediately obvious that the DCT requires eight pressure sources to maintain the capability to actuate each synchroniser mechanism. This need is realised through the use of a sequencing valve and solenoid, a two position multiport valve designed such that each actuating solenoid can pressurise one of two cylinders at any one time. Furthermore, the synchroniser mechanism is designed with undercut splines such that once engaged with the clutch closed, there is no longer any need to apply any load to the mechanism. Therefore, unlike the wet clutch, once the engagement and shifting processes are complete, pressure can be released from the now engaged synchroniser and the sequencing spool valve repositioned.

The result of this design is that it is reasonable to model the pressure output from the sequencing solenoid to any one control cylinder as being equal to the exhaust pressure

when off, or, if the cylinder is being pressurised, a simple step input with time delay to represent delay in the pressure equalisation. Here the flow rate must be assumed to have the capacity to accommodate any requirements for filling the piston, which is quiet acceptable as the pistons have a comparatively small volume, in conjunction with the mechanism having a limited range of motion. The pressure equation is defined in equation 3.24 below:

$$P_{syn} = \begin{cases} P_{exh} & Idle \\ P_{in}\left(1 - e^{(1-t/\tau)\times 10^5}\right) & Engaged \end{cases} \tag{3.24}$$

This eliminates the requirement to model the on/off solenoids and valves, significantly simplifying the synchroniser hydraulic model. The hydraulic control unit is then modelled as two opposing hydraulic cylinders, with hydraulic system presented in Figure 3.21.

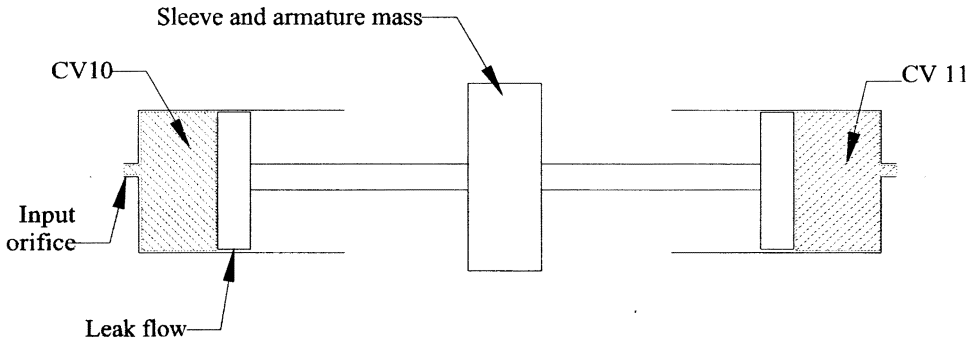

Figure 3.21: Hydraulic shift arrangement for typical DCT synchronisers

In the arrangement in Figure 3.21, the flow into each piston is determined using the orifice equation for sharp edged orifices. Here the orifice coefficient of discharge is combined with the density to form a constant and is assumed to be $4x10^4$ $mm^2s^{-1}N^{-1/2}$ as a result of the orifice geometry, hydraulic fluid and flow type [37]. Fluid flow into or out of each cylinder is directly related to the pressure change across these orifices. Thus the pressure drop is critical to determining the direction of flow for developing numerical solutions.

The pressure for both CV10 and CV11 is a function of input flow from the line pressure in the form of equation 3.24 through orifices, leakage out of the piston, and the rate of change of the control volume represented in equations 3.25 and 3.26.

$$P_{CV10} = \int \frac{\beta}{V_0 + dV} \left(\begin{matrix} C_D \pi \frac{D_{CV10}^{\ 2}}{4} \sqrt{P_{syn} - P_{CV10}} - A_{syn} \frac{dX_{syn}}{dt} \\ - C_D \pi D_S c_{rsyn} \sqrt{P_{CV10} - P_{Exh}} \end{matrix} \right) dt \tag{3.25}$$

$$P_{CV11} = \int \frac{\beta}{V_0 + dV} \begin{pmatrix} C_D \pi \frac{D_{CV11}^{\ 2}}{4} \sqrt{P_{syn} - P_{CV11}} + A_P \frac{dX_{syn}}{dt} \\ - C_D \pi D_S c_{rsyn} \sqrt{P_{CV11} - P_{Exh}} \end{pmatrix} dt \qquad (3.26)$$

The physical model of the synchroniser arm is affected by multiple nonlinearities as a result of its interaction with the synchroniser mechanism. Interacting forces derived from contact with the cone clutch and chamfer, as well as spring resistance and frictional damping forces are modelled as piecewise systems, (see chapter 4 for details). For now the model is as below:

$$\ddot{X} = \frac{1}{M_{SI}} \left(P_{CV10} A_P - P_{CV11} A_P - F_{RESISTANCE} \right) \qquad (3.27)$$

The combination of equations 3.25-3.27 provides a fourth order dynamic system with nonlinearities associated with the mechanical system that it is used for control.

Table 3.2: Synchroniser hydraulic system properties

Parameter	*Value*	*Parameter*	*Value*
M_S (kg)	0.5	$D_{CV\#}$ (mm)	3
A_P (mm^2)	31.416	C_r (mm)	0.01
V_0 (mm^3)	5000	-	-

3.7 MATLAB MODELLING AND INITIAL RESULTS

The hydraulic control system has been modelled in detail with the synchroniser in Matlab using the direct application of the classical fourth order Runge-Kutta method, and for demonstrative purposes, basic simulation results have been presented in the following section. As with the clutch model the bulk modulus and high degree of nonlinearity result in a numerically stiff system. The time step interval for calculations is set as 10^{-7}s.

Outputs from the synchroniser mechanism model in the form of speed and displacement responses are inputs required for determining flow rates in the piston models before the pressure rate change is determined and integration is performed as prescribed in equations 3.25 and 3.26. The response of the actuated cylinder is a result of the feed pressure applied through the orifice; this provides the force to move the synchroniser mechanism. The idle cylinder, however, is reactive; the movement of the assembly

alters the cylinder volume and hence pressure. This causes fluid flow out of this cylinder, and provides a resistive force to the engagement of the mechanism.

Simulation of this model requires the application of a complete synchroniser model as described in Chapter 4. Results in Figures 3.22 and 3.23 show the input pressure and pressure for both the active and idle cylinders. These responses are useful in determining how the system reacts to actuation, in particular the response of the idle cylinder, which provides significant resistance to the engagement of the mechanism.

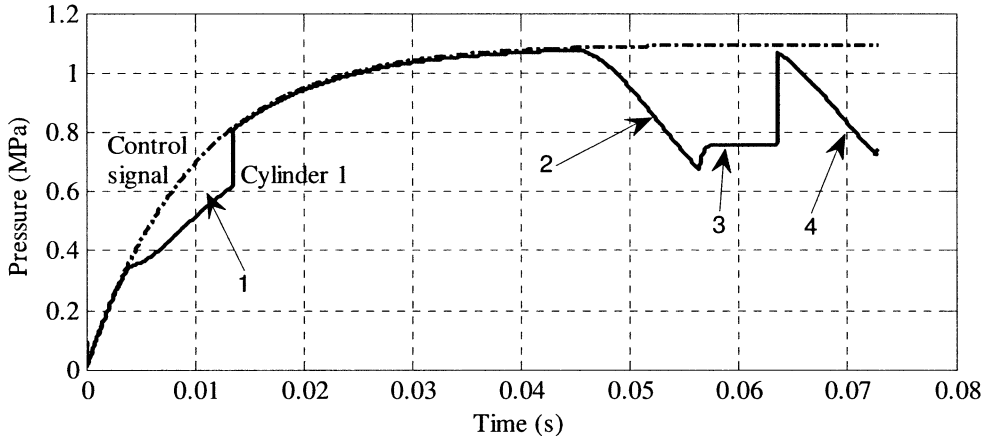

Figure 3.22: Solenoid output pressure and cylinder response pressure

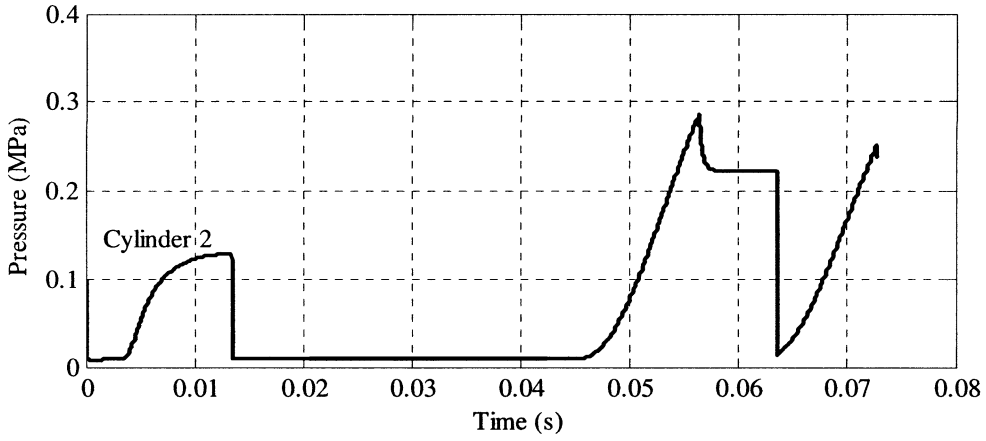

Figure 3.23: Idle cylinder response pressure

From the arrows highlighting particular hydraulic response characteristics in Figure 3.22, (1) is the initial displacement of sleeve to contact; cylinder pressure drops off below maximum, balanced by resistance forces and the pressure in cylinder 2. After contact this pressure rapidly equalises for cylinder 1 as speed synchronisation occurs. At (2) the unblocking of the synchroniser ring occurs, where displacement of the sleeve is constrained by the average torque in the cone clutch counteracting the chamfer torque, resulting in reactive pressures in both active and idle control cylinders. (3) demonstrates release of the sleeve at breakthrough and rebalance of forces as the sleeve

moves forward to contact with the hub chamfers. Similar to (2), (4) is the realignment of hub chamfers with sleeve to constrict its continued displacement.

An inevitable response to restriction of the idle cylinder from an orifice is that it is pressurised during rapid displacements of the synchroniser. Shown in Figure 3.23. Additionally pressure drops are experienced in the active cylinder as associated with the rapid expansion of control volume (see Figure 3.22). The impact of this is minimal as peak pressure is rapidly reattained once the displacement is halted. These results demonstrate the reactive nature of the hydraulic cylinders. These reactions are most notable during unblocking and hub indexing of the synchroniser mechanism, thus it is apparent that the idle cylinder is a impairment to the optimum operation of the synchroniser mechanism in its current state.

3.8 CHAPTER SUMMARY AND CONCLUSION

In this chapter classical physical modelling techniques have been used to develop models of hydraulic systems used for the actuation of a dual clutch transmission system for both clutch shift control and synchroniser engagement. Detailed development of each model and modelling techniques were presented, followed by simulations to demonstrate the actuation of these hydraulic systems. Results included basic operation of the hydraulic solenoid and the same solenoid combined with clutch piston, and hydraulic synchroniser control piston arrangement.

Characteristic curves for the clutch solenoid pressure responses and time delays were generated from a series of step inputs to demonstrate the response of the solenoid to particular inputs. The capacity to achieve the two required needs of the solenoid, high flow capacity in conjunction with accurate pressure control, was demonstrated. This is realised through the two operating ranges of the solenoid, where lower input currents provide pressure control and higher currents provide maximum flow for quick response. The most significant limitation of the solenoid valve is the extended settling times with input currents around 0.8 Amps, a consequence of the interaction of small delays in pressure equalisation and valve overlap.

The response of the solenoid and combined solenoid and clutch piston to both ramp and step inputs was used to demonstrate and identify specific operating characteristics. Observations on the valve nonlinearity in response to these inputs were made, and particular note should be taken of the force balancing on the spool, where the output

pressure must equalise the input magneto motive force before precise control of pressure is realised. This means that this valve in particular will be forced completely open with high flow demands and only throttle pressure once flow demand reduces and the spool is positioned correctly. This is significant for the rapid response of the solenoid to high flow demand conditions without having to modify the control signal.
There are several significant characteristics of the mechanism that provide some areas for improvement. Particularly:

- The capacity for the damper to provide significant isolation of pressure oscillations is limited by high damper pressure for the second input pressure.
- During fill and release transient times the limited flow capacity of the valve in conjunction with the design of spool force balance produces a period of reduced control as the clutch volume is filled. This is more dominant on release of the clutch as emptying times are relatively long, consideration of methods to reduce this duration should be made.
- Finally, the poor settling time at 0.8 Amps is realised from the overlapped nature of the valve, again the spool force balance inhibits ideal response.

The development of the two cylinder hydraulic system for actuation of the synchroniser mechanism was performed in this chapter and simulated using the synchroniser mechanism model developed in Chapter 4 and ideal solenoid response. Results demonstrate the influence of the idle cylinder on engagement, where rapid forward sleeve motion produces a high resistance force to engagement as fluid is forced out of the idle cylinder. This low compressibility of the fluid contributes significantly to both the idle pressure changes and rapid responses of the active cylinder when high resistances are reached. As detailed in later sections, this provides some indication of the double bump phenomenon detailed by Kim, *et al*, [63].
The primary limitation experienced by the application of this method is the use of the numerically stiff bulk modulus; this has required the application of classical fourth order Runge-Kutta methods using very small time steps of the order of 10^{-7}s.

3.8.1 Summary of contributions

This chapter detailed the development and simulation of the essential hydraulic components used for the actuation of the DCT. This includes both clutch and synchroniser control systems. Significant contributions from this chapter are:

- Modelling of the two component hydraulic control system for the dual clutch transmission,
- Identification of the operating characteristics of the modelled solenoid valve, particularly the high flow phase of operation and interaction of overlap and pressure response at points of lower stability, and
- Modelling and application of the two cylinder hydraulic system for engagement of highly nonlinear synchroniser mechanisms.

CHAPTER 4: SYNCHRONISER MECHANISM RIGID BODY MODELLING AND ANALYSIS

4.1 INTRODUCTION

Development of the DCT has been facilitated through the adoption of the synchroniser utilised for interlocking the gear targeted for shifting to its respective shaft. Synchronisation precedes clutch engagement. In conventional manuals the synchroniser is engaged with the clutch open and the target gear freewheeling in the transmission, but in the automated DCT the synchroniser is engaged without release of the currently engaged clutch. The introduction of the synchroniser into this new operating environment facilitates the need to model the actuation of the mechanism in detail as part of the DCT shift process and investigate engagement in this new environment.

A rigid body mechanism model of the synchroniser is developed from theory presented in well established literature. The application of several assumptions is required to develop a reasonable model of the mechanism, some of which are conventional for the synchroniser, while others are a result of the particular characteristics of the DCT. With this mechanism model the investigation of specific characteristics of the synchroniser will be possible, including modification of design parameters, influence of drag torque and different control methodologies.

This chapter is divided into four sections. Firstly important background information on the synchroniser mechanism is discussed to establish the actuation process and known characteristics for synchroniser engagement. This paves the way for the detailed rigid body modelling of the synchroniser mechanism, which is followed by simulations of the mechanism to establish operating characteristics. Finally, dimensionless torques are introduced for evaluating design torques in the synchroniser mechanism, with this evaluation backed by a parameter study of the synchroniser engagement.

4.2 BACKGROUND

The basic synchroniser design has been around as long as there has been the need to change gears in automobiles. The modern synchromesh synchroniser has developed

from long periods of development dating back to the 1930's. The principle of the mechanism is to first achieve speed matching of target gear through a cone clutch, and then interlock the target gear to the shaft using dog gears, referred to in this thesis as chamfers or chamfered splines. In modern transmissions with constant mesh gears only one synchroniser can be engaged at any one time, leading to traction losses when performing a conventional shift in manual transmissions. The application in DCTs is distinguished from conventional manuals by relying on two synchronisers being engaged for power-on shifting. Thus the application of the synchroniser has changed in this new transmission, with one of the two primary clutches engaged whilst the target synchroniser is actuated.

The most popular and prevalent synchroniser is known as the synchromesh. It utilises a cone clutch for speed synchronisation between gear and its respective shaft, and angled chamfers on both cone clutch ring and hub for indexing and interlocking the mechanism [49]. It is preferred in most MT and AMTs as well as the DCT for its high torque capacity, low cost, simple design, and ease of use [47]. Briefly, there are several other types of synchroniser available that are not considered herein. These include pin type synchronisers, which use pins in place of chamfers; multi-plate clutch types, used in place of the cone clutch, and Porsche-type synchronisers, which has a "brake" band that opens out to lock synchroniser mechanism. It is, nevertheless, the synchromesh synchroniser mechanism and its double and triple cone variants that are of interest to this work, primarily as a result of its prevalence over other available mechanisms.

Figure 2.3 presents the typical cross section for a synchroniser mechanism and its major components. These are:

1. Saddle – Rigidly connected to the shaft, it seats the moving components of the synchroniser, such as sleeve, thrust piece and detent. It is externally splined to mate with the sleeve and recesses provide locations for the thrust piece.
2. Sleeve – This is the driven component for actuation. Internal splines mate with the sleeve and spline ends are chamfered to engage ring and gear hub.
3. Detent and thrust piece – The detent provides location for the sleeve in the neutral position and resists initial engagement. The thrust piece pushes the ring forward during the initial displacement period before the ring engages the cone.
4. Ring – Contains the external half of a cone clutch and matching chamfered splines for engaging the sleeve. The torque balance on this component is critical to engagement success.

5. Gear hub – The gear hub contains the matching internal half of the cone clutch to engage the ring during synchronisation, and the final set of chamfered splines that match up with the sleeve during indexing. Overlap in these splines positively engages the gear to the sleeve and completes locking the gear to shaft.
6.

4.3 PROCESS DESCRIPTION

The process of synchronisation has many phases, depending on the author anything from 5 to 11 [47, 64], with different foci of each author resulting in the application of different number of phases for engagement. For the purpose of this thesis it will be broken down into the two primary phases and then again into additional sub-phases. The first phase is where the actual synchronisation occurs, it is generally called speed synchronisation or asynchronisation depending on the literature. Here the cone clutch is engaged by the axial translation of the sleeve and load is applied onto the ring to energise the cone clutch. The frictional engagement causes speed matching of the two halves so that the engine side of the synchroniser matches speed with the vehicle side. This is followed by the lockup of the two halves of the synchroniser, called indexing. This is where meshing of sleeve splines with ring chamfers and the hub chamfers occurs. Allowing positive locking of the gear to the sleeve and hence lay shaft, completing the engagement and enabling torque transfer. These two stages are divided into a total of 6 steps, with each step discussed below in greater detail. This is based on the work of [47, 60, and 64]:

Step 1: Initial displacement (Figure 4.1 (a)) – The engagement process is initiated, axial load builds on the sleeve as pressure increases in the hydraulic piston, the sleeve pushes against the detent which is forced down and breakthrough is achieved. The thrust piece via the ball pin is pushed onto the ring, and translation proceeds ahead of the sleeve. Viscous friction and initial contact in the cone clutch friction torque yields relative angular displacement in the ring, aligning chamfers with those on the sleeve such that the ring blocks sleeve motion

Step 2: Speed synchronisation (Figure 4.1 (b)) – The cone clutch is now energised and the freewheeling component speed is synchronised to the lay shaft speed. With ring in the blocking position, the sleeve load is transferred directly to the cone clutch in its entirety, and the thrust piece and ball pin move back to initial positions through the use of a compression spring. Once the cone clutch

completes synchronisation, torque is reduced in the mechanism and ring unblocking begins.

Step 3: Ring unblocking (Figure 4.1 (b)) – The internal splines on the sleeve can now move over the ring chamfers as a result of the chamfer torque exceeding drag torque on the target gear, rotating the ring to the neutral position.

Step 4: Second displacement (Figure 4.1 (c)) – The blocking torque has rotated the ring into the neutral position, and sleeve moves forward unimpeded until it comes in contact with the hub chamfers. During this stage the capacity for the cone to maintain synchronisation must be considered, with failure resulting in the regeneration of relative speed between sleeve and hub chamfers.

Step 5: Hub indexing (Figure 4.1 (c)) – Hub indexing phase begins with contact between sleeve and hub chamfers. Initial alignment is entirely random, resulting from the influence of many uncontrolled variables. A similar chamfer torque to the blocking torque is generated in the hub and target gear is aligned such that sleeve splines interlock with the hub splines to complete the engagement process.

Step 6: Completion (Figure 4.1 (d)) – With the splines fully meshed with the gear dog, positive locking occurs between the two sets of mesh teeth through deliberate undercutting of the two sets of teeth [47].

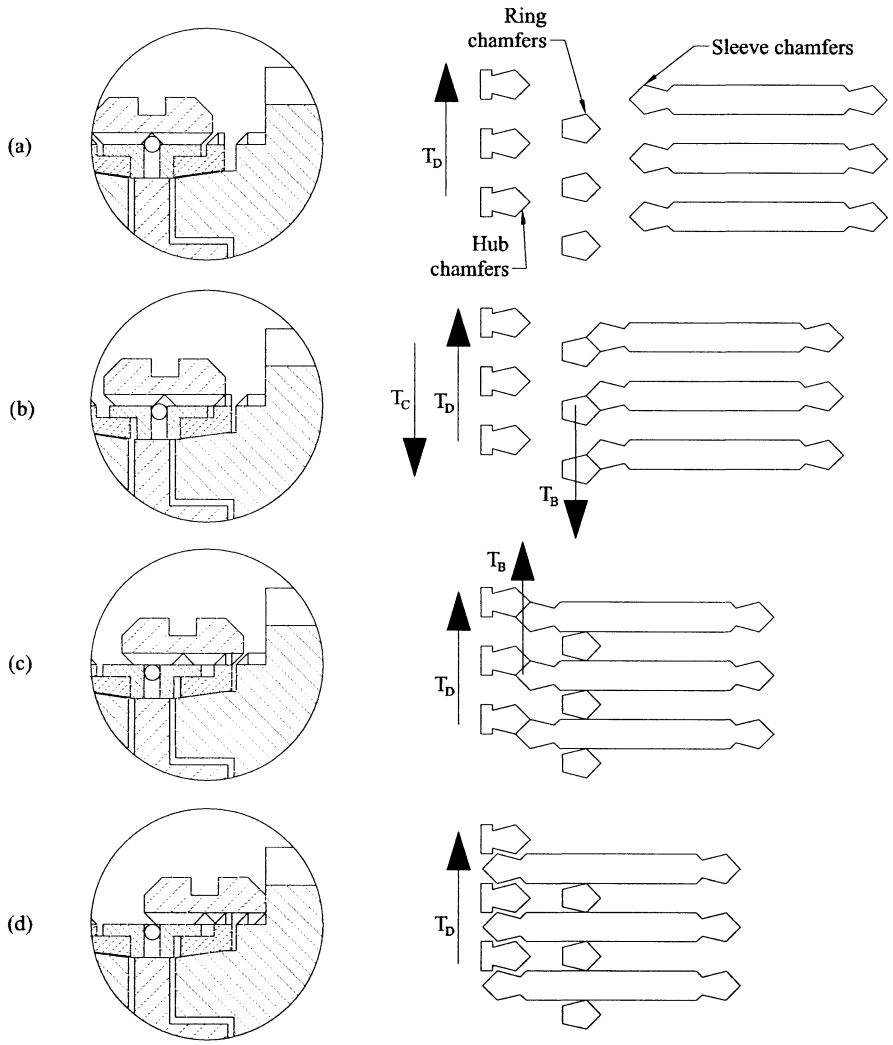

Figure 4.1: Steps of synchroniser engagement

4.3.1 Important considerations for synchronisers

4.3.1.1 Failure modes

The actuation of the synchroniser mechanism is highly reliant on the balance of different torques throughout the shift process. This is most notable in the relation between torques generated in the cone, indexing chamfers, and through drag torques generated in the freewheeling mechanism. Tolerance stacks and other factors also play a significant role in some failures, however these will not be considered herein as such failures can be eliminated through good design. Only failure modes relating to operational variables are considered.

- Block out – This failure mode is realised if drag torque exceeds cone torque during synchronisation, or post speed synchronisation when the drag torque exceeds the ring unblocking or indexing torques.

Subsequently the sleeve cannot realign the ring to allow it to pass through to the next stage of engagement.

- Clash – This process failure occurs when the indexing torque exceeds the cone torque during speed synchronisation, typically as a result of low cone torque generated from poor oil wiping. This is often realised as an audible noise generated from sleeve and hub chamfer coming into contact, and results in damage to hub or sleeve chamfers.
- Partial clash – Similar to clash in that it is a result of relative speed between sleeve and hub chamfers causing damage to the mechanism. However it is achieved through the mechanism de-synchronising after unblocking of the synchroniser ring. As such the impact energy is lower, however there is still the potential for there to be damage to chamfer tips.

4.3.1.2 Limitations to design parameters

Two critical limitations to cone and chamfer designs are friction lock of the cone and minimum chamfer angle to prevent block out. The friction locking of the synchroniser mechanism is critical to the successful function of the mechanism. If there is self locking it becomes difficult for the release of the cone during indexing of the hub, with the potential to result in block out failure of the mechanism. Refs [49, 137] provides the limit to the minimum cone torque as a function of the cone angle as being:

$$\mu_C < \tan \alpha \qquad (4.1)$$

For shallow cone angles typical to synchronisers $\tan \alpha \approx \alpha$ and $\sin \alpha \approx \alpha$. Therefore equation 4.1 can be modified to $\mu_C < \sin \alpha$. Seizure of the ring will prevent both realignment of the synchroniser during indexing, and disengagement of the mechanism when required, however it is common for designs to target $\sin \alpha = \mu_C$.

Obviously, and as implied by Lovas, *et al,* [64], error angles are designed into the synchroniser cone to ensure that there is some aspect of seizure prevention. This would suggest that it may be practicable to overcome this limitation. However when considering the detail provided by [47], notably the capacity for wear of different friction materials, it would be expected that, over time, uneven loading brought about by error angles will result in wearing of the mechanism such that friction seizure would again be likely over the transmission lifetime.

To design the chamfer angle to meet block out prevention requirements consider the interaction of cone and indexing/blocking torques. As detailed in Socin & Walters [49], by assuming that the chamfer friction is zero, thence maximising the chamfer torque, the minimum chamfer angle is designed thus:

$$\tan\beta \geq \frac{R_I \sin\alpha}{R_C \mu_C} \tag{4.2}$$

4.3.1.3 Multi-cone Synchronisers

A common variation to standard synchronisers is the multi-cone synchroniser, where multiple interlinked cones are used to multiply the friction generated in the cone clutch. The principle is not dissimilar to multi-plate clutches. A typical example of the synchronisation of triple cone synchroniser is presented by ref [50]. The two equations presented below should be considered with reference to the model development presented later in this chapter. Two separate versions were used, independent triple cone synchronisers and coupled triple cone synchronisers. The second version couples the first and third cones, and the second cone and hub as two separate halves of the mechanism, creating three friction surfaces, with two degrees of freedom. Generally used on low gears with high initial slip speed and drag torque, the synchronisation torque for the coupled synchroniser is then derived as:

$$\pm T_S = \frac{1}{I_{FW} + I_V}\left\{\frac{I_{FW} I_V \omega}{t_0} + T_C I_{FW} - T_D I_V\right\} \tag{4.3}$$

where T_S is synchronisation torque, I_V is vehicle inertia, I_{FW} is inertia of the freewheeling components, T_C cone torque, T_D drag torque, t_0 is time constant, and ω is relative cone speed. This equation defines the net torque on the target gear but cannot be used in this sense as the time constant "t_0" in particular is unknown. However, the initial solution provided for the cone torque can be utilised in the mechanism. That is:

$$T_C = F_A\left\{\frac{\mu_1 R_1}{\tan\alpha_1} + \frac{\mu_2 R_2}{\tan\alpha_2} + \frac{\mu_3 R_3}{\tan\alpha_3}\right\} \tag{4.4}$$

where F_A is net sleeve load, $\alpha_\#$ is cone angle, $R_\#$ is mean cone radius, $\mu_\#$ cone dynamic friction. In a similar manner equations for a coupled double cone synchroniser can be developed.

4.3.1.4 Cone friction coefficient and materials

There are a range of materials used as friction surfaces in typical synchroniser mechanisms. Traditional materials include brass with or without thin coated molybdenum on friction surfaces. More popular non-metallic linings now include paper based friction materials or carbon-fibre based linings [47]. It is suggested that paper and carbon fibre based linings are more desirable as they produce more stable friction coefficients under a wider range of operating conditions [138], but are limited by wear and degradation of friction surfaces. That being said the selection of friction coefficient component is limited by the very oil wiping process during initial displacement. This should be expanded to include both static and dynamic friction coefficients, to ensure ring release is possible under any circumstance. Nevertheless, further investigation of the friction material is likely only to lead to small improvements in synchroniser performance, as opposed to significant gains sought in this research.

4.4 DCT APPLICATION AND COMPARISON TO MANUAL TRANSMISSION

The application of synchronisers to DCTs alters the operating environment of the mechanism. The clutch is no longer released before engagement, drag torque is now derived from the slipping speed of the clutch as well as the absolute speed of gears, and the actuation process is performed with no driver feedback.

Synchroniser actuation in the DCT is performed as a pre-shift operation, where the mechanism is completely engaged prior to the initiation of shifting, with the engine still driving the wheels. The most important changes to the synchroniser mechanism when moving from any MT to DCTs are the change in control of the mechanism and the application of drag torque. Traditional actuation of the mechanism is through the driver applying a load through the leavers and linkages, as such forces peak as increased resistance is felt by the driver as suggested by refs [60, 63, and 64]. The synchroniser now is engaged using compact hydraulic actuators, and, as a consequence, is able to both provide a peak load to the engagement and respond more rapidly to changes in resistance. A large component of feedback is lost during engagement, where a driver observation in manual transmissions is now replaced by a limited closed loop system.

In Figure 4.2 the layout of the DCT is shown, highlighting the components that will be affected during synchronisation of fourth gear. Accordingly, with common primary

shafts, consideration of the impact of the synchroniser mechanism requires only the inclusion of the components between the target synchroniser and open clutch in the dynamic model. As such, for a fourth gear synchronisation simulation, this would only include the highlighted components detailed in Figure 4.2. Gears two and six, four separate bearings and clutch 2 contribute to reflected inertia of the mechanism as well as resultant drag torque from gears, bearings, clutch and shafts.

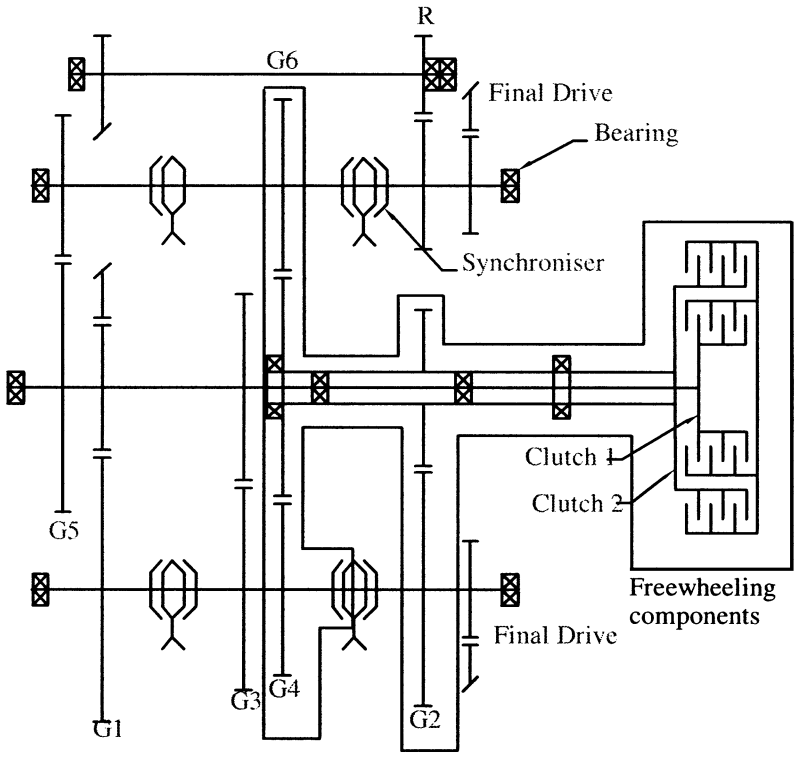

Figure 4.2: Typical transmission Layout for DCT, including synchronisers

The application of drag torque in manual transmissions is characterised by having both clutch release prior to synchronisation and unidirectional drag, where upshifts are aided by drag and downshifts are resisted. Given the application of the wet clutch to the DCT system, pre-shift engagement of a synchroniser results in maximum drag being realised after the synchronisation process, as peak differential speed is achieved here at the wet clutch. Additionally, the direction of drag torque is dependent on the engaged and target gear, as well as engine and gear speeds

4.5 MODEL DEVELOPMENT

The development of synchroniser mechanism model as applied to the DCT is performed through coding in the Matlab simulation environment. Each stage of the synchroniser modelling is detailed and discussed step by step in this section. There are several

assumptions that have been made here to simplify the modelling process. These include the structure of the mechanism, the constant vehicle speed over the synchronisation period, and the impact of temperature.

In literature such as M'Ewen [53], the vehicle inertia is included in the theory equations that are used to define the synchroniser mechanism. However it is well established that the synchroniser inertia is much less than that of the vehicle, or $I_V >> I_S$. It can therefore be expected that the impact of synchronisation on the vehicle is negligible, and vice versa. Unlike MTs the DCT also is capable of compensating for any loss of power in the vehicle during synchronisation as the engine is continuously driving the wheels prior to shifting. Therefore the synchroniser can be easily modelled by assuming that the components downstream of the sleeve are effectively grounding the mechanism. This results in a much simpler model of the mechanism, as shown in Figure **4.3**, with only sleeve, freewheeling velocities and freewheeling inertia considered:

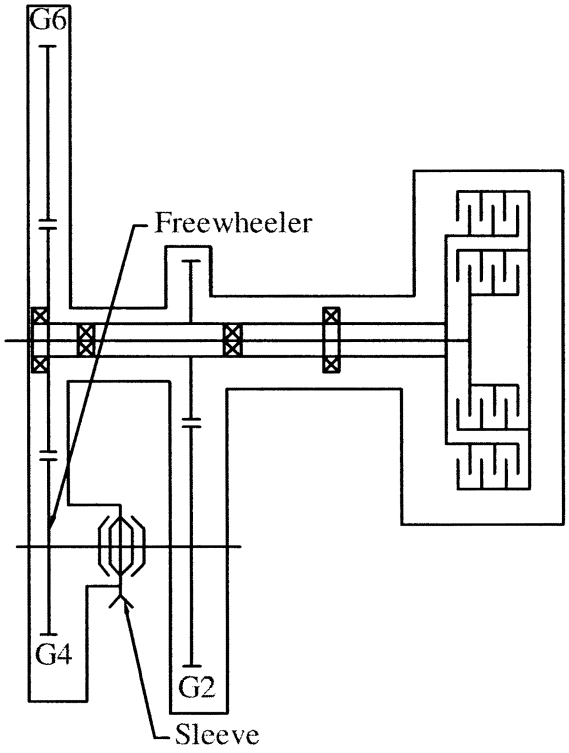

Figure 4.3: Simplified synchroniser model components for drag and inertia, studying 4th gear

In conjunction with the above assumption, it is necessary to assume that the speed of the vehicle is constant over the synchronisation period. Given that the entire engagement period is generally less than 100ms, this is quiet acceptable. As there is already one gear engaged in the transmission, the clutch speed will also be held constant. This will affect the total clutch drag in the system.

The influence of temperature on the process of synchronisation has two separate functions. Firstly, variation in local and absolute temperature has a significant effect on the magnitude of drag torques. Changenet & Velex [73] provide excellent demonstration on the impact of local temperature change on different drag torques. Indeed, improvements in accuracy of up to 5% are possible when including such variation in the model. For this case, however, the influence of temperature is ignored as such accuracy of the drag model is not noteworthy without experimental validation. The second influence is on the wear and damage to the synchroniser cone clutch, where overheating of the clutch will cause permanent damage to the friction surfaces. Again, as these effects are not of interest to this research, they will be excluded.

Step 1: Initial Displacement to Contact and Ring Blocking

In the initial phase of the synchronisation process the sleeve moves from the neutral position to engage the hub. Here the ring is pushed in advance of the sleeve to friction contact the cone clutch hub. In doing so it must first overcome the detent load, used to maintain the disengaged sleeve in a neutral position. During this time the target gear will freewheel at a speed that minimises net drag torque for any given transmission sped. As the sleeve loads the ring onto the hub, however, two fluid phenomena are encountered. First, the cone must load up the lubricant film and wipe it off the cone surface, and second, the film generates a viscous friction contact between ring and hub. This initiates the speed synchronisation process, and begins rotating the ring into the blocking position.

The equation of motion that describes the sleeves motion is:

$$m_{S+R}\ddot{x}_S = P_{CV10}A_P - P_{CV11}A_P - F_{DETENT} - F_{FILM} - F_{LOSS} \qquad (4.5)$$

where m_{S+R} is sleeve and ring mass, and F_{LOSS} is seel drag losses The hydraulic actuation forces are calculated as the cylinder pressure multiplied by the piston head area, using the detailed model of the hydraulic system presented previously in Chapter 3. The detent force is calculated as the break through load described in ref [51]:

$$F_{DETENT} = 3F_R \frac{\mu_{DETENT} + \tan\theta_D}{1 - \mu_{DETENT}\tan\theta_D} \qquad (4.6)$$

where F_{DETENT} is detent force, F_R is radial force, θ_D is detent contact angle, μ_{DETENT} is detent friction coefficient.

The force required to break down the film is [67]:

$$F_{FILM} = 16K_{GR}\pi\mu\dot{X}\sin^2\alpha R_m\left(\frac{b}{h(t)}\right)^3 \tag{4.7}$$

where F_{FILM} is film squeezing force, K_{GR} is groove coefficient, μ transmission fluid viscosity, b is semi-width of the contact generatrix in the cone [66], R_m is cone mean radius, $\dot{X}$ is sleeve velocity, and h is film thickness. If there are no grooves [67]:

$$K_{GR} = 1 \tag{4.8}$$

Or, for circumferentially grooved cones [67]:

$$K_{GR} = \frac{1}{n^2}\left[1+(1-n)\frac{a}{b}\right]^3 \tag{4.9}$$

where a is grooved width, and n is number of grooves. In this instance the minimum film thickness is taken from Paffoni, *et al,* [67] and Hamrock [139], and the force required to achieve this film thickness is compared to the maximum force generated and a determination of wiping is made. The minimum film thickness is ([139]):

$$h_{\min} \geq \Lambda\sqrt{R_R^2 + R_H^2} \tag{4.10}$$

where Λ is empirical constant that is dependent on the lubrication case ($1>\Lambda>5$) , R_R is RMS roughness of the ring, and R_H is RMS roughness of the hub. It is assumed that both surfaces are ground finished with RMS of 0.4μm and Λ=5. Additional forces that make up the losses in the system include drag of seals in the hydraulic system and friction losses in the mechanism. These generic losses are included in the F_{LOSS} parameter as a single value, dependent on load in the system.

With the displacement of the sleeve defined, the motion of the ring must now be modelled. First of all it can be assumed that the ring is pushed ahead of the sleeve. This is a result of the thrust piece being pushed by the sleeve to maintain a gap between ring and sleeve chamfers. As it moves to contact the hub, the oil on the cone surfaces creates viscous shear if there is a relative speed between the two contact surfaces, as is typically the case. This viscous torque the rotational displacement of the ring to the blocking position can be modelled. The only acting torque on it is that generated by viscous cone contact. The ring's equation of motion is thus:

$$I_R\ddot{\theta}_R = -T_C \tag{4.11}$$

where I_R is inertia of the ring, and $\ddot{\theta}_R$ is ring acceleration.

The integration of this equation leads to the calculation of the rings rotation to the blocking position, restricted by either the strut contact or chamfer engagement. The limit of its rotation from the neutral position, where it can move clockwise or counter clockwise, depending on the direction of torque, is:

$$\delta = \frac{\pi}{N_{CH}} \tag{4.12}$$

where δ is angular displacement between consecutive chamfers, and N_{CH} is number of chamfers on one ring. It is important to note here that the rotation of the ring is its relative motion compared to the sleeve chamfers. Thus the acceleration and rotation of the ring calculated here are only relative to the sleeve. The viscous contact torque in the cone clutch prior to full contact is described by Paffoni, Progri & Gras [66] as being:

$$T_C = 4\pi\mu R_C^3 b\frac{\dot{\theta}_S}{h} \tag{4.13}$$

where R_C is mean cone radius $\dot{\theta}_S$ and is cone relative speed. Similar to the ring, the hub and freewheeling components are affected by the viscous friction, but in the impact of drag torque must also be considered. The details of drag torque model are presented in Chapter 5 in detail, and a general loss term will be used here as T_D. Thus, the dynamic equation of motion of the freewheeling mechanism is:

$$I_{FW}\ddot{\theta}_{FW} = T_C + T_D \tag{4.14}$$

where $\ddot{\theta}_{FW}$ is freewheeling component acceleration. Equations 4.5, 4.11, and 4.14 define the dynamic state of the simplified synchroniser model for rigid body analysis up to the point of friction contact of the ring with the hub.

Step 2: Speed synchronisation

During the process of synchronisation the primary consideration is the matching of speeds between freewheeling components and the sleeve and shaft. Critical consideration must be given to the torques acting on the ring to ensure continued blocking of the sleeve, as it prevents the continued displacement of the sleeve during and after speeds are synchronised. The synchronisation of the freewheeling components

is a function of inertia and torques affecting these components. Therefore the equation of motion can be written for the freewheeling inertia as being:

$$I_{FW}\ddot{\theta}_{FW} = T_C + T_D \tag{4.15}$$

In Step 1 the cone torque was a function of viscous shear; it is now dry friction contact between ring and hub, with friction torque then a function of cone angle, friction coefficient and load. The piecewise model of the cone torque, including viscous contact torque is limited by the displacement of the sleeve and slipping speed of the cone. This is defined as:

$$T_C = \begin{cases} 4\pi\mu R_C^3 b\dfrac{\dot{\theta}_S}{h} & x_S < 2 \\ \dfrac{\mu_D F_A R_C}{\sin\alpha} & x_S \geq 2, \dot{\theta} \neq 0 \\ T_D + I_{FW}\ddot{\theta}_{FW} & x_S \geq 2, \dot{\theta} = 0 \\ \dfrac{\mu_{C,S} F_A R_C}{\sin\alpha} & x_S \geq 2, \dot{\theta} = 0, T_D > T_C \end{cases} \tag{4.16}$$

where μ_C is cone dynamic friction, $\mu_{C,S}$ is cone static friction, and x_S is sleeve displacement. Equation 4.16 consists of viscous cone torque below X=2mm; beyond this point is the friction contact phase. The piecewise model consists of dynamic friction torque if there is slip in the cone, and average static friction torque limited by the static friction coefficient.

The piecewise model of cone torque states that during the non contact region, X<2mm, there is viscous contact in the cone, with X>2mm there is dry friction in the cone until slip speed reaches zero. With the cone locked, torque is then the average drag torque and acceleration of the freewheeling components. This is limited by the final element of the model, the static friction of the closed cone clutch.

Step 3: Ring unblocking

In the blocking position, the ring prevents the displacement of the sleeve while the cone torque exceeds blocking torque and the ring cannot realign to the neutral position. The general equation for the blocking torque is defined below, as:

$$T_B = F_A R_I \frac{1-\mu_I \tan\beta}{\mu_I + \tan\beta} \tag{4.17}$$

where R_I is pitch radius of chamfers, T_B is blocking torque, μ_I is chamfer friction coefficient, and β is chamfer angle. However it is necessary for the ring to be rotated back to the neutral position and allow the continued displacement of the sleeve. Thus, for the ring to be maintained in the blocking position, consider a free body diagram of the ring, as in Figure 4.4 below:

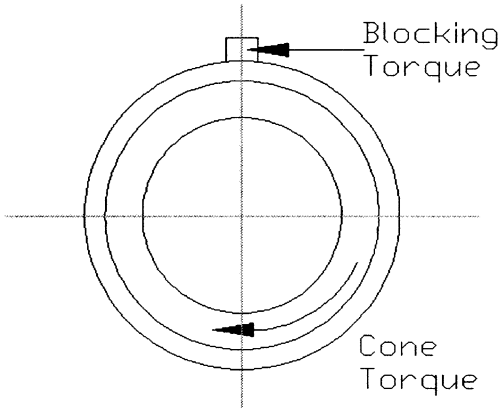

Figure 4.4: Ring free body diagram during speed synchronisation

By summing the torque for the ring and with the assumption that the ring is in the blocking position, to maintain this balance in the blocking position the resulting inequality is:

$$T_B \leq T_C \tag{4.18}$$

Unblocking of the ring will occur if equation 4.18 fails. This is generally a result of successful synchronisation in the piecewise cone torque model, where the cone torque reverts to being a function of drag torque alone. From equation 4.16 it is obvious that with normal process actuation once synchronisation is complete, the torque load in the cone clutch is now equal to the drag torque and any acceleration of the target gear, facilitating the unblocking of the ring; with ring and freewheeling components moving in unison. The equation of motion then becomes:

$$(I_{FW}+I_R)\ddot{\theta}_{FW}=T_B+T_D \tag{4.19}$$

In this context, the magnitude of both drag and blocking torques becomes critical. If both torques are acting in the same direction, or if the drag torque is less than that generated in the blocking chamfers then the sleeve can move through the chamfers and unblock the ring. Or, more succinctly:

$$T_B > T_C \tag{4.20}$$

According to equation 4.20 during ring unblocking the resistance to sleeve displacement reduces, with decreased load the sleeve can now move forward, constrained by the realignment of ring and target gear. Thus the sleeve displacement is controlled by the unblocking of the mechanism, and the dynamic equation of motion is:

$$m_S \ddot{x}_S = P_{CV10} A_P - P_{CV11} A_P - \frac{\tan\beta\left(T_D + (I_{FW} + I_R)\ddot{\theta}_{FW}\right)}{R_I} - F_{LOSS} \qquad (4.21)$$

The result of equations 4.14 to 4.16 is successful operation of the speed matching phase of synchronisation, with the cone and drag torque combining to accelerate freewheeling components, and the target gear will match the speed of the lay shaft. The unblocking of the ring is again a consideration of equations 4.17 to 4.21 The complex relationship between these equations of motion makes it necessary to model these phases, combined into a single grouped stage of the actuation of the synchroniser mechanism, where blocking and cone lock up algorithms continually check torque balances. At the completion of ring unblocking the ring is aligned in the neutral position and the sleeve can now move freely forward to engage the hub chamfers.

Step 4: Second displacement

In the post-speed synchronisation of the freewheeling components the sleeve proceeds to move to contact with the hub and index the gear, achieving locking of the synchroniser mechanism. Before it reaches this point, consider the forces acting on the sleeve, including hydraulic loads, from cylinders losses from seal drag, and the sliding of the sleeve over the ring. This friction force potentially plays a significant role in the maintaining cone lock. The continued engagement of the sleeve is calculated as:

$$m_S \ddot{x}_S = P_{CV10} A_P - P_{CV11} A_P - \frac{\mu_R T_D}{R_I} - F_{LOSS} \qquad (4.22)$$

During this phase of the engagement process particular attention must be paid to the continued engagement of the cone clutch. Of importance is if the cone clutch maintains locking during this phase. Using the piecewise model in equation 4.16 it is assumed that reduction in cone torque or increase in drag will disengage the cone. With the ring trapped by the sleeve in the neutral position there is no load directed on to the cone via the sleeve. At a very basic level the only axial force applied to the ring is the sliding of

the sleeve, resulting in the reaction friction force to that proposed in equation 4.23. Thus the cone torque is:

$$T_{CONE} = \frac{\mu_R T_{DRAG}}{R_I} \times \frac{\mu_{C,S} R_C}{\sin\alpha} \tag{4.23}$$

This results in a noteworthy variation to the torque balance that can result in the regeneration of slip in the cone clutch, and subsequent partial clash of the mechanism. The two torques acting on the freewheeling components are drag and cone torques, and if the drag torque is greater than the cone torque described in equation (4.23) then there will be the development of slip in the mechanism. Or to maintain synchronisation:

$$T_D \leq T_C \tag{4.24}$$

These two alternate solutions to the continued preservation of synchronisation in the clutch lead to two different results. If the freewheeling components de-synchronise then the equation of motion must be determined using equation 4.15 with cone torque supplemented by equation 4.23. Alternatively engagement proceeds without slip in the cone clutch. Either way step 4 ends with contact between sleeve and hub chamfers, thus bringing about indexing of the hub.

Step 5: Indexing

The process of indexing is not dissimilar to the unblocking of the ring, however there is more variation in initial conditions than for step 3. From the previous section the relative velocities of sleeve and hub are determined for rotating velocity and axial translation of the sleeve. The initial sleeve displacement at the point of contact is defined from the alignment of hub and sleeve chamfers. In general, the initial alignment of these chamfers prior to indexing is impossible to determine, with repeated shifting and realignment of chamfers being impractical to reasonably trace, and the introduction of uncertain variables such as drag torque in conjunction with well established torques does little to aid determination of alignment change. Furthermore, tiny variations in temperature, drag, and other variables including vehicle incline, cornering, *et cetera*, lead to a non-repeatable process in translation from physical experimentation to numerical simulation. Thus the initial alignment can be either preset in the simulation or generated with a pseudo-random number. From these initial alignment and speed conditions the indexing of the hub and the concurrent translation of sleeve can be

determined. Most benefit is realised by choosing the chamfer alignment at the beginning of this step, so that results can easily be observed with respect to known initial conditions.

Figure **4.5** provides four typical scenarios for the engagement of the synchroniser mechanism. For instances of engagement presented in Figure 4.5 (b) and (c), where the sleeve motion and thus relative rotation are negative, the friction force is altered to the reverse direction in the chamfers. Ideally all alignments should be like Figure 4.5 (a) with the chamfer now able to directly interlock. If the slip speed opposes the torque, as in Figure 4.5 (b), the chamfer torque must first brake the mechanism before it is possible to actively engage the chamfers. Also desirable is Figure 4.5 (c), with chamfers torque aided by the relative speed, enabling successful engagement. For tip-on-tip engagement the sleeve must wait for slip speed and drag torque to realign the mechanism. Obviously conditions in Figure 4.5 (b) and (d) will both contribute to the delay in mechanism engagement, with refd [60, 65] both demonstrating these results. This is particularly true for Figure 4.5 (b) where significant delay in engagement may result from slip speed resisting the chamfer engagement.

By combining the direction of motion with the contact flank, see Figure 4.6 for examples of flank contact, a piecewise model of indexing torque can be derived as:

$$T_I = \begin{cases} F_A R_I \dfrac{1-\mu_I \tan\beta}{\mu_I + \tan\beta} & \lambda + ve, \dot{x} + ve \\ F_A R_I \dfrac{1+\mu_I \tan\beta}{\mu_I - \tan\beta} & \lambda + ve, \dot{x} - ve \\ -F_A R_I \dfrac{1+\mu_I \tan\beta}{\mu_I - \tan\beta} & \lambda - ve, \dot{x} + ve \\ -F_A R_I \dfrac{1-\mu_I \tan\beta}{\mu_I + \tan\beta} & \lambda - ve, \dot{x} - ve \end{cases} \tag{4.25}$$

where λ is chamfer flank contact, and T_I and indexing torque. Within the mechanism the ring has been enclosed in the sleeve and essentially cannot move, thus it is excluded from the model at this point. However, there still is the case of sliding of sleeve over ring as it pushes the hub to the indexed position, resulting in the generation of some minor of cone torque as described by equation 4.23. The equation of motion of the target gear as it is indexed is then:

$$I_{FW}\ddot{\theta}_{FW} = T_I + T_C + T_D \tag{4.26}$$

The indexing of the hub is essentially identical to ring unblocking, however with the ring enclosed in the sleeve it is excluded from the inertia. The force balance thus includes hydraulic pressure, resistance from drag and freewheeling components, and the losses. i.e.:

$$m_S \ddot{x}_S = P_{CV10} A_P - P_{CV11} A_P - \frac{\tan\beta\left(T_D + I_{FR}\ddot{\theta}_{FW}\right)}{R_I} - F_{LOSS} \qquad (4.27)$$

where m_s is sleeve mass. Once the sleeve has pushed through the chamfers, the mechanism locks via sleeve splines and hub chamfers overlapping. The sleeve will move forward without any restrictions to engagement, and is ignored from the modelling section.

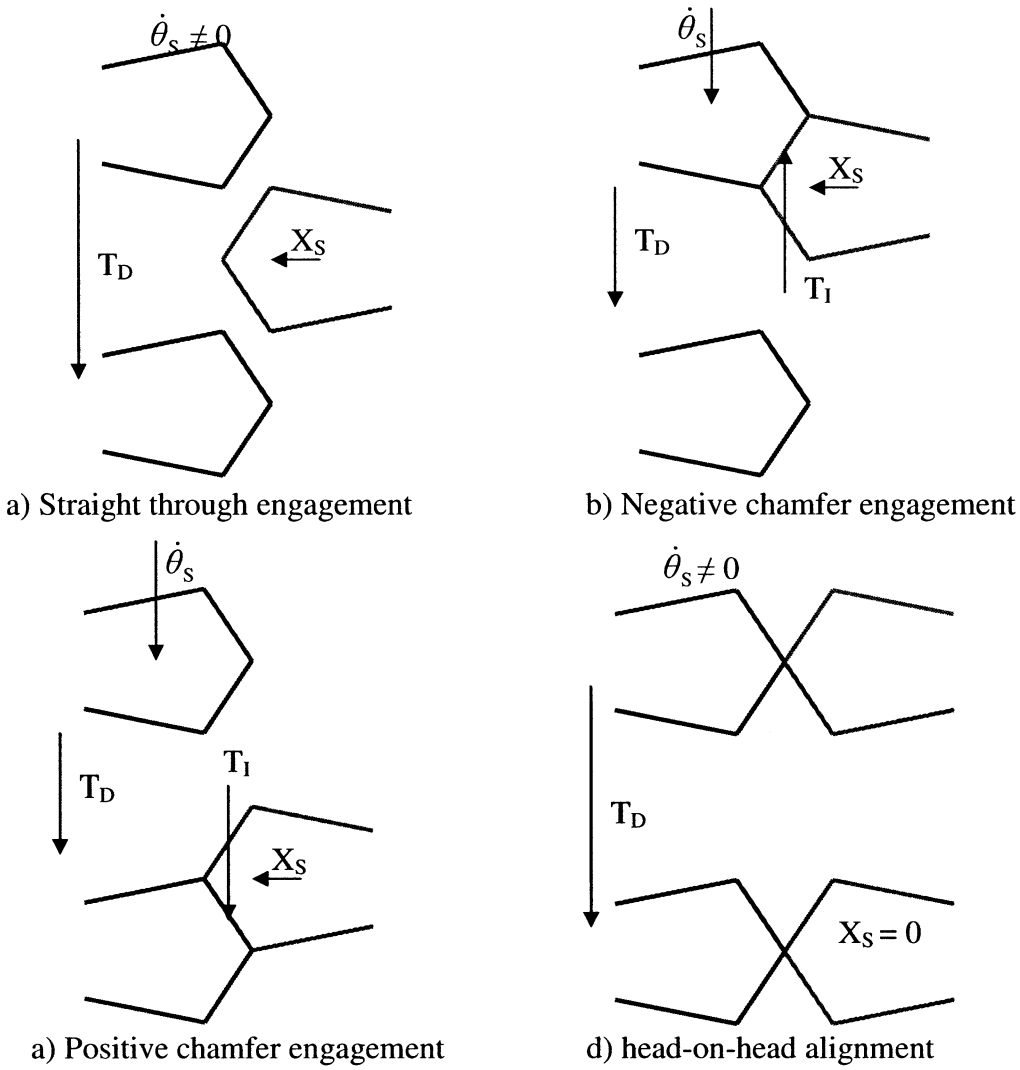

Figure 4.5: Possible variations in chamfer alignment

The contact force and kinematic diagrams are presented in Figure 4.6 for the four different flank contact possibilities considering the different slip speeds in the mechanisms. If indexing is dominant, that is, the resulting torque is in the same direction as the slip speed, then the engagement moves forward. If the reverse is true then the sleeve can be forced backwards.

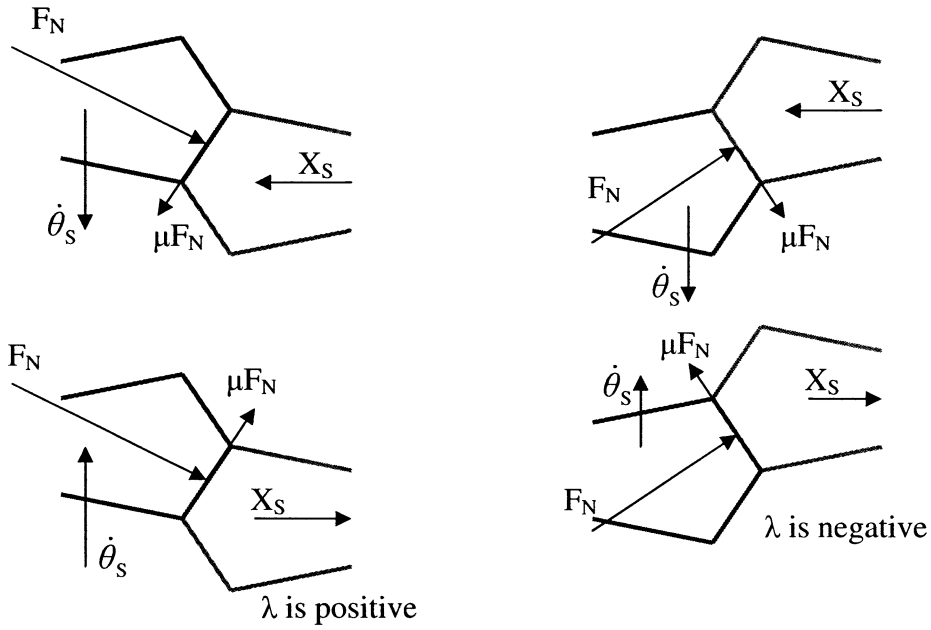

Figure 4.6: Resultant forces on the chamfers

To summarise the displacement of the sleeve, and the consideration of different torques and forces acting on the mechanism different torques, forces, and inequalities are grouped in Figure 4.7. Above the line are steps under consideration. Below the line are the torques and forces that play critical roles in ensuring the completion of goals for each phase of engagement.

Detent loading, Sleeve displacement to cone,	Ring blocking, synchronisation of target gear,	Displacement of sleeve to hub chamfers, Cone lock	Indexing of hub chamfers to lockup of target gear
F_{BTL}	T_C	$F_{S1,2}$	$F_{S1,2}$
F_{Film}	$F_{S1,2}$	T_D	T_D
$T_{C,V}$	T_D	T_C	T_I
$F_{S1,2}$	T_I	$T_C > T_D$	

Figure 4.7: Synchronisation process modelling summary

4.5.1 Model Parameters and initial conditions

The synchroniser mechanism parameters used for the following simulations are tabulated below. For the multi-cone synchronisers for gears 1 and 2 the cone angle and radius should be taken as the total of the three friction surfaces. For first gear in particular a larger pitch radius must be used for the chamfers, to counter high drag torque developed at the end of speed synchronisation.

Table 4.1: Synchroniser model parameters

Gear	*1st*	*2nd*	*3rd*	*4th*	*5th*	*6th*
Inertia (kg-m^2)	0.071	0.028	0.014	0.009	0.009	0.007
Gear ratio	3.45	2.05	1.45	1.08	1.11	0.92
Cone angle (°)	7					
Cone radius (mm)	47.5					
Cone friction coefficient	0.12					
Number of cones	3	3	1	1	1	1
Chamfer angle (°)	50	50	55	55	55	55
Chamfer radius (mm)	95	60	60	60	60	60
Chamfer friction coefficient	0.04					

The combination of standard drag torques found in a transmission and wet clutch drag results in the disengaged freewheeling gears rapidly reaching steady state speeds while idling. To determine the initial speeds of target gears, simulations of freewheeling analysis for target upshifts and target downshifts are run. Here the target gear is allowed to freewheel and the drag torques and cone shear come to equilibrium. The steady state speed of the sleeve is constant speed at 1500RPM or approximately 157 rad/s. Reference speeds are tabulated below:

Table 4.2: Steady state gear speeds for engaged speed of 1500RPM (157.1 rad/s)

Gear	*1st*	*2nd*	*3rd*	*4th*	*5th*	*6th*
Upshift speed (rad/s)	-	280	233	224	208	202
Downshift speed (rad/s)	103	123	127	137	138	-

4.6 NUMERICAL SIMULATIONS

This section is devoted simulations of synchroniser engagement using the model developed in this chapter, in conjunction with the hydraulic system model developed in Chapter 3 and the drag torque model developed in Chapter 5. It is divided into three subsections covering basic engagement simulation for demonstrative purposes, the influence of general environmental variables such as particular gear synchronisations, vehicle speed variation, and different operating temperatures. In the final subsections dimensionless torque evaluation of cone and chamfer torques are presented and a parameter study is performed for these design variables, to evaluate respective influences. The variability of gear synchronisation is a result of internal parameters such as gear and mechanism parameters and choice of up or down shift, or the vehicle speed during shifting, alignment of indexing chamfers, and even the operating temperature and nominal operating pressure of the transmission. In following sections simulations of all these variables is conducted to ascertain the time dependency of different engagement conditions. This will aid in the understanding of how precisely the engagement time can be predicted.

4.6.1 Basic simulations

The first simulation performed will be used to demonstrate the engagement of the synchroniser mechanism, such that the description of the process (section 4.3) should be considered with reference to these results. The target gear is 4^{th} with 3^{rd} gear currently engaged in the transmission. The sleeve speed is set to 1500RPM, an equivalent engine speed of about 2200RPM.

The individual steps of engagement are indicated in Figure **4.8** (c), demonstrating the control cylinder pressures. Figure 4.8 (a) and (b) represent the cone slip speed and sleeve displacement, respectively. The cylinder pressure in particular represents the response of the hydraulic system to the nonlinear contact model. Results are reflective of the described process for each stage and indicate the response of the hydraulic system to the demands of actuation. During the initial displacement to contact, Step 1, the pressure rises to counter the oil squeezing, detent, and friction loads and slides forward to energise the cone clutch as the sleeve loads up the ring. The forward motion reduces the rate of pressure increase as the cylinder expands prior to contact indicating that throttling in the orifice restricts engagement. During ring blocking and synchronisation,

Step 2, pressurisation continues in line with the solenoid output with no sleeve motion, but during ring unblocking, Step 3, as the sleeve moves forwards again, pressure begins to drop, limited by resistance load from the ring. This indicates that the solenoid orifice provides limited flow below that required. From here the second unrestrained displacement occurs, Step 4, and the sleeve pushes forward with limited resistance until there is contact with the hub chamfers. Pressure increases rapidly at the contact point and then decreases as the chamfers are realigned and the cylinder expands, Step 5, until it finally reaches the fully displaced position.

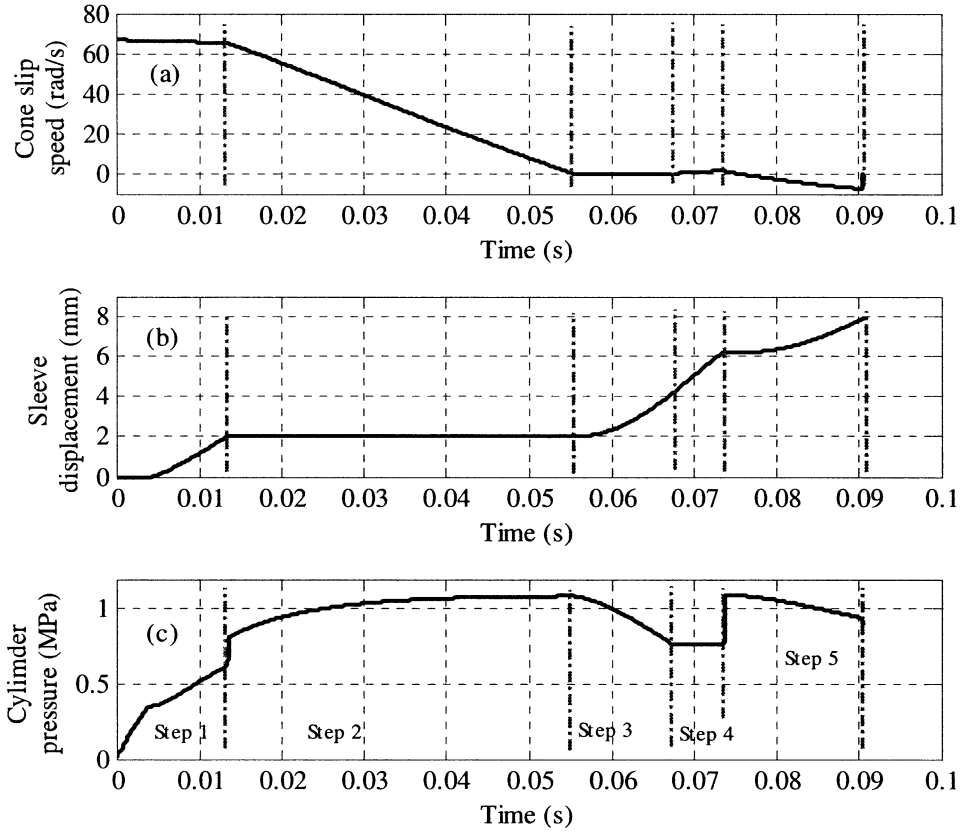

Figure 4.8: Synchronisation process breakdown, showing cone slip speed (top), sleeve displacement (middle), and hydraulic pressure (bottom)

Two obvious bump phases linked to the process engagement are observed. First, at the beginning of the ring blocking and synchronisation stage, where a step increase to hydraulic pressure is observed from contact between sleeve and ring chamfers resulting in rapid halting of the sleeve's motion. The second when a similar contact event occurs as the sleeve engages the hub chamfers for hub indexing, again resulting in restriction of sleeve motion. These two step changes are consistent with the "double bump" phenomenon or "second load" discussed by refs [57, 63], with the study of synchroniser engagement in manual transmissions, suggesting that the phenomenon is a result of

abrupt halting of the sleeve rather than peak loading as the driver increases force on the gear lever.

The variation in cone speed, Figure 4.8 (a), shows the freewheeling target gear begin at its steady state condition, above the target speed for an upshift, as the cone is engaged speeds synchroniser rapidly and synchronisation is maintained during unblocking of the ring. Beyond this point there is no load on the cone and a small amount of slip is reintroduced into the cone. Recovering this slip is performed by the chamfers and results in slowed indexing of the mechanism. Figure 4.8 (b) shows the sleeve move backwards as the relative speed is reduced by chamfers at the beginning of indexing.

4.6.2 Up and down shift synchronisations for all gears

In this section a series of upshifts and downshifts have been simulated to demonstrate typical results for each gear using the steady state conditions in Table 4.2 and parameters from Table 4.1. Sleeve speed is set at a constant speed of 1500RPM and the target gear is set at its steady state speed for up or down shift and engagement is simulated with an actuation pressure of 1.1MPa.

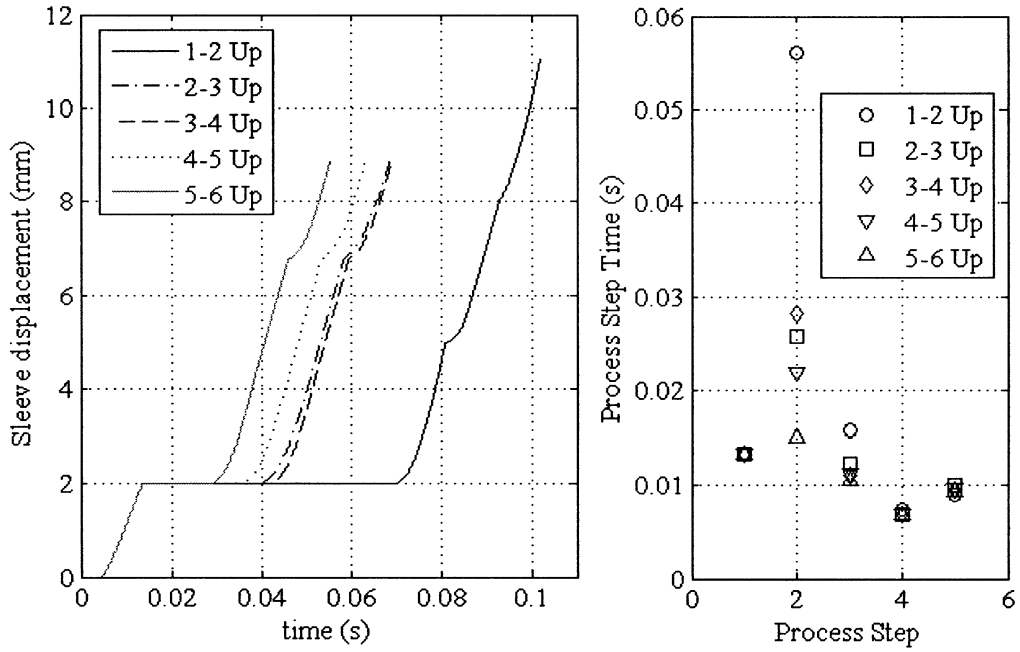

Figure 4.9: Up shift synchroniser engagement simulations for all gears, (left) sleeve displacement of gears 2-6 with sleeve speed of 1500RPM, (right) duration for each step

The synchronisation of each gear for a typical upshift is demonstrated in Figure 4.9 with the duration of engagement shown for reference. Each of the engagements is

reasonably fast, lasting less than 70ms for all but 2nd gear. For this gear speed synchronisation is much higher than for other gears with a larger speed differential and high drag torque, both resulting from the higher reduction ratio in the gear.

The two displacement Steps, 1 and 4, are very consistent; this is also the case with indexing. However, unlike displacement steps, indexing is governed by different values for indexing and drag torque depending on the gear, thus a slight variation in the duration. Both synchronisation, Step 2, and ring unblocking are variable, with the former being more so than the latter. While Step 2 is dependent on initial slip speed and local drag torque variation, unblocking is more dependent on drag torque generated.

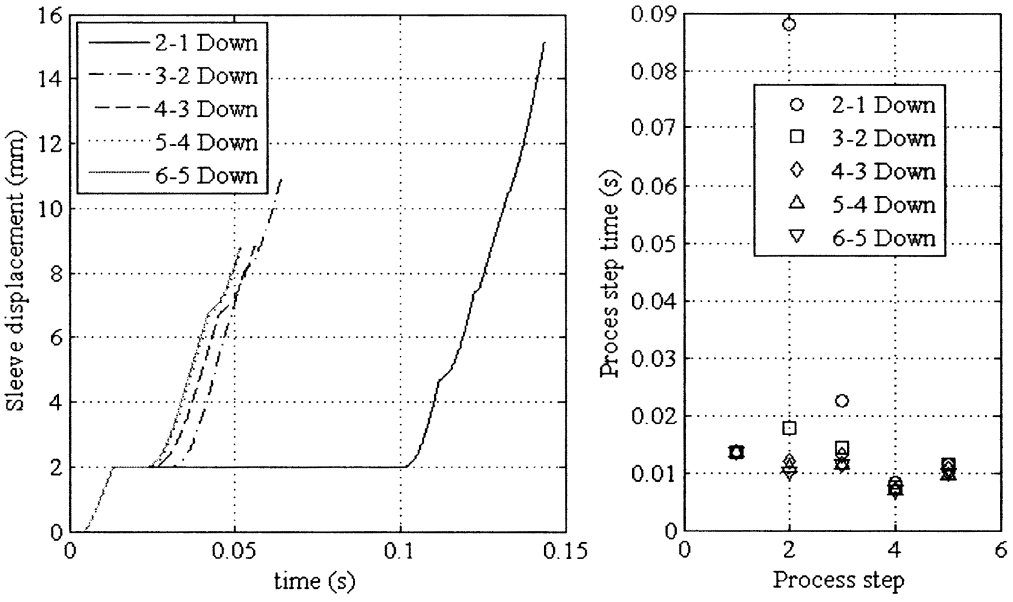

Figure 4.10: Sleeve displacement for downshifts of gears 1-5 with sleeve speed of 1500RPM

Comparing the downshift results in Figure 4.10, again the duration of the entire process occurs in less than 70ms for most cases, however the lowest gear shift again being significantly longer engagement periods. This is a result of the higher drag torque produced from the increasing differential speed at the clutch acting in conjunction with the high initial differential speed; the use of triple cone synchronisers in first and second gears is insufficient to reduce the duration further. Therefore variation in engagement time is a result of the variation in initial slip speed for each gear and the drag torque produced. Different gear inertia should be considered secondary to these influences.

4.6.3 Variation of chamfer alignment

These next simulations use a 3rd to 4th gear upshift, specifically targeting the variation in alignment of sleeve and hub chamfers at the beginning of indexing. Given the random nature of alignment variation predefining the alignment can be used to demonstrate the significance of engagement results. Simulations performed are for a 4th gear upshift synchronisation with 3rd gear engaged, With the range of alignment, δ, (equation 4.12) in one sixth fractions between 0 and δ are performed. Note θ_H is chamfer alignment.

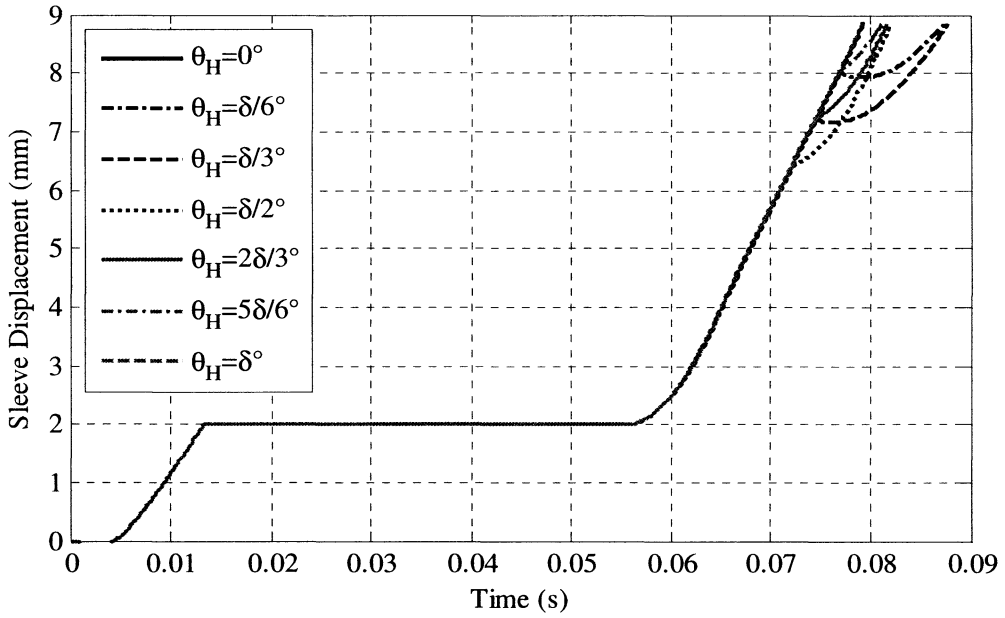

Figure 4.11: Demonstration of variation associated with chamfer alignment

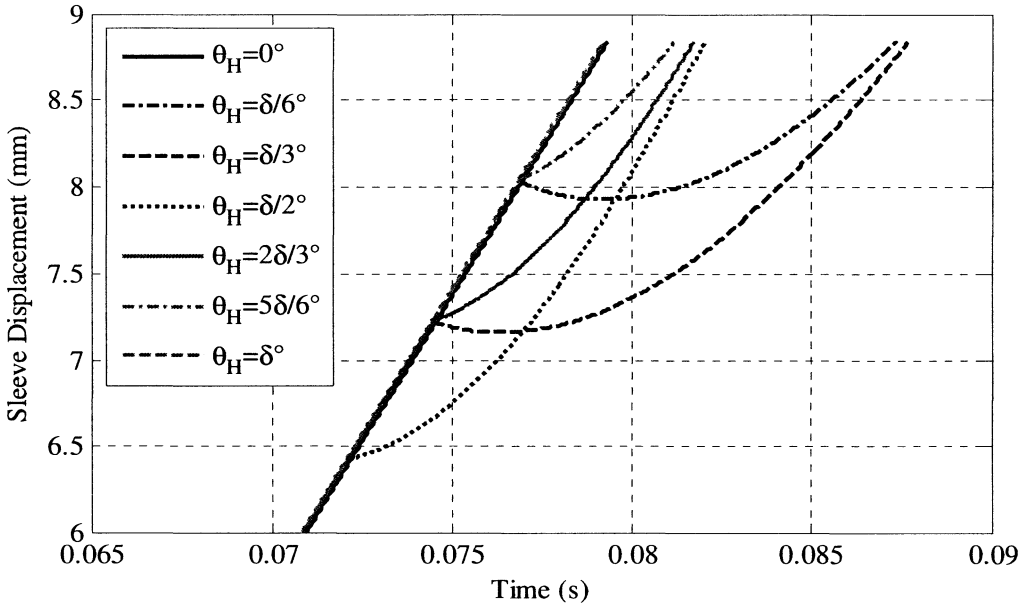

Figure 4.12: Variation in chamfer alignment simulations focusing on indexing only

The alignment results in special cases of sleeve displacements, where the indexing torque is either aided by the slip speed or resisted. As indicated by Figure 4.12, in the case of resistance these results demonstrate that the sleeve chamfers are pushed backward as the chamfer brakes the regenerated slip before moving forward to complete the engagement. This can be extrapolated to the results presented by ref [65], where the hub chamfers may climb backwards over the tip to advantageous alignment. This would likely require higher slip speeds and drag torques, or alignments closer to $\theta_H = \delta/2$, to eventuate than used in these simulation.

Angles below $\delta/2$ indicate that the regenerated slip coincides with the resulting direction of chamfer torque to provide advantageous engagement. This is characterised by engagement proceeding without reversal of sleeve motion. Conversely, for alignments greater than $\delta/2$, but less than the straight through condition there is disadvantageous engagement. Here the regenerated slip coincides with an indexing torque in the opposing direction. Indexing torque must then overcome the regenerated slip speed before realignment can progress.

4.6.4 Effect of varying sleeve rotational speed

The effect of increased sleeve speed is studied next using the same parameters as previous sections, this time the sleeve speed is varied between 1000 and 3000 RPM, with increments of 500RPM.

Results shown here in Figure **4.13**, N_S is sleeve speed in RPM, demonstrate that with the tripling of the sleeve speed the duration of engagement has almost doubled. This result is expected here. The influence on detrimental chamfer alignment is also demonstrated, where, at high speed, it is inferred from the indexing step of engagement that drag torque increases and slip speed at the beginning of indexing subsequently increases. Thus the sleeve moves further backward requiring more time to recover regenerated slip speed and continue with nominal engagement. The introduction of this regenerated slip into the mechanism through high drag torque is also likely to produce partial clash of the synchroniser mechanism. Results show higher slip speeds initiate impact contact in the sleeve and gear hub chamfers. This can lead to excessive wear and long term damage to the chamfer tips [49]. This also exposes the transmission to block out failures at the synchroniser ring and hub through the reduction in indexing torque.

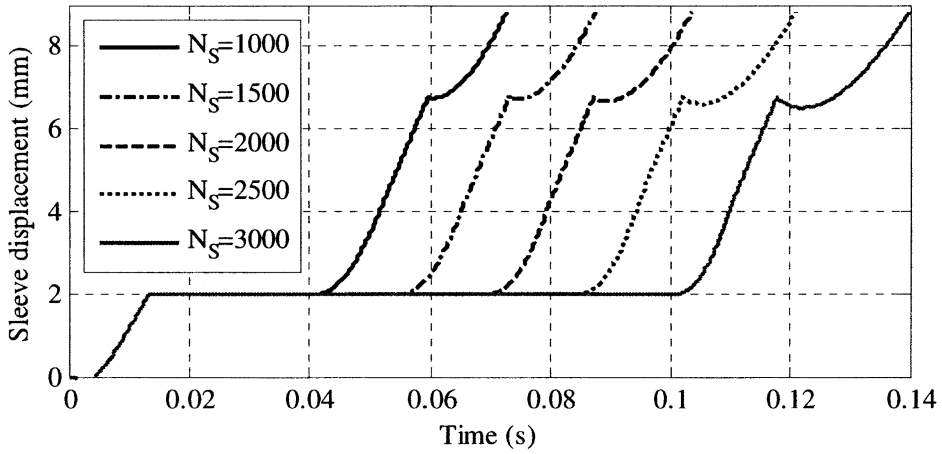

Figure 4.13: Influence of sleeve speed on engagement for a 3rd -4th gear upshift synchronisation

4.6.5 Influence of maximum hydraulic pressure

The next consideration is for the variation in input pressure of the mechanism. A typical 3rd to 4th gear shift is simulated with variation to the actuation pressure only, modified from a minimum of 0.4MPa through increments of 0.4MPa to a maximum of 2MPa, results are shown in Figure 4.15 (a) and (b).

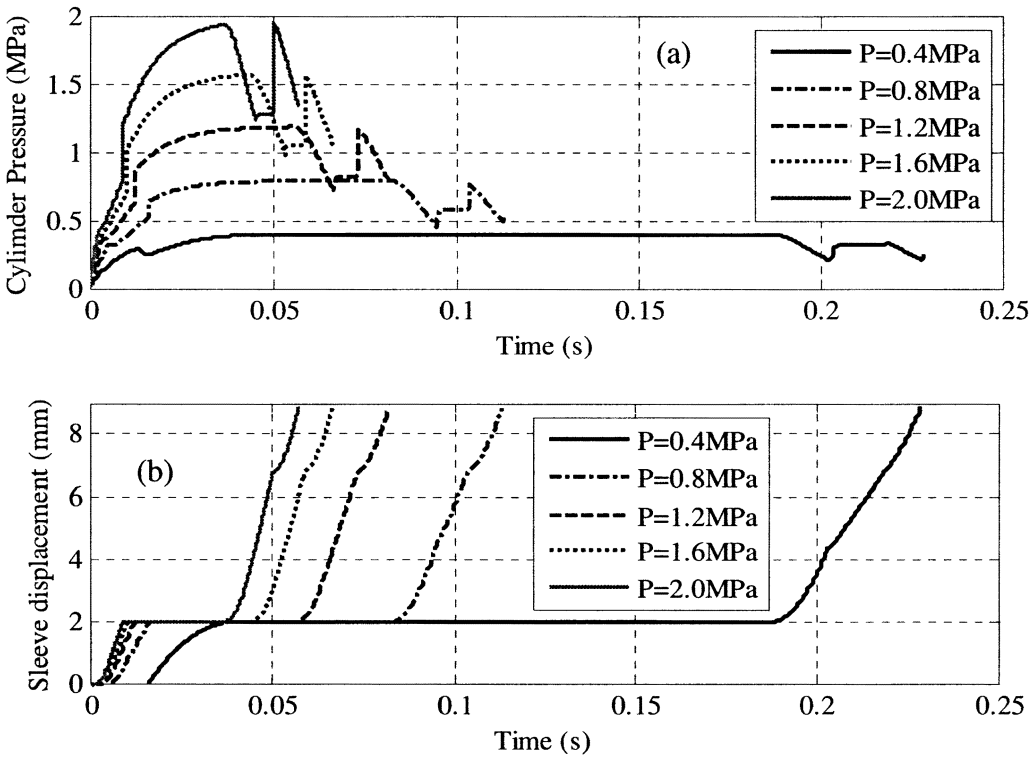

Figure 4.14: 3rd -4th gear upshift synchronisation with variations in control pressure from 0.4-2MPa, (a) cylinder pressure and (b) sleeve displacement

From Figure **4.14** the influence of modifying the synchroniser pressure can be observed. Given a constant time delay of 50ms a nominal peak pressure of 2MPa can reduce the engagement time by one third in comparison to the midrange pressure of 1.2MPa. The minimum pressure of 0.4MPa is barely able to overcome the detent and friction forces to push through and continue engagement, thus the engagement time is extended significantly. Overall the most significant improvement in performance is for speed synchronisation, with duration significantly reduced. Performance reductions in the other steps is also improved, but to a lesser degree, resulting from the rapid expansion of the cylinders as the mechanism moves forward, reducing the peak force during displacement steps of engagement.

4.6.6 Simulations with varied nominal transmission temperature

Evaluations of the effects of changes in the steady state operating temperature on the mechanism are also necessary, as variation in drag torque is significantly affected by changes in the automatic transmission fluid operating temperature, as may be experienced in cold starts, for example. The fluid characteristics at different operating temperatures are presented in Table 4.3 below from Kemp & Linden [140]. Again similar initial conditions and operating parameters are used as with previous simulations in this chapter.

Table 4.3: ATF parameters

Parameters	0°C	40°C	60°C	Units
Viscosity	0.239	0.029	0.015	Pa s
Kinematic viscosity	$2.7\text{x}10^{-4}$	$3.4\text{x}10^{-5}$	$1.8\text{x}10^{-5}$	m^2/s
Density	881.2	853.4	839.4	Kg/m^3

The results presented in Figure **4.15** and Figure **4.16** are for the synchronisation of 5^{th} gear with 4^{th} gear engaged from steady state conditions. The ambient temperatures and corresponding fluid parameters are presented in Table 4.3. Comparison of the high temperatures of 40° and 60° indicates that lower variation in fluid properties, particularly viscosity, has minimal influence on the actuation process, with both 40°C and 60°C sleeve displacements in Figure **4.15** having negligible variation. However, the more significant result is presented for the 0°C results. Figure **4.15** suggests that the high viscosity increases the sleeve displacement time to contact and the synchronisation

time, and that the excessive drag induces ring block out. With the inclusion of Figure **4.16** the extended displacement time is confirmed with excessive drag torque exceeding the available cone torque, thence making synchronisation impossible.

The most significant observable result in this table is the change in viscosity between zero and forty degrees centigrade. This indicates that there will be a sizeable increase in drag torque acting on the mechanism, at least one order of magnitude higher than at other temperatures.

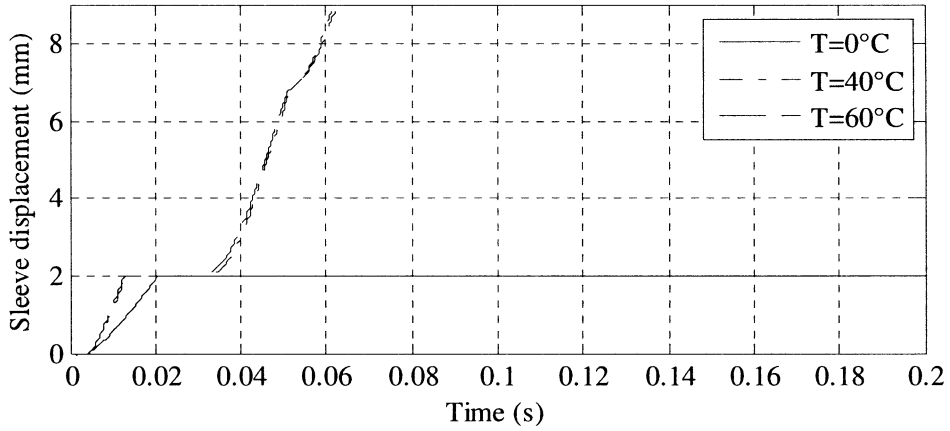

Figure 4.15: Sleeve displacement with variation in ambient transmission temperature

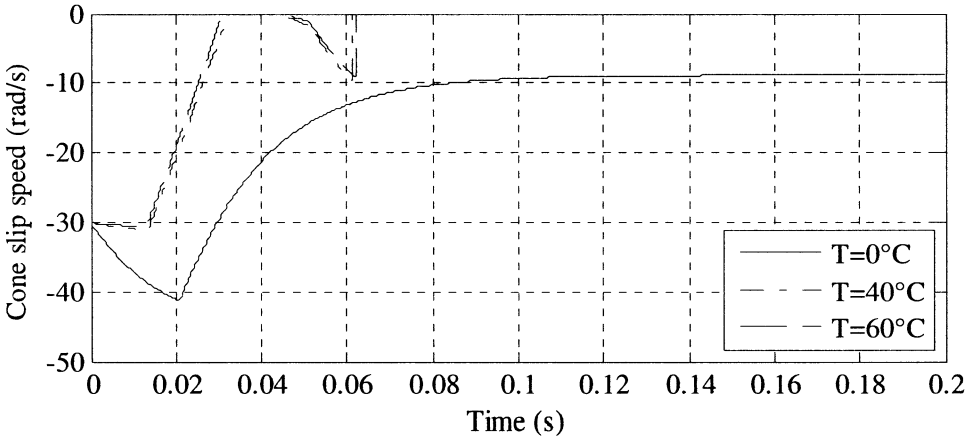

Figure 4.16: Cone slip speed with variation in ambient transmission temperature

4.6.7 Summation of simulation results

The evaluation of each of these environmental and design variables that characterise the design and general operation of the DCT indicates that there is considerable variation in the duration of engagement of the synchroniser must be expected in the general vehicle operating environment. While physical characteristics such as the inertia, gear ratio,

and operating pressure can be controlled to some degree through design, there are limitations to the ability to modify these parameters without compromising the transmission design, *i.e.* lower gear ratios are critical for vehicle performance at low speeds. The influences of chamfer alignment, initial sleeve speed, and operating temperature are also significant in influencing the engagement of synchronisers, but, by and large, these variables are difficult to control from the design perspective. Heating the ATF or performing synchronisations at low speeds immediately after gearshift are possible solutions to reducing this variability, but controlling randomness of the chamfer alignment is impractical.

4.7 DIMENSIONLESS TORQUE ANALYSIS

Effectively, the synchroniser mechanism actuation is defined with the use of three torques; drag torque, cone clutch torque, and indexing torque. The drag torque is not easily defined and, despite this, there have been many attempts to model drag in various forms as applied to transmission systems (see Chapter 5). Indeed, the effect of drag torque on the simulation and control of synchroniser mechanisms needs to be investigated [49].

With respect to the cone clutch synchronisation time is evaluated from the target gear inertias, initial and final speeds, and applied loads as:

$$t_S = \frac{(\dot{\theta}_{S,f} - \dot{\theta}_{S,i})I_{FW}}{T_C \pm T_D} \tag{4.28}$$

where t_S is synchronisation time. As T_D approaches $-T_C$, t_S approaches infinity, or if $T_D \geq -T_C$ synchronisation is impossible. Alternatively for unblocking of the synchroniser ring consideration of the requirements to move from the blocking to neutral position must be evaluated. See Appendix A for detailed derivation of equation. Unblocking time:

$$t_B = \sqrt{\frac{2\delta \cdot I_{FW}}{T_D + T_B}} \tag{4.28}$$

where t_B is unblocking time. Thus, as T_D approaches $-T_B$, t_B approaches the square root of infinity, thence block out occurs if $T_D \geq T_B$. In terms of indexing, the drag torque will only affect the direction of rotation, and only if $T_D = T_I$ will there be an indexing issue. Thus blocking is given a higher priority as a reference torque than its indexing

counterpart. Additionally, consideration of the torque inequality $T_C \geq T_B$ during speed synchronisation to prevent early unblocking of the mechanism and subsequent failure is required.

To evaluate the cone, indexing, and applied drag torques on the mechanism in a more general manner, one can consider the development of pseudo dimensionless groups of torques by dividing unique torque equations by the applied load, F_A, and a cone radius R_C; chosen to provide a common reference for all torques.

To fully realise the application and variation of the cone and indexing torques in the design of synchroniser mechanisms, the two torque equations 4.16 and 4.17 can be defined as dimensionless quantities, as:

$$\Pi_C = \frac{T_C}{F_A R_C} = \frac{\mu_C}{\sin\alpha} \tag{4.30}$$

And:

$$\Pi_I = \frac{T_I}{F_A R_C} = \frac{(1-\mu_I \tan\beta)}{(\mu_I + \tan\beta)} \cdot \frac{R_I}{R_C} \tag{4.31}$$

where Π signifies dimensionless groups for cone, indexing and drag torques. If the radius ratio is maintained as a constant, the two dimensionless groups are defined by the design angles and friction coefficients only. The use of cone radius is important to maintain the continuity of the system, such that a consistent comparison is achieved.

Throughout the synchronisation process, however, the most significant uncontrolled variable is the developed drag torque. To be able to completely realise the application of these dimensionless variables it is necessary to quantify the drag torque acting on the synchroniser and then reduce it to a similar dimensionless quantity. It is then logical to divide the drag torque by the operating radius of the cone clutch such that the normalised drag torque can be evaluated directly against dimensionless cone and indexing torques. Thus:

$$\Pi_D = \frac{\left|\sum T_D\right|}{F_A R_C} \tag{4.32}$$

This provides two dimensionless equations for analysis of the design variables of synchronisers. The purpose for the development of dimensionless variables to describe the torques acting on the synchroniser mechanism is to provide a broad ranging understanding of the influence of certain parameters on the mechanism. Here

modification to cone and chamfer parameters will enable the further understanding of their specific influence. Equations 4.31 and 4.32 are plotted below for a range of angles and friction coefficients. The cone torque map has been developed over a range of operating conditions, with the cone angle, α, varied from 6° to 10° degrees, and the cone friction coefficient, μ_C, varied from 0.06 to 0.16. In some instances of variation the selected cone angle and friction coefficient breach the static limit that causes cone lock of $\mu_C < \sin\alpha$. Using this limit the maximum normalised torque is at $\Pi_C = 1$.

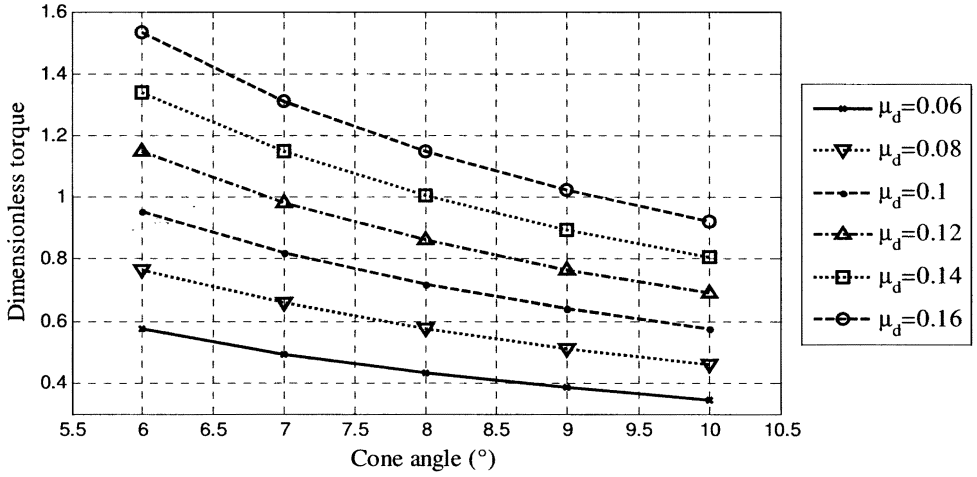

Figure 4.17: Dimensionless cone torque

Variation of the friction and cone angle parameters, as shown in Figure 4.17, produce substantial variation in the developed torque. Higher torques are achieved using shallower cone angles and higher friction coefficients, but are limited by the friction lock described by Vyrabov [137]. Even with the use of design error angles, it is ill advised to use parameters that exceed this limit as gradual wear of the cone surface will reduce the error angle leading to lock of the cone.

For the indexing torque map a radius ratio, R_I/R_C, of 1.2 is used to provide adequate sizing of components, though a range from 1.1 – 1.3 is reasonable. Using a value of less than one implies that the chamfers are internal from the cone. Chamfer coefficient μ_C is varied from 0.0 to 0.1, and β is varied from 50° to 70°.

Evaluation of chamfer torques developed in Figure 4.18 provides significant demonstration of the ability of the derived torque to match that generated in the cone. Only with the ideal friction case of $\mu_C = 0$ is the cone torque limit reached, and for more typical friction coefficients and chamfer angles the dimensionless value is in the band of 0.6 to 0.7, suggesting that the early unblocking of the synchroniser ring is more a result of ineffective wiping of the cone surface or through other loss of cone friction than

inducement from the chamfers. Unlike the variation in the cone torque, increasing friction coefficient reduces the torque developed as it acts against the direction of torque developed from the flank contact, and also plays a smaller role in variation in comparison to chamfer angles.

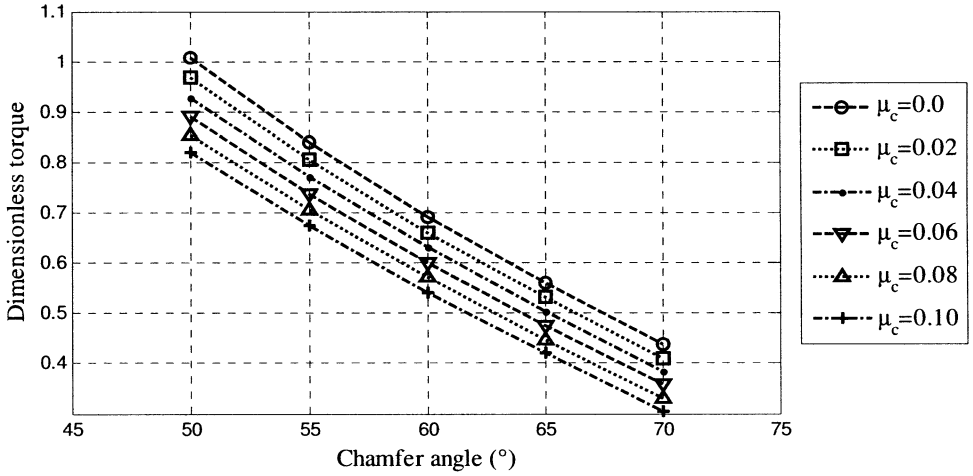

Figure 4.18: Dimensionless blocking/indexing torque

Using a dimensionless version of the drag torque immediately demonstrates the inadequacy of even triple cone synchronisers for first gear to perform at high speeds. For second gear this is true for application of a single cone synchroniser. The most significant issue in developing a drag torque map is that there is considerable variation from gear to gear, depending on both current gear ratio and target gear ratio, making any drag torque map unique to the transmission under consideration. The maps presented in Figures 4.19 and 4.20 are for both up and down shifts of all gears, using a range of operating speeds. Thus the peak drag torque can be established over a reasonably wide range of operating conditions. It is important to note here that simulations are performed using an operating temperature of 40°C. Variation in temperatures, particularly use of zero or subzero operating temperatures will have significant effect on the drag torque developed.

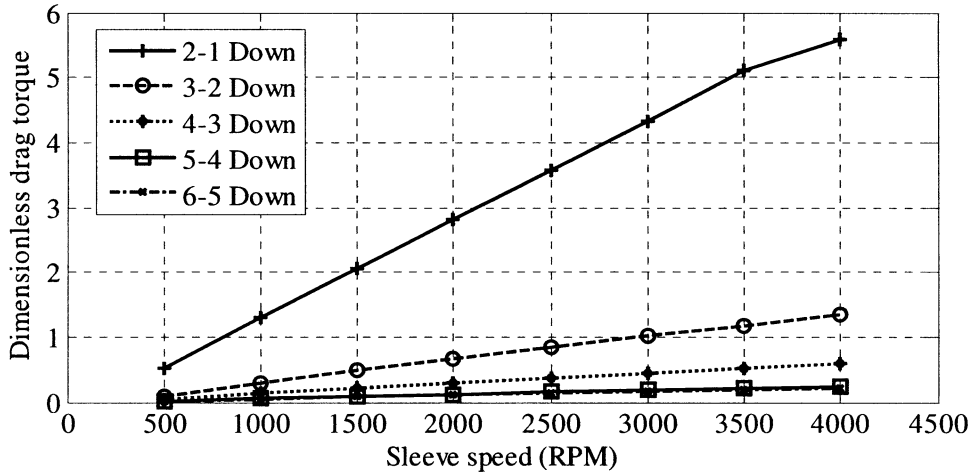

Figure 4.19: Dimensionless drag torque for downshifts

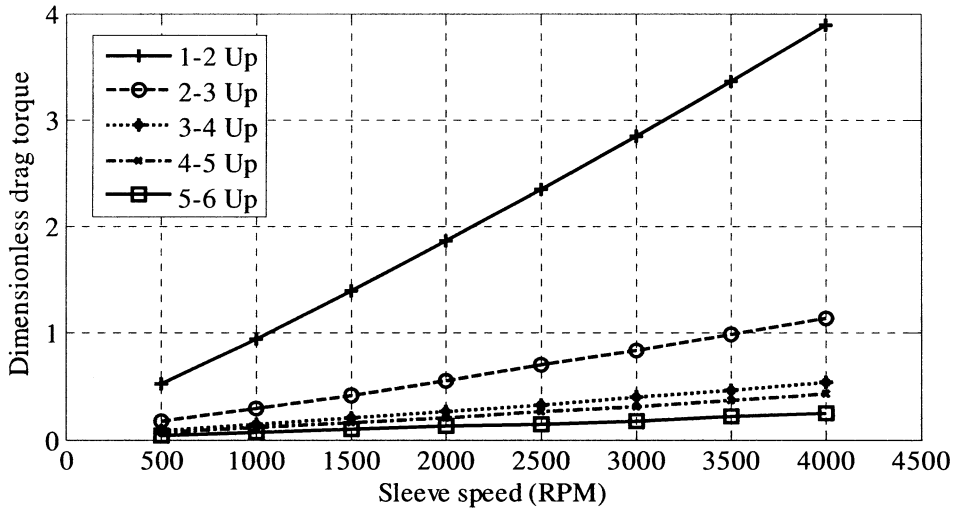

Figure 4.20: Dimensionless drag torque for up shifts

Significant variation arises in the dimensionless drag torques for up and downshifts as a result of conflicting drag components. The absolute component of drag, that which is linked to the gear speed, acts only against this speed whilst the drag torque associated with the relative speed in the wet clutch pack can act with or against the absolute drag torque. This is clearly demonstrated in Figures 4.19 and 4.20 where difference in normalised drag is minimal at low speeds, but for high speed upshifts, the difference in drag torque is substantially higher.

The comparison of Figure 4.19 and 4.20 with Figure 4.17 demonstrates that there is ample capability for cone torque overcoming drag torque in most applications whilst under standard operating conditions. Generally speaking this is also true for the indexing torques, Figure 4.18. However poor selection of chamfer angle suggests that there could be significant resistance to unblocking or indexing of the mechanism under certain conditions. Obviously the higher drag developed in lower gears as a result of the

differential speeds will increase the resistance load on indexing torque. Thus more acute chamfer angles are required for lower gears.

As a comparative example of the different influence of up and down shift drags when selecting parameters, one can compare several gear selections. For fourth gear, in both up and downshifts at normal operating temperatures, dimensionless drag is below 0.4 for the entire operating range. Beginning with the cone torque requirements, to minimise synchronisation time, the maximum dimensionless torque is chosen given the friction limit. So with a friction coefficient of 0.12, the maximum friction angle is about 7.5°. Considering nominal operating conditions, the dimensionless indexing torque must be less than the cone torque but greater than the dimensionless drag torque. If the friction component is assumed to be 0.06, then, for a dimensionless value of 0.7, the chamfer angle will be at 57°. By comparison, a first gear synchroniser, at peak engine speeds, already has a dimensionless torque value for downshifts at 80% of the dimensionless cone torque. Thus multi-cone synchronisers are most definitely required under even standard operating conditions. Furthermore, with these conditions it may be necessary to increase the pitch diameter of the chamfers, or choose more aggressive chamfer angles to overcome this drag torque. Alternate solutions must consider the operation of the wet clutch, such as evacuation of the open clutch pack of AFT during synchronisation under adverse operating conditions, for example.

In this section the development of dimensionless torque variables is performed for the improved understanding of the influence of drag torque on the design and operation of the synchroniser mechanism and provides guidance for the design and selection of cone and chamfer angles. Conducive to this is the relating of cone and chamfer torques to the less well understood drag torque, where utilisation of the operating radius of the cone and peak hydraulic force provides a simple method for evaluating the drag torque over a wide range of operating conditions.

4.8 DESIGN PARAMETER STUDY

Confirmation of the results demonstrated by the dimensionless analysis of the synchroniser mechanism, particularly when considering the four selected design variables, is best realised through the performance of a parameter study of the mechanism. Thus the following section details the results achieved through variation of these four variables independently using numerical simulations. It should be noted that

some of these variations will deliberately breach design limitations set out at the beginning of this chapter. The nominal parameters and initial speed for the simulations are listed in Table 4.4.

Table 4.4: Parameters and initial conditions for parameter variation simulations

Parameter	*Value*	*Parameter*	*Value*
Cone angle	7°	Chamfer angle	60°
Cone friction coefficient	0.12	Chamfer friction coefficient	0.02
Actuation pressure	1.1MPa	Sleeve speed	1500RPM
Engaged gear	3	Target gear	4

First target is the variation in synchroniser cone angle, with results shown in Figure 4.21, with the friction coefficient of 0.12 cone angles of 6° and 7° are less than the friction limit of $\mu_C < \tan \alpha$. As prescribed in equation 4.24, it would be expected that a decrease in cone angle results in an increase cone torque, hence decreasing the synchronisation time. Results of the simulation demonstrate decreasing the cone angle has the effect of reducing synchronisation time in a reasonably linear form, with a one degree decrease correlating to a decrease in synchronisation time of less than 10ms. This is countered by the change in angle increasing the oil squeezing resistance during initial displacement at 0.01s, though the duration of this change is much smaller than 1ms per degree of cone angle.

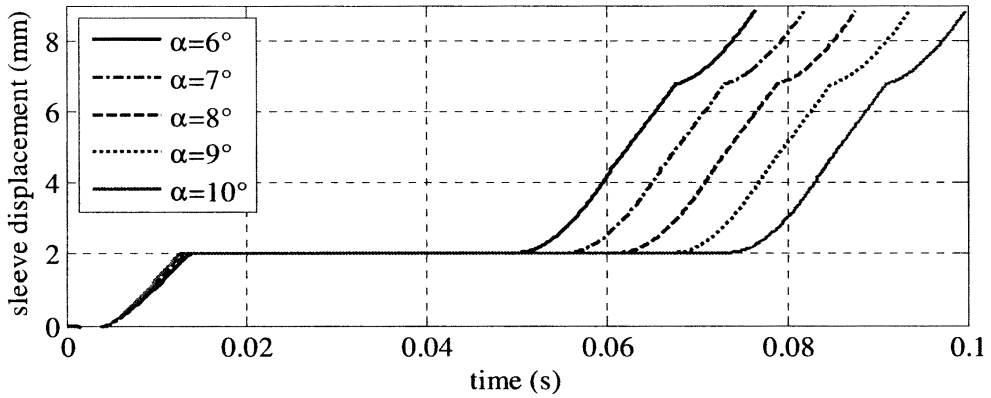

Figure 4.21: Parameter modification to cone angle

Secondly, the cone friction coefficient is varied through a range of $\mu_C = 0.06$ to $\mu_C = 0.16$. With the cone angle set to 7° friction coefficients above $\mu_C = 0.10$ breach the friction limit convention. The results presented in Figure 4.22 demonstrate a nonlinear change to the increase in cone friction, with the influence of increasing μ_C by a factor of 0.2 having less and less significance above $\mu_C = 0.10$. However, it is clearly

demonstrated that the use of higher friction coefficients is more desirable, particularly as limitations to cone angles are included. These simulation results are consistent with the dimensionless friction results presented in Figure 4.17, where modification to friction coefficient is demonstrated as nonlinear but cone angle change produces linear variation in dimensionless cone torque.

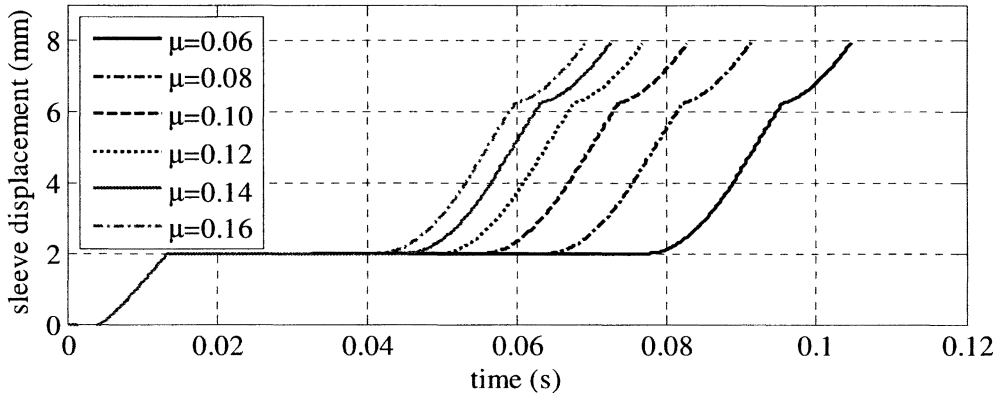

Figure 4.22: Parameter modification to friction coefficient

Next variation of chamfer angle is simulated, with modifications to β between 55° and 75° degrees. Typically β may be up to 65°, but more acute angles may be necessary given the nature of drag torque in the wet clutch. The results in Figure 4.23 demonstrate a trade off in the mechanism design, where, if the chamfer toque is to be increased at a particular pitch radius, a longer sleeve displacement is required. This equates to about one millimetre for every 5 degree change, and can add to the transmission design envelope. The results show that with continued increase to the chamfer angle the overall process time is extended, which is offset by the reduced displacement. This is a result of lower blocking torques increasing the ring unblocking and hub indexing times. The selection of chamfer angle then brings about a peculiar balance, where overall engagement time can be minimised by either using a blunt angle with a more compact design, but exposing the mechanism to the potential for block out at the ring, or by using an acute chamfer angle to increase the blocking and indexing torques at the risk of causing premature unblocking of the ring and longer displacements.

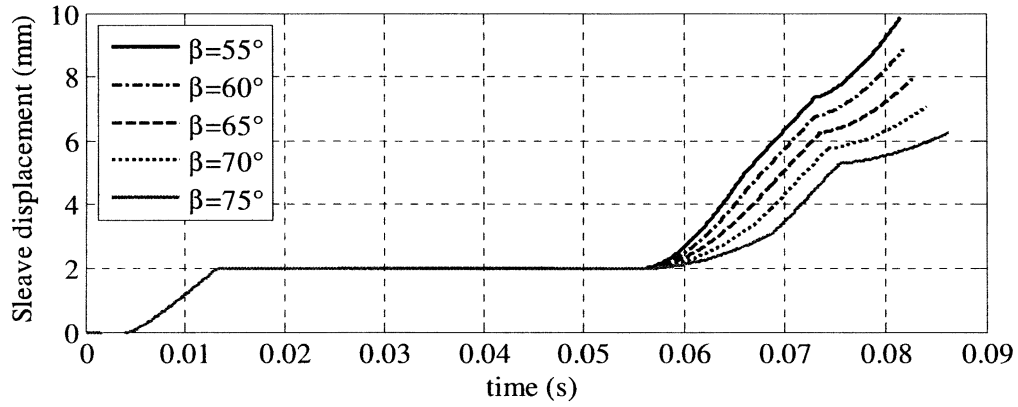

Figure 4.23: Chamfer angle parameter modification

Finally, the chamfer coefficient of friction is modified, between the ideal of μ_C=0 and μ_C=0.1, Figure 4.24 presents the sleeve displacement for the entire process. Results demonstrate that the friction coefficient has the least significance of influence of each design parameter, where, over the entire range of variation, reduction in simulation time varies by approximately 3ms. Thus, while it is favourable to minimise the chamfer friction, the reduction has little impact on the actuation of the system in terms of response times. The primary benefit is rather associated with the increased indexing torque as the friction loss is minimised.

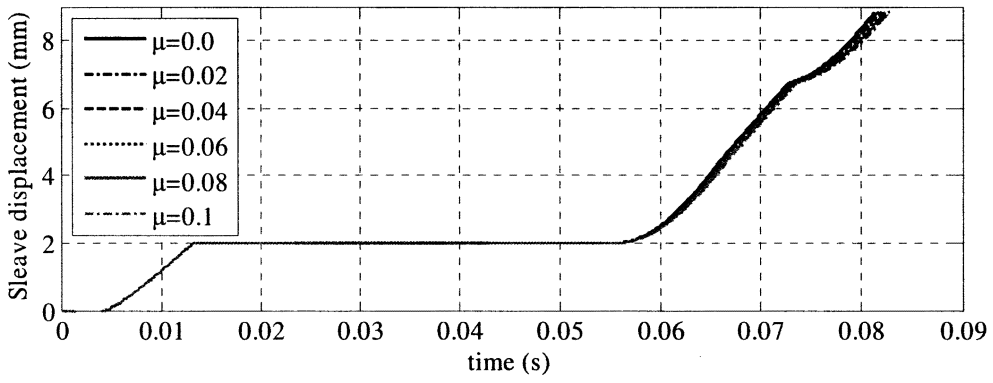

Figure 4.24: Parameter modification to chamfer friction

Thus, the comparison of chamfer variables leads to the conclusion that the chamfer friction coefficient is of minimal importance in comparison to the chamfer angle. This again verifies the dimensionless results shown in Section 4.7. These results implied that the significance in changing chamfer angle greatly surpasses modification to the friction coefficient. In this section the overall result has shown the use of cone and chamfer angles to maximise torque in the synchroniser mechanism, with friction variation being of lesser significance for the cone friction surfaces.

4.9 CHAPTER SUMMARY AND CONCLUSION

This chapter has focused on the development of an understanding of how the synchronisation process works within the framework of DCTs. In doing so several assumptions regarding the influence of synchronisation of vehicle dynamics and vice-versa were made. Through these assumptions and available literature on synchronisers, a detailed model of the mechanism engagement characteristics was created for studying the performance of the synchroniser under a range of operating conditions and through modifications to the mechanism's design.

Numerical simulations of synchroniser engagement were divided into two sections: (1) the study of different variables in the transmission system and during normal operation; and (2) the parametric investigation of critical synchroniser design parameters. From the simulations in Section 4.6 it was possible to discern the performance of a typical synchroniser under a wide range of operating conditions, using 4^{th} gear as the target for synchronisation with 3^{rd} gear engaged in the transmission.

Significant findings with respect to variables of alignment, temperature, vehicle speed and actuation pressure, as well as those resulting from general simulations are:

- After unblocking of the synchroniser ring a lack of load on the cone clutch leads to loss of synchronisation of the target gear which is further influenced by high drag torques,
- High drag torques and slip speeds generated after ring unblocking can lead to the partial clash of chamfers at the initial stages of indexing, increasing wear of the chamfer tips and potentially introducing block out failures [49],
- In conjunction with this, randomness of chamfer alignment results in engagement conditions where the chamfer torque must first eliminate the slip speed before it can initialise indexing of the mechanism. A particular result of this is that, as the slip direction is dependent on shift type; unidirectional chamfers cannot be used in wet clutch DCTs.
- There is heavy dependence on the duration of synchronisation and hub indexing (as per above) resulting from the initial speed of the sleeve, insofar that higher speeds increase both drag torque and duration of engagement, and
- The impact of high hydraulic pressure is most prevalent for speed synchronisation as the maximum load supplied increases cone clutch torque.

Development of a method for estimating synchroniser parameters using dimensionless variables has provided a useful tool for investigating the influence of specific design parameters on the synchroniser itself. Evaluation of these parameters was complimented with a parametric study of synchroniser engagement using a range of design variables. From this it is concluded that:

- Significant increases to the cone torque with modification of angle or friction are numerically possible, but cannot be achieved as a result of the cone friction limit, suggesting that cone torque is important for reducing engagement time.
- The influence of chamfer friction is minimal on the engagement process for both ring unblocking and indexing, however
- The chamfer angle can provide reduction in engagement time at a cost of sleeve displacement.

4.9.1 Summary of contributions

Significant contributions and findings that have resulted from this chapter are:

- The development of a rigid body model of the synchroniser mechanism for simulations of engagement in a DCT,
- Integration of a synchroniser mechanism model with hydraulic control system to simulate automated engagements,
- Identification of the specific operating characteristics of the synchroniser in the DCT. This includes the re-introduction of slip during post ring unblocking, synchroniser engagement and its impact on repeatability of engagement.
- The introduction of a dimensionless method for parameter design of synchroniser mechanisms through the use of dimensionless indexing, cone and drag torques.

CHAPTER 5: DRAG TORQUE MODELLING AND ANALYSIS

5.1 INTRODUCTION AND BACKGROUND

In modern automatically controlled transmission systems sources of damping play a significant role in the design of controllers, where low damping decreases the system stability. In this sense the AT has the distinct advantage over DCTs of high damping available in the hydrodynamic torque converter, with the majority of shift transients are significantly damped, improving shift quality. For the DCT, with no torque converter, other torsional damping mechanisms must be sought. As such understanding of the influence of drag torque in transmission systems will lead to improved design of the system and refinement of control parameters.

As demonstrated with synchroniser modelling, drag torque also plays a major role in the actuation of this mechanism. Particularly when considering synchronisation time and energy as well as the implications of potential failure modes. It then becomes important to precisely model the drag torque on the synchroniser where it is suggested that it can be considered a constant, as prescribed by ref [47, 65]. It is more important to investigate its variation over the entire synchroniser engagement process, and a detailed model as suggested by ref [52, 64] is most definitely required.

Therefore this chapter is devoted to the development of a suitable drag torque model for a wet clutch DCT. This includes two separate applications: (1) to characterise transmission damping and (2) study the impact on synchroniser engagement. This chapter is broken down into discussion on the sources of drag and methods for modelling; looking particularly at the techniques applied by other authors and results. Then the literature for each source of drag is detailed and the appropriate method chosen, with justification for the application of particular methods. Finally applications of drag torque is demonstrated and discussed for both the transmission, with basic linearization for the lumped inertia model, and synchroniser mechanism rigid body model, with model verification and simulation undertaken.

5.2 SOURCES OF DRAG

There are two forms of drag that are found in transmission systems, load dependent losses, and speed dependent losses. Heingartner & Mba [72] identify these two sources of drag torque and further break them down to friction losses in bearing and gear teeth, and windage losses in the gears and bearings. These sources are typical for Lovas, *et al,* [64], Changenet, Oviedo-Marlot & Velex [73], and Anderson and Lowenthal [69]. However, in considering the DCT there are two additional sources of drag torque that must be included in the drag analysis, viscous shear in clutches and concentrically arranged shafts.

Figure 5.1 provides a line diagram for a typical dual clutch transmission. This particular transmission is known as a dual lay shaft DCT, with gear pairs set on two separate lay shafts, linked through the final drive gears. Of interest to the development of drag torque in the transmission system is the arrangement of the compact dual clutch pack and associated concentrically aligned shafts. Open wet clutches friction and hub plates are separated by gaps in the order of ~0.1mm through which transmission lubricant passes, with slip in the open clutch the resulting in viscous shear torque in the transmission. It is also quiet reasonable to assume that the concentric shafts are lubricated, particularly as this is a requirement of the bearings used to separate the shafts. This will generate another source of viscous shear.

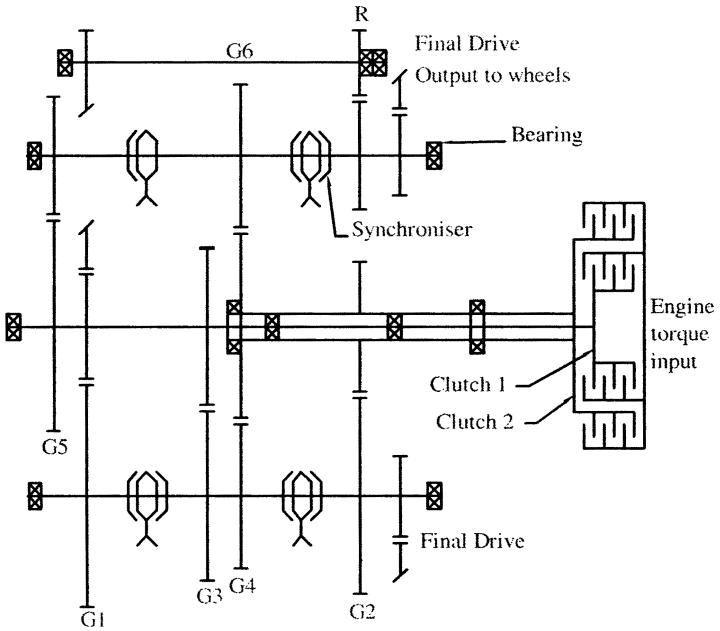

Figure 5.1: DCT transmission layout

As it is established that this transmission is lubricated using spray type methods as opposed to dip lubrication of the gears, it is possible to eliminate churning of gears as a source of system drag. Therefore, from Figure 5.1, the sources of drag are windage losses in the twelve bearings, drag generated at the gears as a result of tooth friction and windage of gears in the air-lubricant mixture, as well as viscous shear losses in both concentrically aligned shafts and the open clutch packs.

5.3 EFFECTS OF DRAG

The role of drag torque in the DCT includes both a significant contributor to system damping and synchroniser engagement, as well as the traditional role as a source of efficiency reduction in the powertrain. For the basic lumped inertia model damping excludes torsional dampers or dual mass flywheels which are used to isolate engine vibrations and are dependent on powertrain configuration. Modelling of these losses are then important for the simulation of the DCT. These are treated differently by different authors. Lei, Wang & Ge [26] ignores these losses in the model, Kulkarni, Shim & Zhang [23] and Zhang, *et al,* [22] model losses as a lumped damping at the differential, while Goetz [1] model losses at gears and clutches, with this method more representative of the transmission structure.

It is argued here that over-simplification of the drag torque leads to inaccurate results for damped responses of the torsional system. Therefore detailed models of drag torque will be built in line with Goetz [1] application of losses, and expanded to include the use of established literature for modelling different drag torques. This model will be used to build a better understanding of the effects of damping on the DCT and establish the requirements for damping to improve the shifting responses.

In consideration of the synchroniser mechanism, drag torque plays a significantly different role. As has been alluded to in the previous chapter, the most significant uncontrollable variable that influences the engagement of the synchroniser is the drag torque. References such as [49, 50] provide insight into the importance of drag torque on the synchroniser. Equations presented in both references detail the influence of drag torque on synchronisation time and energy. Furthermore, the detailed work of ref [49] demonstrates the significance of drag torque in specific application to the engagement process, and potential failure modes. Specifically:

- Block out – post synchronisation block out develops when there is excessive drag acting on the target gear, blocking torque is insufficient to realign the ring to allow the sleeve to pass.
- Hard shifting – where high drag resists speed synchronisation and chamfer alignment process, reflected in increased shift effort felt by the driver, similar to block out above.
- Partial clash – here synchronisation is successful, however excessive drag reinitiates slip in the mechanism and low speed clash develops.

In most instances these failure modes are minimised through good design practices, but cannot be completely eliminated. Razzacki [51] also details the application of drag to the synchroniser mechanism. In conjunction with other authors, there is one common conclusion. For a manual transmission the drag torque is coupled to the type of shift, up or down. Thus the determination of numerical sign references the shift rather than the speed of particular components. The structure and shifting method of DCTs – *i.e.* pre-selection of target gear without clutch disengagement – changes this significantly. Consideration must now be for the velocities at the point source of drag alone; otherwise incorrect application of drag torque will result. these sources are summed from the known drag torques in a transmission. See equation 5.1 below:

$$T_D = -sign(\omega_G)(T_W + T_F + T_B) - sign(\Delta\omega_{CL})(T_{CL} + T_{SH} + T_B) \qquad (5.1)$$

where ω_G is gear speed, $\Delta\omega_{CL}$ is clutch slip speed, T is torque, and subscripts are W is gear windage, SH is inter-shaft shear, B is bearing losses, CL is clutch windage, D is drag, and F is gear friction. From a practical perspective detailed modelling of the drag torque acting either on the synchroniser or the DCT as a whole can be numerically cumbersome. From a design perspective Lechner & Naunheimer [47] suggests the use of constants, approximately 2Nm at the clutch, for the drag torque as an estimate to improve the ease at which design variables can be estimated. Alternatively, for DCTs, individual losses can be giving as a percentage of output torque based on the overall efficiency of the transmission.

Such an assumption does not account for the variation of drag torques through different speeds, particularly as viscous, speed dependent drags tend to be more dominant at higher speeds, i.e. windage. From the simulation perspective this cannot capture the variation inherent in drag torque, nor the influence that it imparts on both DCT and

synchroniser. It is therefore necessary to model individual component drag torques as point sources and apply results onto DCT and synchroniser, as required.

5.4 DRAG TORQUE MODELLING

The literature survey identified several different demonstrations of the modelling of combined drag torques for the study of losses in gears and transmissions. From this research the state-of-the-art was identified in the study of drag torque. This provides a frame of reference for the following sections where individual sources of drag are discussed, identifying different methods for simulating each source of drag and the selection of the most appropriate method for simulations. These were identified as bearing losses, gear windage and friction, and concentric shaft and open clutch drag torques.

5.4.1 Bearing drag

Bearing losses have been analysed by Harris [77] for a variety of bearing designs, considering both speed and load dependent losses on individual bearings. This work is commonly considered to be the state-of-the-art on the topic, with similar results being applied through many other papers [60, 76]. Alternative bearing models are presented in [78] for radial and axial loaded bearings based on a bearing manufacturer's research. To maintain independence of this model from manufacturer specific information, Harris [77] will be applied in this simulation.

$$\begin{aligned} &T_B = 10^3 f_V (\nu N)^{2/3} d^3 \\ &for\ \nu N > 2\times10^{-3} m^2/s\,\text{min} \\ &T_B = 16 f_V d^3 \\ &for\ \nu N < 2\times10^{-3} m^2/s\,\text{min} \end{aligned} \qquad (5.2)$$

where N is rotational speed (RPM), f is friction, ν is kinematic viscosity, and subscript V is windage.

5.4.2 Gear tooth friction drag

Most techniques used to model friction losses in gear teeth are dependent on both rolling and sliding friction, and modelling has become quite popular for both spur and helical gears of single mesh cycles. Other modelling methods consider more simple assessment of the losses for time averaged model that lead to more compact and efficient models for transient simulations.

Early work in Anderson and Lowenthal [69] requires the numerical integration of instantaneous rolling and sliding velocities along the path of contact. This must be divided into separate regions depending on contact point of the meshed tooth, and incorporates load sharing between teeth, dividing the line of contact into shared and single tooth contact regions. Michlin & Myunster [83] provide an example of vector analysis of the contact topography of two teeth in mesh. The line of action of the mesh is divided into four zones relative to the pitch point. From this reference point equations are varied to account for vector change. Friction load at different stages can then be calculated. Methods such as these become quiet cumbersome for modelling the time dependent variation of losses over multiple gears for an extended period and are more useful when investigating the mesh itself.

Time averaged models are presented in Changenet, Oviedo-Marlot & Velex [73] provides an initial method for the evaluation of tooth friction power losses, with an alternative presented in BS ISO/TR 14179-1:2001 [76]. Both of the presented equations are functions of input torque, gear geometry, and friction. However in each case the gear geometry is treated quiet differently. The model selected by Changenet, Oviedo-Marlot & Velex [73] has the helix angle in the denominator and other geometry, such as module, in the numerator. This is reversed for the BS/ISO model [76] and, as a result it would be expected that the two results that are produced are substantially different. The BS/ISO model [76] will be adopted in this chapter over other models as the rigorous analysis required in the development of the model to be utilised as an ISO standard ptovides higher surety of its quality. Further, [72] has also demonstrated its acceptability to numerical modelling. Power losses are determined, with the result divided by rotational speed to result in torque loss:

$$T_F = \frac{P_M}{\omega_G} = \frac{fTN\cos^2\beta}{9549M} \times \frac{1}{\omega_G} \tag{5.3}$$

Where:

$$M = \frac{2\cos\alpha(H_s + H_t)}{H_s^2 + H_t^2} \tag{5.4}$$

$$H_s = (\gamma - 1)\left[\sqrt{\frac{r_{o2}^2}{r_{w2}^2} - \cos^2\alpha} - \sin\alpha\right] \tag{5.5}$$

$$H_t = \left(\frac{\gamma + 1}{\gamma}\right)\left[\sqrt{\frac{r_{o1}^2}{r_{w1}^2} - \cos^2\alpha} - \sin\alpha\right] \tag{5.6}$$

where α is transverse operating pressure angle, β is operating helix angle, γ is gear ratio, r is radius, H is sliding ratio, M is mesh mechanical advantage, P is mesh power loss, and subscripts are s is start of approach, t is end of approach, o1 is pinion outside radius, o2 is gear outside radius, w1 is pinion operating pitch radius, and w2 is gear operating pitch radius. In the lay shaft arrangement for the transmission type, all even and odd gear pairs are attached to a common shaft that is connected to the clutch pack. The load for an individual gear is then the acceleration of its attached freewheeler on the lay shaft. For the gear pair under investigation the load is considered to be the acceleration of all components between it and the clutch pack, giving a much higher inertia than the freewheeling gears. It is therefore possible to ignore the considerably smaller resistance of non-targeted freewheeling gears over that of the gear targeted during both synchronisation and shift transient modelling.

5.4.2.1 Gear tooth friction coefficient

Diab, Ville & Velex [74], while focusing on the assessment of friction coefficient, provides demonstration of the accuracy of the preceding method. With the use of an appropriate friction coefficient the tooth friction force can be calculated accurately. Xu, *et al,* [84] reviews many of the current friction models and identifies a flaw in that as the sliding velocity approaches zero at the pitch point the corresponding friction coefficient approaches infinity; this is a major issue with most current models as it create numerical issues. Elasto-hydro dynamic lubrication (EHL) is identified as the most suitable method for developing friction models by Xu, *et al,* [84], though it is not considered practical in terms of computational requirements and multiple parameter studies. EHL

simulations were instead used by Xu, *et al,* [84] to develop a new empirical friction model, relating multiple variables to generate the mathematical model. Like all friction models this is limited by the lubricant used in the simulation, information available on gearing, and experimental validation.

An alternative friction model is presented by Benedict & Kelley [85] and popularised in [73] and [82]. This model is an empirical correlation of fluid properties with gear speed and load, and as previously discussed, has the disadvantage of tending to infinity at the pitch point. A significant part of both of these models is that both include rolling and sliding velocities in the model, required for accurate determination of the friction coefficient. However, as with the discussion of previous methods, this requires precise calculation of tooth surface velocities, incorporating tooth geometry and relative alignment. Thus such a method is still overly complex for this model.

To simplify this issue, a constant friction coefficient will be applied to the model based on the available literature on gear tooth friction. This will reduce the computational complexity of the model while maintaining a reasonable degree of accuracy, particularly as the helical gear mesh results in multiple contact points over several gear teeth at any instant. Effectively an average loss will be determined. Such assumptions have been taken by He, Cho & Singh [132], Xu, *et al,* [84] and Diab, Ville & Velex [82], with the latter providing reasonable reference to an average friction coefficient.

5.4.3 Gear windage drag

Gear windage is defined as the drag of a gear as is rotates in air or an air-oil mixture, whilst churning is the drag generated as a gear rotates in oil. Both forms of loss are considered speed dependent. Churning losses arise from the partial submersion of a gear in lubricant, with the drag developed from viscous resistance of the fluid [88, 90]. The churning of gears through transmission fluid is consistent with dip-type lubrication of the gear train. To minimise the losses in the DCT, spray-type lubrication is generally adopted. This is associated with windage drag alone, therefore churning losses will be excluded from the model.

Similar to the churning of the gear through lubricant, modelling of gear windage in an air or air-oil mixture is based on experimentation involving discs or drums rotating in

this mixture, Schlichting [141] examines this work. A review into the effects of windage power losses was conducted by Eastwick & Johnson [95] who seeks to provide designers with the most appropriate information for the development of high efficiency gearboxes. Significantly, it is identified that the literature tends to utilise the same experimental apparatus to validate models as used to develop the empirical model. Thus "successful" results must be considered with some scepticism, as there is a lack of independence in the validation of results. Alternative evaluation using simulations by Al-Shibl, Simmons & Eastwick [94] applies CDF techniques to the question of windage power losses to determine the ability to practically model this form of loss. Though it was possible to model these losses with reasonable accuracy there was a propensity for models to underestimate the windage at high speeds.

Anderson and Lowenthal [70] provide an initial model for the windage of gear-pinion pairs, using gear geometry, speed, and viscosity to correlate experimental data. Dawson [92] provides a second empirical model based on experiments that measure the deceleration of gears. Results were gathered for a varied range of gear parameters; however only air is used as the working fluid, and therefore the extent of impact of oil vapour is unknown. Diab, *et al,* [93] provides two separate models for the windage of gears in air-oil mixtures. The first method is based on pi-theorem, as performed in the previous models of refs [70] and [92], and considers a combination of viscosity, speed, and geometry in developing an empirical model. The second method applies fluid flow analysis in developing separate equations for gear tooth faces, using friction force generated on a "disc" surface, and teeth, where fluid flow is deflected by the proceeding tooth onto next tooth, generating a second resistance moment. This has the advantage of being independent of correlation using experimental equipment that limits the alternate research. Diab, *et al,* [93] demonstrates good comparison of both of these methods, using a small number of experiments. However, as is suggested, the independence of the second method from experimental data provides it with an increased degree of confidence. Referring to ref [93] the dimensionless coefficient equations for gear faces are:

$$C_{W,1} = 2.586\pi \frac{1}{\sqrt{\mathrm{Re}^*}}\left(\frac{R^*}{R}\right)^5 + \frac{0.178\pi}{4.6}\left[\frac{1}{\mathrm{Re}^{*0.2}} - \frac{1}{\mathrm{Re}^{*0.2}}\left(\frac{R^*}{R}\right)^5\right] \qquad (5.7)$$

For gear teeth:

$$C_{W,2} = \xi \frac{Z}{4}\left(\frac{b}{r_p}\right)\left[1+\frac{2(1+X_A)}{Z}\right]^4 (1-\cos\phi)(1+\cos\phi)^3 \tag{5.8}$$

Where:

$$\phi = \frac{\pi}{Z} - 2(inv\alpha_P - inv\alpha_A) \tag{5.9}$$

Finally, gear windage torque is determined as:

$$T_W = 0.5(C_{W,1} + C_{W,2})\rho\omega^2 R^5 \tag{5.10}$$

where C is drag torque dimensionless coefficient, X is profile coefficient, Z is module, b is face width, r is radius (* denotes radius at critical Reynolds number), Re is Reynolds number (* denotes critical Reynolds number), and subscripts A is tooth tip, and P is pitch point.

5.4.4 Wet Clutch drag

In the open multi-plate wet clutch pack a differential velocity will result in the generation of a viscous shearing torque that resists the slip speed of adjacent friction surfaces. The ideal case is a relatively simple problem, demonstrated by the work of Kitabayashi, Yu Li & Hiraki [81] that provides demonstration of the drag torque that is accurate in low speed ranges. It has been demonstrated by Yaun, *et al,* [79] that this method is not applicable at higher speeds, and an alternate method is provided for an improved model that has reasonable accuracy at both high and low speeds. Here, at high speed, a reduced effective radius is developed from the interaction of surface tension, centrifugal force and mass conservation. At high speed, centrifugal force pushes lubricant out of between the clutch plates in rivulets and reduces the effective contact area; this is countered by capillary action which draws the ATF against centrifugal motion. Therefore the balancing of these two forces can be used to estimate a reduced outer radius.

The effective drag torque is calculated using Yaun, *et al,* [79] method by:

$$T_{Cl} = 2\pi \int_{r_1}^{r_0} \frac{\mu \omega r^3}{h} \left(1 + 0.0012 \mathrm{Re}_h^{0.94}\right) dr \tag{5.11}$$

where the characteristic Reynolds number is defined by:

$$\mathrm{Re}_h = \frac{\rho \omega r h}{\mu} \tag{5.12}$$

To determine the revised outer clutch radius two turbulent flow coefficients are found:

$$f = \begin{cases} 0.885 \mathrm{Re}_h^{-0.367} & (\mathrm{Re}_h \geq 500) \\ 0.09 & (\mathrm{Re}_h \leq 500) \end{cases} \tag{5.13}$$

$$G_r = \frac{1}{12}\left(1 + 0.00069\, \mathrm{Re}_h^{0.95}\right) \tag{5.14}$$

where μ is dynamic viscosity, ρ is density, ω is rotational velocity, Gr is turbulent flow coefficient, and subscripts h is fluid spacing, I is inside, and O is outside. It is convenient to note here that through application of mass conservation principles Equations 5.12 to 5.14 can be solved at the inner clutch radius, particularly as fluid is pumped from the inner to outer radius. To account for the variation of radius, the analysis continues with the solving of the Reynolds equations using centrifugal and surface tension forces. The result is arranged in polynomial form, with the roots being solutions to the effective outer radius. This is then used in Equation 5.11 as the outer radius if it is less than the existing outer radius:

$$\frac{\rho\omega^2}{2}\left(f + \frac{1}{4}\right) r_o^2 - \frac{\mu Q}{2\pi r_m h^3 G_r} r_o + \frac{\mu Q}{2\pi r_m h^3 G_r} r_i - \frac{2\pi \cos\theta}{h} - \frac{\rho\omega^2}{2}\left(f + \frac{1}{4}\right) r_i^2 = 0 \tag{5.15}$$

where Q is flow rate. Aphale, *et al,* [142] provides an alternative using solutions for the Naiver-Stokes equations that are solved in ref [79] and similarly assumes that the centrifugal forces play a significant role in the fluid flow in the clutch. However, at the same time, it is assumed that viscous forces do not play a significant role in the distribution of forces. This results in some limitations to the results that are presented. Thus the method proposed in ref [79] is used for modelling the clutch drag.

5.4.5 Concentric shaft drag

Particular to the DCT is the arrangement of concentric shafts that connect the gear train to the clutches. The arrangement of rotating concentric shafts is presented in Schlichting [141] as an example of Couette flow, or simple shear flow. It is represented thus:

$$T_{SH} = 4\pi\mu h \frac{r_O^2 r_I^2}{r_O^2 - r_I^2} \Delta\omega_{CL} \tag{5.16}$$

The application of this equation requires the assumption that there is a continuous flow of lubricant through the annular area. This is justified as there are bearings separating these shafts which must be lubricated at all times.

5.4.6 Summary of modelling methods

Drag torques associated with a spray lubricated wet clutch DCT were identified for investigation in this chapter. Modelling of these drag torques has relied on the evaluation of available literature for bearing losses, gear tooth friction, gear windage, as well as viscous drag in the clutches and concentrically aligned shafts. The chosen models presented in this section must now be applied for the development of linearised drag torque losses to be used as damping coefficients in the DCT lumped inertia model, and as a net drag torque model for simulating the engagement of the synchroniser mechanism. The chosen models have therefore been considered as the state-of-the-art for respective sources of drag torques. Heingartner & Mba and Changenet, *et al,* [72, 73] have both taken similar literature and utilised it to perform detailed investigations of drag torque losses for geared transmissions. In the following sections these models will be reapplied in different methods for specific applications to DCTs.

5.4.7 Drag torque modelling parameters

The parameters that have been used to model drag torque are primarily based on the information available in Stokes [143], are as follows:

Table 5.1: Drag torque data for gear modelling

Gear	*1st*	*2nd*	*3rd*	*4th*	*5th*	*6th*
Helix angle (°)	32	32	32	32	32	32
Pressure angle (°)	20	20	20	20	20	20
Transverse pressure angle (°)	23	23	23	23	23	23
Pressure angle at tooth tip (°)	25	25	25	25	25	25
Teeth on gear	45	45	45	41	39	35
Teeth on pinion	13	22	31	38	35	38
Outside radius of gear (mm)	65.5	57	50.5	44.5	42.25	36.75
pitch radius of gear (mm)	62.25	54.125	47.75	41.75	40.375	36
Gear	**1st**	**2nd**	**3rd**	**4th**	**5th**	**6th**
Outside radius of pinion (mm)	41.75	29.5	30.75	41.75	38.5	41.75
pitch radius of pinion (mm)	18.5	26.625	33	39	36.625	41
Face width (mm)	18	16	15	15	17	16

5.5 APPLICATION TO THE DCT FOR DYNAMICS MODELS

Modelling of the dual clutch transmission applies lumped stiffness and inertias to the development of a complete powertrain model, incorporating engine, flywheel and any torsional damper, transmission, propeller shaft, differential, axle, wheels and vehicle inertia in Chapter 8. Significant sources of damping associated with the transmission and differential can therefore be included as damping elements, coupled between inertial elements or linking inertia elements to ground.

Given the complexity of the equations that have been used to describe local sources of drag and indeed necessity to integrate equation 5.11 for each time step during numerical modelling, it is illogical to directly apply equations to individual damping elements. It is reasonable to simulate individual damping elements over a reasonable range of speeds, and then linearise the results to develop damping coefficients that provide reasonable approximation of the relevant drag equations. Graphical linearisation becomes much

more useful to modelling than the linearisation of equations particularly as the friction model combines both speed and torque in the determination of any drag torque.

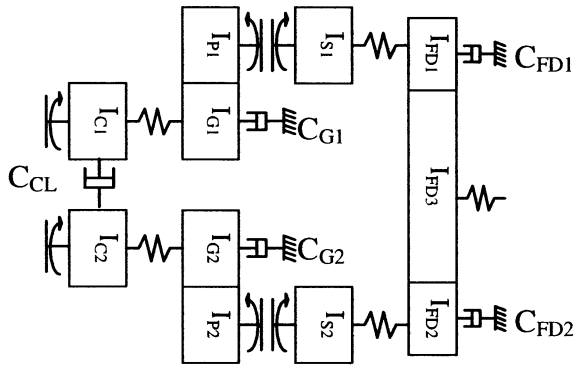

Figure 5.2: Transmission and differential finite element layout

The transmission layout in Figure 5.2 represents the location of individual damping sources that are to be incorporated into the transmission model. There are four individual damping sources that are absolute, or grounded, and one damping element coupling the clutch packs. The absolute damping elements include drag from multiple bearings, and active and idle gear windage drag, but only friction losses from active gears – those under synchronisation or engaged in the transmission. Friction losses have been excluded from other gears primarily as the only acting torque on idler gears is the acceleration of the pinion; therefore the applied torque is significantly less than that present in the active gear pairs. For the coupling of the two open clutch packss drag torque is derived from clutch shear, shaft shear, and bearings separating the shafts. Thus damping will be substantial between the two clutch packs.

5.5.1 Linearisation of drag torques for finite element models

To develop reasonable estimations of the drag torque damping in the system it is necessary to perform simulations over a reasonable range of operating conditions for identified damping elements. As identified in Figure 5.2 these are:

- Coupling damping in the wet clutch, concentric shafts, and associated bearings
- Lumped gear and bearing damping for engaged and target gears, and
- Losses in the final drive gears.

To estimate the torque load on each gear the engine torque look up table model will be applied as an input torque directly to the transmission over the chosen speed range with a 50% throttle angle condition, reasonably estimating the torque load in each gear pair, with consideration of the influence of ratio change.

To perform linearisation of the approximated losses in the transmission the drag torques are mapped over a reasonable range of speeds and a linear curve fitting is used form the "Curve Fitting" toolbox in Matlab, making use of the least squares method for curve fitting. This method relies on minimising the difference between the approximated curve and the known data. The main limitation of this method is that outliers will have significant influence on the final parameters as the procedure tries to minimise the difference. Fortunately, this method is applied to a small quantity of simulated data as opposed to a large volume of experimental data this limitation has minimal influence.

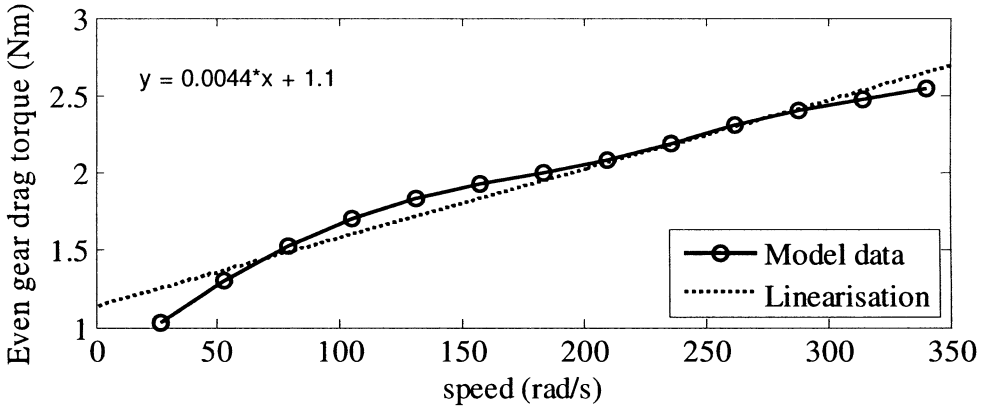

Figure 5.3: Linearised damping for even gears

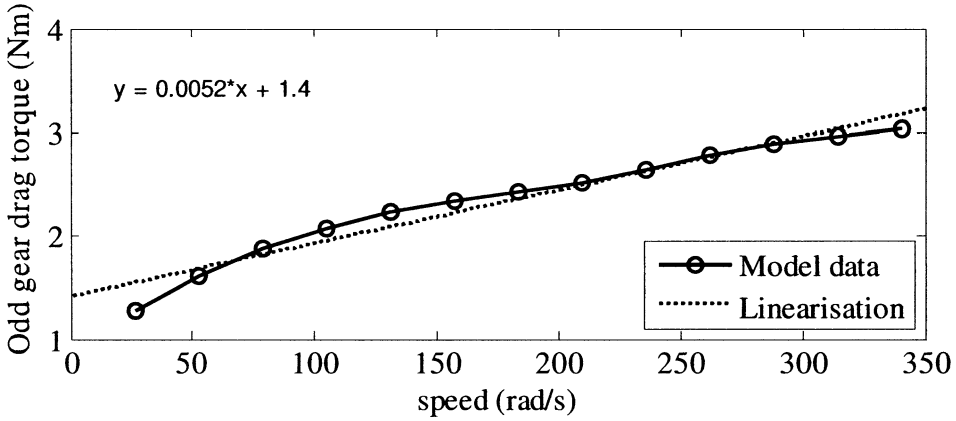

Figure 5.4: Linearised data for odd gears

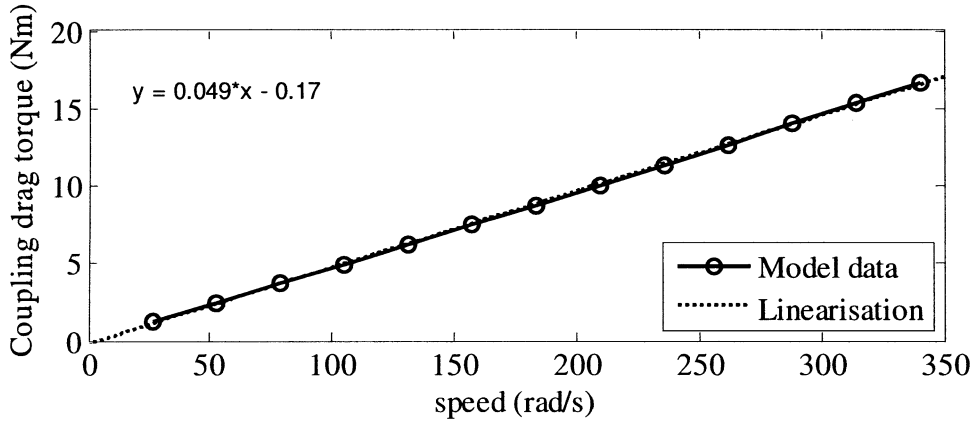

Figure 5.5: Linearised data for coupling drag

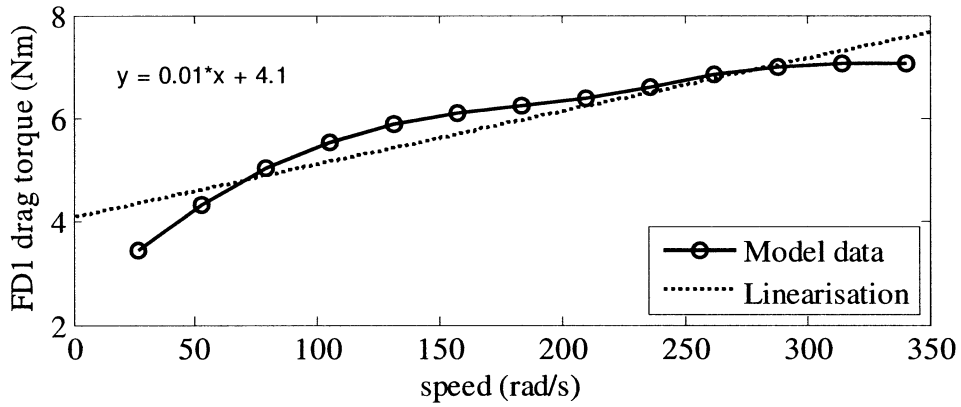

Figure 5.6: Linearised data for final drive 1

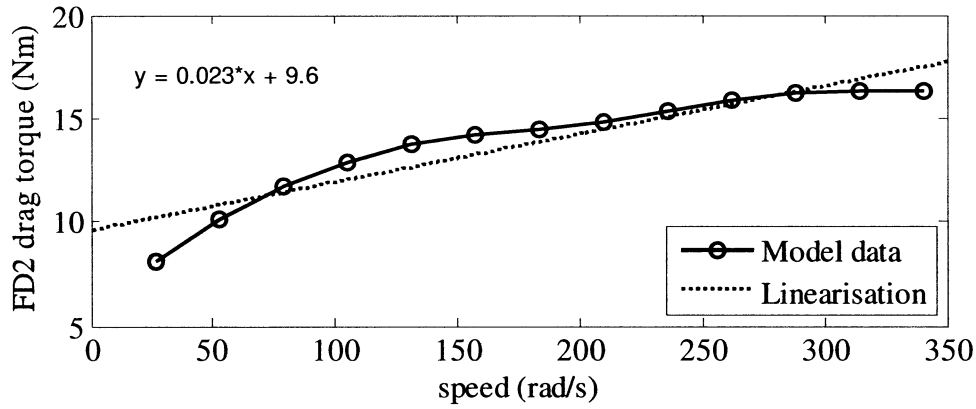

Figure 5.7: Linearised data for final drive 2

In reviewing the results of Figures 5.3 to 5.7 the results present a reasonably accurate linear result in the comparison for simulation and linearisation. For odd and even gear and both final drive damping results there is variation of friction and windage losses contributing to the overall variation in drag losses. The dominance of friction is evident in figures 5.6 and 5.7, where torque multiplication significantly increases the torque

load. In Figures 5.3, 5.4, 5.6, and 5.7 there are significant torque offsets in the linear model, but as these values are constant, thence independent of speed, they will not influence the dynamic model and can be excluded from the system. For gear coupling drag in Figure 5.5 the model is already very linear. This is a result of the assumption that the hydraulic fluid pump is capable of continually maintaining sufficient flow rate to submerge the clutch plates under all operating conditions.

Overall these results are typical to transmission damping and demonstrate that the dual clutch transmission in particular has only light damping. From these results the final damping coefficients are detailed in the table below. These damping coefficients will be used in the simulation and modelling of the full vehicle powertrain in Chapter 8 of this thesis.

Table 5.2: Summary of damping coefficients

	Damping coefficient (Nm.s/rad)
Even Gear (4^{th})	0.0044
Odd Gear (3^{rd})	0.0052
Clutch coupling	0.049
Final drive 1	0.010
Final drive 2	0.023

5.6 APPLICATION TO THE SYNCHRONISER

The synchroniser mechanism model requires a different application of drag torque owing to the different modelling technique in Chapter 4. The synchroniser is considered as a rigid body, with high shaft stiffnesses and low inertia. The local natural frequencies are far in excess of those which will have significant influence on the mechanism during engagement. Thus in the application of drag torque to the synchroniser mechanism, damping is of little interest. It is, however, important to establish a reasonably accurate resistance torque model for the synchronisation process. Particularly as it is a speed and load dependent variable that effects the duration of

engagement and can potentially initiate several different failure modes during engagement.

In building the rigid body model for an activated synchroniser mechanism drag torque acting on the synchroniser is only those sources between the cone and the open clutch are considered. Thence, as can be deduced from Figure 5.1, drag torque is unique to the individual gear, and, indeed with the reduction pairs, lower ratios will endure significantly higher drag torques. Similar to the work described in Razzacki [52] and Lovas, *et al,* [64], a reflected drag torque model is built by determining individual sources of drag reflected on the lay shaft and then using gear multiplication to apply it to individual synchronisers.

In Figure 5.8 below the highlighted sources of drag torque for the engagement of 2^{nd}, 4^{th} and 6^{th} are presented. This includes windage from each of these friction pairs, tooth friction from the targeted gear for synchronisation, concentric shaft drag, bearing losses, and shear in coupled wet clutches. The drag torque can be represented as Equation 5.1. Drawing on such a drag torque model provides improved simulation accuracy of the likes of Liu &Tseng [60], where a constant drag torque is utilised in simulations as the time dependent variance in drag can now be considered. This is particularly important in the DCT as drag will be a function of both the slip speed in the clutch and gear speed.

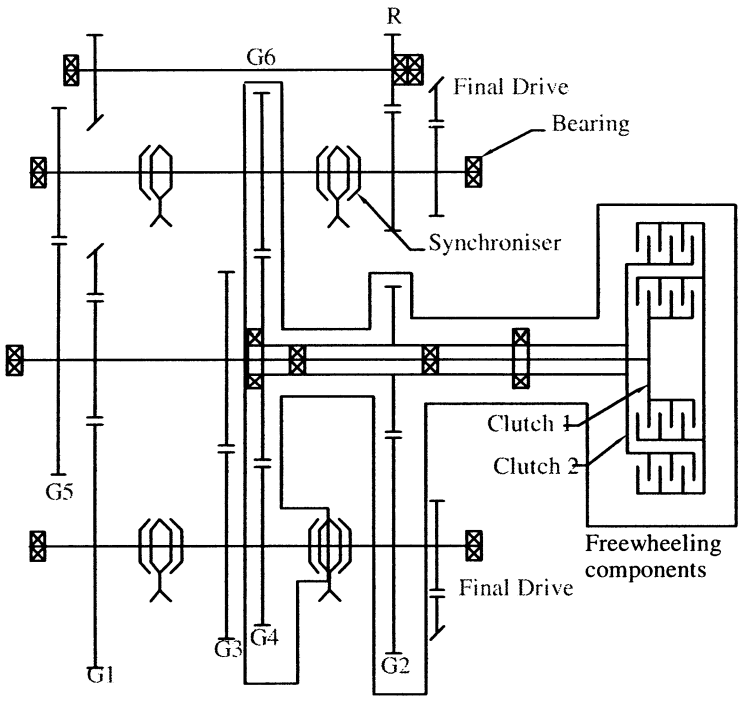

Figure 5.8: highlighted sources of drag torque that will affect the synchronisation of 2nd 4th and 6th gears

5.6.1 Model verification

It is also important to verify the developed drag as being a reasonable representation of drag torque acting on a synchroniser; this can be performed using synchronisation time and energy. The determination of speed synchronisation time is considered to be highly important to the selection of synchroniser design parameters [49]. It is a function of reflected inertia, initial and final speed, and net torque on the target gear. Defined as:

$$t_s = \frac{(\omega_f - \omega_i) I_{FW}}{T_C \pm T_D} \tag{5.18}$$

Synchroniser energy calculations are based on the kinetic energy change resulting from synchronisation, and the net energy required overcoming drag loss. Socin and Walters [49] define it, with the sign selection based on the shift type, as:

$$KE_s = \frac{(\omega_f - \omega_i)^2 I}{2} \pm E_D \tag{5.19}$$

where KE is kinetic energy, E is energy, and subsripts are D for drag and S for synchronisation. The drag energy loss is defined, assuming speed change is linear and drag constant as:

$$E_D = \int T_D d\theta = (\omega_f - \omega_i) T_D \cdot t_s \tag{5.20}$$

The other affect of drag torque in terms of duration is on the unblocking of the ring and the indexing of the hub. As the duration of hub indexing depends heavily on the alignment, it is preferable to evaluate the influence of drag for unblocking of the synchroniser ring. From appendix A:

$$t_B = \sqrt{\frac{2\delta \cdot I_{FW}}{T_D + T_B}} \tag{5.21}$$

In both equations 5.17 and 5.18 the "±" is applied based on shifting of the manual transmission, with upshifts being aided by drag and downshifts resisted by these losses. In the DCT this must now consider the speed change and direction of drag torque, with upshift and downshift drag torque resisting the speed synchronisation. This is a result primarily of the high clutch drag during the engagement process resisting all accelerations of the target gears from the steady state speeds.

Typically, without substantial knowledge of the acting drag torque on the mechanism, it is accepted that an average drag torque is used as an approximate solution. Lechner & Naunheimer [47] suggests that a reasonable approximation of torque loss of 2Nm is used as a design assumption for passenger vehicles, and can be used to estimate synchronisation time and energy for the evaluation of the accuracy of the drag model. In this instance it is reasonable to apply these equations numerically to the synchroniser model, and use the estimation provided by Lechner & Naunheimer [47] for the drag torque for comparative evaluation of simulation results.

The use of equations 5.17 to 5.19 for the estimation of synchronisation time and energy generated in the cone clutch provides some insight into the interaction of the applied torques on the mechanism. As previously stated, these estimation methods assumed that the drag torque resists all engagement of the mechanism. With the variation of drag over the duration of the synchronisation process, the resulting synchronisation time and energy must be significantly influenced. Initial conditions and model parameters are available in Tables 4.1 and 4.2.

Figures 5.9 and 5.10 present a comparison of the upshift and downshift synchronisation time and energy, respectively, between numerical results from simulations and defined theoretical results from ref [47]. These results suggest that the numerical determination of synchronisation time thorough simulation demonstrates very reasonable agreement with the classical theory presented by Lechner & Naunheimer [47]. However theoretical results consistently underestimate the simulations, particularly for low gears. This is most predominantly a result of the inability of theoretical results to evaluate the variation of drag torque over the synchronisation process as speeds change in the DCT for fixed clutch speed. Using assumed direction of drag torque for theoretical energy calculations highlights the independent nature of drag torque in the DCT and is the most significant limitation to theoretical calculation using equations 5.18, 5.19 and 5.21.

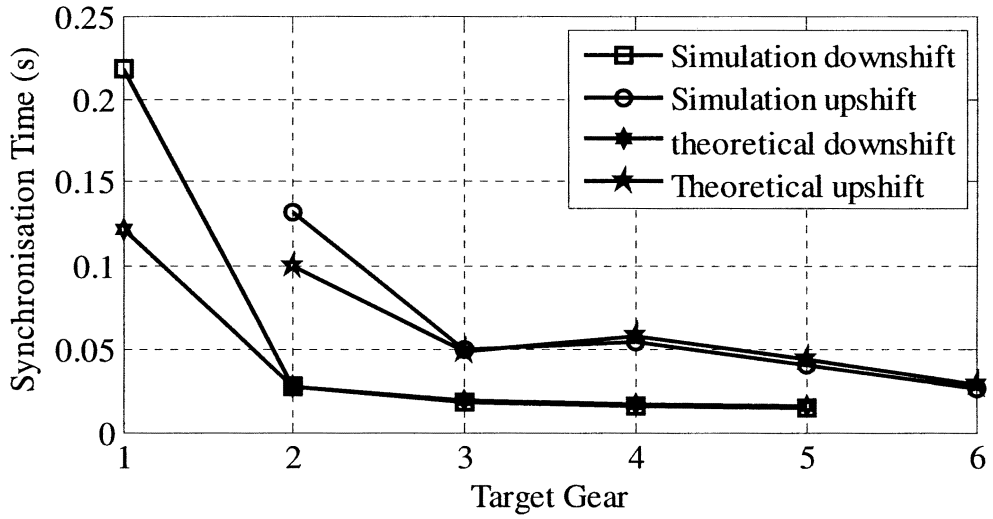

Figure 5.9: Synchronisation time for upshifts and downshifts

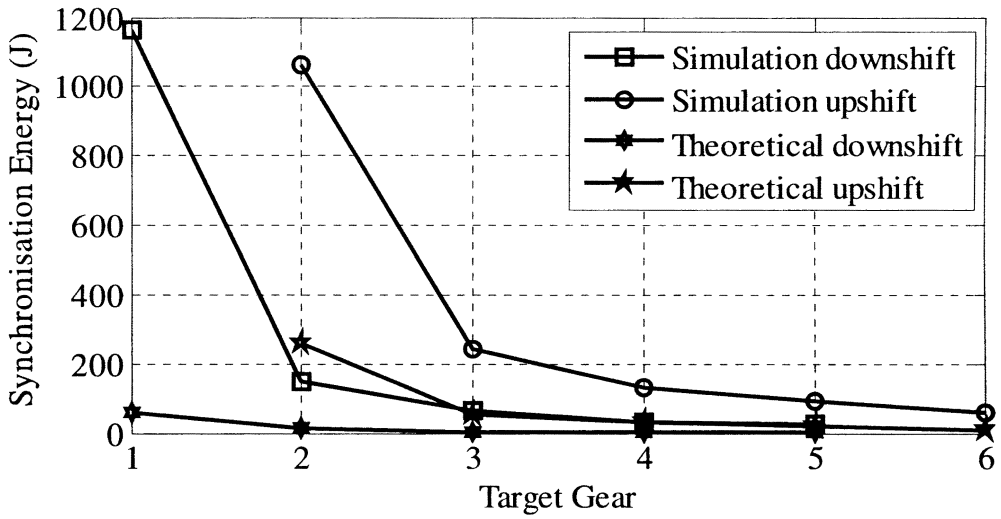

Figure 5.10: Synchronisation energy for upshifts and downshifts

The comparison of assumed drag torque with numerically calculated drag in Figure 5.11 demonstrates this variation, and is the most significant variation between theoretical and numerical results. Upshifts into second gear and downshifts into first gear demonstrate that the theory considerably underestimates the mean numerical drag, a result of very high differential speed in the wet clutch. Furthermore drag torque during downshifts with drag torque based on the absolute gear speed and clutch slipping speed, results in the relative motion of the clutches provide drag in the opposite direction to that generated from gearing. Thence opposing drag torques reduce the total drag torque acting in the model.

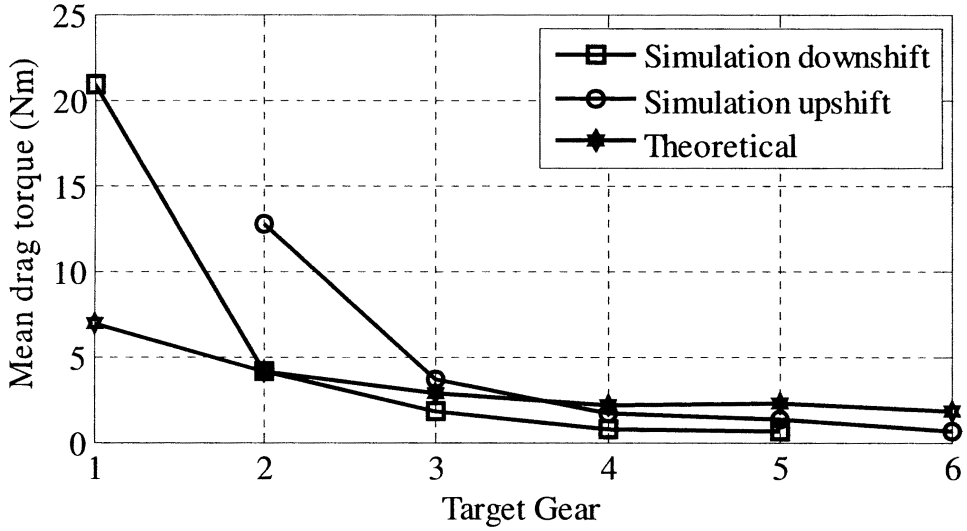

Figure 5.11: Assumed and numerical mean drag torques at the synchroniser

In Figure 5.12 the unblocking times are shown for both up and down shifts, using numerical results from simulations and developed in Equation 5.20. The upshift and downshift solutions for Equation 5.20 show identical results from the equation calculated as the change is sign of the drag torque is reflected in the blocking angle and the blocking torque. The simulated results are close but not identical for up and down shifts as there is the variation of relative and absolute drag torques during different shift types. Simulated and theoretical results present reasonable comparisons, however theoretical method tends to overestimate results by as much as 50% in some cases. This is an issue with the assumed direction and estimation of peak drag torque.

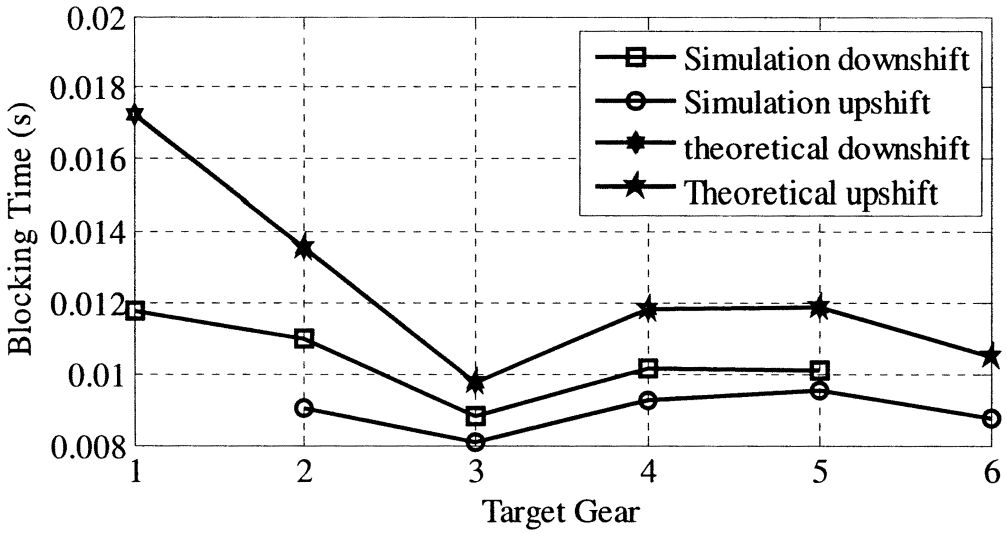

Figure 5.12: Unblocking time variation based on different drag torques

5.6.2 Numerical simulations of drag torque

5.6.2.1 Breakdown of drag torques

To demonstrate the influence of individual sources of drag torque on the mechanism simulations will be performed for a standard 3-4 upshift and for a 5-4 downshift. Results include a reference sleeve displacement plot and the breakdown of the total drag torque into individual sources of drag, with charts for absolute drag torque, associated with the gear speed, and relative drag, associated with the clutch slip speed.

These results for drag torque demonstrate the different influences of individual component drags. In both Figure 5.13 (b) and (c) graphics the bearing associated losses for absolute and relative speeds are very low, with the inter-shaft drag loss being similarly low. Friction losses in the gear teeth are highly dependent on the acceleration of the gear, affecting its direction of application, while windage gear losses are the second most dominant of the losses. Variation in friction losses results from torque loads on the gear increasing as it is accelerated during synchronisation and indexing.

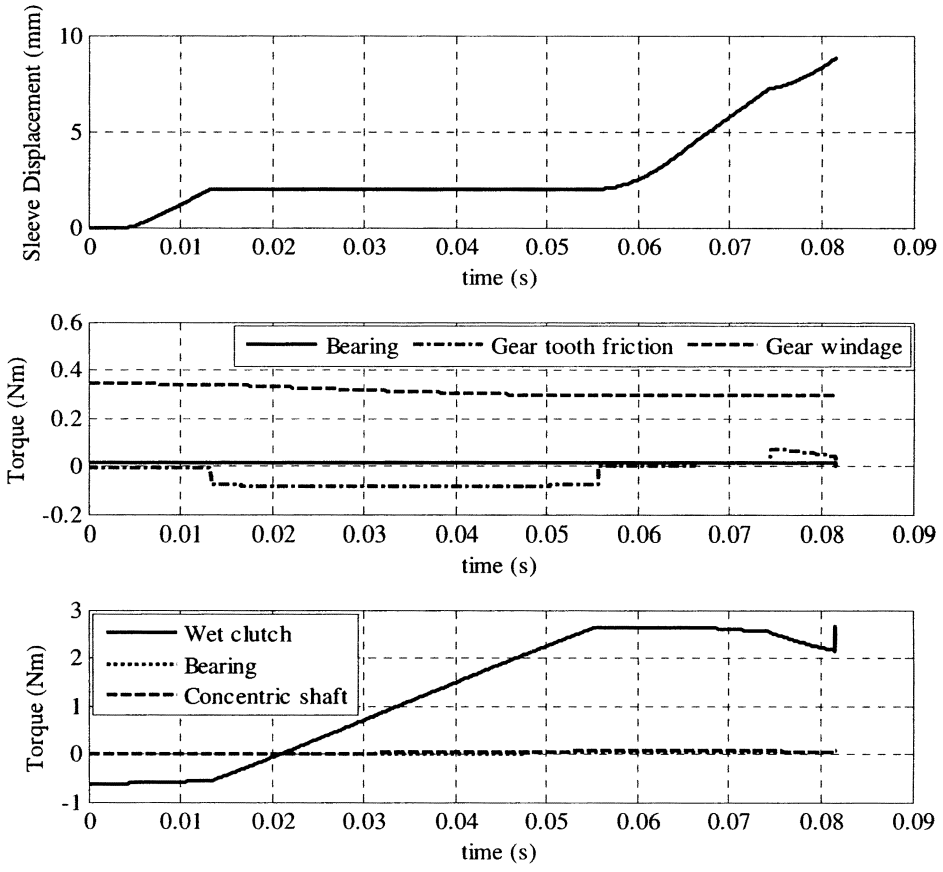

Figure 5.13: Drag torques for a 3-4 upshift. (a) Synchroniser sleeve displacement, (b) absolute drag torque, (c) relative drag torque

By far the most dominant loss is associated with the viscous shear in the wet clutch shown in Figure 5.13 (c), with results being substantially higher than for any other drag torque. Steady state conditions viscous drag is negative, however once the cone is engaged and the gear accelerated to the target speed the wet clutch loss reverses in direction and peaks once synchronisation is complete. This suggests that the resistance to synchronisation is maximised as the mechanism approaches slip speed in the cone of zero. Wet clutch drag is therefore the most significant drag torque, and contributing significantly to the variability of drag over the synchronisation process.

The results in Figure 5.14 demonstrate a similar result for those presented for upshifts. The downshift results, however, have shorter synchronisation duration as a result of the lower overall drag torque and initial steady state slip speed. Indeed the absolute drag torque in gears is countered by the relative drag in the clutch and the direction of this drag is maintained, unlike upshifts. Still, the peak drag torque also resists synchronisation and is achieved as the synchronous point is reached. Additionally a second peak is realised as indexing increases the slip speed further.

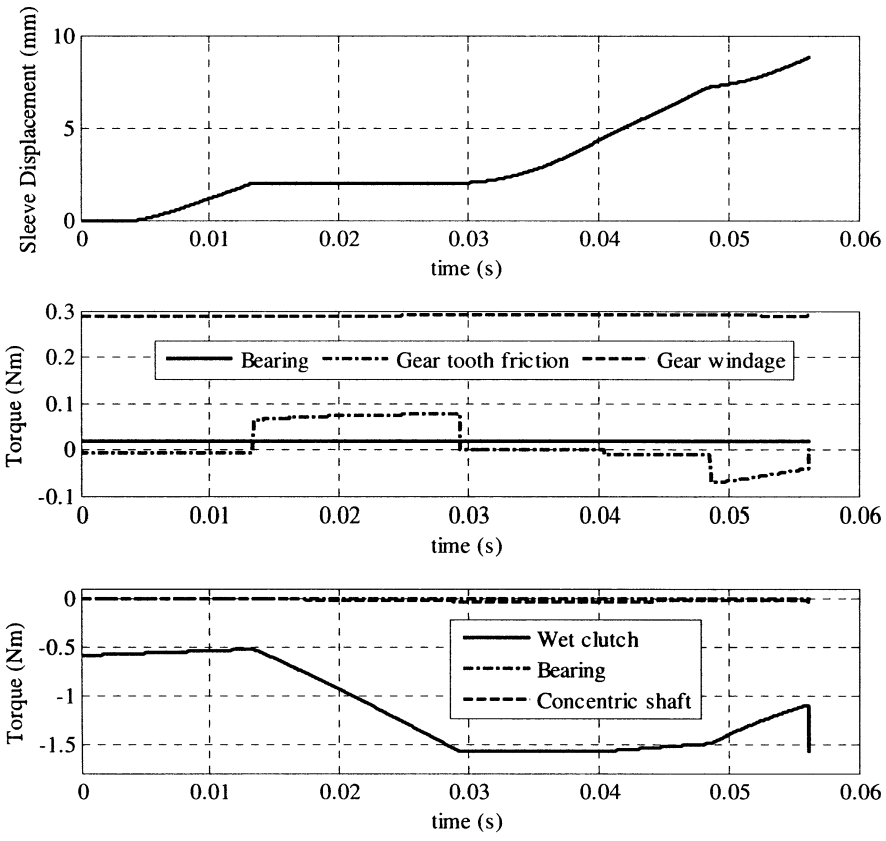

Figure 5.14: Drag torques for a 5-4 downshift. (a) Synchroniser sleeve displacement, (b) absolute drag torque, (c) relative drag torque

From the results presented in Figure 5.13 and Figure 5.14 important characteristics of the drag torque model are drawn. First, drags associated with windage and frictional losses are significantly less dominant in the process than the viscous losses in the multi-plate wet clutch. Furthermore, the losses generated by the wet clutch reach a peak once speed synchronisation has been completed, and can be exacerbated during indexing. This peak drag torque is potentially a significant contributor to block out and partial clash failures [49].

5.6.2.2 Drag torque variation between gears

As peak drag torque is achieved at the end of speed synchronisation, consideration of how these drag torques vary between different gears is now given. Therefore a series of simulations were performed to demonstrate variation in drag torque over the speed synchronisation of each gear, with unblocking and indexing ignored, in preparation for up and down shifts. Results are presented in the Figure 5.15 and 5.16.

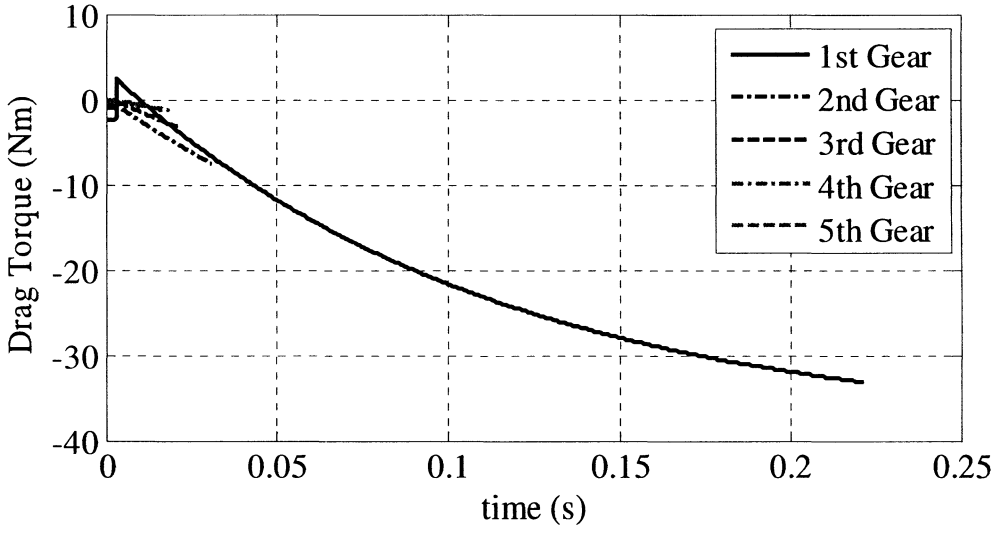

Figure 5.15: Drag torques developed during synchronisation for downshifts

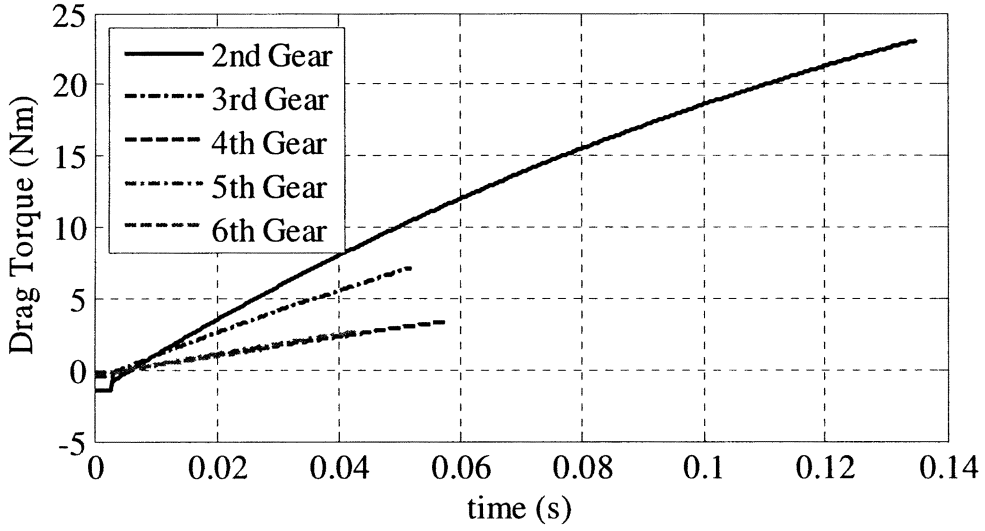

Figure 5.16: Drag torques developed during synchronisation for upshifts

Figure 5.15 presents the drag torque variation during speed synchronisation, beginning with contact of cone friction surfaces and ending when cone slip speed is zero for downshifts, whilst Figure 5.16 presents similar results for upshifts. These results suggest that drag torque always resists the engagement of the mechanism as a result of increased resistance in the wet clutch. Peak drag torques are reached as the cone clutch completes speed synchronisation and the slip in the wet clutch is maximised. Thus the drag torques peak at the point of synchronisation with maximum differential speed in the wet clutch, and with torques counterbalancing in downshifts, the peak drag torques are reduced.

Comparison of drag torque developed for different upshifts and downshifts demonstrates the significance of torque multiplication developed in the gear ratio, and the influence of fixed speed of the engaged gear. Most notably, the high speed differential between first and second gears results in the development of large drag torques from the open clutch once synchronised. This is further exacerbated through the gear ratios of both these gears, and, along with significant differential speeds, provides the reasoning for the application of multi-cone synchronisers; reducing synchronisation time and providing sufficient torque capacity to the mechanism such that high drag torque is overcome in short time frames.

5.7 CHAPTER SUMMARY AND CONCLUSION

In this chapter the process of developing damping coefficients of damping for a transmission model and modelling of the drag torque acting on a synchroniser mechanism within the frame of reference of the dual clutch transmission have been presented. This has focused on the inclusion of multiple sources of drag torque found in a DCT and applying literature based models to provide a reasonable estimation of drag torque. This includes losses associated with bearing, gear windage and friction, and the identified losses unique to the DCT of coupled shaft and clutch shear torques.

The application of lumped inertia methods to the establishment of a vehicle powertrain model incorporating a dual clutch transmission has required the estimation of damping coefficient parameters for the transmission system. Research by Changenet, Oviedo-Marlot & Velex [73] and Heingartner & Mba [72] have demonstrated the capacity to reproduce reasonable models of the drag torques affecting geared systems. By applying similar methods to those presented it has been possible to create the local drags at a various points in the transmission system. This has included wet clutch drag torque as the most significant contributor to overall drag torque. This is consistent with arguments put forward by the likes of Certez, *et al,* [8], Berger [3], and Wheals, *et al,* [11] that cite the significant drag torque developed during normal operations as a primary reason for seeking the development of a dry DCT.

Methods for estimating synchronisation time and energy have been used for comparison to literature based models of drag acting on a synchroniser for verification of the proposed models, with results that are quiet reasonable given the available information used to develop these drag models. Additionally the significance of the inclusion of wet clutch drag in the model should not be underestimated, particularly as it has been demonstrated to be the most significant source of drag torque in the mechanism. This is demonstrated in both Figure 5.13 (c) and Figure 5.14 (c), where maximum drag is achieved at synchronisation. This can negatively impact on ring unblocking, secondary displacement, and hub indexing. Also notice that manual transmission drag torque aids upshifts by slowing the target gear, but resists the downshift. This is no longer the case with the dominant drag in the clutch pack resisting all shift types for the majority of the process time.

The main issue to come from this aspect of research is the need for validation and verification of results. Several significant assumptions associated with the transmission architecture and sources of drag were made, such as the exclusion of oil churning and use of a constant gear friction coefficient. The influence of these assumptions would require more detailed evaluation than applied in this chapter, but as there is no experimentation, this is beyond the scope of this project.

5.7.1 Summary of contributions

This chapter covered the development of a reasonable drag torque model for application to a damping model in a dual clutch transmission powertrain model and as a resistance model for a simplified synchroniser mechanism model. The specific original contributions and findings of this chapter are:

1. Application of detailed drag torque models to estimate damping in a dual clutch transmission, including coupled wet clutches,
2. Application of the wet clutch losses as a source of drag torque in transmission modelling,
3. The development of a drag torque model for synchroniser mechanisms in a wet clutch DCT,
4. Demonstration of the contribution of wet clutch drag torque to actuation of a synchroniser mechanism in a DCT,
5. Identification and demonstration of two drag torque components in the synchroniser mechanism, related independently to gear speed and clutch slip speed, and
6. Identification of peak drag torques present during the synchronisation process for wet clutch DCTs.

CHAPTER 6: POSITIVE CONTROL OF DETRIMENTAL CHAMFER ALIGNMENTS IN SYNCHRONISERS

6.1 INTRODUCTION

The alignment of sleeve and hub chamfers before indexing commences is identified as a significant issue in synchroniser engagements for DCTs. The variation in chamfer alignment during hub indexing contributes significantly to uncertainty to engagement times. It is completely random and considered impractical to control for a variety of reasons, primarily cost. Secondly, identification of the regeneration of slip in the cone and its potential to detrimentally effect engagement of the chamfers needs to be resolved, particularly as it affects duration of chamfer alignment. The combination of these two issues leads to significant variation in the engagement of synchroniser chamfers, extending the engagement process significantly.

In terms of mechanism control, highly stable and repeatable engagement processes are desirable to enable reliable preshift preparation for automated transmissions. Simulation results have demonstrated some limited capacity for repeatability in simulation of synchroniser engagement time, particularly relating to the alignment of chamfers at the beginning of synchronisation, resulting in variations of synchroniser engagement of the order of 10ms, depending on operating conditions of the synchroniser and design of the mechanism. Further exploration of this issue is therefore required. This chapter undertakes the demonstration of a popular feedback control method for synchroniser engagement and simulation of different active alignment techniques will be developed in order to improve the repeatability of the hub indexing stage of synchroniser engagement.

As regeneration of slip in the synchroniser through the no load condition on the cone clutch post ring unblocking has been identified as a significant contributor to the phenomena of detrimental chamfer alignments, and can be considered as part of the origin of engagement delay. Elimination of the slip regeneration is considered to be one method for reducing variation in delay of chamfer alignment. To solve this issue an

alternative thrust piece design is presented that will continue to apply partial load to the clutch after ring unblocking and reduce the regeneration of slip in the cone clutch.

6.2 CONTROL OF DETRIMENTAL CHAMFER ALIGNMENT

In Chapter 4, it was demonstrated that, for specific conditions, this chamfer alignment can negatively influence the engagement of the mechanism. Specifically, it was identified that if the momentum gained through regeneration of slip in the cone clutch was of the opposing direction to the torque generated in the chamfers, the chamfers had to first brake and synchronise the target gear before engagement could proceed. This process is further hampered by the drag torque on the mechanism, as it increases regenerated slip, and also counters indexing torque under certain alignment conditions.

Figure 6.1 provides demonstrations of both good and poor chamfer alignments. Consistent with the earlier description the poor alignment is revealed by the chamfer torque having the opposing direction to drag and regenerated slip. It causes the extension of engagement, and is thus undesirable for repeatability of process; it is dependent on the shift regime and will differ for up and down shift situations.

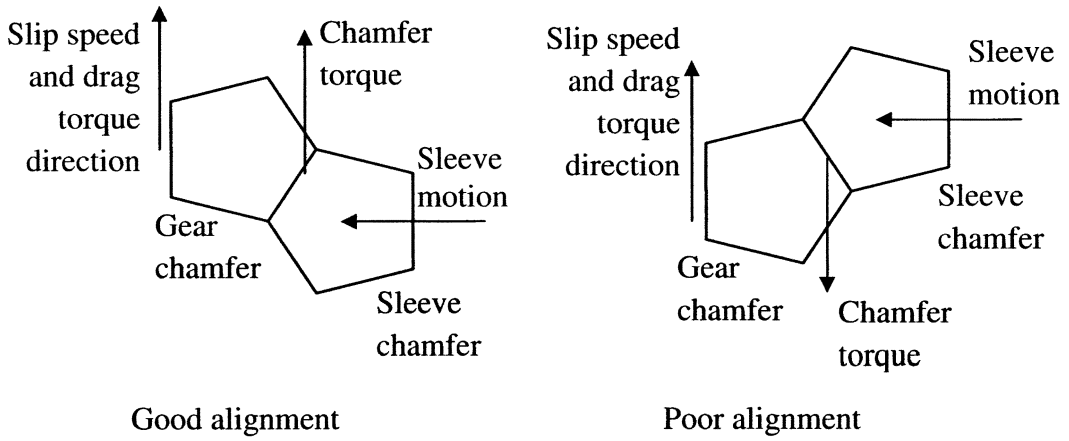

Figure 6.1: Example of good and poor chamfer alignments during synchroniser engagement

Figure 6.2 is an example of the tip on tip alignment of chamfers in the DCT. It represents a small portion of possible alignments, but if it eventuates it presents an unreasonable extension to the engagement of the mechanism, relying on higher drag torques in the wet clutch to initiate chamfer alignment.

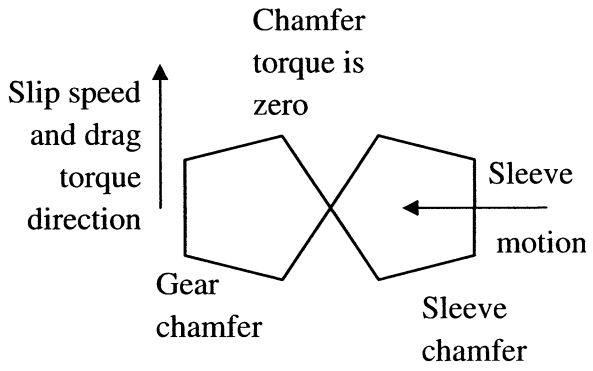

Figure 6.2: Example of tip-on-tip alignment condition

The issue of detrimental chamfer alignment is demonstrated with two groups of simulations. The first series use the wet clutch DCT drag torque model, with a combination of chamfer alignments for both up and down shifts used to demonstrate the issued identified previously. The second group of simulations is for the dry clutch DCT, again with different alignments and for up and down shifts. This significance of this variation is that the dry clutch will significantly change drag torque acting on the synchroniser, simulated by removing the wet clutch component of the drag torque. For comparison the generic drag torque equations for wet clutch is shown in equation 5.1 it is modified below for dry clutch transmissions as shown in equation 6.1:

$$T_D = -sign(\omega_G)(T_W + T_F + T_B) - sign(\Delta\omega_{CL})(T_{SH} + T_B) \qquad (6.1)$$

6.2.1 Baseline simulations

A series of baseline simulations will be carried out to demonstrate these particular chamfer alignment issues. The synchroniser parameters are consistent with those presented in Chapter 4, and the initial sleeve speed is 1500RPM.

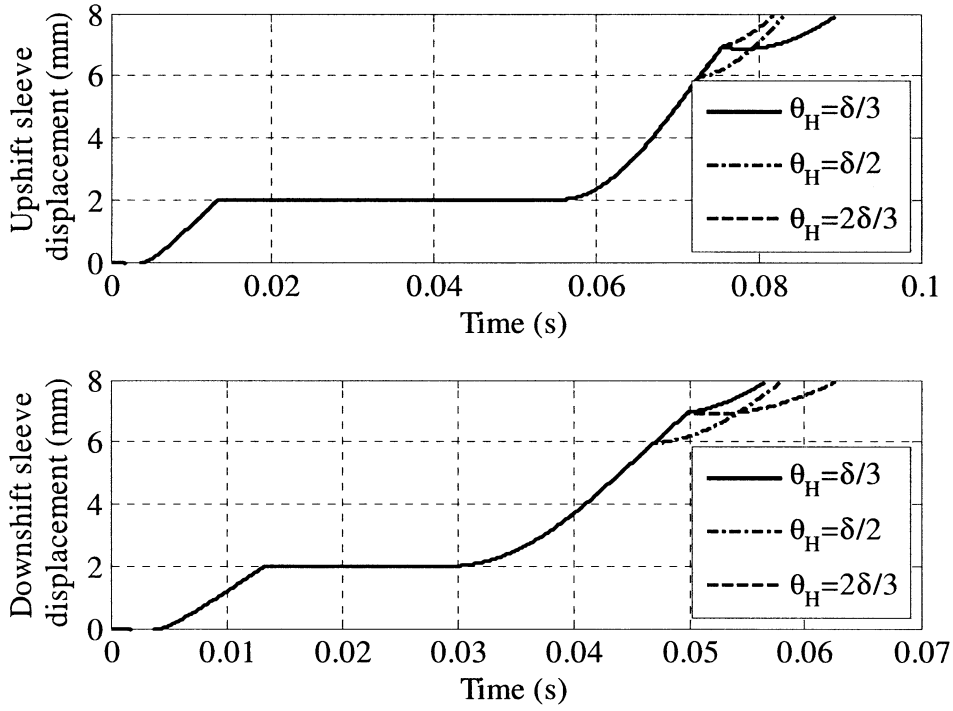

Figure 6.3: Demonstration of different alignment issues for wet clutches, fourth gear is synchronised with third gear engaged (top) and fifth gear engaged (bottom)

The simulations in Figure 6.3 present the variation of alignment in the synchroniser mechanism for up and down shifts, targeting fourth gear. For the up shift synchronisation (top), engaged in 3rd gear and targeting 4th, $\theta_H = 2\delta/3$ is representative of good alignment, where both drag and chamfer torques having the same direction enabling rapid alignment. At $\theta_H = \delta/2$ the tip-on-tip alignment condition is experienced, with high drag torque re-aligning the chamfers to an advantageous alignment before successful engagement. Finally, with $\theta_H = \delta/3$ the poor alignment condition results, where the chamfer torque must first brake the hub and target gear speed before continuing with the engagement, resulting in the sleeve moving backward. For specific alignment angles it is possible here for the sleeve to be forced backwards over the tip of the hub chamfers, moving from poor to good alignment conditions. The difference in these results is the duration of the indexing of the hub, with the poor alignment extending engagement.

Conversely, for the down shift synchronisation from 5th gear (bottom) $\theta_H = 2\delta/3$ results in poor alignment. Again $\theta_H = \delta/2$ for the tip-on-tip condition, and $\theta_H = \delta/3$ with good alignment. In terms of good, tip-on-tip, and poor alignments the results are similar to upshift simulations, but the different direction of drag torque resulting from

slip in the wet clutch changes the direction of regenerated slip, reflected in the variation in detrimental chamfer alignments in up and downshift simulations. With the change in the detrimental alignment condition, for the up shift present where $\theta_H = \delta/3$, while for the down shift present with $\theta_H = 2\delta/3$, the chamfer torque is used to brake this relative motion before proper engagement can occur. Thus the it is suggested that the use of unidirectional chamfers or similar designs are not possible for the wet clutch DCT.

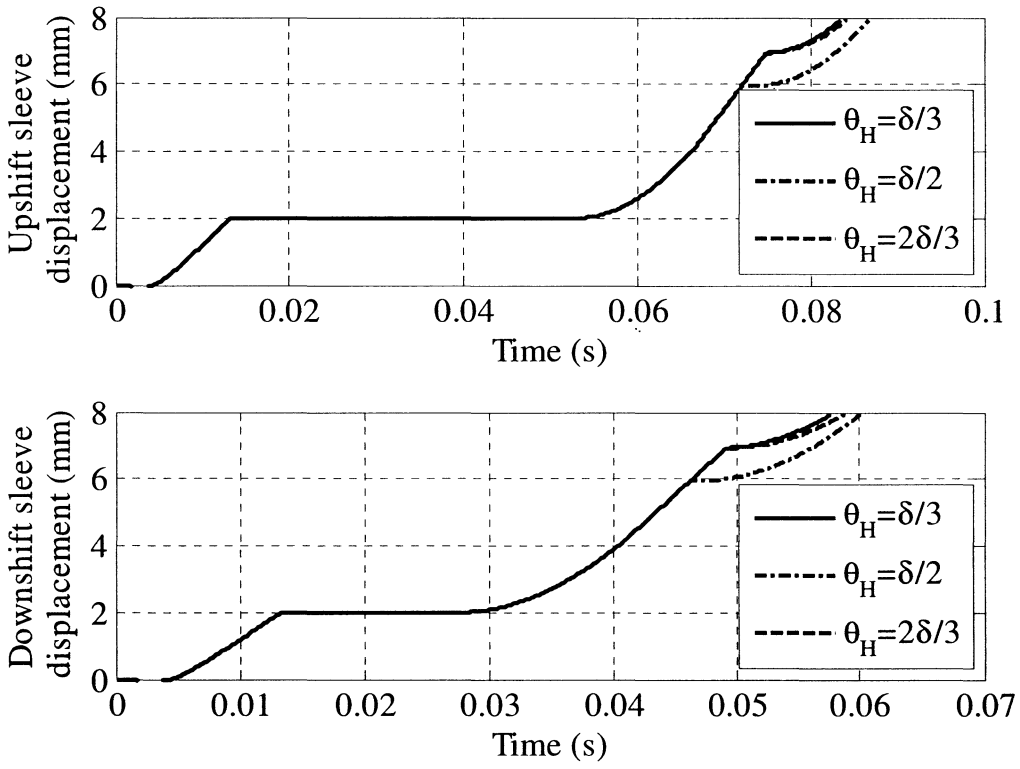

Figure 6.4: Demonstration of different alignment issues for dry clutches, fourth gear is synchronised with third gear engaged (top), and fifth gear engaged (bottom)

Figure 6.4 indicates a different result comparing wet to dry clutch simulations. The results demonstrate that detrimental alignment is present in $\theta_H = 2\delta/3$ for both up and down shift synchronisation simulations, a consequence of lower peak drag torque now being dominated by the absolute torque rather than the relative drag in the wet clutch. Additionally, with much lower drag, regenerated slip and subsequent braking period is reduced significantly.

The tip-on-tip issue presented in $\theta_H = \delta/2$ takes longer to engage than the simulation of adverse alignment issue. This is a consequence of the low drag torque taking longer to realign chamfers. These results are poorer for the downshifts than upshifts as the relative and absolute components of the drag torque counteract each other and reduce

the total drag present in the system for the downshift synchronisation. This affects the rate at which drag can realign chamfers before continuing with the engagement. Indeed it may be possible under the correct conditions for the two different drag torques to cancel out the drag acting on the system and prevent drag realignment from the tip-on-tip condition.

The results in Figure 6.3 and Figure 6.4 demonstrate that under certain circumstances it is possible to develop conditions where detrimental alignment of chamfers occurs. These conditions are heavily dependent on the drag torque present, slip regeneration and alignment of chamfers. The consequence being extended engagement of the mechanism as a result of the restricted alignment of sleeve chamfers with the hub during indexing.

6.3 FEEDBACK CONTROL OF THE SYNCHRONISER

Feedback control of the chamfer engagement is realised through tracking the displacement of the sleeve. It was demonstrated previously that the forward motion of the sleeve is associated with positive chamfer engagement. If the sleeve stops or is reversed during the chamfer engagement process then there is detrimental chamfer engagement. For this condition the idle hydraulic cylinder should be engaged to push the sleeve back and then re-engage the chamfers.

Figure 6.5 represents the control algorithm used in this feedback control. It identifies either the stopping or reversal of the sleeve, both of which indicate a detrimental engagement of the mechanism, and overrides hydraulic control. In this method the idle cylinder is pressurised and the control cylinder is released to rapidly push the sleeve backwards and allow the chamfers to re-align. These are demonstrated in the following simulations using ideal input pressures when overriding the engagement control, minimising engagement responses to provide best possible engagement.

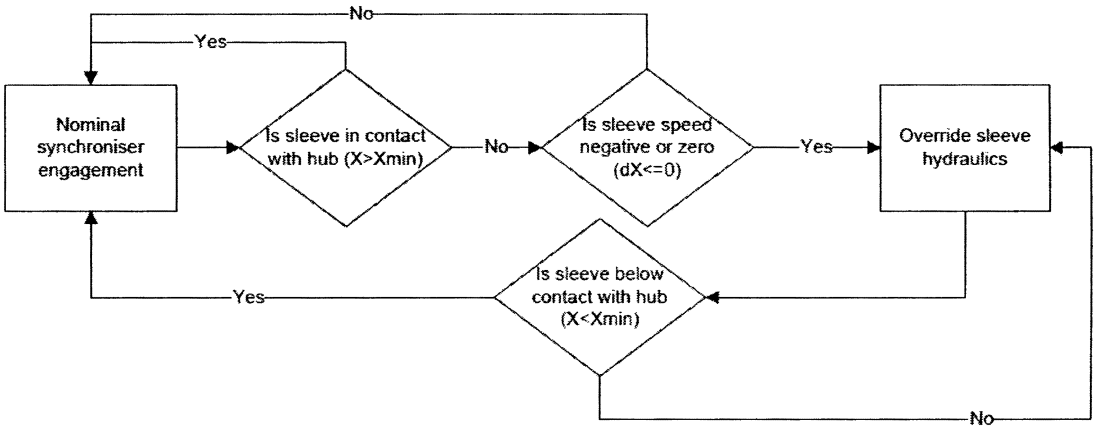

Figure 6.5: Synchroniser engagement override control algorithm

6.3.1 Simulations

To demonstrate the actuation of the synchroniser mechanism, simulations of the synchroniser engagement identical to those performed in section 6.2 will be performed with the inclusion of the override control algorithm. For this algorithm the override pressure will be ideal and not include any time delay characteristics during override control, demonstrating the ideal control of the mechanism, and minimising delay in the engagement.

Closed loop control of chamfer alignment in the synchroniser with wet clutch drag is shown in Figure 6.6. In the upshift (top) results the poor alignment with $\theta_H = \delta/3$. There is activation of the override control and the sleeve is pushed back to before the beginning of chamfer alignment before restarting the engagement. This allows the drag torque and existing slip to realign chamfers and restart engagement. For detrimental alignment of the downshift, Figure 6.6 (bottom), similar results to Figure 6.3 prevail for detrimental alignment. With both of these overridden engagements, there is significant delay as the hydraulic control system responses to the control signals and the sleeve moves back, stops and again engages the chamfers. It should be noted that it is possible for the realignment to engage the detrimental chamfer flank a second time and the poor alignment condition will be repeated as the new chamfer alignment is still uncontrolled.

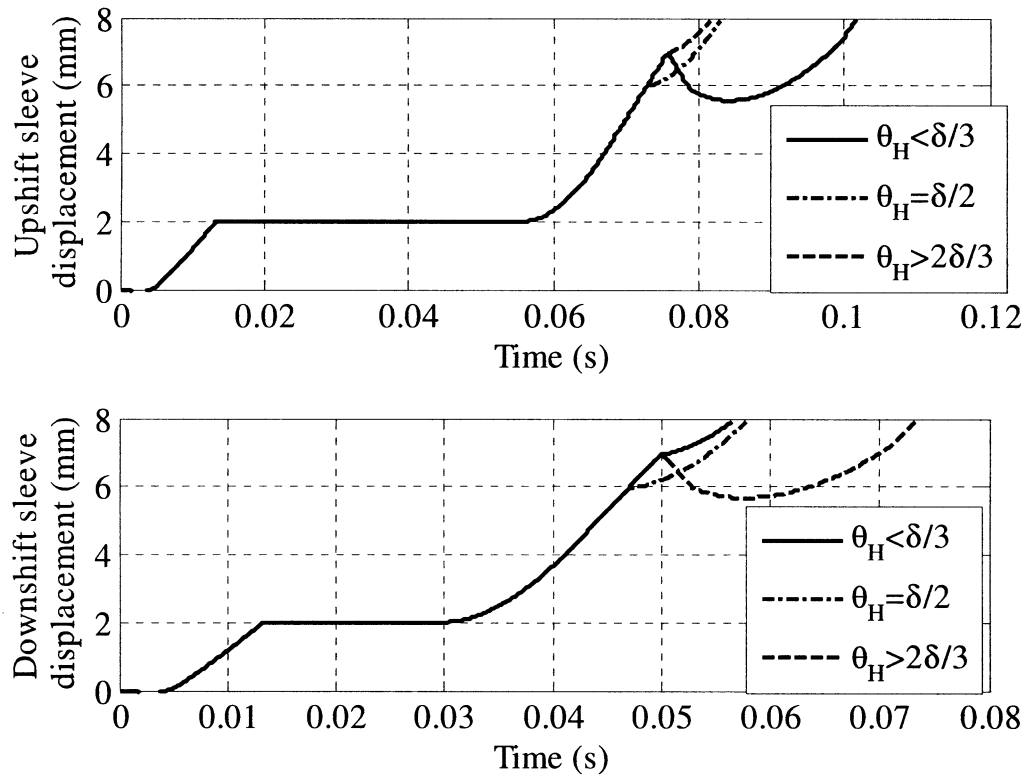

Figure 6.6: Sleeve displacement results for closed loop alignment control of wet clutches for upshift (top) and downshift (bottom)

Figure 6.7 shows the hydraulic cylinder pressures for the active cylinder corresponding to the simulations in Figure 6.6. In particular, reference to the upshift results and the downshift result corroborate the sleeve displacement in Figure 6.6. When alignment control is activated pressure rapidly drops in the active cylinder and builds up in the idle cylinder as the override algorithm takes control. With rapid backward motion of the sleeve, when the active cylinder is again pressurised it must stop sleeve motion and reengage the hub chamfers. The results demonstrate that the use of active control extends the overall engagement time of the mechanism by approximately 20ms, substantially more than the uncontrolled engagement.

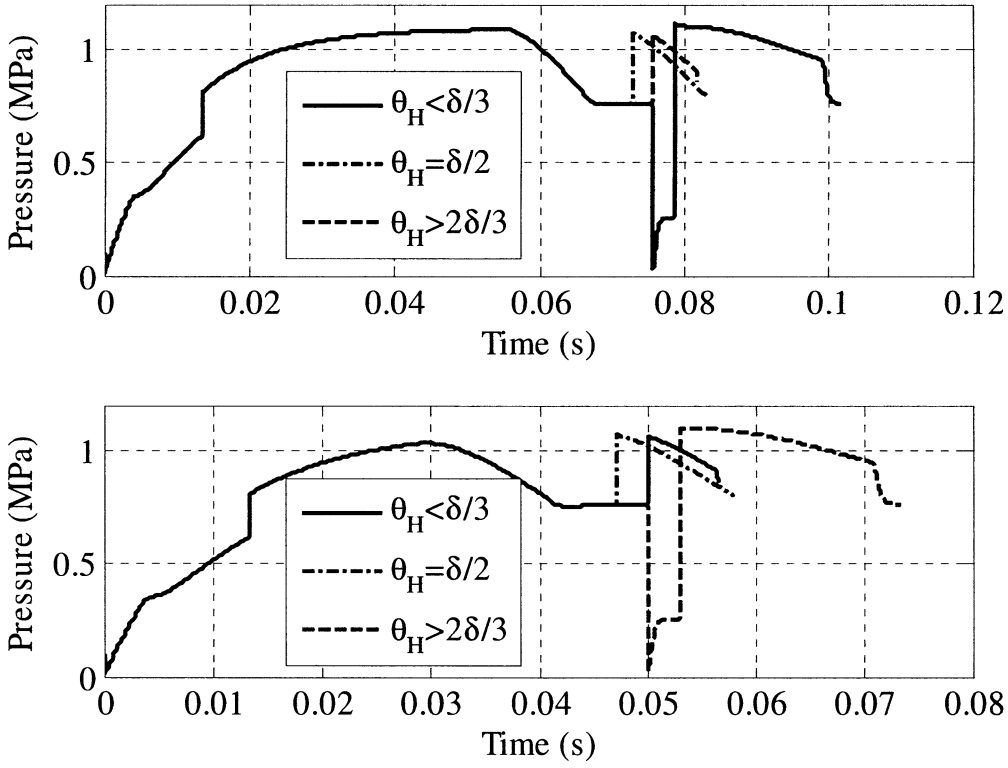

Figure 6.7: Active and idle cylinder pressures for closed loop alignment control of wet clutches for upshift (top) and downshift (bottom)

The simulation results in Figure 6.8 present the active alignment control for dry clutches DCT synchroniser engagement. In both cases alignment control is activated when $\theta_H = 2\delta/3$ indicating that there is minor detrimental engagement of the chamfers, with closed loop control overriding the engagement of the mechanism. However Figure 6.4 suggests that this is unwarranted. The results in Figure 6.9 are for the cylinder pressures corresponding to Figure 6.8, demonstrate the triggering of the release of the active cylinder to restart chamfer engagement of the synchroniser.

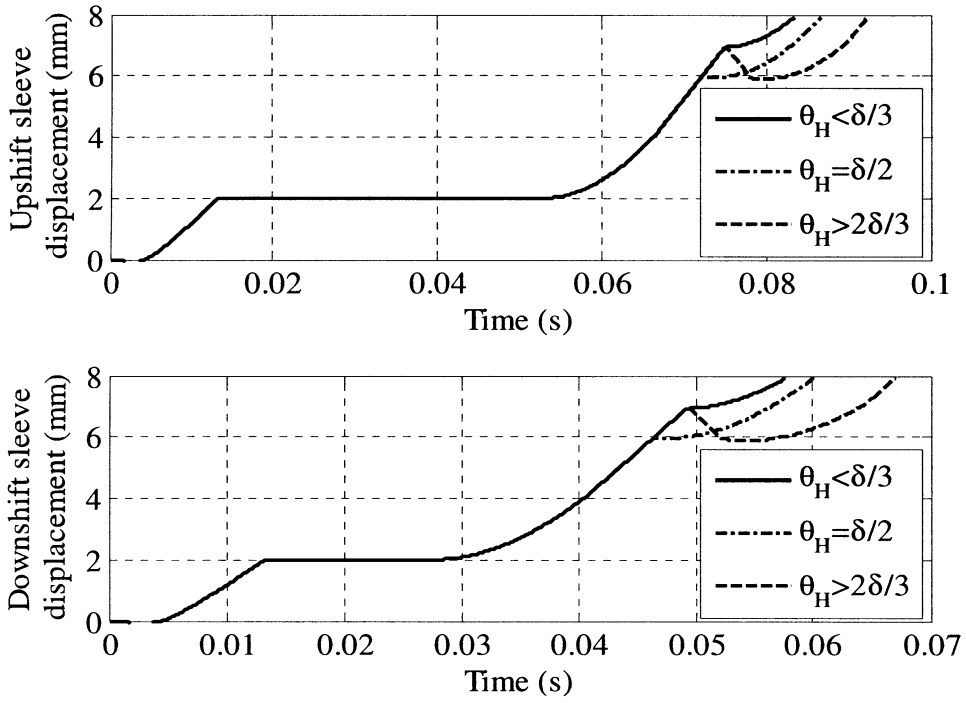

Figure 6.8: Sleeve displacement results for closed loop alignment control of dry clutches for upshift (top) and downshift (bottom)

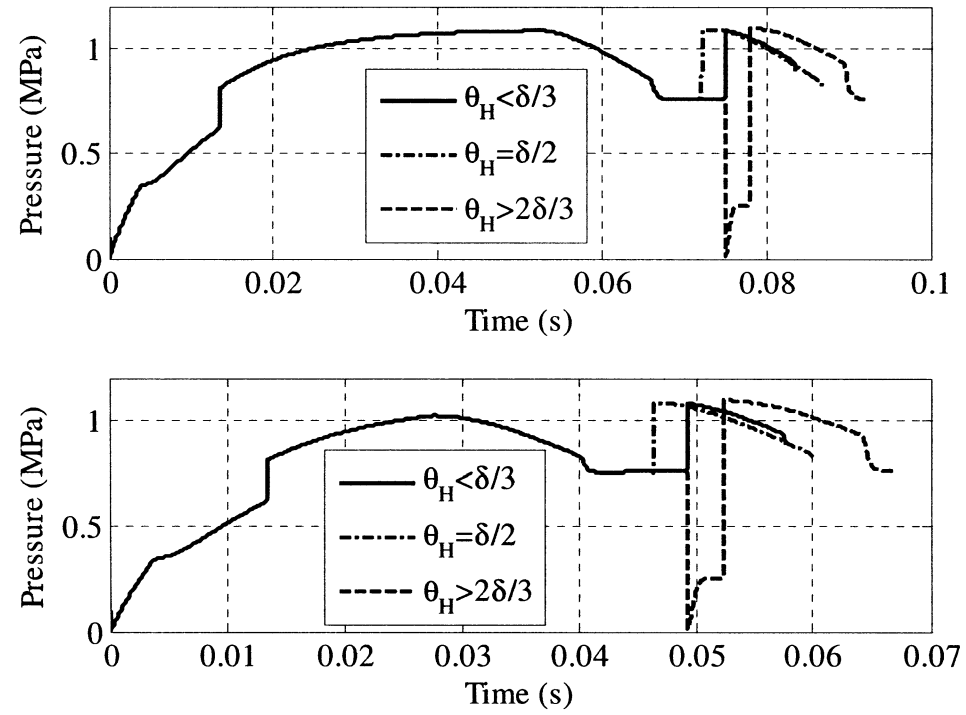

Figure 6.9: Active and idle cylinder pressures for closed loop alignment control of dry clutches for upshift (top) and downshift (bottom)

The simulations presented in Figures 6.6 to 6.9 demonstrate that the use of active alignment control does not entirely resolve this issue of poor chamfer alignment. There

are two problems that will still be present even if a feedback method is implemented in the synchroniser mechanism. First and foremost, in each of these simulations the override control significantly increased the engagement time of the synchroniser by between 10 and 20ms in each case. Thus while it does not reduce the engagement time this method positively controls the engagement, which may be preferred over the passive control even with extended delay of engagement.

Secondly, and potentially more significantly, when forcing the sleeve backwards, with no tracking of relative chamfer alignment there is a significant probability that the same result will entail. That is to say the sleeve may move backwards and as it moves forward to re-engage the hub it will engage again in a detrimental alignment. This is primarily a result of there being no positive control of the alignment if the mechanism, repeated engagements may ensue.

These issues demonstrate the difficulty in finding a simple method for override control that will provide minimal delay and a repeatable engagement time. This is a product of the difficulty inherent in even tracking the two separate chamfer sets positions relative to each other, owing to the compact nature of the synchroniser and cost involved in deploying any such tracking and control system. Thus any methods for tracking alignment of the synchroniser chamfer alignment are costly in real terms. Alternate methods must then be considered.

6.4 DISTURBANCE METHOD SIMULATIONS

Reverting back to the main issue at hand, if the engagement of the chamfers proceeds under normal operating conditions, the variation in rate of engagement and detrimental alignment that have been detailed at the beginning of this chapter above are persistent. There will remain the constant possibility of detrimental chamfer alignment and chance for tip-on-tip block out of the synchroniser. An alternative solution is proposed in that an external disturbance is introduced into the system to generate torsional vibrations to aid the realignment of synchroniser chamfers during indexing. This concept is consistent with ref [49] insofar that high vibration is identified as a source of premature unblocking of the synchroniser ring. The two methods are presented here are:

- Case 1: the use of an eternally applied torque, or

- Case 2: introduction of impulse by changing inertia of part of the subsystem.

These two mechanisms should be considered as blind control of synchroniser chamfer alignment, where detrimental alignment is not detected and activation of the mechanisms are performed for each engagement independent of alignment conditions. Such that once a minimum displacement is achieved the mechanism is triggered and engagement continues normally whilst under the influence of the suggested excitation mechanism.

For both methods an extra degree of freedom is introduced through the inclusion of a shaft element and inertial disk. For Case 1 an externally applied load of 20Nm is applied to this element to generate an additional load on the synchroniser and increase the rate of rotation. The direction of the applied load is with the slip speed of the clutch as this relative speed is the same direction as the drag torque and thus increases the effective resistance torque to override the chamfer torque in poor alignment conditions. Alternatively, Case 2 applies an impulse by instantaneously increasing the inertia of the additional element. Thereby providing the addition of vibration response in the synchroniser model to increase the rate of chamfer realignment and reduce indexing time. Conceptually, the intention is to introduce an external excitation that will provide sufficient oscillations to increase the rate of engagement of the chamfers.

6.4.1 Case 1: Externally applied torque

Application of an externally applied torque to the synchroniser model that will generate an oscillatory response requires the addition of an extra degree of freedom to the system. Beginning with the original rigid body synchroniser model an extra degree of freedom is added to the system to represent a simple friction clutch; the two are connected using a stiffness element, (see Figure 6.10. In terms of physical application it is more desirable to apply the external torque in the same direction as drag torque to increase the rate of engagement. It is therefore suggested that the new system could reasonably be based on a small clutch interlocking the two primary shafts. The resulting model would then have a slip speed derived from the clutch slip, and one mechanism can be applied for all gears in the transmission.

Figure 6.10: Schematic for Case 1, external excitation through an applied torque

The equations of motion of the proposed model in Figure 6.10 are then:

$$\begin{bmatrix} I_C & 0 \\ 0 & \gamma^2 I_{FW} + I_P \end{bmatrix} \begin{Bmatrix} \ddot{\theta}_C \\ \ddot{\theta}_P \end{Bmatrix} = -\begin{bmatrix} K_C & -\gamma K_C \\ -\gamma K_C & \gamma^2 K_C \end{bmatrix} \begin{Bmatrix} \theta_C \\ \theta_P \end{Bmatrix} + \begin{Bmatrix} -T_{CONT} \\ T_{SYN} \end{Bmatrix} \quad (6.2)$$

where θ_C is control system rotation DOF, θ_P is pinion DOF, I_C is control system inertia, I_P is pinion inertia, K_C is control shaft stiffness, T_{CONT} is control torque, and T_{SYN} is synchroniser torques. Defining the external torque, T_{CONT}, is rather simple. By making the torque relative to clutch slip, most notably for wet clutch DCTs, it is in the same direction as the relative drag torque. Therefore the best use of T_{CONT} is to counteract the chamfer torque and rely on the combined external torque and drag torque to perform the realignment. For these simulations, an applied torque of 20 Nm is more than sufficient to overcome the chamfer torque, which is generally 8 to 10 Nm. For the purposes of the simulations I_C is 1^{-3} kg-m^2, and K_C is 1^4 Nm/rad. This is representative of the addition of a small inertia to the system on a reasonably stiff shaft.

To maintain continuity the same initial conditions and parameters are used here as for previous simulations in the section. The control torque is actuated only once there is contact between sleeve and hub chamfers. This is chosen as it will not add to the regeneration of slip in the cone clutch and only come into effect once there is chamfer engagement. The torque will be applied to all engagement types, ignoring the need for closed loop control for detrimental engagements.

The results of using a mechanism to apply an external torque during hub chamfer engagement in the wet clutch DCT are presented in Figure 6.11 above. Overall the engagement time is not significantly affected through the addition of additional

component inertia. The delay associated with the tip-on-tip condition during engagement is successfully reduced with the additional torque aiding realignment. However, the results for poor chamfer alignment are approximately equal to the results presented in Figure 6.3. This suggests that there is limited influence of this mechanism for wet clutch type DCTs as a result of the multiple arrangements of the indexing and drag torques. However, positive control of chamfer alignment is still achieved for the synchroniser without the delay associated with the closed loop control simulations.

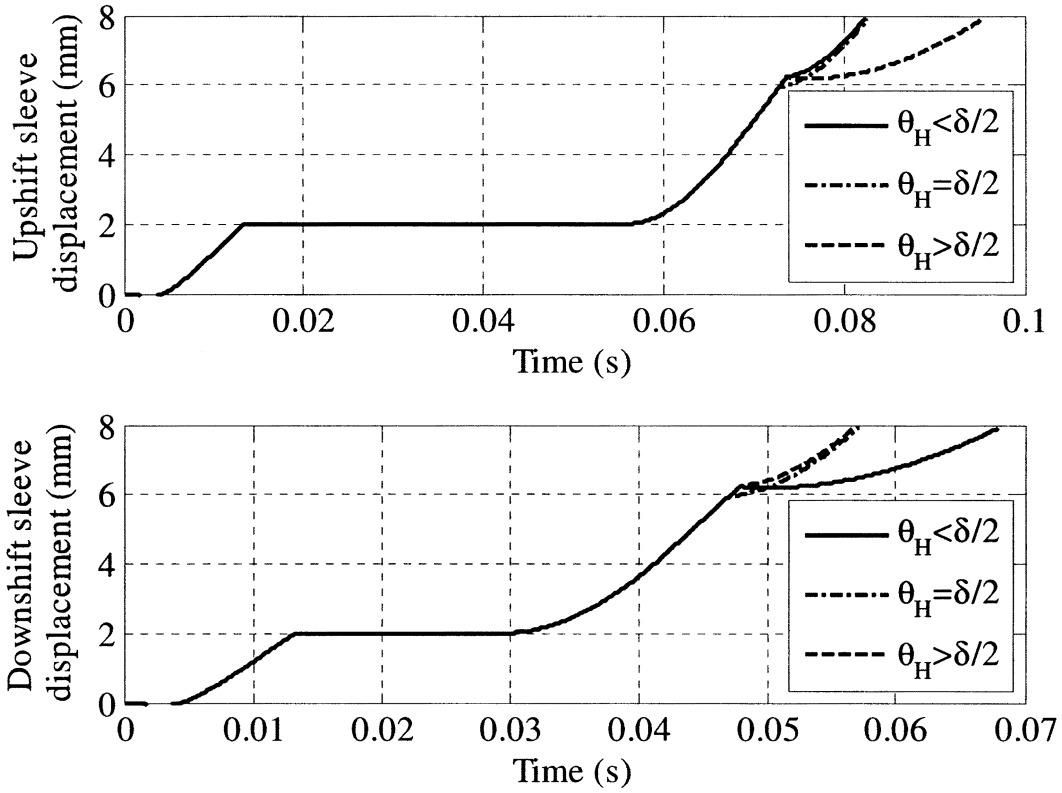

Figure 6.11: control of chamfer alignment in a wet clutch DCT using an externally applied torque for upshift (top) and downshift (bottom)

The same externally applied torque is simulated here for a dry clutch DCT. Figure 6.12 results show improved performance over the wet clutch type simulations. Compared to the baseline dry clutch control, the delay associated with tip-on-tip contact conditions is reduced. Thus positive alignment control is achieved to override this type of engagement. However delay results in the chamfer alignment for downshifts with $\theta_H=\delta/3$ with control torque and chamfer torque being of opposite direction. Again the majority of the engagement times are about equal, but when chamfer torque opposes the applied torque the overall engagement times are slightly increased.

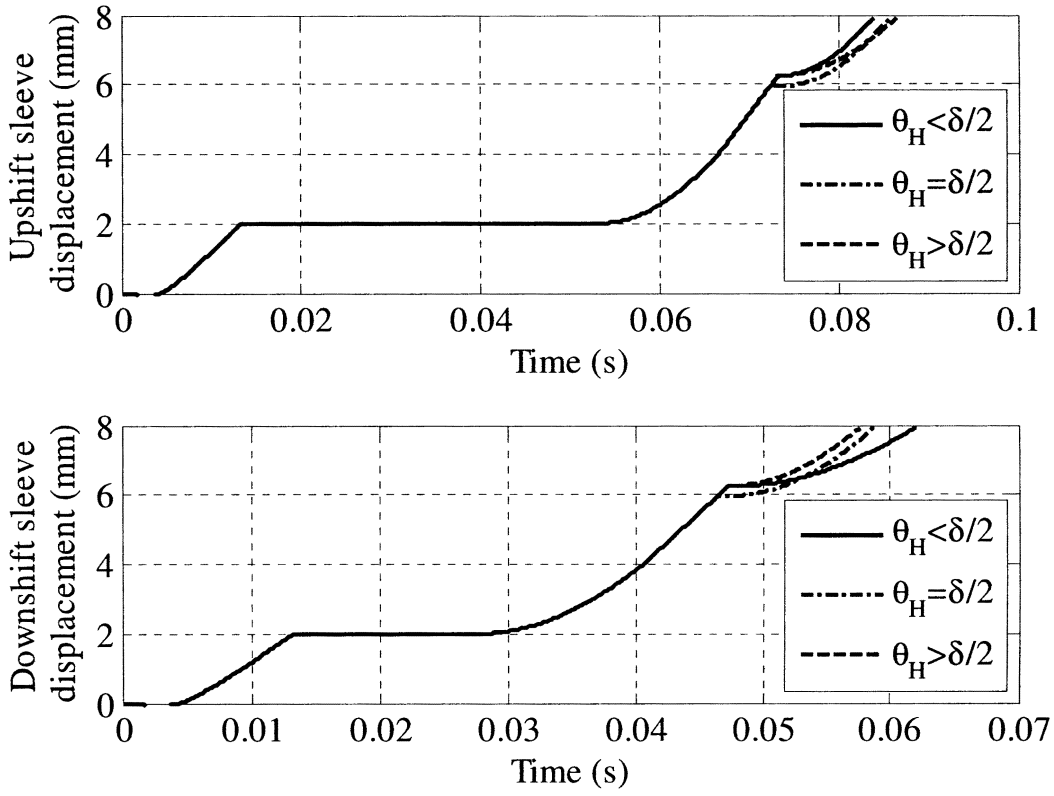

Figure 6.12: Control of chamfer alignment in a dry clutch DCT using an externally applied torque for upshift (top) and downshift (bottom)

Applying additional torque to the synchroniser mechanism during the hub indexing phase has the potential to overcome the issue of synchroniser tip-on-tip engagement and detrimental chamfer engagements, particularly for dry clutches as well as wet clutches to a lesser extent. This is a result of additional torque aiding re-alignment, but with the applied torque partially reducing the effects of chamfer torques in cases when chamfer and control torque are opposed. This is a similar result to Figure 6.3 if the synchroniser engages without the use of any control tool; however the use of a tool to override engagement provides positive control for the synchroniser alignment. Comparison to the closed loop method in Figure 6.9 is more noteworthy, with the delay associated with hydraulic control eliminated from the engagement. Accordingly, the suggested method provides active control of alignment without inclusion of engagement delay in Section 6.3.

6.4.2 Case 2: Impulse from inertia change

By generating an impulsive response in the synchroniser, the excitation may be used to realign the indexing chamfers and aid engagement. Again, the combined synchroniser

and excitation mechanism can be considered a two degree of freedom system, two inertias connected by a single shaft (see Figure 6.13). The inertia of the freewheeling target gear is already known, and with the exciter on the primary shaft, its impulse is increased by the inclusion of the gear ratio.

Conceptually the inertia change is not unlike a centrifugal governor, where above certain speeds there is an increase in rotating inertia that prevents continued acceleration. Unlike this governor, the change in inertia is not controlled using proportional control to limit shaft speed. Rather the inertial change is initiated through an external signal once contact between sleeve and hub is determined, the inertia then provides a step response increase to inertia and excitation is initiated to aid chamfer alignment.

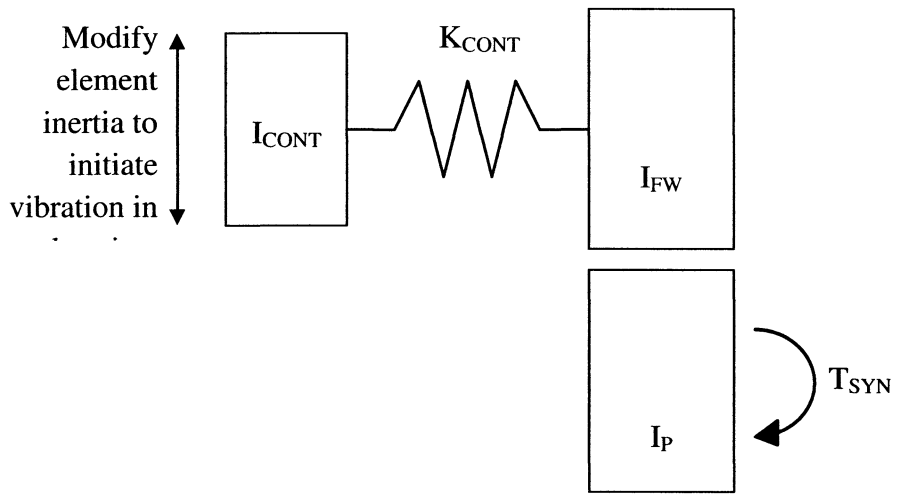

Figure 6.13: Example model of Inertia change system for Case 2

The equation of motion is very simple for the free vibration of the system. Using Newtonian mechanics in matrix form for Figure 6.13:

$$\begin{bmatrix} I_C & 0 \\ 0 & \gamma^2 I_{FW} + I_P \end{bmatrix} \begin{Bmatrix} \ddot{\theta}_C \\ \ddot{\theta}_P \end{Bmatrix} = -\begin{bmatrix} K_C & -\gamma K_C \\ -\gamma K_C & \gamma^2 K_C \end{bmatrix} \begin{Bmatrix} \theta_C \\ \theta_P \end{Bmatrix} + \begin{Bmatrix} 0 \\ T_{SYN} \end{Bmatrix} \tag{6.3}$$

The inertia I_C, must be considered as a step response, using:

$$I_C = \begin{cases} I_{C0} & X_S < X_C \\ I_{C0} + \Delta I & X_S \geq X_C \end{cases} \tag{6.4}$$

Where I_C is control system inertia ($_0$ for initial, Δ for change in inertia), X_S is sleeve displacement and X_C is the minimum contact displacement to the hub chamfers. The torque T_{SYN} represents the net torque acting on the synchroniser. It should be

considered variable and unknown, particularly as drag torque is dependent on both slip and absolute speeds of the clutch and target gear, respectively. Additionally, as the inertia of the target gear, $\gamma^2 I_{FW} + I_D$, varies for each gear, it must be concluded that a chosen inertia change must be unique to a given engagement condition.

Table 6.1: Simulation model properties for excitation method

	Stiffness (Nm/rad)	*Initial inertia (Kg-m^2)*	*Final inertia (Kg-m^2)*
Wet	1e5	0.0001	0.0100
Dry	1e6	0.0001	0.0100

Again the same synchroniser parameters and initial conditions are used for the simulations, with the inertia change initiated once a minimum displacement is achieved. Similarly to previous simulations both wet clutch and dry clutch drag torque models for the synchroniser will be applied to the simulations.

The application of a high inertia change to generate impulsive vibrations aiding the chamfer engagement during indexing is demonstrated in Figure 6.14, indicating that there are some limitations to the proposed design. During upshift synchronisations the impulsive response enhances engagement, reducing the indexing phase of engagement. However, issues arise in the downshift, for the tip-on-tip engagement the vibration peaks and retreats before the sleeve can completely engage, suggesting that the impulsive response encourages a detrimental alignment, with torsional vibration then forcing the sleeve backwards. This is reflected in the detrimental alignment condition, where the sleeve speed is halted by the vibration, similar to uncontrolled detrimental engagement before the sleeve is dragged backwards of the tip of the chamfer to advantageous chamfer alignment. This indicates that the induced vibration needs to be tuned for each gear and engagement type, increasing complexity of control.

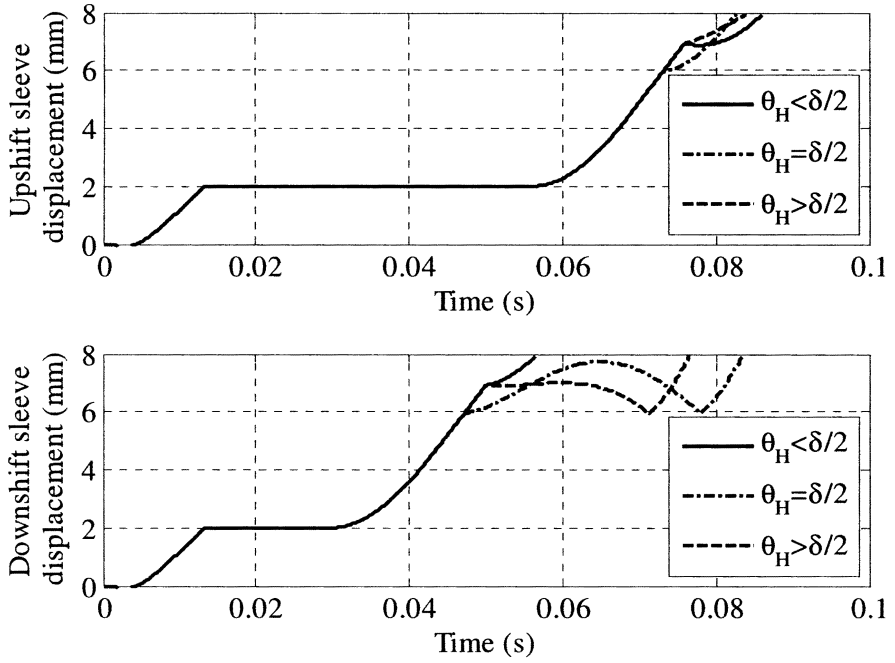

Figure 6.14: Control of chamfers for a wet clutch DCT using torque impulse for upshift (top) and downshift (bottom)

Chamfer engagement with inertia changes for the dry clutch are demonstrated in Figure 6.15. These results are positive. With significantly lower drag torque on the synchroniser the impulse rapidly realigns both up and downshift engagements for advantageous and detrimental alignment conditions. Indeed for both shift types the rate of chamfer engagement is increased, demonstrating successful engagement using positive control with inertial vibration.

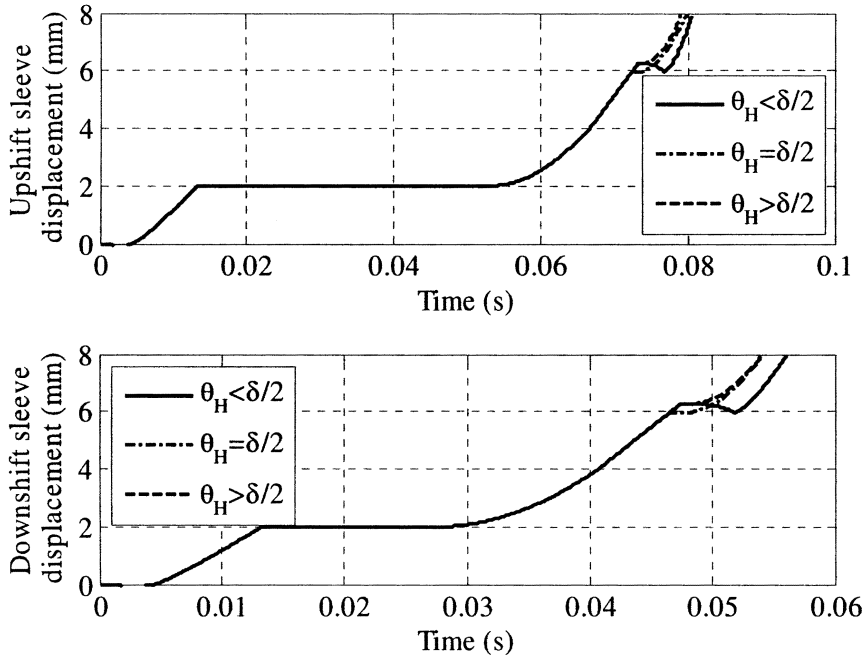

Figure 6.15: Control of chamfers for a dry clutch DCT using torque impulse for upshift (top) and downshift (bottom)

The results presented for the suggested mechanism in Case 2 indicate that there is some potential for improving the engagement of the synchroniser mechanism using impulsive changes to inertial resistance of the system. However, the influence of drag torque has been demonstrated for downshift synchronisation in a wet clutch DCT. Where the alignment tool would otherwise increase the rate of engagement, the impact of variable drag and chamfer torque is to counteract the positive influence of vibrations, to the extent that, for wet clutches, closed loop control of the mechanism, Figure 6.6, achieves a similar delay in successful engagement (Figure 6.14). Therefore this method for active chamfer control has some positive capabilities with further research needed into the selection of inertia and stiffness.

6.5 MINIMISATION OF SLIP REGENERATION

The most significant aspect delay results from the regeneration of slip in the cone clutch after it is released post ring unblocking. Specifically, after ring unblocking is completed the sleeve no longer applies a load on the cone clutch. As a result drag torque is the dominant torque acting on the target gear, and slip ensues. It is suggested here that if the cone clutch was continually partially energised after the unblocking of the ring then the regeneration of slip in the cone clutch can be limited. There are currently two methods for applying a load on the ring and hence the cone clutch:

1. Thrust piece during initial displacement, where the ring is pushed ahead of the sleeve using thrust piece and detent to ensure that relative rotation of the ring is possible, before chamfers are engaged
2. During synchronisation and ring unblocking, the cone clutch is energised directly from the sleeve via the ring chamfers. After ring unblocking this is released with sleeve chamfers moving past the ring

Obviously the second method of loading cannot be used as the sleeve continues to move forward. Additionally, the load on the thrust piece is dependent on the detent spring and once the ball is released from the groove load discontinues. It is therefore proposed that the detent groove is modified on the sleeve to include a second contact component. This divides the thrust piece groove into three separate regions, shown in Figure 6.16:

1. Initial contact position, where the traditional action of the thrust piece is performed, the ball is forced down by the groove until it is released.
2. The ring contact region requires that a no load condition is met with the thrust piece and all load is via the ring chamfers for the cone clutch. Therefore the ring contact region is designed to allow free motion of the sleeve.
3. Secondary contact region is used specifically so that the thrust piece is forced into ring contact again, thereby partially energising the cone clutch. This will enable the cone clutch to restrict the capability for slip regeneration in the mechanism.

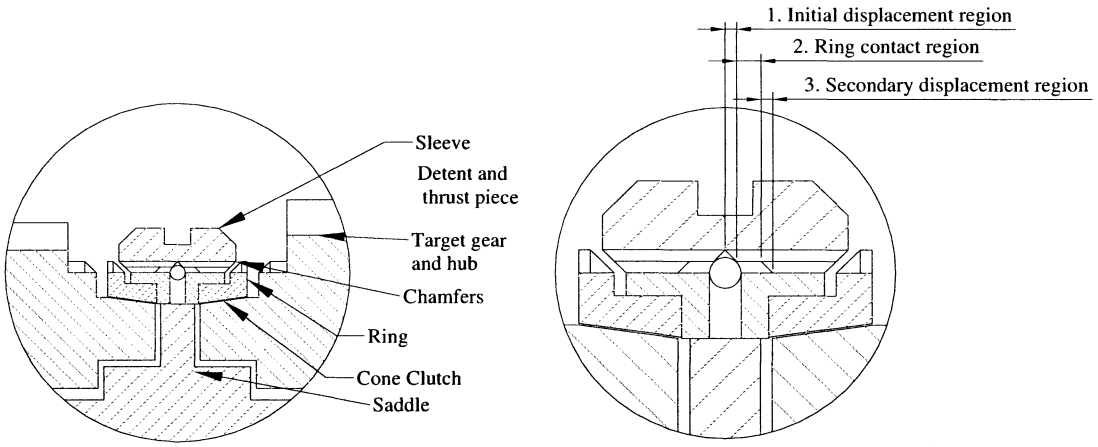

Figure 6.16: Detailed cross section of double contact thrust piece

The detailed double contact sleeve is presented in Figure 6.16 above. During contact region 1 the thrust piece performs its traditional role of pushing the ring ahead of the sleeve. In region 2, there is free motion of the sleeve, de-energising the thrust piece and allowing the direct contact of sleeve and ring to load the cone clutch. The length of this region should equal or exceed the contact length of ring chamfers, thus once unblocking is complete the thrust piece is again forced into contact with the ring. Finally, in region 3, the secondary ring contact energises the cone clutch for a second time, both reducing the possibility of slip regenerating and providing a method for again synchronising the target gear to shaft speed.

To model the effect of using a double contact thrust piece concept the cone torque defined in Equation 4.23 in Chapter 4 during the secondary displacement of the sleeve can be redefined to include forces applied through the detents springs during the secondary contact period, see Equation 6.5 below:

$$T_{CONE} = \left(\frac{\mu_R T_{DRAG}}{R_i} + 3K_S tan(\theta_D)(X_0 + \Delta X)\right) \times \frac{\mu_C R_C}{sin(\alpha)} \qquad (6.5)$$

Note that X_0 represents the preload in the spring resulting from the initial displacement. This equation is modelled in Matlab only during the secondary displacement period. It therefore assumes that the thrust piece is in contact with the ring immediately after ring unblocking, and releases once the minimum displacement for contact in hub chamfers is reached. Otherwise the same synchroniser parameters and initial conditions are again applied for simulations of up and down shift synchronisation only in the wet clutch model, with this higher drag torques.

Simulations of the application of a simple double contact thrust piece in the rigid body synchroniser are shown above in Figure 6.17. These results show considerable improvement over comparative simulations in Figure 6.3 with substantial reduction of engagement time for the detrimental alignment case for both up and down shift synchronisations. This results directly from reduction in slip generated in the cone clutch as a consequence of the load on the cone clutch after ring unblocking. However, these results also indicate a small amount of slip still generates in the cone, slowing the engagement in the detrimental alignment case. Thus the engagement with this double contact thrust piece is only partially successful, but the use of stiffer springs or alternate loading methods will improve the results, particularly with lower gears that experience higher drag torques and therefore higher slip speeds.

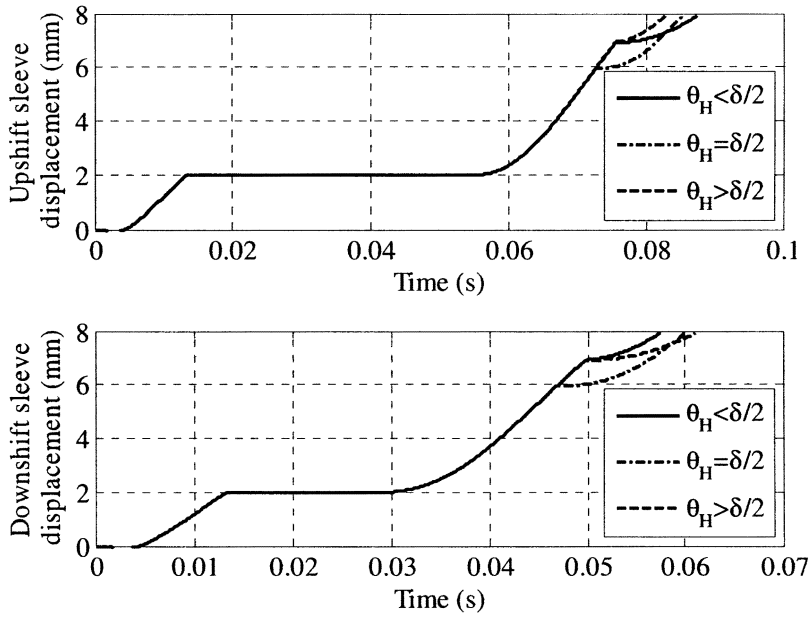

Figure 6.17: Simulations of engagement with double contact thrust piece in wet clutch DCT, (top) upshifts and (bottom) downshifts

6.6 CONCLUSIONS

This chapter has sought to present alternate methods for reducing negative effects of chamfer engagement identified as the regeneration of slip after indexing and random nature of chamfer alignment during hub indexing for both dry clutch and wet clutch DCTs. It was found that the engagement of the synchroniser in wet clutch DCTs is highly dependent on the chamfer flank on which it engages, with the two possible outcomes being the advantageous alignment with these two torques having the same direction and aiding engagement, or detrimental alignment where drag torque and chamfer torque are opposing. Here, the chamfer torque generated must eliminate any built up momentum in the mechanism before proceeding with normal chamfer alignment, contributing to the extension of the overall process time. For dry clutch DCTs, an additional issue arises in the tip-on-tip engagement condition where there is insufficient drag torque to rapidly realign the chamfers as demonstrated in the wet clutch DCT. To resolve these issues three methods were demonstrated for the aiding of engagement of the mechanism:

1. The currently used method of active control of chamfer alignment using the sleeve speed and position for closed loop control,
2. The employment of an externally applied torque to aid the chamfer engagement, and
3. Use of a step change in inertia to generate an excitation to aid in chamfer realignment.

Each of these suggested methods has its own limitations, particularly with increased delay in certain engagement conditions. Where closed loop control has an increased engagement time, it also cannot guarantee successful realignment. Each of the two alignment tools was capable of providing decreased engagement under only some of the conditions. These methods were not completely successful, but they did provide positive control for all alignment conditions. This positive control is a clear benefit over closed loop control; however results have shown a significant requirement for tuning of excitation tools to specific conditions.

The source of detrimental engagements, excluding tip-on-tip alignment, is the regeneration of slip in the synchroniser mechanism after the ring is unblocked. Targeting the source of the problem is the last alternative suggested, where the thrust piece design is modified to include two contact points such that the cone clutch can be

partially energised post ring unblocking and before chamfer engagement. Simulations demonstrated that this was capable of partially eliminating the regenerated slip, with higher axial load required for the cone clutch to minimise regenerated slip. This load can be achieved with the implementation of nonlinear spring stiffness.

6.6.1 Summary of contributions

This chapter has sought solutions to the detrimental engagement of synchroniser chamfers during hub indexing. Three novel solutions were suggested:

1. Chamfer realignment using an externally applied torque,
2. Use of external excitation to initiate realignment, and
3. The modification of thrust piece design to introduce a secondary detent contact condition

CHAPTER 7: INVERTED SYNCHRONISER MECHANISM DESIGN

7.1 INTRODUCTION

This chapter focuses specifically on the development of an alternative synchroniser mechanism design resulting from the dimensionless study and parameter investigation performed in Chapter 4. Results presented have demonstrated the limited capacity for typical design solutions to be utilised in the reduction of synchronisation time. The use of high friction coefficients or lower cone angles is limited by the friction lock phenomenon when disengaging the mechanism, while the adoption of aggressive chamfer angles to reduce chamfer realignment duration at ring and hub have low risk-reward tradeoffs in terms of resilience against drag torque or against clash failure. Thus a modified synchroniser design, required to further reduce the engagement times, is presented that includes improving cone torque without significantly changing the mechanism overall design envelop or practical design and manufacturing methods.

Therefore this chapter is divided into sections investigating improvements to the synchroniser arrangement and chamfer design impacts, including simulations. This is followed by the introduction of a modified synchroniser mechanism design which retains many of the principal operating characteristics of traditional synchroniser mechanisms while improving available torque. The novelty of the design is discussed, and specific improvements over the standard synchroniser identified before conclusions are drawn.

7.2 RATIONALE FOR SYNCHRONISER IMPROVEMENTS

Consideration of how to further reduce the engagement time of any synchroniser mechanism leads to the identification of two separate possible design characteristics that can be investigated for further development, identified as the size of the cone clutch radius and friction coefficient, and chamfer angle and radius. The parameter study has provided some indication of the possible options for design improvement. Through

maximising the cone torque present in the mechanism, the speed synchronisation time is minimised and drag resilience improved. This is important to the reduction of overall process time and in chamfer design. The influence of variation of the cone parameters is limited by the friction lock limit of the cone, as previously indicated by equation 4.1 of Chapter 4. These results arrive at an issue, what other methods can be used to maximise the cone torque.

Choice of chamfer angle presents similar limitations; restrictions, however, are based on the designed cone torque and drag torque. Evaluation of the chamfer design identified that the friction loss component of the torque has minimal influence on the engagement of the mechanism. The chamfer angle is much more influential, affecting both the torque generated and the displacement required for engagement. These two competing requirements are significant in determining the engagement time for ring unblocking and hub indexing, and are both highly coupled, making good parameter selection difficult to manage. Consideration of the synchroniser design envelop is also important as compactness and low inertia will benefit transmission performance.

7.3 IMPACT OF INCREASING CONE RADIUS

The dimensionless analysis presented in Chapter 4 incorporated three torques that play significant roles in the synchroniser process; cone clutch torque, indexing chamfer torque, and drag torque. The first two of these are easily defined from constitutive equations in Chapter 4, equations 4.30 and 4.31. The dimensionless drag torque is less precisely known, with theory presented in Chapter 5 to build a representative drag torque model, and modified to dimensionless drag in Chapter 4 equation 4.32.

Dimensionless equations show the design requirements that must be met by the synchroniser mechanism. The dimensionless cone torque equation has peak torque, in accordance with theory presented in Vyrabov [137] and Stringer [37], about equal to one ($\Pi_C \approx 1$) to gain maximum possible torque from the cone angles and friction coefficients without breaking the friction limit. Thus cone angle and friction coefficient must be considered as fixed. Increasing the cone torque is therefore the result of increasing the mean cone radius.

The dimensionless chamfer torque must maintain the limit with respect to cone torque, in that $\Pi_C > \Pi_I$. As the mean cone radius is in the denominator, a higher cone radius will reduce the dimensionless indexing torque. Hence it becomes possible to increase actual indexing torque if cone radius is increased. Thence the chamfer angle can be designed to allow for the increase in cone torque. The result is therefore to improve resilience of the synchroniser mechanism to drag torque.

Finally, the dimensionless drag torque, equation 4.32, must be less than hte dimensionless cone and indexing torques. However, this torque in particular is not constant but rather dependent on a range of variables such as gear speeds, loading, and temperature. By increasing the cone and chamfer torques the resilience of the synchroniser to high drag is increased. This is observed in equation 4.32, i.e. the increase in R reduces the dimensionless value of the drag torque. This results in an increased resilience of the cone to higher drags, and contributes to reduction in synchronisation time. For the dimensionless indexing torque a similar result is achieved; the dimensionless value of indexing torque is reduced for an increase in mean cone radius. However, the ability of the indexing torque to overcome drag is unchanged.

To demonstrate the potential improvement realised from modifying the mean cone radius, simulations of the synchroniser engagement for a 4th gear synchronisation with 3rd gear engaged in the DCT are performed. The mean cone radius is modified through a range including typical synchroniser mechanisms, and is equal to and greater than the indexing chamfers. The results in Figure 7.1 demonstrate the variation in engagement times result from the modification to the mean cone radius. There is no influence of the modification of the cone radius on the indexing of the ring and hub. However by increasing R it is possible to reduce the speed synchronisation time significantly; in this case a reduction > 10ms is achieved for a ratio of 1.4, over a typical ratio of 0.6 to 0.8. This suggests a synchroniser with cone clutch external of ring and chamfers as a possible design solution.

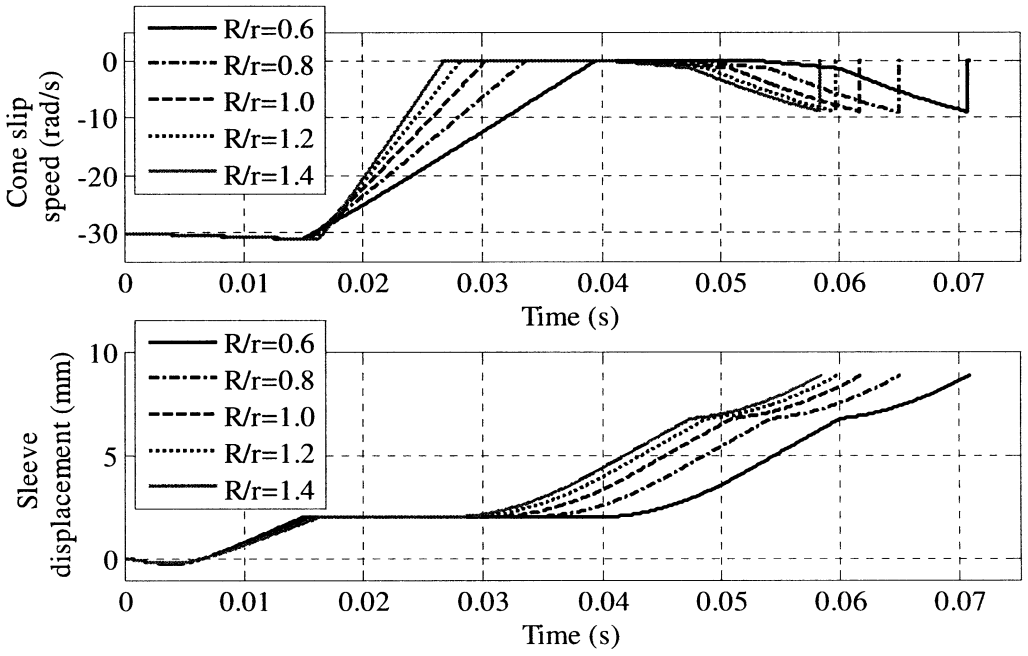

Figure 7.1: Synchroniser engagement simulations with variation to the cone clutch mean radius, (top) Cone clutch slip speed during synchronisation of gear, and (bottom) sleeve displacement simulation

Speed synchronisation is not the only role that is played by cone torque. It affects the total drag torque that the synchroniser can overcome during engagement process, and influences the maximum indexing torque available. The indexing torque in particular must be less than the dynamic friction torque generated in the cone clutch during speed synchronisation, but greater than the drag torque during all other stages. By increasing the cone friction torque through the increase of the cone mean radius it is therefore possible to increase the indexing chamfer torque to match this change through either more acute chamfer angles or through a larger chamfer pitch radius. For example, it is possible for the chamfer angle to be modified to increase the torque. This will result in the increase of sleeve displacement, but the chamfer radius can then be reduced to compensate for sleeve displacement, or *vice versa*. Thus it is possible to maintain or improve the chamfer torque when reducing the chamfer radius, and produce a significant increase to the cone torque. It is still necessary, though, to balance the increased chamfer torque with the requirement for sleeve displacement.

7.4 CHAMFER DESIGN IMPROVEMENTS

The development of an external cone on the synchroniser mechanism requires the balancing of both cone and chamfer torques. One advantage of the external cone is the capacity to increase the generated chamfer torque to further reduce process engagement times. To do so, a study of the chamfer angle and pitch radius will demonstrate any improvements that will result from the modification of the design.

The parameter δ is one of the most important aspects that contribute to ring unblocking and hub indexing in the synchroniser mechanism. It is the rotational displacement required to realign the ring into the neutral position, and is defined by the number of chamfers present on the ring, see equation 4.12. This rotation also significantly contributes to the displacement required by the sleeve to pass through the ring, defined as (see Appendix B for derivation):

$$\Delta x_S = \frac{\delta}{2} \cdot \frac{r}{\tan\beta} \tag{7.1}$$

where r is chamfer pitch radius. Comparing chamfer torque equation to equation 7.1 demonstrates the contradicting requirements, i.e. reducing the pitch radius and increasing the chamfer angle benefits the decrease in sleeve displacement requirements, it has negative effects on chamfer torque. Therefore there must be a balance achieved between these contradicting requirements.

Equation 7.1 indicates the required sleeve displacement is proportional to the pitch radius, r, of the indexing chamfers, and inversely proportional to the tangent of the chamfer angle, β. Both of these parameters are very important to the magnitude of indexing torque developed, with the traditional radius limited design maintaining chamfers outside of the cone radius.

To understand how important these two parameters are on indexing torque a simple parameter variation is performed. Assuming that there are thirty-five (35) chamfers, both chamfer angle and pitch radius are modified through a reasonable range of values. In conjunction with sleeve displacement, the dimensionless chamfer torque must be considered with reference to variation in these same two parameters of chamfer radius and angle.

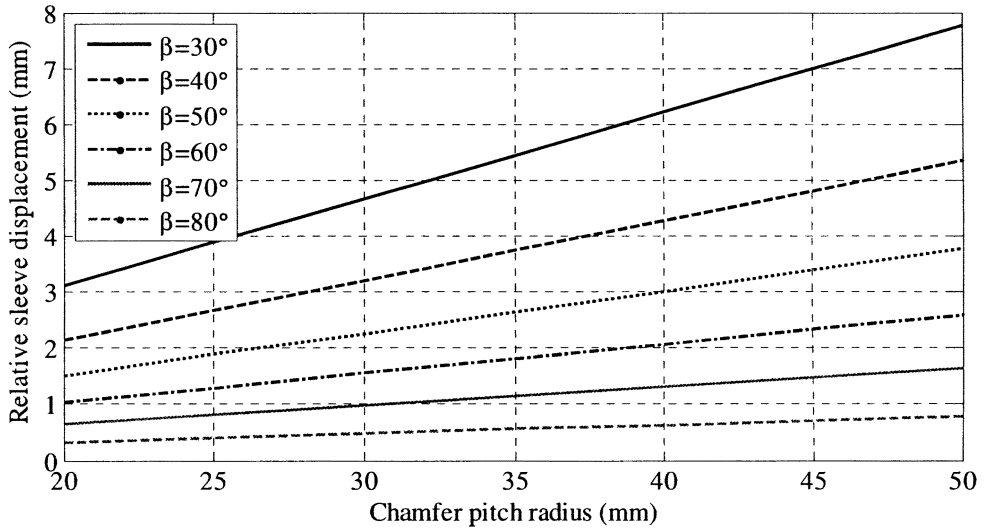

Figure 7.2: sleeve displacement variation with chamfer angle and pitch radius change

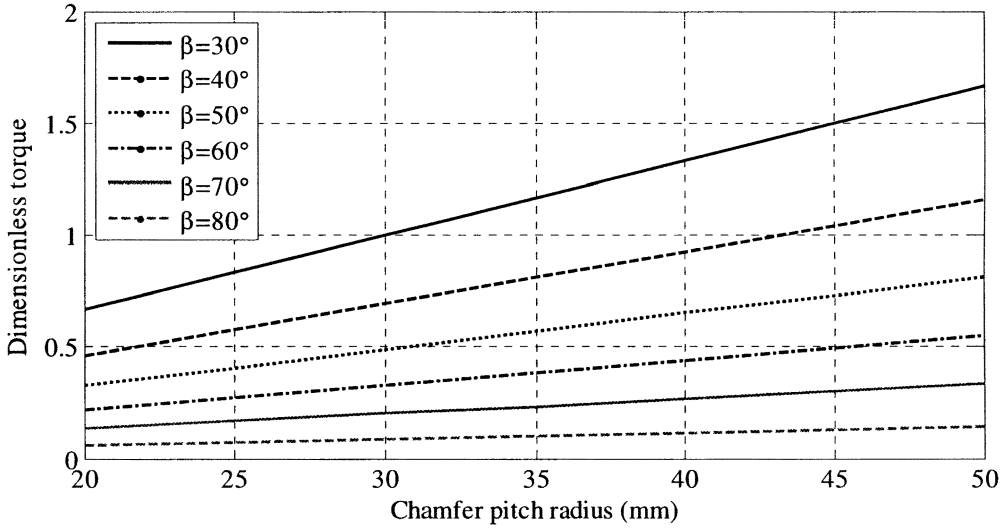

Figure 7.3: dimensionless chamfer torque as a function of chamfer angle and operating radius

The results of this parameter variation in Figures 7.2 and 7.3 demonstrate the two conflicting requirements, where an increase in the chamfer angle will provide an increase in torque, but also increases the displacement, with both these results similar to what occurs from an increase in the chamfer pitch radius. It must be concluded that these variables alone are not sufficient to determine the effect of the trade off between sleeve displacement and chamfer torque. Finally, consider the influence of the number of chamfer splines that will fit on each chamfer pitch radius on the sleeve displacement. Substituting equation 4.12 into equation 7.1 provides the equation for sleeve displacement as a function of the number of chamfers.

$$\Delta x_S = \frac{\pi}{N_C} \cdot \frac{r}{\tan\beta} \tag{7.2}$$

Figure 7.4 demonstrates the influence of pitch radius and the number of chamfers on sleeve displacement. For a constant chamfer angle the condition holds that the reduction of pitch radius leads to the reduction of sleeve displacement. Figure 7.5 shows the result of varying the chamfer angle and number of chamfers for a constant pitch radius, with the blunter chamfer angle leading to a reduction of sleeve displacement. Thus a good balance of desired torque, derived from the chamfer angle and pitch radius, and sleeve displacement, stemming from the number of chamfers as well as pitch radius and chamfer angle, is required in design and selection of chamfers.

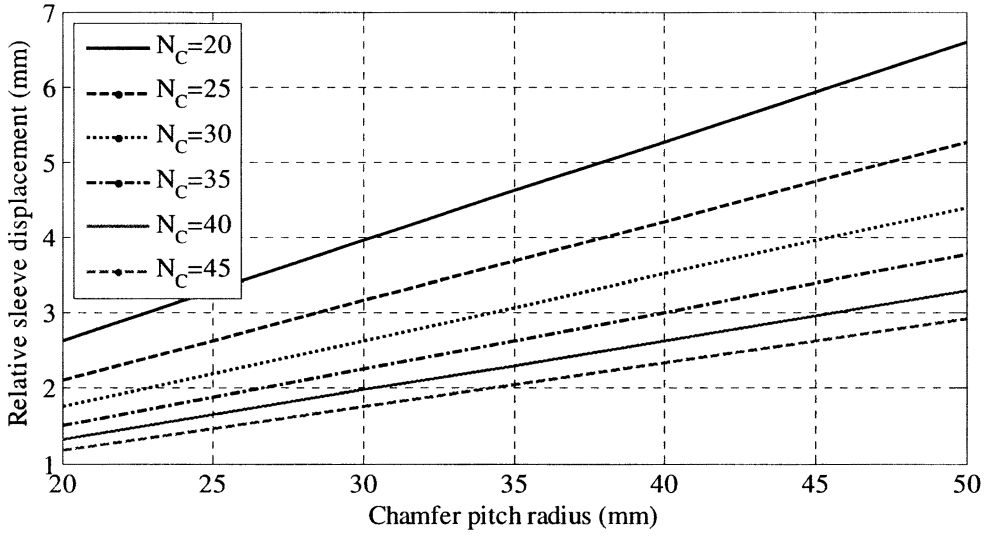

Figure 7.4: Variation of sleeve displacement with modification to the chamfer pitch radius and number of chamfers at a chamfer angle of 50 degrees

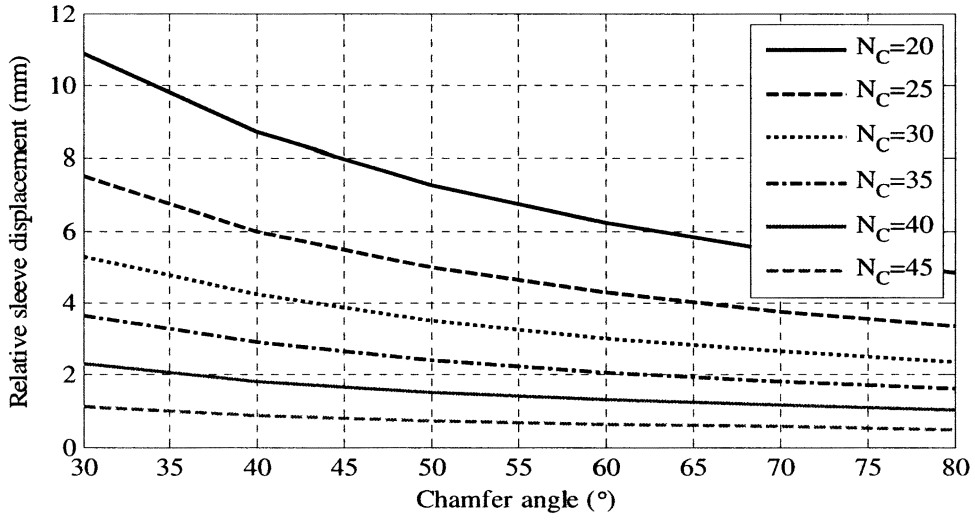

Figure 7.5: Variation of sleeve displacement with modification to the chamfer angle at a constant pitch radius of 40mm

To compare the influence of the chamfer angle and pitch radius on the mechanism engagement, a constant dimensionless chamfer torque is chosen from Figure 4.19 of approximately 0.6. The number of chamfers is maintained constant in Table 7.1. Note that the maximum chamfer torque is calculated with an assumed pressure of 1.1 MPa and a piston head diameter of 20mm.

Table 7.1: Simulation parameters

	Original	*Sim 1*	*Sim 2*	*Sim 3*	*Sim 4*
Pitch radius (mm)	60	40	40	50	50
Chamfer angle (deg)	65	50	55	50	55
Number of chamfers	45	45	45	45	45
Required displacement (mm)	2	2.3	1.6	2.9	2
Max. chamfer torque (Nm)	8.7	10.7	7.2	13.4	9.1

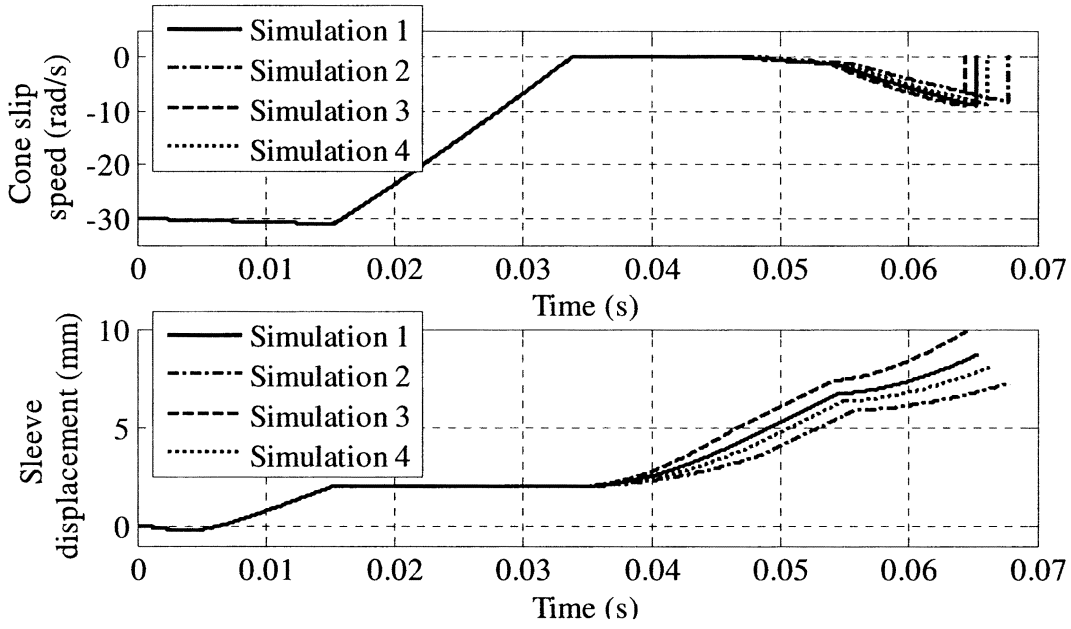

Figure 7.6: Synchroniser engagement simulations with variation to chamfer design according to Table 2, (top) cone clutch slip speed, and (bottom) Sleeve displacement

The results of modifying the chamfer pitch radius and angle are presented in Figure 7.6 for the sleeve displacement and cone slip speed. These simulations confirm the results shown in Figures 7.2 to 7.5, where the balance between shorter sleeve displacement and higher chamfer torque can produce marginal variations in the engagement time. It is reasonable conclude that higher chamfer torque holds more advantages over shorter

sleeve displacements. Particularly as shown in Simulation 3, by producing higher chamfer torque the overall engagement time is reduced significantly. However these same parameters produce the longest sleeve displacement. Conversely, Simulation 2 demonstrates the shortest sleeve displacement with lower chamfer torque and as a consequence the longest engagement time. Thus, on balance, the approximate doubling of the required displacement is sufficiently counteracted by the shorter engagement time.

7.5 THE INVERTED CONE DESIGN

Maximising the cone and optimising the chamfer torque and geometry suggests that the best possible synchroniser design is achieved with the cone external of sleeve and chamfers; converse to traditional synchroniser designs. This enables the maximising of the cone and chamfer torque without significantly changing the fundamental operating components of the synchroniser. As such the design of an inverted cone mechanism must provide certain characteristics inherent to traditional synchroniser mechanisms to ensure reliability in actuation, most notably is the use of a thrust piece and detents.

Figure 7.7 presents a suggested design of the new synchroniser mechanism. All the major components found in other mechanisms are used here and the actuation process is essentially identical to traditional designs. While the chamfers are now internal to the cone, the use of more acute chamfer angles will compensate for the reduced pitch radius. The simplicity of the ring contact with the thrust piece is lost; the design must cater for the thrust piece that is not retained by the sleeve. This is achieved through the use of guides to locate thrust pieces in the sleeve. Two detents are used; the inner detent locates the sleeve on the saddle and provides resistance during initiation of engagement. The second detent is used to provide relative motion between the thrust piece and sleeve during the initial stages of engagement, allowing the ring to be pushed ahead of the sleeve and rotate to the blocking position.

The saddle is smaller than synchromesh synchronisers as more internal space is required to house the sleeve, with internal sleeve surface splined to mount on the saddle, and the outer surface chamfered splines to engage the ring and hub, and recess is suggested for the trust piece.

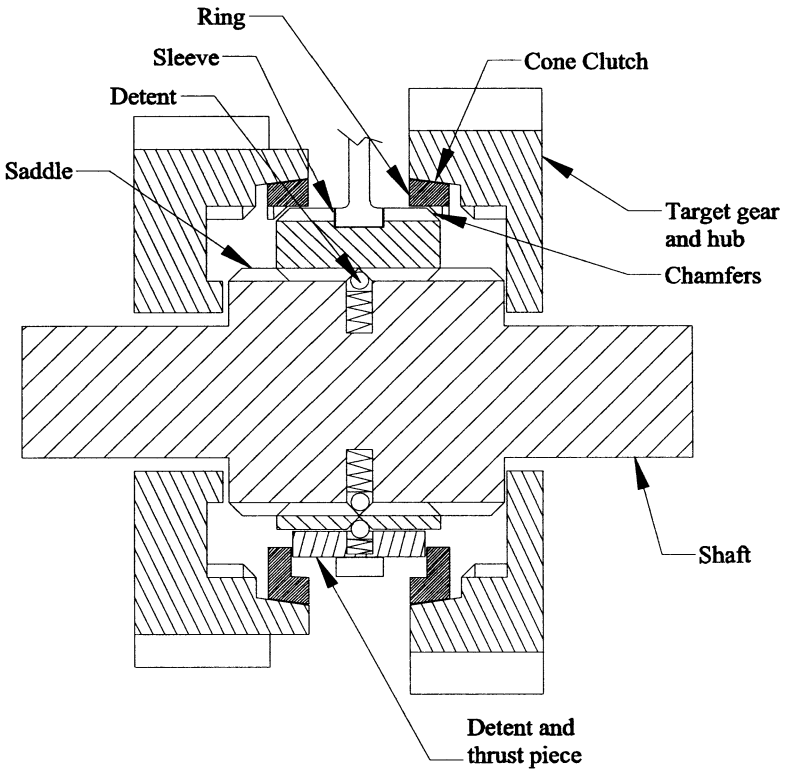

Figure 7.7: Typical section of inverted synchroniser mechanism

While the external half of the cone clutch, traditionally on the ring, is now located on the target gear, this is key to the design as it can provide more torque than traditional synchronisers. One particular benefit of this chamfer and cone arrangement is the possibility to undercut the gear and use the otherwise unused gear volume to house the synchroniser or part thereof. Thus the envelope of the gear and synchroniser combined can be reduced, making the overall transmission design more compact.

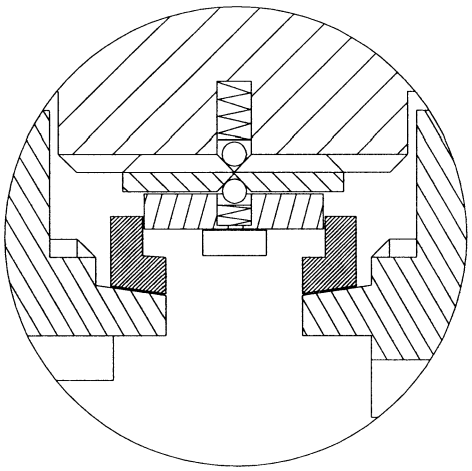

Figure 7.8: Detail of thrust piece and detents

In traditional mechanisms, the thrust piece is located on the inside of the sleeve, and retracts to the saddle during engagement. In the inverted design this is no longer possible as the ring is located outside of the sleeve. To overcome this design limitation, the thrust piece is recessed in the sleeve, and a secondary detent replaces the original single detent design. Thus, as the sleeve is energised and moves forward, the thrust piece detent retracts as the thrust piece pushes the cone clutch closed, enabling the ring to rotate to blocking position before chamfer comes in contact in a similar manner to the traditional design. The recess is required so that there is sufficient space for contact between the ring and thrust piece to initiate engagement successfully, and to provide space to retract the thrust piece as the sleeve moves past the ring. Figure 7.9 details the displacement of thrust piece as several different steps of engagement.

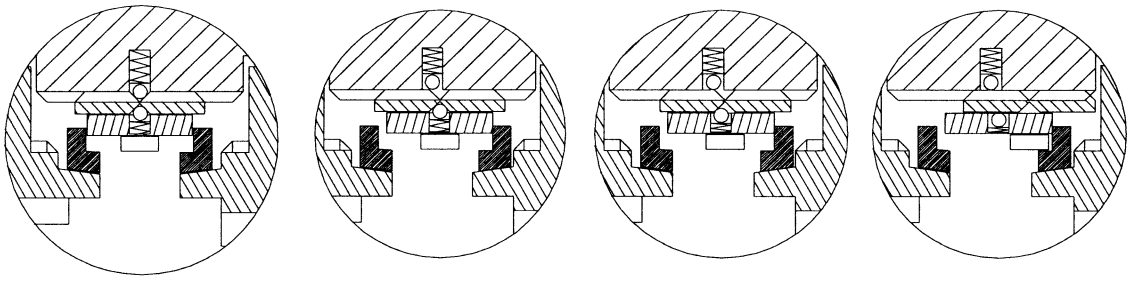

Figure 7.9: Detailed thrust piece positions, from left to right (1) neutral position, (2) at end of initial displacement before sleeve and ring chamfers engaged, (3) During synchronisation with sleeve and ring chamfers engaged and thrust piece detent retracted, and (4) at full displacement with thrust piece dented fully retracted and gear completely engaged.

Therefore the designed inverted synchroniser mechanism provides several key improvements over traditional synchroniser designs. These are:

- Increased cone torque to reduce synchronisation time,
- Increased chamfer torque to reduce indexing and ring unblocking time,
- Improved resilience to variation in drag torque through higher cone and chamfer torques, and
- More compact design through the overlapping design of synchroniser and gear.

7.5.1 Simulations

The inverted synchroniser mechanism design aims to provide reduced synchroniser engagement times through the increasing of cone and chamfer torques, and potentially

also through reduction of overall sleeve displacement required for engaging the mechanism. Figure 7.1 demonstrates the result of increased cone mean operating radius, while Figure 7.6 displays the effect of modifying the chamfer angles and operating radius during engagement. In this section, two separate shifts are used for simulation of the full inverted cone engagement. Synchronisation of 4^{th} gear with 3^{rd} engaged, and synchronisation of 4^{th} gear with 5^{th} engaged. Two separate cone radii will be used for each engagement, and a combination of chamfer angles and pitch radii will be applied to demonstrate variation resulting from different designs. The initial displacement and secondary displacement have been maintained at the initial length of 2mm used in previous simulations for consistency.

Table 7.2: Inverted cone design simulation parameters and dimensionless parameters

Parameter	*Original*	*Sim 1*	*Sim 2*	*Sim 3*	*Sim 4*
Cone Radius (mm)	*47.5*	57	57	66.5	66.5
Chamfer angle (°)	*65*	40	30	40	30
Chamfer pitch radius (mm)	*60*	30	30	30	30
Maximum cone torque (Nm)	*16.2*	19.4	19.4	22.6	22.6
Maximum chamfer torque (Nm)	*8.7*	11.4	16.4	11.4	16.4

The maximum cone and chamfer torque calculations presented in Table 7.2 provide demonstrative evidence of how the use of this mechanism arrangement will improve over standard designs. At a basic level of comparison, the maximum cone and chamfer torques are designed to exceed drag torque generated in the transmission, modification of the cone and chamfer designs enables significant increases to maximum applied torque. Considering that high drag torque contributes significantly to the failure modes of the synchroniser mechanism, it is reasonable to conclude that by increasing the cone and chamfer torque, the mechanism is more resilient to the effects of drag torque. Simulation results presented in Figure 7.10 are carried out using parameters in Table 7.2

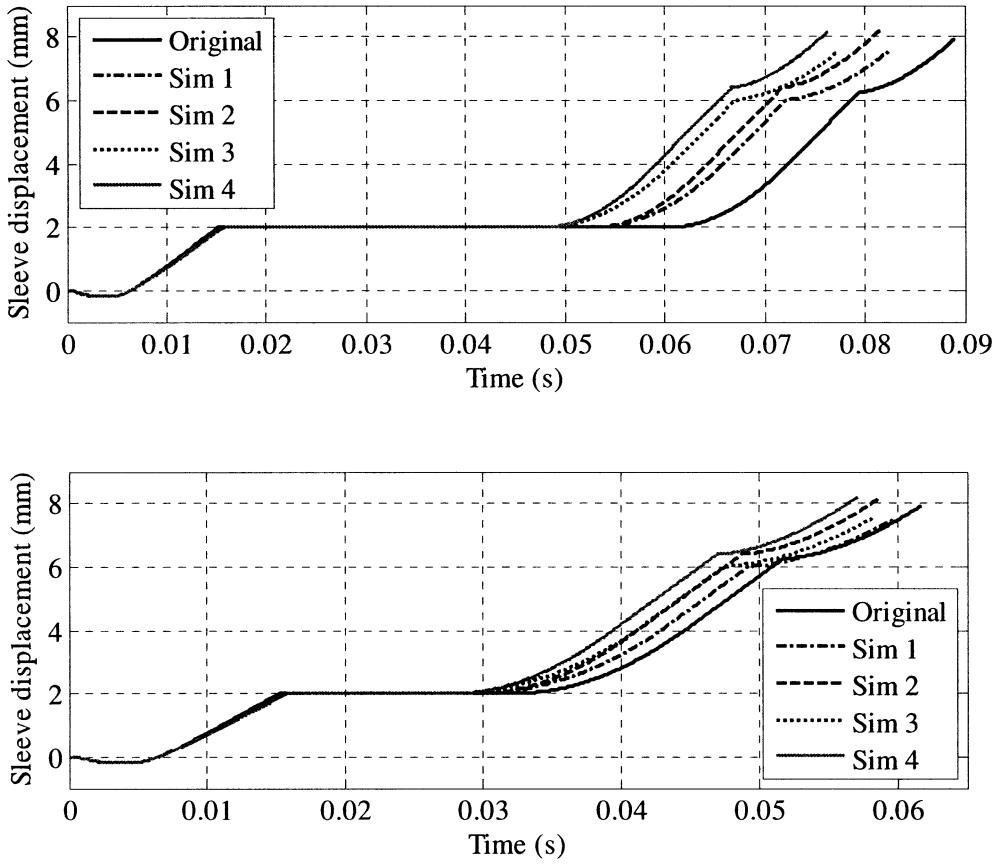

Figure 7.10: Simulations of the inverted cone synchroniser mechanism, (top) above 3rd to 4th gear synchronisations, and (bottom) below 5th to 4th gear synchronisations

Figure 7.10 presents the simulation results for a series of up and down shift gear synchronisations with variation to the mean cone radius, chamfer pitch radius, and chamfer operating angle. The combination of larger cone radius and modified chamfers provides simulation results that consistently improve on the results possible with the original mechanism. This is a result of the inverted mechanism being capable of providing higher operating torques in the cone and chamfers than the original mechanism, providing faster actuation and increased resilience to resistive drag torques with similar sleeve displacement requirements. This displacement can be further improved through the study of the clearance requirements during both initial displacement and secondary displacement [51]. Consistent with previous simulations, the use of higher chamfer torques is demonstrated to outweigh any possible improvement that can be gained by decreasing the sleeve displacement during ring unblocking and chamfer indexing. For up shifts the total synchronisation time is reduced to between 75 and 85 ms for each of the new simulations. For the down shifts

this is around 55 ms for each of the alternative models. Both up and down shift synchronisations therefore represent a reasonable reduction in engagement times.

Results Sim 1 and 3 in Figure 7.10 both demonstrate the restrictive use of longer sleeve displacement requirements, with mixed results. The upshift synchronisations tend to show a significant improvement over the baseline results, however with down shifts these results are much more marginal. This is due to the reduction in synchronisation time being attenuated during chamfer engagement phases, providing further cause for suggesting higher chamfer torques provides greater benefits. The new synchroniser design can therefore provide improved engagement performance over traditional synchromesh synchronisers through increases to the synchroniser cone torques and the application of increased chamfer torque improving engagement in place of shorter displacement requirements.

7.6 CONCLUSIONS

This chapter proposed the design of an inverted synchroniser mechanism. In developing this design two aspects of the synchroniser were investigated. Simulation of modification to the ratio of cone radius to chamfer pitch radius shows that, for a constant chamfer radius, increasing the cone radius reduces the duration of speed synchronisation, suggesting the better synchroniser design will have the cone clutch external of the chamfers. By increasing the cone torque it is then possible to increase the chamfer torque. The principle design parameters of synchroniser chamfers were then investigated to determine best design for maximising chamfer torque against sleeve displacement. Simulation results show that increasing the chamfer torque reduces the engagement time more than compensating for longer displacements of the sleeve.

Based on these results the inverted synchroniser mechanism is suggested. This is characterised by having the cone external of the chamfers, increasing the cone torque, with the investigation into the chamfer modifications used to increase chamfer torque in response to the high cone torque. Simulation results of the new synchroniser mechanism with modifications to the rigid body model developed in Chapter 4, demonstrate that the modified synchroniser design is capable of reducing the duration of engagements of the mechanism by around 15ms for upshift synchroniser engagements and 8ms for downshift engagement.

This design is characterised by having the same operating principles as the conventional synchromesh synchroniser including cone, chamfer, sleeve, and thrust piece designs, with minor modifications to the thrust piece operation, for a similar design envelope. The suggested design provides improved performance in terms of reduced engagement and higher synchroniser torques through the application of current synchroniser mechanism technologies in an alternative arrangement. Furthermore, by inverting this design the synchroniser can be located internally of the gear for a more compact design.

7.6.1 Summary of contributions

This chapter has two original contributions:

1. Through the design and development process, an alternative method for investigating different requirements of the synchroniser chamfer design and selection was presented. Using parametric analysis of characteristic parameters for the mechanism.
2. The inverted synchroniser mechanism, which is significantly different from current synchroniser designs and provides decreased engagement times through the increased cone and chamfer torques. Additionally, the new design arrangement provides more compact synchroniser and gear arrangement.

CHAPTER 8: DYNAMIC MODELLING OF A DCT POWERTRAIN WITH INTEGRATED SYNCHRONISERS

8.1 INTRODUCTION

In Chapters 3, 4, and 9 of this thesis the contributors to transmission torques required for shifting in the DCT are studied. Modelling and control of the hydraulic clutch control system for shift transient studies was performed in Chapters 3, the modelling and engagement of the synchroniser mechanism in Chapter 4, and a shift control methodology and shift transient studies are conducted for a 4DOF powertrain model in Chapter 9. In this chapter lumped stiffness-inertia torsional models of the powertrain will be developed for different powertrain states to investigate transient vibration. These models include those capable of shift transient studies and synchroniser mechanism engagements, combining major components of the powertrain into a single model. The major powertrain components – such as engine, flywheel, transmission, or differential – are lumped as inertia elements, interconnected with torsional stiffness and damping elements to represent a multi-degree of freedom powertrain model.

This chapter is then divided into five sections covering the development of a lumped mass model of the powertrain. The first section is devoted to the introduction of modelling theory and free vibration analysis. In the second section the different states of the powertrain are identified through the combination of open and closed clutches and synchronisers. Next, in section three, the lumped inertial powertrain is presented and specific assumptions regarding the model development are identified. In section four, the model matrices and free vibration analysis is presented for the states that are studied during the transient period. Section five presents mathematical models of the applied torques to the powertrain. Finally concluding remarks are made.

8.2 LUMPED MASS MODELLING THEORY AND APPLICATION

The application of the torsional lumped inertia models to complex structures such as vehicle powertrains is a popular method for determining powertrain characteristics such as damped natural frequencies and modal shapes or studying the transient response of the powertrain under different operating scenarios. Methods for applying these modelling techniques can be found in many sources of literature, such as Rao [144]. For inertial elements the equations of motion are derived from Newton's Second Law where "*the net force on a particle of constant mass is proportional to the time rate of change of its linear momentum*" [144] or the sum of the moments on an object is equal to it's inertia multiplied by angular acceleration. Presented mathematically, with "i" as the i^{th} element in a structure consisting of n degrees of freedom, as:

$$\sum M_i = I_i \ddot{\theta}_i \tag{8.1}$$

where M is the applied moment, I is the inertia, $\ddot{\theta}$ and is angular acceleration

The process for developing a lumped inertia model is best demonstrated using simple example of a two degree of freedom system. Consistent with the powertrain a semi-definite model, insofar that it is not physically connected to the ground, will be used with no grounding stiffness, to provide free vibration characteristics, such as the rigid body mode. Consider the generic model in Figure 8.1, applying Newton's second law to masses M_1 and M_2 separately, and using two independent coordinates x_1 and x_2.

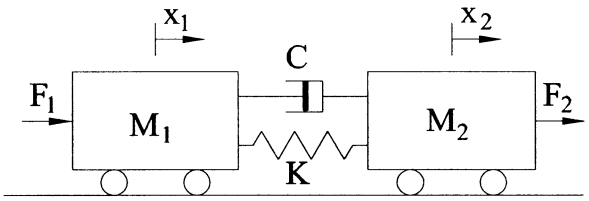

Figure 8.1: Semi-definite two degree of freedom system

The equations of motion of this system are written using the linear analogue of equation 8.1, as:

$$M_1 \ddot{x}_1 + C(\dot{x}_1 - \dot{x}_2) + K(x_1 - x_2) = F_1 \tag{8.2}$$

$$M_2 \ddot{x}_2 + C(\dot{x}_2 - \dot{x}_1) + K(x_2 - x_1) = F_2 \tag{8.3}$$

where x is displacement, $\dot{x}$ is velocity, $\ddot{x}$ is acceleration, K is stiffness coefficient, M is mass, F is force, and C is damping coefficient. Or in matrix form:

$$\begin{bmatrix} M_1 & 0 \\ 0 & M_2 \end{bmatrix}\begin{Bmatrix} \ddot{x}_1 \\ \ddot{x}_2 \end{Bmatrix} + \begin{bmatrix} C & -C \\ -C & C \end{bmatrix}\begin{Bmatrix} \dot{x}_1 \\ \dot{x}_2 \end{Bmatrix} + \begin{bmatrix} K & -K \\ -K & K \end{bmatrix}\begin{Bmatrix} x_1 \\ x_2 \end{Bmatrix} = \begin{Bmatrix} F_1 \\ F_2 \end{Bmatrix} \quad (8.4)$$

So from these equations the acceleration of the two masses is dependent on the coupled stiffness and damping of the system as well as the applied forces. Thus in vibration the response of mass 1 will influence mass 2, and vice versa.

To apply this method to a powertrain, components are reduced to a series of lumped inertias connected via torsional stiffness and dampers. For example, the differential is conveniently modelled as a lumped inertia, the propeller shaft combines both mass and stiffness. Thus it is possible to provide a reasonable approximation of the response of the powertrain system through the use of lumped inertia multi-degree of freedom models. The complex nature of powertrains, structured with multiple branches and gear pairs are all defined using interconnected elements. For transient analysis, loading exists in the form of externally applied torques from engine, clutches, synchronisers, and vehicle resistance.

8.2.1 Free vibration analysis

The first assessment of any powertrain system model is the free vibration analysis of the system. The natural modes of any system characterise the response under generalised forcing conditions. Typical methods for determining the free vibration response of a powertrain system include undamped or damped free vibration analysis.

8.2.1.1 Undamped free vibration

Undamped free vibration analysis requires the system to either be undamped or assumed as such to apply this method. The undamped free vibration of a system is then:

$$\mathbf{M}\ddot{x} + \mathbf{K}x = 0 \quad (8.5)$$

To then determine the natural frequencies of the system and corresponding modal shapes harmonic motion is assumed. This results in the defining of acceleration and displacement vectors using the solution:

$$x = X\cos(\omega t + \phi) \tag{8.6}$$

$$\ddot{x} = -X\omega^2\cos(\omega t + \phi) \tag{8.7}$$

where X is amplitude coefficient, ω is frequency, and ϕ is phase angle. These results are substituted into the matrix model, arriving at:

$$\mathbf{M}\left(-X\omega^2\cos(\omega t + \phi)\right) + \mathbf{K}X\cos(\omega t + \phi) = 0 \tag{8.8}$$

The nontrivial solutions for equation 8.8 require that the amplitude vector, X, and the harmonic component, cos(ωt+φ), are not nonzero, thus the result:

$$-\mathbf{M}\omega^2 + \mathbf{K} = 0 \tag{8.9}$$

The solutions of $\lambda = \omega^2$ that satisfy equation 8.9 are natural frequencies of the system. To find the modal shapes of the system at a particular natural frequency, the natural frequency is substituted back into equation 8.8, the harmonic component is eliminated from the equation, and nontrivial solution ($X \neq 0$) to the modal vector provides the modal shape at the applied natural frequency.

8.2.1.2 Damped free vibration

Using the state space method solutions to damped natural frequency and modal shapes can be defined as solutions to the eigenvalue problem. Beginning with the damped, unforced equation of motion, and taking the inverse of the mass (inertia) matrix:

$$\ddot{x} + \mathbf{M}^{-1}\mathbf{C}\dot{x} + \mathbf{M}^{-1}\mathbf{K}x = 0 \tag{8.10}$$

The state vectors are chosen as:

$$x = \begin{Bmatrix} x \\ \dot{x} \end{Bmatrix}, \text{ and } \dot{x} = \begin{Bmatrix} \dot{x} \\ \ddot{x} \end{Bmatrix} \tag{8.11}$$

a & b)

The state matrix can then be defined as:

$$\mathbf{A} = \begin{bmatrix} \mathbf{0} & \mathbf{I} \\ -\mathbf{M}^{-1}\mathbf{K} & -\mathbf{M}^{-1}\mathbf{C} \end{bmatrix} \tag{8.12}$$

Where **0** represents a zero matrix of size n by n, where n is the degrees of freedom, and **I** is the identity matrix. The solutions to the eigenvalue problem provide then matrices for the eigenvalues, representing paired damped natural frequencies with real and imaginary components, and eigenvectors, paired columns representing the modal shape corresponding to a particular natural frequency. From the eigenvalues it is then possible to retrieve the natural frequencies, damped natural frequencies, and damping ratio for the system. Where the natural frequency can be taken as the absolute value of a particular eigenvalue, or for the eigenvalue $\lambda = a + ib$, the natural frequency is:

$$\omega_n = \sqrt{a^2 + b^2} \tag{8.13}$$

The damping ratio is then:

$$\zeta = \frac{|a|}{\omega_n} \tag{8.14}$$

And, the damped natural frequency is:

$$\omega_d = \omega_n \sqrt{1 - \zeta^2} \tag{8.15}$$

where ω_n is natural frequency, ω_d is damped natural frequency, and ζ is damping ratio.

To complete the analysis the eigenvectors are then studied. Taken as part of the result of the eigenvalue problem, a paired column of eigenvectors represents the modal shape of a particular natural frequency, or, more generally, the relative displacements of inertial elements from the neutral point. Thus it is possible to define many of the important characteristics of a dynamic system and associate natural frequencies with particular modal responses.

8.3 POWERTRAIN STATES

The dual clutch transmission chosen for this investigation is arranged with two concentric wet clutches attached to concentrically arranged primary shafts, shown in Figure 8.2. Even gears are grouped on the external shaft and clutch, with odd gears on the internal primary shaft. Synchronisers are located on the two lay shafts, with bi-directional sleeves for gears 1 and 3, 2 and 4, and 6 and reverse, with 5th gear on a single synchroniser. For one gear to be engaged a clutch and synchroniser must both be

closed, however, before shifting two synchronisers are closed, and one clutch. There are specific limitations to this, only one clutch can be locked at any one time, and one synchroniser for each primary shaft may be locked at any one time. Thus the sophistication of the DCT can be reduced for analysing different shift states to one synchroniser representing odd gears and one representing even gears.

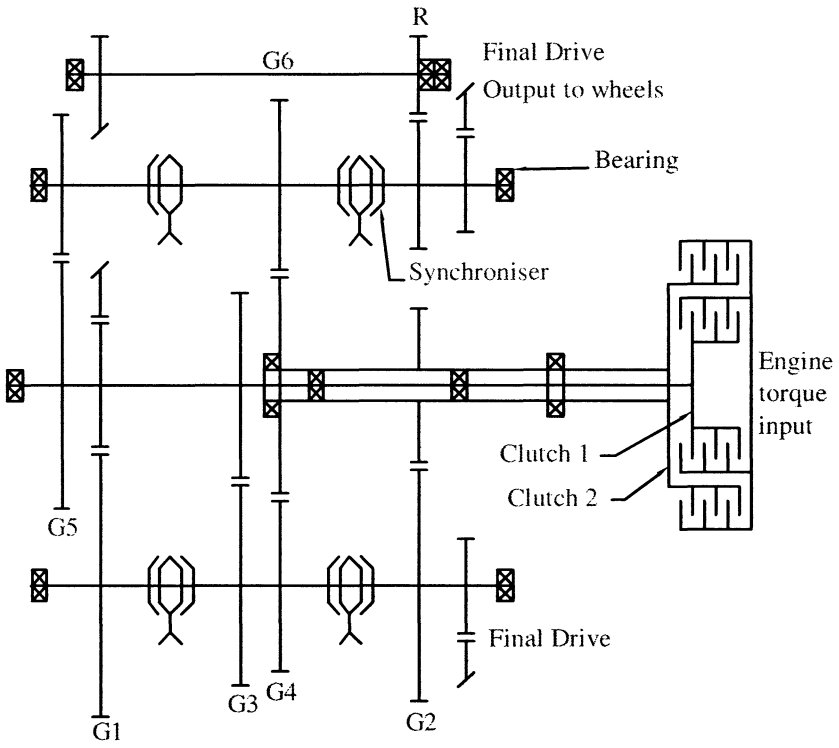

Figure 8.2: Layout of dual clutch transmission

The simplified transmission model utilises two multi-plate clutches and two synchronisers, with parameters for each clutch and synchroniser dependent on the gear selected. Each clutch and synchroniser should therefore be considered as a power switch to determine the powertrain state, and thence degrees of freedom, system matrices for each state. Table 8.1 below presents the engaged clutch and/or synchroniser for each of the seven states. Each state is defined here as:

- Open refers to the neutral state where all gears and synchronisers are open
- Prelaunch refers to the state where only the odd synchroniser (S1) is closed
- Closed (odd) refers to the odd clutch and synchroniser being closed
- Closed (even) where the even clutch and synchroniser are closed
- Shift Closed (odd) with the odd clutch and both synchronisers closed in preparation for a shift

- Shift Closed (even) with the even clutch and both synchronisers closed in preparation for a shift
- Shift where both synchronisers are closed and clutches are open in slipping states

Given that there are a total of seven (7) possible states there must be seven (7) different system matrices required for developing a transient shift model.

Table 8.1: System states for shifting of DCT, "O" signifies open, "X" signifies closed

#	*State*	*C1*	*C2*	*S1*	*S2*	*NDOF*
1	**Open**	O	O	O	O	17
2	**Prelaunch**	O	O	X	O	16
3	**Closed (odd)**	X	O	X	O	15
4	**Closed (even)**	O	X	O	X	15
5	**Shift Closed (odd)**	X	O	X	X	14
6	**Shift Closed (even)**	O	X	X	X	14
7	**Shift**	O	O	X	X	15

8.4 POWERTRAIN MODEL

To model the powertrain economically several simplifications can be made to the transmission and powertrain, thereby reducing the degrees of freedom. For the transmission the idling gears not targeted for synchronisation or shifting can be grouped as a single lumped inertia on the primary shaft, added to engaged gear inertia. Within the gear pairs themselves, and the engaged synchroniser, backlash is initially ignored, combining inertias through gear ratios. With the synchroniser closed, clearances in the splines have a torsional backlash, and are also ignored. The propeller shaft is divided into four smaller inertias, while symmetry in the wheels and hubs pair the lumped inertias. As a result the lumped mass model is reflected in Figure 8.3, with open synchronisers and clutches shown below. Equations are derived in the subsequent sections.

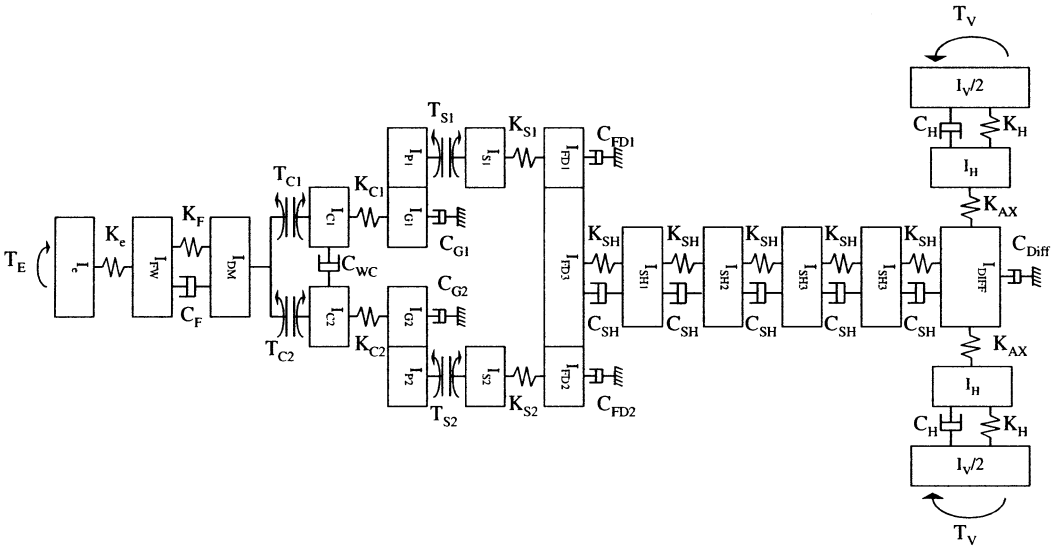

Figure 8.3: Simplified powertrain dynamic model with clutches and synchronisers

8.4.1 Engine, flywheel and clutch drum models

For general simulations the engine is modelled as a single degree of freedom with input torque from a lookup table. This ignores engine harmonics, as it is a more convenient method when considering engine control during shift transients. Nevertheless a harmonic engine model is presented later in this chapter. Though it is possible to replace the flywheel with a clutch drum inertia only, the inclusion of this flywheel enables the easy introduction a dual mass flywheel (DMFW) model to study the dynamic effects during shifting. Thus for the initial simulations flywheel stiffnesses are representative of the output shaft stiffness without hysteresis damping. These will be introduced when investigating shifting with transient engine torques.

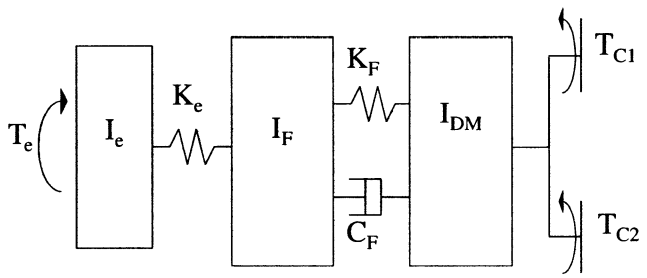

Figure 8.4: Engine, flywheel, and clutch drum model elements

The equations of motion for the engine, flywheel, and drum elements are:

$$I_e\ddot{\theta}_e - K_e(\theta_F - \theta_e) = T_e \tag{8.16}$$

$$I_F\ddot{\theta}_F + K_e(\theta_F - \theta_e) - K_F(\theta_{DM} - \theta_F) - C_F(\dot{\theta}_{DM} - \dot{\theta}_F) = 0 \tag{8.17}$$

$$I_{DM}\ddot{\theta}_{DM} + K_F(\theta_{DM} - \theta_F) + C_F(\dot{\theta}_{DM} - \dot{\theta}_F) = -(T_{C1} + T_{C2}) \tag{8.18}$$

where θ is angular displacement, $\dot{\theta}$ is angular velocity, T is torque, and subscripts e is Engine, F is flywheel, DM is drum, and C1 and C2 for clutch 1 and clutch 2, respectively.

8.4.2 Dual mass flywheel

In some manual transmissions the isolation of engine vibration is generally realised through torsional dampers or dual mass flywheels, limiting the transmission of engine harmonic torques to the clutch. Comprising of two inertia elements, primary inertia connects to the engine, while the secondary inertia is integrated with the clutch drum. Inertias are connected using a long moderately stiff arc spring with an angular displacement up to 110°. Centrifugal loading on the spring provides frictional resistance and hysteric damping between inertias.

Literature available on DMFW presents many different design configurations that can include multiple springs, or integrated dampers (for example ref [110, 111]). These models are more of a refinement on the fundamental design rather than new work; therefore a basic DMFW will be developed and integrated in to the model with easily manipulated configuration. The layout of this model is as per Figure 8.5, with the model equations of motion in equations 8.19 (a & b) and 8.20 (a & b).

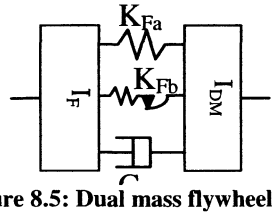

Figure 8.5: Dual mass flywheel elements

The equations of motion are divided into two groups, with or without dynamic friction component, with hys signifying hysteresis components

If $|K_{Fa}(\theta_F - \theta_D)| < T_{hys}$

$$I_F\ddot{\theta}_F + K_e(\theta_F - \theta_e) - K_{Fa}(\theta_{DM} - \theta_F) - K_{Fb}(\theta_{DM} - \theta_F) - C_F(\dot{\theta}_{DM} - \dot{\theta}_F) = 0 \quad (8.19a)$$

$$I_{DM}\ddot{\theta}_{DM} + K_{Fa}(\theta_{DM} - \theta_F) + C_F(\dot{\theta}_{DM} - \dot{\theta}_F) + K_{Fb}(\theta_{DM} - \theta_F) = -(T_{C1} + T_{C2}) \quad (8.20a)$$

Or when $|K_{Fa}(\theta_F - \theta_D)| > T_{hys}$

$$I_F\ddot{\theta}_F + K_e(\theta_F - \theta_e) - K_{Fa}(\theta_{DM} - \theta_F) - sign(\theta_{DM} - \theta_F)T_{hys} - C_F(\dot{\theta}_{DM} - \dot{\theta}_F) = 0 \quad (8.19b)$$

$$I_{DM}\ddot{\theta}_{DM} + K_{Fa}(\theta_{DM} - \theta_F) + C_F(\dot{\theta}_{DM} - \dot{\theta}_F) + sign(\theta_{DM} - \theta_F)T_{hys} = -(T_{C1} + T_{C2}) \quad (8.20b)$$

Model parameters that are of concern are taken from literature available for the DMFW. Gilliard & Singh [116] correctly point out that there is limited information available for the modelling of DMFWs, Schnurr [113] is one among several LuK affiliated authors that provide some details for typical inertia and stiffness data that can be applied. However it is Yamamoto, *et al,* [115] that provides the most relevant details regarding design of the stiffness using selected inertias for primary and secondary flywheels to ensure the local natural frequency is below idle speed of the engine. Typical values in ref [113, 115] range between 10 and 100 Nm for hysteresis, while results in Gilliard & Singh [116] indicate an approximate hysteresis values of 10 - 20Nm.

Both the models of ref [115, 116] utilise a hysteresis spring element with conventional springs, with the later including a damping component in the DMFW. Some form of these models are typical of many other authors. The configuration utilised in this paper combines conventional spring damper relationship with a hysteresis friction element, (see Figure 8.5). With the high inertia of the clutch drum and flywheels already present the current values are maintained, stiffness of the flywheel spring is modified to K_2 = 300Nm/rad, K_{2a} = 1000Nm/rad, hysteresis torque T_{hys} = 10Nm, and damping is C_2 = 5Nm.s/rad.

8.4.3 Transmission and synchroniser model

Within the transmission model clutch hubs, gears and the synchronisers are modelled as lumped inertias and shafts as stiffness elements. Damping is associated with the drag torques that results from system losses. Equations used to derive these torques have been previously detailed in Chapter 5, and summarised in Table 5.2. The transmission model is presented in Figure 8.6 below, with stiffness, damping and inertia elements. For each possible gear the compliant elements will vary based on the location within the transmission, and the inertia of gears, and pinions will also vary depending on the gear selected. In later sections, a model for the contact nonlinearity in the gear mesh and closed synchroniser model will be applied. Investigations into the effects on transmission performance with contact nonlinearities under different driving conditions, including shift transient performance, are conducted.

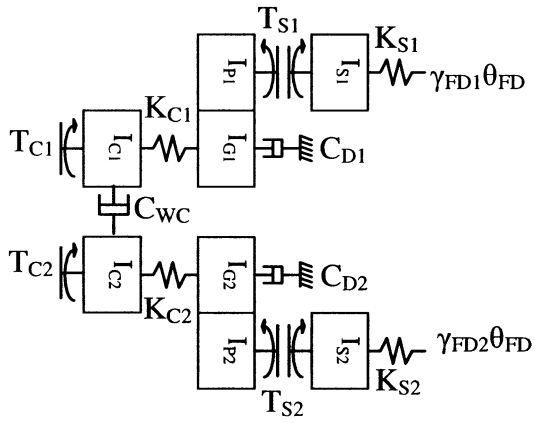

Figure 8.6: Clutch and simple transmission model elements

This results in six equations of motion for the transmission that are developed from the combined gears, synchronisers and clutches. These are:

$$I_{C1}\ddot{\theta}_{C1} - K_{C1}(\theta_{G1} - \theta_{C1}) - C_{WC}(\dot{\theta}_{C2} - \dot{\theta}_{C1}) = T_{C1} \tag{8.21}$$

$$\left(I_{P1}/\gamma_1^2 + I_{G1}\right)\ddot{\theta}_{G1} + K_{C1}(\theta_{G1} - \theta_{C1}) - C_{D1}\dot{\theta}_{G1} = -T_{S1}/\gamma_1 \tag{8.22}$$

$$I_{S1}\ddot{\theta}_{S1} - K_{S1}(\gamma_{FD1}\theta_{FD3} - \theta_{S1}) - C_{SD1}\dot{\theta}_{S1} = T_{S1} \tag{8.23}$$

$$I_{C2}\ddot{\theta}_{C2} - K_{C2}(\theta_{G2} - \theta_{C2}) - C_{WC}(\dot{\theta}_{C1} - \dot{\theta}_{C2}) = T_{C2} \tag{8.24}$$

$$\left(I_{P2}/\gamma_2^{\,2} + I_{G2}\right)\ddot{\theta}_{G2} + K_{C2}(\theta_{G2} - \theta_{C2}) - C_{D2}\dot{\theta}_{G2} = -T_{S2}/\gamma_2 \tag{8.25}$$

$$I_{S2}\ddot{\theta}_{S2} - K_{S2}(\gamma_{FD2}\theta_{FD3} - \theta_{S2}) - C_{SD2}\dot{\theta}_{S2} = T_{S2} \tag{8.26}$$

where subscripts P for pinion, G for gear, S for synchroniser, γ is gear ratio, and 1 and 2 refer to odd and even gear, respectively. Equations 8.21 to 8.26 represent the open synchroniser and clutch modes. If there is locking of the clutch and/or synchronisers these equations are changed to reduce the degrees of freedom represented by the locked mechanism. If either of the two clutches is locked, equation 8.15 is merged with either equation 8.21 or 8.24 of the model.

$$\begin{aligned}&(I_{C1} + I_{DM2})\ddot{\theta}_{DM2} + K_{DM}(\theta_{DM2} - \theta_{DM1}) + C_{DM}(\dot{\theta}_{DM2} - \dot{\theta}_{DM1})\\&-K_{C1}(\theta_{G1} - \theta_{DM2}) - C_{WC}(\dot{\theta}_{C2} - \dot{\theta}_{DM2}) = 0\end{aligned} \tag{8.27}$$

$$\begin{aligned}&(I_{C2} + I_{DM2})\ddot{\theta}_{DM2} + K_{DM}(\theta_{DM2} - \theta_{DM1}) + C_{DM}(\dot{\theta}_{DM2} - \dot{\theta}_{DM1})\\&-K_{C2}(\theta_{G2} - \theta_{DM2}) - C_{WC}(\dot{\theta}_{C1} - \dot{\theta}_{DM2}) = 0\end{aligned} \tag{8.28}$$

If either of the two synchronisers is locked equations 8.22 and 8.23 or 8.25 and 8.26 are reduced to two separate equations which represent the locked synchroniser mechanism.

$$\begin{aligned}&\left(\frac{(I_{S1} + I_{P1})}{\gamma_1^{\,2}} + I_{G1}\right)\ddot{\theta}_{G1} + K_{C1}(\theta_{G1} - \theta_{C1})\\&-\frac{K_{S1}}{\gamma_1^{\,2}}\left(\gamma_{FD1}\theta_{FD3} - \frac{\theta_{G1}}{\gamma_1}\right) + \left(C_{D1} + \frac{C_{SD1}}{\gamma_1^{\,2}}\right)\dot{\theta}_{G1} = 0\end{aligned} \tag{8.29}$$

$$\begin{aligned}&\left(\frac{(I_{S2} + I_{P2})}{\gamma_2^{\,2}} + I_{G2}\right)\ddot{\theta}_{G2} + K_{C2}(\theta_{G2} - \theta_{C2})\\&-\frac{K_{S2}}{\gamma_2^{\,2}}\left(\gamma_{FD2}\theta_{FD3} - \frac{\theta_{G2}}{\gamma_2}\right) + \left(C_{D2} + \frac{C_{SD2}}{\gamma_2^{\,2}}\right)\dot{\theta}_{G2} = 0\end{aligned} \tag{8.30}$$

The equations derived here, 8.18 and 8.21 to 8.30 are interchangeable depending on the state of the mechanism as indicated in Table 8.1. This changes the degrees of freedom of the dynamic model, again shown in Table 8.1, and changing natural frequencies, damping ratio, and modal shapes of the powertrain.

8.4.4 Final drive

In the dual lay shaft type DCT, final drive gears are used to link independent lay shafts to a single output shaft. Thus the final drive is the integration of three inertial gear components, utilising shaft stiffness elements to link the gear set to both the transmission and the drive shaft. The final drive components are reduced to a single inertia that links transmission lay shafts and the drive shaft by assuming no backlash in the gears. Damping elements are based on the drag torque model in Chapter 5 and coefficients found in Table 5.2.

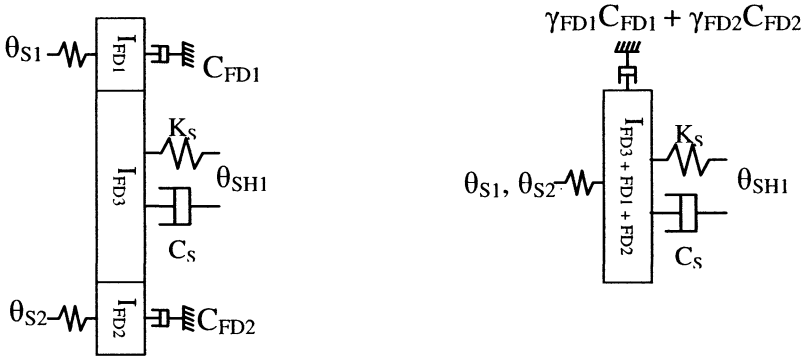

Figure 8.7: final drive and reduced differential model elements

The resulting equation of motion is:

$$\begin{aligned}&\left(\gamma_1^2 \cdot I_{FD1} + \gamma_2^2 \cdot I_{FD2} + I_{FD3}\right)\ddot{\theta}_{FD3} + \gamma_{FD1}K_{S1}\left(\gamma_{FD1} \cdot \theta_{FD1} - \theta_{S1}\right)\\&+ \gamma_{FD2}K_{S2}\left(\gamma_{FD2} \cdot \theta_{FD2} - \theta_{S2}\right) - K_{FD3}\left(\theta_{SH1} - \theta_{FD3}\right)\\&-\left(\gamma_{FD1}C_{FD1} + \gamma_{FD2}C_{FD2}\right)\dot{\theta}_{FD3} - C_{SH}\left(\dot{\theta}_{SH1} - \dot{\theta}_{FD3}\right) = 0\end{aligned} \tag{8.31}$$

where FD refers to final drive. Note here that if any synchroniser is closed, the degree of freedom represented by the synchroniser is replaced with the gear degree of freedom divided by the gear ratio, thus maintaining consistency of results, assuming S1 synchroniser is closed.

$$\begin{aligned}&\left(\gamma_1^2 \cdot I_{FD1} + \gamma_2^2 \cdot I_{FD2} + I_{FD3}\right)\ddot{\theta}_{FD3} + \gamma_{FD1}K_{S1}\left(\gamma_{FD1} \cdot \theta_{FD1} - \frac{\theta_{G1}}{\gamma_{G1}}\right)\\&+ \gamma_{FD2}K_{S2}\left(\gamma_{FD2} \cdot \theta_{FD2} - \frac{\theta_{G2}}{\gamma_{G2}}\right) - K_{FD3}\left(\theta_{SH1} - \theta_{FD3}\right)\\&-\left(\gamma_{FD1}C_{FD1} + \gamma_{FD2}C_{FD2}\right)\dot{\theta}_{FD3} - C_{SH}\left(\dot{\theta}_{SH1} - \dot{\theta}_{FD3}\right) = 0\end{aligned} \tag{8.32}$$

8.4.5 Propeller shaft model

The shaft is modelled as a four degree of freedom system in Figure 8.8, connected with torsional stiffness and a small damping component to maintain stability of the powertrain. Four lumped masses represent the shaft inertias, and are sufficient for generating the first four natural frequencies associated with the shaft.

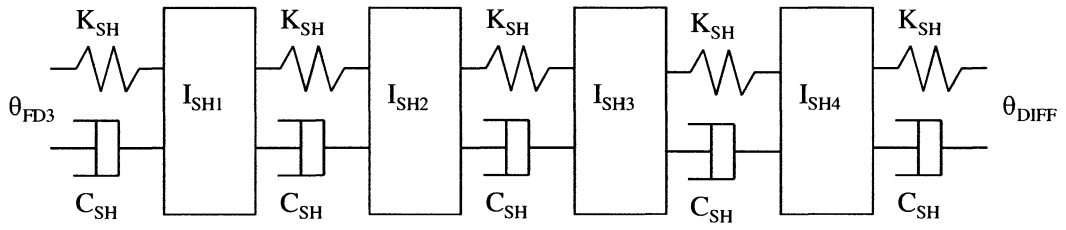

Figure 8.8: Shafts model elements

Equations of motion for these shaft elements are identical as it is assumed that the shaft is of constant cross-sectional geometry. The equation of motion for each shaft element is detailed below, where SH# subscript refers to one of the four shaft elements:

$$I_{SH1}\ddot{\theta}_{SH1} + K_{SH}(\theta_{SH1} - \theta_{FD3}) - K_{SH}(\theta_{SH2} - \theta_{SH1}) + C_{SH}(\dot{\theta}_{SH1} - \dot{\theta}_{FD3}) - C_{SH}(\dot{\theta}_{SH2} - \dot{\theta}_{SH1}) = 0 \quad (8.33)$$

$$I_{SH2}\ddot{\theta}_{SH2} + K_{SH}(\theta_{SH2} - \theta_{SH1}) - K_{SH}(\theta_{SH3} - \theta_{SH2}) + C_{SH}(\dot{\theta}_{SH2} - \dot{\theta}_{SH1}) - C_{SH}(\dot{\theta}_{SH3} - \dot{\theta}_{SH2}) = 0 \quad (8.34)$$

$$I_{SH3}\ddot{\theta}_{SH3} + K_{SH2}(\theta_{SH3} - \theta_{SH2}) - K_{SH3}(\theta_{SH4} - \theta_{SH3}) + C_{SH}(\dot{\theta}_{SH3} - \dot{\theta}_{SH2}) - C_{SH}(\dot{\theta}_{SH4} - \dot{\theta}_{SH3}) = 0 \quad (8.35)$$

$$I_{SH4}\ddot{\theta}_{SH4} + K_{SH3}(\theta_{SH4} - \theta_{SH3}) - K_{SH4}(\theta_{DIFF} - \theta_{SH4}) + C_{SH}(\dot{\theta}_{SH4} - \dot{\theta}_{SH3}) - C_{SH}(\dot{\theta}_{DIFF} - \dot{\theta}_{SH4}) = 0 \quad (8.36)$$

8.4.6 Differential, axle, and wheels and tyre models

The differential and axle splits the drive torque to both rear wheels, in this case a one-to-one ratio as the final drive is incorporated in the transmission. The differential is modelled as a lumped mass with damping to ground as a result of its efficiency loss. Stiffness elements connect driveshaft and axles to the differential.

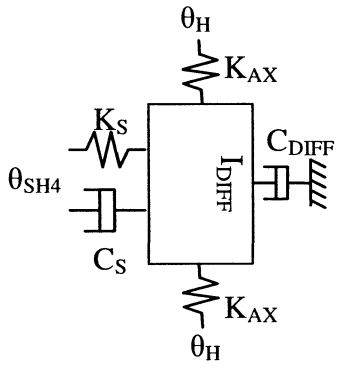

Figure 8.9: Differential and axle elements

$$I_{DIFF}\ddot{\theta}_{DIFF} + K_{SH4}(\theta_{DIFF} - \theta_{SH4}) - 2K_{AX}(\theta_H - \theta_{DIFF}) + C_{SH}(\dot{\theta}_{DIFF} - \dot{\theta}_{SH4}) - C_{DIFF}\dot{\theta}_{DIFF} = 0 \quad (8.37)$$

where subscripts DIFF refers to differential, AX is axle, H is wheel hub. The wheel model integrates the hub and tyre inertia with the flexural rigidity of the tyre wall. Moreover, the tyre inertia receives torque from the rolling resistance of the vehicle and the tyre must also include the vehicle inertia to accurately reflect the load on the transmission. This inertia is typically several orders of magnitude larger than that of any other powertrain component. Accordingly the wheel is modelled as in Figure 8.10.

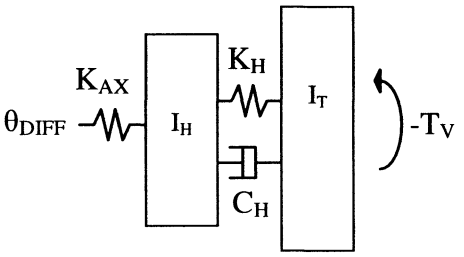

Figure 8.10: Hub and tyre model elements

The equations of motion for the wheel hub and tyre are presented below.

$$I_H\ddot{\theta}_H + K_{AX}(\theta_H - \theta_{DIFF}) - K_H(\theta_T - \theta_H) - C_H(\dot{\theta}_T - \dot{\theta}_H) = 0 \quad (8.38)$$

$$I_T\ddot{\theta}_T + K_H(\theta_T - \theta_H) + C_H(\dot{\theta}_T - \dot{\theta}_H) = -T_V/2 \quad (8.39)$$

where T is tyre and V is vehicle. It is assumed here that the axles, hub and wheels are symmetrical about the differential. This reduces the number of degrees of freedom by two for the model, without substantially affecting results. In line with theory presented

in Rao [144], parallel bodies can be summed together, therefore equations 8.38 and 8.39 are effectively doubled. Results are as follows:

$$2I_H\ddot{\theta}_H + 2K_{AX}(\theta_H - \theta_{DIFF}) - 2K_H(\theta_T - \theta_H) - 2C_H(\dot{\theta}_T - \dot{\theta}_H) = 0 \quad (8.40)$$

$$2I_T\ddot{\theta}_T + 2K_H(\theta_T - \theta_H) + 2C_H(\dot{\theta}_T - \dot{\theta}_H) = -T_V \quad (8.41)$$

This concludes the derivation of the lumped inertia model mathematical equations. The equations 8.13 to 8.40, excluding those related to particular parameters such as DMFW, provide the foundations for the lumped mass model at each of its 7 states. Inertia, stiffness, and damping matrices are each presented at later stage of this chapter.

8.4.7 Model Parameters

At this stage it is most useful to define the parameters that are employed in this model to represent the powertrain model. The gear ratios are presented below in Table 8.2, and lumped mass, stiffness, damping, and gear ratios for the finite element model are then presented in Table 8.3.

Table 8.2: Transmission and final drive gear ratios

Gear	*1st*	*2nd*	*3rd*	*4th*	*5th*	*6th*	*Final 1*	*Final 2*
Ratio	3.45	2.05	1.45	1.08	1.11	0.92	3.14	4.06

Table 8.3: Powertrain parameters to be applied to the nDOF models

Parameter	*Description*	*Inertia (kg-m²)*	*Parameter*	*Damping (Nms/rad)*
I_e	Engine	0.4	C_F	2
I_{FW}	Flywheel	0.2	C_{WC}	0.049
I_{DM}	Clutch drum	0.2	C_{G1}	0.0044
I_{C1}	Clutch hub 1	0.0072	C_{G2}	0.0052
I_{G1}	Gear 1	0.0006	C_{FD1}	0.01
I_{P1}	Pinion 1	0.005	C_{FD2}	0.023
I_{S1}	Synchroniser 1	0.0145	C_{SH}	0.1
I_{C2}	Clutch hub 2	0.0125	C_{DIFF}	0.25
I_{G2}	Gear 2	0.0013	C_H	4
I_{P2}	Pinion 2	0.005	**Parameter**	**Stiffness (Nm/rad)**
I_{S2}	Synchroniser 2	0.0094	K_E	95000
I_{FD1}	Final drive 1	0.0028	K_F	200000
I_{FD2}	Final drive 2	0.16	K_{C1}	210000
I_{FD3}	Final drive 3	0.0009	K_{S1}	560000
$I_{SH1} - I_{SH4}$	¼ propeller shaft	0.0007	K_{C2}	870000
I_{DIFF}	Differential	0.16	K_{S2}	470000
I_H	Hub	0.6992	K_{SH}	165000
I_V	Vehicle + tyre	67.5585	K_{AX}	165000
-	-	-	K_H	20000

8.5 LUMPED INERTIA MODEL MATRICES AND FREE VIBRATION ANALYSIS

Previously the equations of motion were derived for each element of the powertrain. These included elements from engine, dual mass flywheel, transmission, differential, output shafts and wheels. Table 8.1 presented the 7 different states for the transmission that are required to produce a sufficiently accurate dynamic model for the analysis of responses of the powertrain to synchroniser and clutch engagement, as would be experienced in a broad range of operating conditions. These equations of motion must be integrated into inertia, stiffness and damping matrices in conjunction with vectors for input torques, and angular displacement, velocity and acceleration to provide suitable tools for analysing the transient conditions of control of the DCT as shown in Section 8.2. However as the primary investigation of this thesis is the investigation of shift transient dynamics, only models for states 3 to 7 will be presented in Appendix C. Third and fourth gears are used for free vibration analysis.

The matrix models in Appendix C are used in transient simulations in following chapters and for free vibration analysis in Section 8.5.1.

8.5.1 DAMPED FREE VIBRATION ANALYSIS

Damped free vibration analysis is conducted for states with both synchronisers and one clutch engaged, these being state 5 and 6. Natural frequencies, damping ratios, and modal shapes can all be found in Tables 8.4 and 8.5. States 3, 4 and 7 are not included as under transient conditions the gear ratio is considered to be variable, and as such free vibration results are not constant [120]. To be able to justify the powertrain models as being reasonable representations of typical powertrains consider the information provided in the free vibration results.

The main results present in Table 8.4 are the:

1. Presence of the rigid body mode (0Hz), indicating that the powertrain is capable of unrestricted free rotation, i.e. the powertrain has free rotating motion to drive the vehicle.
2. Shuffle mode (6Hz), this is a global powertrain mode usually of the range 2-10Hz [45]

3. Global mode dominated by wheel hubs at 34Hz, consistent with Crowther [120]. However combining of wheels in Section 8.4.6 eliminates one of the two modes.
4. Local mode dominated by the flywheel at 98Hz
5. Local mode dominated by the differential at 225Hz
6. Local mode dominated by the Clutch 2 and Gear 2 at 231Hz
7. Local mode dominated by the Flywheel, Drum and Gear 2 at 325Hz
8. Frequencies above 1000Hz are primarily local modes dominated by gears and propeller shaft elements, consistent with the description of clonk in ref [45].

The results in Table 8.5 present a similar breakdown in terms of mode shapes and natural frequencies to the results identified above. Note that the natural frequencies in Tables 8.4 and 8.5 are compared to other available literature for AT powertrain model, such as ref [45, 119, 120]. The damping ratios are typically near an order of magnitude lower than comparable models. This verifies the assertion that DCT powertrain are significantly less damped than conventional automatics.

Table 8.4: Free vibration analysis of powertrain with 3rd gear and clutch 1 engaged, synchroniser two engaged with 4th gear. Results show natural frequencies, damping ratios and modal shapes

ω_n (Hz)	ζ (%)	STATE	θ_e	θ_F	θ_{D+C1}	$\theta_{G1+P1+S1}$	θ_{C2}	$\theta_{G2+P2+S2}$	θ_{FD}	θ_{SH1}	θ_{SH2}	θ_{SH3}	θ_{SH4}	θ_{Diff}	θ_H	θ_V
0	0.00	1	1.00	1.00	1.00	1.00	0.74	0.74	0.22	0.22	0.22	0.22	0.22	0.22	0.22	0.22
6	0.20	2	0.99	0.99	1.00	1.00	0.75	0.75	0.22	0.23	0.24	0.26	0.27	0.28	0.28	-0.10
34	1.26	3	-0.55	-0.52	-0.50	-0.47	-0.33	-0.33	-0.10	0.11	0.31	0.51	0.72	0.88	1.00	0.01
98	0.06	4	-0.24	1.00	-0.31	-0.32	-0.24	-0.24	-0.07	-0.08	-0.09	-0.10	-0.11	-0.09	-0.06	0.00
225	0.43	5	-0.05	0.26	-0.15	-0.11	-0.05	-0.05	-0.02	0.20	0.40	0.61	0.80	1.00	-0.11	0.00
231	0.17	6	0.11	-0.87	0.42	0.87	1.00	0.97	0.24	0.22	0.19	0.16	0.12	0.03	0.00	0.00
325	0.16	7	-0.05	1.00	-0.71	-0.78	-0.55	-0.53	-0.17	-0.13	-0.08	-0.04	0.01	0.06	0.00	0.00
736	0.01	8	0.00	-0.13	0.08	0.14	-0.09	0.04	0.06	0.66	0.99	1.00	0.73	-0.04	0.00	0.00
1070	0.65	9	0.00	0.00	0.00	0.09	0.12	0.02	-0.08	0.38	0.77	1.00	0.98	-0.05	0.00	0.00
1284	0.04	10	0.00	0.00	0.00	-0.01	0.02	-0.01	-0.01	0.67	1.00	0.88	0.42	-0.01	0.00	0.00
1926	0.01	11	0.00	0.00	0.00	0.00	0.00	0.00	-0.01	1.00	0.65	-0.55	-0.98	0.01	0.00	0.00
2040	1.21	12	0.00	0.00	0.00	-0.04	0.39	-0.45	0.05	-0.49	-0.90	-0.40	1.00	-0.02	0.00	0.00
2803	1.52	13	0.00	0.00	0.00	0.00	0.00	0.00	0.00	-0.89	0.18	1.00	-0.58	0.01	0.00	0.00
3294	1.63	14	0.00	0.00	0.00	0.00	0.00	0.00	0.00	-0.69	1.00	-0.73	-0.01	0.00	0.00	0.00

Table 8.5: Free vibration analysis of powertrain with 4th gear and clutch 2 engaged, synchroniser one engaged with 3rd gear. Results show natural frequencies, damping ratios and modal shapes

ω_n (Hz)	ζ (%)	STATE	θ_e	θ_F	θ_{D+C1}	$\theta_{G1+P1+S1}$	θ_{C2}	$\theta_{G2+P2+S2}$	θ_{FD}	θ_{SH1}	θ_{SH2}	θ_{SH3}	θ_{SH4}	θ_{Diff}	θ_H	θ_V
0	0.00	1	1.00	1.00	1.00	1.00	0.74	0.74	0.22	0.22	0.22	0.22	0.22	0.22	0.22	0.22
6	0.19	2	0.99	0.99	1.00	1.00	0.75	0.75	0.22	0.23	0.25	0.26	0.28	0.29	0.29	-0.10
34	1.26	3	-0.55	-0.53	-0.50	-0.47	-0.33	-0.33	-0.10	0.11	0.31	0.51	0.72	0.88	1.00	0.01
98	0.06	4	-0.26	1.00	-0.29	-0.31	-0.25	-0.25	-0.07	-0.08	-0.09	-0.10	-0.11	-0.09	-0.06	0.00
226	0.41	5	-0.04	0.23	-0.14	-0.10	-0.04	-0.04	-0.01	0.20	0.41	0.61	0.80	1.00	-0.11	0.00
231	0.19	6	0.10	-0.84	0.41	0.80	1.00	0.96	0.23	0.21	0.18	0.14	0.11	0.02	0.00	0.00
315	0.13	7	-0.06	1.00	-0.71	-0.78	-0.40	-0.43	-0.16	-0.12	-0.08	-0.04	0.01	0.06	0.00	0.00
875	0.04	8	0.00	-0.01	0.01	0.05	-0.06	-0.06	0.00	0.61	0.97	1.00	0.69	-0.03	0.00	0.00
1079	0.67	9	0.00	0.00	0.01	-0.20	0.13	0.04	-0.06	0.39	0.77	1.00	0.98	-0.05	0.00	0.00
1503	0.03	10	0.00	0.00	-0.01	-0.07	0.00	-0.05	0.02	0.93	1.00	0.46	-0.11	0.00	0.00	0.00
1832	0.01	11	0.00	0.00	0.00	0.05	0.01	0.00	-0.01	1.00	0.69	-0.44	-0.90	0.01	0.00	0.00
2040	1.22	12	0.00	0.00	0.00	-0.12	0.11	-0.20	0.04	-0.50	-0.90	-0.40	1.00	-0.02	0.00	0.00
2803	1.52	13	0.00	0.00	0.00	-0.01	0.00	0.00	0.00	-0.89	0.18	1.00	-0.58	0.01	0.00	0.00
3294	1.63	14	0.00	0.00	0.00	0.00	0.00	0.00	0.00	-0.69	1.00	-0.73	-0.01	0.00	0.00	0.00

8.6 MODELLING INPUT TORQUES

In the following sections of this chapter four separate torques are modelled for application to the DCT. This includes two versions of the engine torque, one mean torque model and one transient torque model that include engine harmonics, models for the clutches, synchroniser model derived from the previous rigid body model in Chapter 4, and the vehicle torque model.

8.6.1 Engine models

8.6.1.1 Mean torque model

In Chapter 2, Section 2.3.9 several different methods were identified for modelling and control of the vehicle engine. These predominantly included the use of lookup tables or empirical models to provide a mean torque from the engine. The use of mean engine torque models is convenient and simple method for control of DCT powertrains as complexity of the control model and computation requirements is reduced. Mean engine torque models also isolate the powertrain from the transient engine vibration that can otherwise mask transients developed in the transmission.

The engine model chosen is a basic look up table using engine speed and throttle input data to produce an output torque, with torque mapped as a function of engine speed and throttle, shown in Figure 8.11. The model is representative of a typical V6 petrol engine with a peak torque of 340Nm at 3000RPM and peak power of 150kW at 5000RPM.

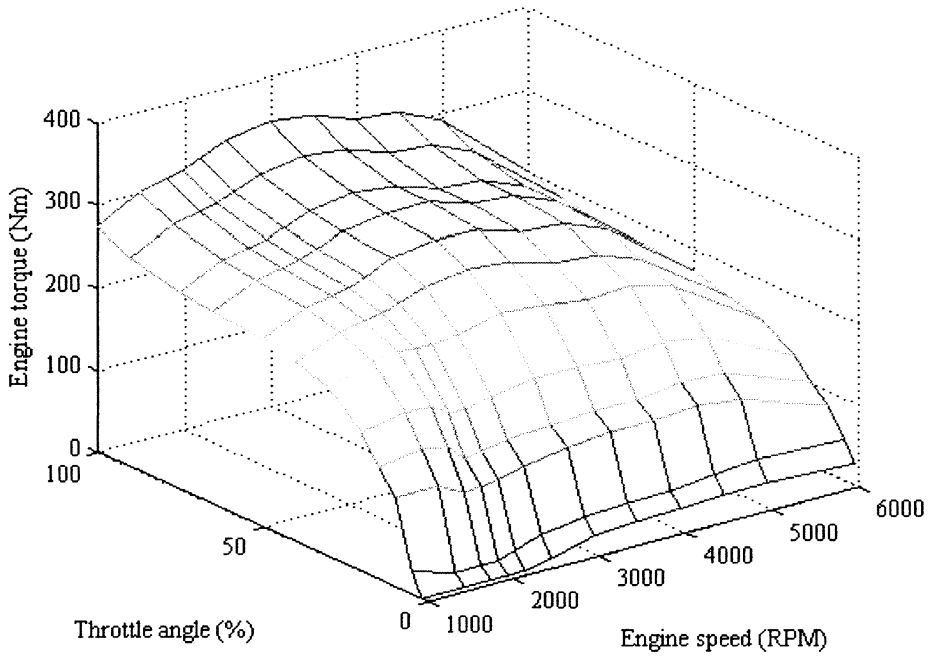

Figure 8.11: Engine torque map

8.6.1.2 Harmonic engine torque model

Harmonic torques in the engine result from the variation in pressure in individual pistons as they fire, angular spacing in the firing sequence and the variation in inertia on the crank shaft as pistons and connecting rods rotate in the engine. Taylor [107] provides a method for calculating the torques resulting from these three variations, both of which are applied to produce the transient torque engine model detailed below. The engine model is based on a V10 engine with a 65° V-bank. Paired pistons are used to reduce the degrees of freedom from 10, i.e. one for each piston, to 5, with each piston pair coupled to the next using crankshaft stiffness. In developing the transient engine model and, more particularly, for the development of a controller, only limited information is available for assimilation in addition to the pressure distribution. This information is detailed in Table 8.6.

Table 8.6:Transient engine model parameters

Parameter	*Value*	*Parameter*	*Value*
Piston mass (kg)	0.404	**Piston diameter (m)**	0.09
Paired cylinder inertia (kgm^2)	0.003038	**Crank radius (m)**	0.0235
Paired crank stiffness (Nm/rad)	260000	**Connecting rod length (m)**	0.103
V-bank (°)	65	**Firing order**	1 4 3 7 10 9 6 5 2

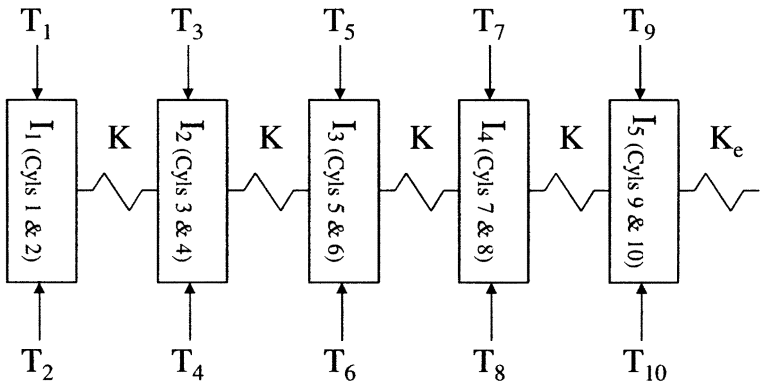

Figure 8.12: 5 degree of freedom transient engine torque model

In Figure 8.12 $T_{\#}$ is cylinder torque, $I_{\#}$ is lumped inertia, and K the crankshaft stiffness. Figure 8.12 is the 5DOF engine model used for transient vibration study, the five inertia elements represent the lumped inertia of crankshaft, connecting rod and pistons.

Though the inertia of piston and connecting rod is not constant, the Taylor [107] torque model for the engine compensates for the variation in inertias, and by lumping the inertia of the connecting rod as two separate masses in at the piston and crank shaft, the effective torque model can be further simplified.

$$\begin{bmatrix} I_1 & & & & \\ & I_2 & & & \\ & & I_3 & & \\ & & & I_4 & \\ & & & & I_5 \end{bmatrix} \begin{Bmatrix} \ddot{\theta}_1 \\ \ddot{\theta}_2 \\ \ddot{\theta}_3 \\ \ddot{\theta}_4 \\ \ddot{\theta}_5 \end{Bmatrix} + \begin{bmatrix} K & -K & & & \\ -K & 2K & -K & & \\ & -K & 2K & -K & \\ & & -K & 2K & -K \\ & & & -K & K+K_e \end{bmatrix} \begin{Bmatrix} \theta_1 \\ \theta_2 \\ \theta_3 \\ \theta_4 \\ \theta_5 \end{Bmatrix} = \begin{Bmatrix} T_1+T_2 \\ T_3+T_4 \\ T_5+T_6 \\ T_7+T_8 \\ T_9+T_{10} \end{Bmatrix}$$

(8.42)

The pressure profiles for two rotations of the crankshaft is shown in Figure 8.13, The applied torque consists of both gas and variable inertia torques, and are defined by Taylor [107] for the nth piston in equations 8.43 and 8.43 below. Similar equations are used to define the torque from varying piston and connecting rod inertias. Here $\dot{S}$ is the piston velocity and is approximated as a function of crank angle by using a Fourier series.

$$T_n = T_P + T_t \tag{8.43}$$

where:

$$T_t = -M_P \ddot{S} \frac{\dot{S}}{\omega_e}$$

$$T_P = PA_P \frac{\dot{S}}{\omega_e}$$

$$\frac{\dot{S}}{\omega_e} = -R_C(\sin\theta + 2a_2 \sin 2\theta ...)$$

$$\ddot{S} = \frac{d}{dt}\dot{S}$$

(8.44 a, b, c & d)

where A_P is piston area, M_P is piston mass, P is instantaneous piston pressure, $\dot{S}$ is piston speed, θ is crank angle, T_P is piston torque, and T_t is inertia change torque.

The transient engine torque can be calculated using this model, and is demonstrated below for a short interval, resulting in a mean engine torque of 373Nm, but without the

inclusion of losses. This torque is constant across a range of speeds. The pressure distribution over one cycle is shown in Figure 8.13 and a time series plot of the engine torque is shown in Figure 8.14, resulting from the presented model.

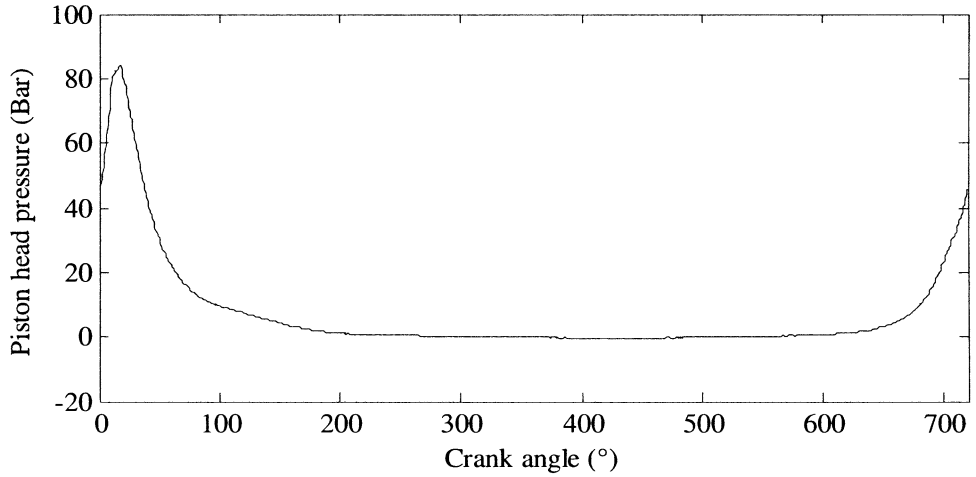

Figure 8.13: Piston head pressure map over 4 strokes

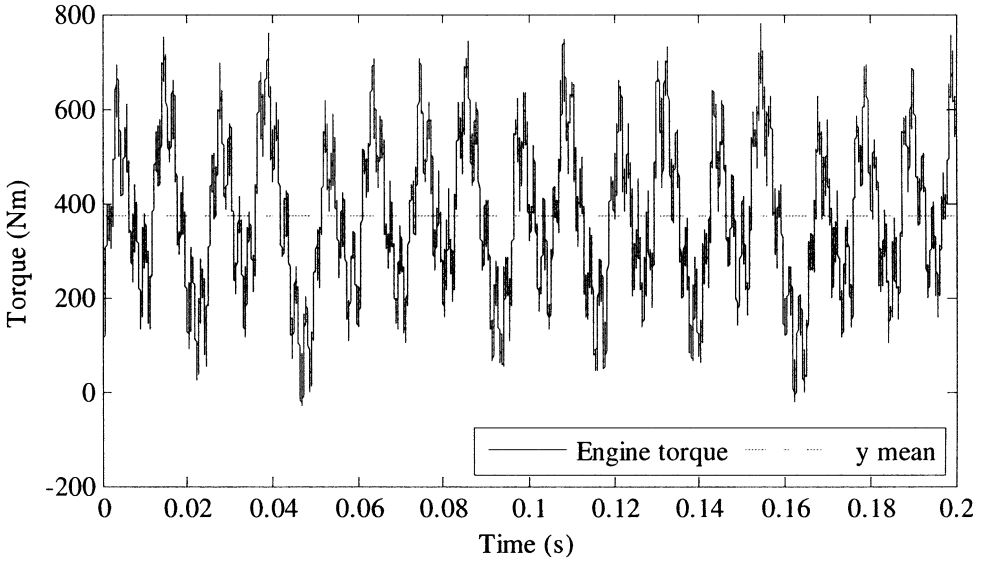

Figure 8.14: Transient engine torque simulation results

8.6.1.3 Harmonic engine control method

The most difficult aspect of using a transient torque model is how to control the engine torque during the shift transient. Ideally multiple piston head pressures would be available at a range of different throttle angles and spark advance locations, and it would then be possible to interpolate this data to vary the output torque in each piston. But with data for only wide open throttle available, an alternate solution must be sought to approximate the change in pressure distribution of the piston head for different

throttle angles. With much of the information unavailable for a detailed engine model in this research a simplified control approach is chosen. Consider that the method described below requires many assumptions to enable the development of a useful controller for the engine with limited engine details. Results will therefore be indicative of engine harmonics output but more development is needed for an accurate model.

The first assumption relates to the initial pressure for the system, i.e. that the pressure during intake strokes is the same for all possible variations in throttle angle, thus it is the same for both known and assumed pressure data during the intake stroke. To then calculate the pressure through the compression and expansion strokes the ideal gas law is applied to the system. Where not enough information is available for a standard Otto cycle model, and an ideal model will contain discontinuous pressure changes that may provide a source of excitation.

$$P_{BDC}V_{BDC} = m_T R T_{\square} \tag{8.45}$$

where V is piston volume, R is ideal gas constant m_T is mass of gas, and T is piston temperature. Considering at BDC, before compression that pressure and volume are the same for all pressure signals, and assuming mass and temperature are constant for all cycles – though this is not the case it is a required assumption – the ideal gas law can be applied over the compression and expansion engine strokes, with m_T, R, and T_P being constant over the cycle. During the exhaust and intake strokes the pressure is assumed to be the same as for the data in Figure 8.13. The resulting profile is shown in Figure 8.15.

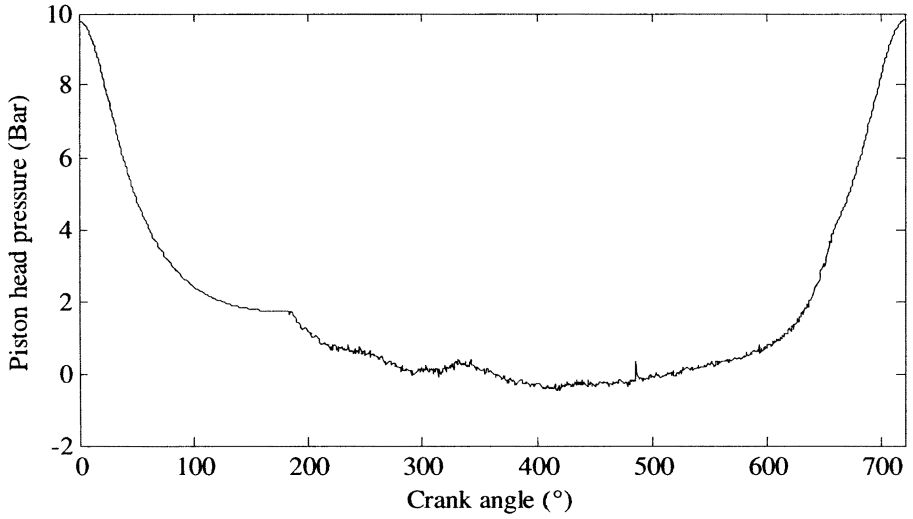

Figure 8.15: Calculated cylinder pressures for assumed 0% and 10% throttle angles

The known pressure cycle in Figure 8.13 and the assumed cycle in Figure 8.15 represent the wide open throttle (100%) and closed throttle (0%) pressure distributions, and linear interpolation is used to obtain a variation in output torque for each cylinder. Thus simulations of engine transient torques will produce torque harmonics with varying mean and peak-to-peak torques, providing a representative simulation of torque harmonics responding from the firing of individual engine cylinders.

This data represents the results with the inclusion of significant assumptions with respect to the actual determined pressure. In a real internal combustion engine it is expected that the change in throttle angle modifies the quantity of fuel injected and the spark advance. This will obviously result in the modification to the timing of peak pressure compared to crank angle, and the resulting engine output torque. However with the data available this is impossible to reasonably replicate.

As a final comment to this section, the goal of building a transient torque model has been to demonstrate the effect nonlinear engine torques on transients in a dual clutch transmission. With limited data available, a reasonable model of transient torques in the engine has been built, but with many of the variables required to develop a detailed engine model missing, the model has the capability to provide mean torque variation with engine harmonics. It must be concluded that the engine transient response is only effectual as a source of vibration, and its implementation will only be indicative of real response.

8.6.2 Clutch torque model

The clutch engagement is modelled using a piecewise torque model, where:

$$T_C = \begin{cases} 0 & X < X_0 \\ n\mu_D \dfrac{r_0^3 - r_I^3}{r_0^2 - r_I^2} \times F_A & X \geq X_0, \left|\Delta\dot{\theta}\right| \geq 0^* \\ T_{avg} & X \geq X_0, \left|\Delta\dot{\theta}\right| < 0^*, T_{avg} < T_{C,S} \\ n\mu_S \dfrac{r_0^3 - r_I^3}{r_0^2 - r_I^2} \times F_A & X \geq X_0, \left|\Delta\dot{\theta}\right| < 0^*, T_{avg} \geq T_{C,S} \end{cases} \tag{8.46}$$

where μ_D is dynamic friction coefficient, μ_S is static friction coefficient, $\Delta\dot{\theta}_{SL}$ is clutch slip speed, n is number of friction surfaces, r_I is inside radius, r_O is outside radius, F_A is

axial force, T_C is clutch torque, T_{avg} is average torque, X is piston displacement and, X_0 is contact displacement for friction plates. Here the initial piston displacement defines contact between clutch plates. With clutches open coupled damping clutch elements accounts for viscous coupling of clutch elements. The remaining components of the piecewise clutch model are identical to those found in ref [119, 120]. It includes dynamic and static friction components with the static friction calculated as the average torque, shown below in equations 8.47 to 8.49, where if average torque exceeds the static friction limit, torque moves to the static limit for transition to dynamic friction.

$$T_{AVG} = \frac{T_{C1a} + T_{C1b}}{2} \tag{8.47}$$

$$T_{C1a} = I_{DM}\ddot{\theta}_{DM} + K_{FW}(\theta_{DM} - \theta_{FW}) + C_{FW}(\dot{\theta}_{DM} - \dot{\theta}_{FW}) - T_{C2} \tag{8.48}$$

$$T_{C1b} = I_{C1}\ddot{\theta}_{C1} - K_{C1}(\theta_{G1} - \theta_{C1}) - C_{WC}(\dot{\theta}_{C2} - \dot{\theta}_{C1}) \tag{8.49}$$

8.6.3 Synchroniser model

The development of an applicable synchroniser mechanism model to the DCT is not as simple as the application of the clutch model. For the synchroniser, consideration of the engagement process is required to reasonably apply the rigid body model as a torque in the powertrain model, and is a primary reason why it is not implemented in Goetz [1]. To begin, it is assumed that as the inertia of the ring is small compared to the rest of the powertrain, it can be ignored. Instead torque inequalities that are used to define initiation of ring unblocking are used during speed synchronisation to ensure normal engagement of the synchroniser. As the focus of this aspect of the investigation is the transient powertrain dynamics, this assumption should not significantly affect the results of synchroniser engagement.

Implementation of the synchroniser model then focuses on the response torques that result for a given sleeve position. The sleeve location is calculated using the differential equations derived in Chapter 4, controlled using the same pressure model in Chapter 3, and the resulting positions are used in combination with slip speed and relative rotation to determine the torque resulting from synchroniser actuation, be it cone torque, blocking or indexing torque, or idling torque.

Given the high stiffness of the compressible hydraulic fluid, directly applying the synchroniser model over the duration of the simulation would require excessive computational time during both transient and steady state conditions. Therefore the hydraulic pressure and sleeve displacement are generated as a subroutine in Matlab such that once the transient period is initiated, the stiff control system is activated and solved using the direct application of the 4th order Runge-Kutta method to the hydraulic pressure and sleeve displacement using equations in Chapters 3 and 4.

The previously developed piecewise cone clutch model in chapter 4 must be redefined to include the inertia and stiffness components that replace drag torque. For synchroniser 2 equation 8.25 is rearranged to keep the synchroniser torque, T_{S2}, as the subject. This can be done similarly for synchroniser 1. As such the average synchroniser torque for the closed mechanism can be redefined using the equation below:

$$T_{S2,avg} = -\gamma_2\left(\left(I_{P2}/\gamma_2^{\,2} + I_{G2}\right)\ddot{\theta}_{G2} + K_{C2}(\theta_{G2} - \theta_{C2}) - C_{D2}\dot{\theta}_{G2}\right) \tag{8.50}$$

Thus, the average torque component of the piecewise cone clutch model must be re-evaluated in terms of the torque described above. Therefore equation 4.23 from Chapter 4 is modified to include the new average torque as:

$$T_{CONE} = \begin{cases} 4\pi\mu R_m^3 b\dfrac{\dot{\theta}_{syn}}{h} & X_S < 2 \\ \dfrac{\mu_C F_S R_C}{\sin\alpha} & X_S \geq 2, \dot{\theta} \neq 0 \\ T_{S,avg} & X_S \geq 2, \dot{\theta} = 0 \\ \dfrac{\mu_{C,S} F_S R_C}{\sin\alpha} & X_S \geq 2, \dot{\theta} = 0, T_{S,avg} > T_{C,S} \end{cases} \tag{8.51}$$

The torque resulting from blocking and indexing are both unchanged from Chapter 4 (see equation 4.17 and 4.25). The synchroniser then engages in a similar manner to the rigid body model, producing output torques that translate to the powertrain model.

8.6.4 Vehicle torque model

The last torque that needs consideration in the development of the powertrain model is the vehicle torque model. This combines the road incline, aerodynamic drag and rolling resistance of the vehicle to generate an input force on the wheels that resists the vehicle's forward motion unless there is a steep negative incline. The equations for each of these loads and their conversion to a torque are presented below in the following equations.

$$F_{incline} = M_v \times g \times \sin(\theta_{incline}) \tag{8.52}$$

$$F_{aero} = \frac{1}{2} \rho_{air} \times W_v \times H_v \times C_D \times V_W^{\,2} \tag{8.53}$$

$$F_{roll} = M_v \times g \times C_{tire} \tag{8.54}$$

$$F_R = F_{incline} + F_{aero} + F_{roll} \tag{8.55}$$

$$T_R = F_R \times R_{wheel} \tag{8.56}$$

where $\theta_{incline}$ is angle of inclination, ρ_{air} is air density, g is gravity, C_D is coefficient of drag, C_{tire} is dimensionless tire retarding force, F_{aero} is aerodynamic drag load, $F_{incline}$ is incline load, F_{roll} is aerodynamic drag load, F_R is net resistance force, H_v is vehicle height, M_v is vehicle mass, R_{wheel} is wheel radius, T_R is net resistance torque, V_W is linear velocity of driving wheels, and W_v is vehicle width.

8.7 CHAPTER SUMMARY AND CONCLUSIONS

The focus of this chapter was the development of a model of a dual clutch transmission equipped powertrain for use in transient gear shift simulations. The powertrain is characterised as a rear wheel drive, wet clutch DCT with synchronisers to engage gears for shifting. Multiple n-degree of freedom powertrain models have been developed to simulate synchronisation and clutch-to-clutch gear shifts using different arrangements of the one powertrain model. These lumped inertia models are dependent on the different powertrain states identified in Table 8.1. However the open powertrain models were excluded as launch control has not been part of the focus of this research.

In developing the model, provisions have been made for the use of alternative damping systems such as dual mass flywheels, and models have included the linearised drag torques developed in Chapter 5 to approximate damping in the transmission. Additionally, in creating these models assumptions have employed. i.e.:

- Ignore backlash in the gear mesh,
- Ignore temperature dependence of the powertrain and particularly transmission,
- Simplifying branched symmetrical axles and tyres to one branch of the powertrain, and
- Reduce the idling gears to reflected inertia at the active gear.

These assumptions have allowed the development of a simplified powertrain model of the DCT while still capturing the important characteristics of the powertrain, particularly with regard to transient vibration, and damping of the powertrain system. Free vibration analysis in third and fourth gears have shown this powertrain to be consistent with published works on similar powertrain architectures for equivalent planetary automatics. However there is the clear demonstration of significant reduction in powertrain damping compared to these powertrains.

Complementing the lumped inertia of the powertrain are models of engine, clutch, synchroniser, and vehicle torques. Both clutch and vehicle torque models are based on popularly used techniques that can be found in ref [1, 120] among a range of literature. The piecewise model for clutch torque has been extended to include pre-fill phase of the hydraulic piston, with no clutch load without contact of friction surfaces, the dynamic friction, and static friction limited by average clutch torque making up the piecewise components. Vehicle torque models includes road incline, aerodynamic drag and rolling resistances for the torque model. Two engine models have been presented, the first a mean torque lookup table model, useful for control modelling, and the second a 5DOF transient vibration model, with piston head pressure used to simulate engine vibration harmonics similar to the model in ref [108]. Finally, the synchroniser model developed compromised of a stiff model of the synchroniser sleeve that is independent of the lumped inertia model, which is used to determine the torques acting on the powertrain as the mechanism is engaged.

8.7.1 Summary of contributions

In the development of lumped mass models of the DCT powertrain, unique research contributions from this chapter include:

- Development of rear wheel drive powertrain models for the DCT that include the capacity for transients with combined gear synchronisation and clutch-to-clutch gearshifts,
- DCT models with detailed harmonic torque engine models for transient vibration studies, and
- Detailed modelling of the synchroniser mechanism torques acting on the synchroniser and its inclusion in the lumped inertia powertrain model.

CHAPTER 9: SHIFT CONTROL OF DCTS – ISSUES AFFECTING SHIFT QUALITY

9.1 INTRODUCTION

Critical to the development of the dual clutch transmission has been the capacity to apply modern control technologies to achieve the best possible shift quality. Even so, current results by several authors demonstrate that the low system damping present in the DCT equipped powertrain has made providing shifts of the quality equal to those in the AT difficult to reproduce. To that end this chapter investigates the influence of different torques acting on the powertrain during shifting, including both clutch torques derived from the hydraulic control system and those derived in the engine.

From literature research conducted there is demonstration of a wide range of control approaches conducted into DCT studies including open loop [25], closed loop [27], and fuzzy [28] approaches. Popular methods similar to those presented by Goetz, Levesley & Crolla [21] make use of torque and inertia phase control, tending to mask the response during the torque phase with slip speed control. Further, in each case there has been significant simplification of hydraulic control systems. As such there is a large breadth of research into DCT control, but little depth of research into the influence hydraulic system or of various uncertainties and assumptions on control and shift performance.

Briefly, control process and requirements are discussed specifically relating to shift control of DCTs. Then a three/four degree of freedom powertrain model is developed with gear ratio change for the purpose of application to clutch shift control. The basic control architecture is then put forward, including engine and clutch control with the integrated hydraulic systems, previously presented in Chapter 3. To study the influence of torsional aspects of engine and clutch control during shifting, transient simulations are then presented using ideal clutch torque, torque derived from the hydraulic model, and under the influence of error in torque estimation. This is then expanded to include feed forward control of engine torque during the shift transient. To then study the effects of engine harmonics, the model is expanded to include the harmonic torque

model of the engine. Finally aspects of time delay that were demonstrated in Chapter 3 in the initial study of the hydraulic system are incorporated into the control architecture.

9.2 SHIFT CONTROL OF DUAL CLUTCH TRANSMISSIONS

9.2.1 Power shifting process in a DCT

For gearshift control of engine and clutches in the DCT, consideration of torque balance in the system is of critical importance. At the engine, clutch 1, clutch 2 and at the wheels an imbalance in torque, speed and inertia will generate system excitations, i.e. transient response. During shifting, and particularly as the clutches lockup, it is necessary that discontinuous variation of inertia, speed and torque are minimised, particularly with no significant source of damping to minimise response.

Power shifting, or clutch-to-clutch shifting, can be performed in a similar manner to those performed in automatic transmissions where hydraulically actuated friction elements are simultaneously released and engaged to smoothly transfer torque between engaged and target clutches in a manner that minimises loss of tractive load to the road. Consider Figure 9.1 with clutch 1 engaged, the powershift is achieved by releasing clutch C1 pressure to the point of slip, simultaneously clutch C2 cylinder is filled to near contact in friction surfaces. Referring to the detailed description in Moskwa & Hedrick [40], shifting begins with the torque phase, where pressure increased to the target C2 clutch and released concurrently from C1 clutch in a manner that minimises the drop in tractive load to the road to transfer torque between clutches. At the completion of torque phase peak load is on the target clutch, C2, and the previously engaged clutch, C1, has a zero load. This signifies the initiation of the inertia phase, with C1 clutch load maintained at zero, C2 pressure is manipulated to synchronise speeds in the engine and transmission halves of clutch C2. With speeds synchronised C2 pressure is set to a maximum to lock the friction surfaces. During this process the engine torque must be manipulated to first minimise the torque hole during the torque phase, and second to aid in synchronising speeds during the inertia phase.

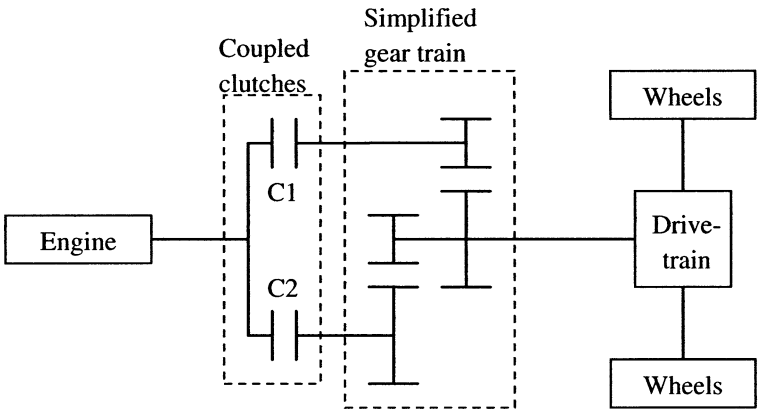

Figure 9.1: General DCT powertrain layout

Shift control is therefore divided into 4 steps:

- Shift preparation, where clutch pressure is released for the engaged clutch and piston filled for target clutch
- Torque phase, with the engaged clutch pressure released and target clutch pressurised to minimise the loss of tractive road load,
- Inertia phase, where target clutch is synchronised, and
- Lockup, with the target clutch pressure maximised to provide friction lock.

9.2.2 Shift requirements

During power shifting there is reliance on the simultaneous release and engagement of two clutch systems without the development of undesirable shift transients and maintain tractive road load. Additionally control of the engine speed is required to ensure rapid acceleration to the required gear speed. Included in this description are the basic requirements for shift control of lightly damped transmission systems.

Considering refs [122-128], there are several requirements that must be considered for both good control of the shift and driver comfort. Three main clutch requirements are:

1. The minimisation of shift time to ensure overheating of the clutch is minimised,
2. Reduce torque overlap, or negative torque, the excess torque in the off going clutch that resists the speed synchronisation of the on-going clutch

3. The control system must estimate the target clutch torque accurately such that the friction torque in the clutch compensates for release of the engine from the powertrain during shift. Failure will provide discontinuous load to the vehicle, introducing vibration and reducing acceleration of the vehicle.

For the driver, shift comfort is imperative. Therefore there must be minimum negative acceleration during and after the shift, with deceleration during the shift equating to a reduction in tractive force, and after the shift poor quality is perceived as transient response. Additionally, vehicle lurch must be minimised, perceived as jerk by the driver and resulting from overestimation of the clutch torque.

Finally, the engine must compensate for the torque hole during the torque phase by adding energy to the powertrain and minimising power loss during this phase. Secondly, emphasis is placed on the need to rapidly accelerate or brake the engine inertia to a new target speed during the inertia phase of shifting. The idle speed is used as the lower bound for engine speed to prevent engine stall during shifting.

9.3 4/3 DOF MODELLING OF THE POWERTRAIN FOR CLUTCH CONTROL

Previously the hydraulic components for clutch control of the DCT were developed in the Simulink environment of Matlab using 13 degrees of freedom (Chapter 3). To perform accurate shift modelling these must be integrated into a compact model of the DCT, with degrees of freedom minimised to provide computationally efficient transient simulations. Comparison of Kirschstein [24] , Liu, *et al,* [27] and Zhang, *et al,* [121], (with 4DOF models) to Goetz, Levesley & Crolla [1, 21], (with a 12DOF model) suggests that it is reasonable to use lower order models to study control methodologies, with higher order models more effective for investigating transient vibration. By ignoring very stiff components higher frequency responses will not be reflected in the mode. Kiencke & Nielson [41] identified these frequencies as not being influential on transient shift control. Therefore a 4 to 3 DOF clutch lockup model is developed using parameters derived from the multi-degree of freedom model developed in Chapter 8.

This model can be considered as the one presented in Figure 9.2, including engine, clutch drum, clutch hub and transmission, and vehicle as separate inertial components of

the system. With synchroniser mechanism excluded from the dynamic system, stiffness and damping elements are used to link engine and drum, and transmission to the vehicle.

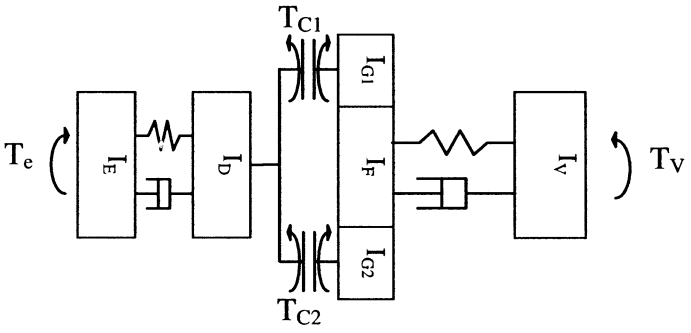

Figure 9.2: 4DOF model of powertrain with both clutches open

For the 4DOF in Figure 9.2 model the equations of motion are as follows:

$$I_E\ddot{\theta}_E = K_D(\theta_D - \theta_E) + C_D(\dot{\theta}_D - \dot{\theta}_E) - T_E \tag{9.1}$$

$$I_D\ddot{\theta}_D = -K_D(\theta_D - \theta_E) - C_D(\dot{\theta}_D - \dot{\theta}_E) + T_{C1} + T_{C2} \tag{9.2}$$

$$I_T\ddot{\theta}_T = K_T(\theta_V - \theta_T) + C_T(\dot{\theta}_V - \dot{\theta}_T) - \gamma_1 T_{C1} - \gamma_2 T_{C2} \tag{9.3}$$

$$I_V\ddot{\theta}_V = -C_T(\dot{\theta}_V - \dot{\theta}_T) - K_T(\theta_V - \theta_T) + T_V \tag{9.4}$$

where C is clutch, D is clutch drum, E is engine, T is transmission, V is vehicle, and 1, 2 refers to clutch or gear number. After clutch lockup the model reduces to a 3DOF system, as presented in Figure 9.3.

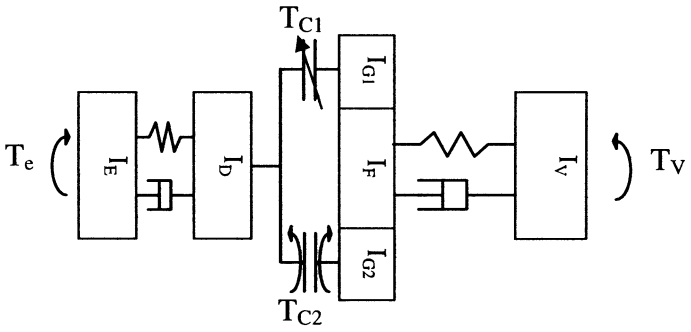

Figure 9.3: 3DOF dynamic model of powertrain with clutch one closed

The equations of motion are:

$$I_E\ddot{\theta}_E = K_D(\gamma_1\theta_T - \theta_E) + C_D(\gamma_1\dot{\theta}_T - \dot{\theta}_E) - T_E \tag{9.5}$$

$$\begin{aligned}(I_D + \gamma_1^2 I_T)\ddot{\theta}_D &= -\gamma_1 K_D(\gamma_1\theta_T - \theta_E) - \gamma_1 C_D(\gamma_1\dot{\theta}_T - \dot{\theta}_E)\ldots \\ &+ K_T(\theta_V - \theta_T) + C_T(\dot{\theta}_V - \dot{\theta}_T) + \left(1 - {}^{\gamma_2}\!/_{\gamma_1}\right)T_{C2}\end{aligned} \tag{9.6}$$

$$I_V\ddot{\theta}_V = -C_T(\dot{\theta}_V - \dot{\theta}_T) - K_T(\theta_V - \theta_T) + T_V \tag{9.7}$$

Significantly, Equation 9.6 provides the capacity to include the reaction to the premature engagement of the open clutch pack and the impact it has on the shifting. The piecewise model of the clutch shown in equation 9.8 is used as the clutch friction for both T_{C1} and T_{C2}, with the input force taken from the hydraulic pressure generated in the controller model from Chapter 3.

Conceptually, the sticking state of the clutch is defined as zero differential clutch speed and the average torque in the closed clutch plates not exceeding that available from static friction limits. The clutch is considered to be the state of slip if the static friction limit is breached by the average torque present in the clutch; however the slip speed can be zero. Using a constant friction coefficient Equation 8.45 is thus:

$$T_C = \begin{cases} 0 & X < X_0 \\ n\mu_D \dfrac{r_0^3 - r_I^3}{r_0^2 - r_I^2} \times F_A & X \geq X_0, \left|\Delta\dot{\theta}\right| \geq 0^* \\ T_{avg} & X \geq X_0, \left|\Delta\dot{\theta}\right| < 0^*, T_{avg} < T_{C,S} \\ n\mu_S \dfrac{r_0^3 - r_I^3}{r_0^2 - r_I^2} \times F_A & X \geq X_0, \left|\Delta\dot{\theta}\right| < 0^*, T_{avg} \geq T_{C,S} \end{cases} \tag{9.8}$$

where X_0 is the contact limit of the clutch plates, and 0* is an approximation of zero such that the state of the clutch can transit from sticking to slipping without being computationally expensive. To eliminate the issue of zero crossing present in Simulink-Stateflow, 0*=0.001rad/s. The dynamic and static frictions are represented diagrammatically below in Figure 9.4.

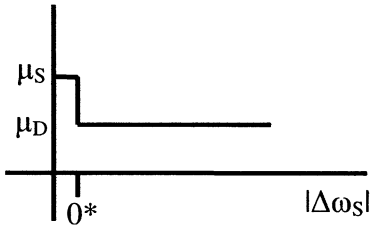

Figure 9.4: friction coefficient representation as a function of slip speed

The average torque at the clutch is then defined using equations 9.2 and 9.3 as:

$$T_{avg} = \left(T_{CD1,2} + T_{CT1,2}\right)/2 \tag{9.9}$$

$$T_{CD1,2} = -I_D\ddot{\theta}_D - K_D(\theta_D - \theta_E) - C_D(\dot{\theta}_D - \dot{\theta}_E) - T_{C2,1} \tag{9.10}$$

$$T_{CT1,2} = \left(-I_T\ddot{\theta}_T + K_T(\theta_V - \theta_T) + C_T(\dot{\theta}_V - \dot{\theta}_T) + \gamma_{2,1}T_{C2,1}\right)/\gamma_{1,2} \tag{9.11}$$

9.3.1 Integration with hydraulic control system

Integration of the hydraulic control system with the 4DOF dynamic powertrain model requires consideration of first, the impact of the highly nonlinear hydraulic controller, and second, the implementation of a model with changing degrees of freedom. For a variable degree of freedom model Matlab® script based execution is highly desirable due to the capacity to manipulate variables, and use event based triggering for control. Countering this is the development of controllers and control algorithms in the Simulink® environment, where controller development, implementation and evaluation are much more accessible. This is however limited by the discontinuities created in the change of degrees of freedom. Consequent zero crossing detection evaluation or discontinuity makes solving the stick to slip clutch transition impractical.

The solution to this problem is the development of a multi degree of freedom powertrain model in Stateflow®, an event driven, or reactive, module for Simulink (see [145] for details on Stateflow). Significant advantage arises in the execution of Stateflow® in that separate NDOF models can be executed depending on state requirements, with seamless transfer of state conditions between stick and slip states. Subsequently, the model is computationally limited by the execution of the stiff hydraulic system model. Given the requirements for analysing the influence of the hydraulic system, this is necessary.

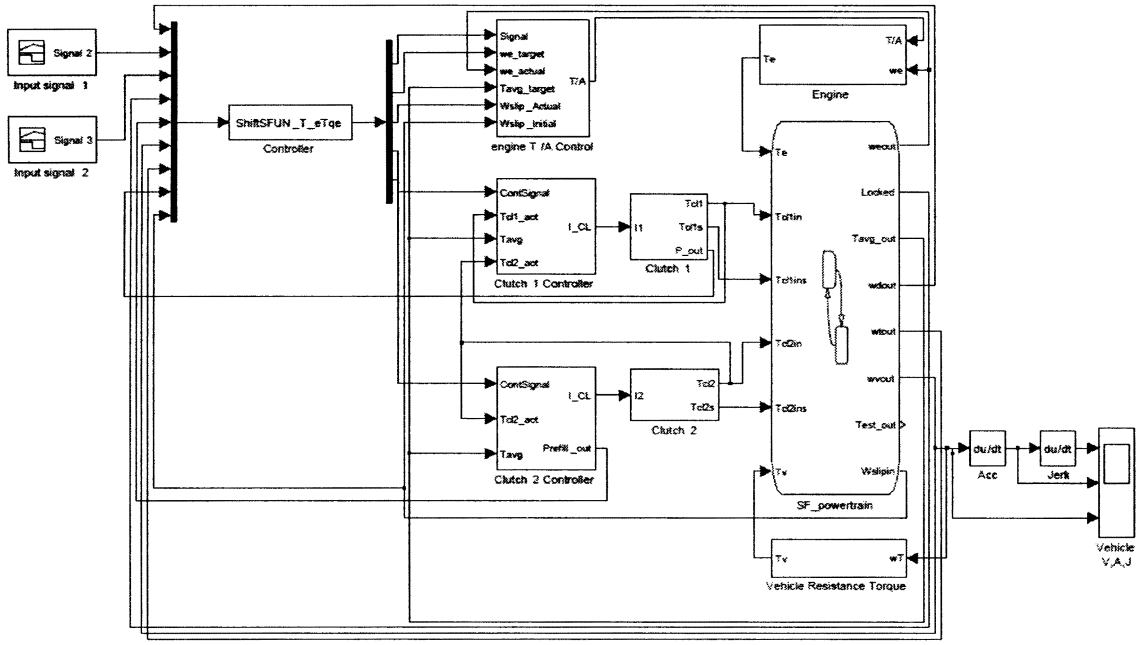

Figure 9.5: Simulink - Stateflow representation of reduced order powertrain with integrated control modules

9.3.2 Parameter estimation

To develop a reasonable mathematical model of the powertrain that reflects the full system model, the natural frequencies and damping ratios of the 4DOF model must reflect the full system model developed in Chapter 8. For the three required states under investigation the natural frequencies and damping ratios are presented below, ignoring the rigid body modes, as:

Table 9.1: Natural frequencies and damping ratios for parameter estimation, for clutch 1 in 3rd gear and clutch 2 in 4th gear

State	*Natural frequencies (Hz)*				*Damping ratios (%)*			
Modes	1	2	3	4	1	2	3	4
Open clutches	18	40	102	230	1.04	0.79	0.05	0.12
CL1 closed	6	34	98	-	0.2	1.26	006	-
CL2 closed	6	34	98	-	0.19	1.26	0.06	-

To maintain results similar to a full powertrain model the inertia elements utilised in the 4DOF model must be consistent with the 15DOF model. Thus it is reasonable to build the inertia matrix using equations 8.1 to 8.4 and reference inertias taken from the combination of multiple elements in the 15DOF inertia matrix. I_e can then be perceived as the engine and flywheel inertia, I_D is the clutch drum inertia, I_T is the inertia of the whole transmission, final drive and half propeller shaft, and I_V is vehicle, hub, differential, and other half shaft inertias. With these four elements used here taken as the combined inertias of the higher degree of freedom model, it is inferred that the average velocity and acceleration of the reduced order model developed here will be essentially the same as the higher order model during transient simulations.

Selection of the stiffness elements is more difficult. First consider now the required stiffness elements. For an accurate representation of the system response the elements must reproduce the lower natural frequencies of the system. Thus stiffness elements that directly represent input and propeller shafts in the powertrain are unlikely to satisfy this requirement. Instead, consider the information that is available. The inertia and natural frequency matrices are known, and the form of the stiffness matrix has been given by equations 8.1 to 8.4. From undamped free vibration analysis it is possible to arrive at the general solution for the system vibration by assuming the harmonic solution to the acceleration and displacements of the system as:

$$\theta_i = \Theta_i \cos(\omega t + \varphi_i) \tag{9.12}$$

$$\ddot{\theta}_i = -\omega^2 \Theta_i \cos(\omega t + \varphi_i) \tag{9.13}$$

And, for undamped free vibration equations 1 to 4 become:

$$0 = (-I_E \omega^2 + K_D)\Theta_E \cos(\omega t + \varphi_E) - K_D \Theta_D \cos(\omega t + \varphi_D) \tag{9.14}$$

$$0 = -K_D \Theta_E \cos(\omega t + \varphi_E) + (-\omega^2 (I_D) + K_D)\Theta_D \cos(\omega t + \varphi_D) \tag{9.15}$$

$$0 = (-\omega^2 (I_T) + K_T)\Theta_T \cos(\omega t + \varphi_T) - K_T \Theta_V \cos(\omega t + \varphi_V) \tag{9.16}$$

$$0 = (-\omega^2 I_V + K_T)\Theta_V \cos(\omega t + \varphi_V) - K_T \Theta_T \cos(\omega t + \varphi_T) \tag{9.17}$$

From here nontrivial solutions to the harmonic response concludes that the sinusoidal components, cos(ωt+φ), and amplitudes, Θ, are not equal to zero, thus the determinant of the coefficients of Θ must be equal to zero.

$$\det\begin{bmatrix} \left(-\omega^2 I_E + K_D\right) & -K_D & 0 & 0 \\ -K_D & \left(-\omega^2 (I_D) + K_D\right) & 0 & 0 \\ 0 & 0 & \left(-\omega^2 (I_T) + K_T\right) & -K_T \\ 0 & 0 & -K_T & \left(-\omega^2 I_V + K_T\right) \end{bmatrix} = 0 \quad (9.18)$$

By taking the determinant of the first column, and introducing the natural frequencies in descending order, an equation for the solution to the natural frequencies, with parameters defined from the natural frequencies detailed in Table 9.1, can be found as:

$$\begin{aligned} &\left[-\left(\omega_1^2\omega_2^2 I_E I_D - \left(\omega_1^2 I_E + \omega_2^2 I_D\right)K_D + K_D^2\right) - K_D^2\right]\times\ldots \\ &\left[\left(\omega_3^2\omega_4^2 I_T I_V - \left(\omega_3^2 I_T + \omega_4^2 I_V\right)K_T - K_T^2\right) + K_T^2\right] = 0 \end{aligned} \quad (9.19)$$

Arriving at two solutions for the stiffness elements by solving for K_D and K_T:

$$K_D = \frac{\omega_1^2\omega_2^2 I_E I_D}{\omega_1^2 I_E + \omega_2^2 I_D} \quad (9.20)$$

$$K_T = \frac{\omega_3^2\omega_4^2 I_T I_V}{\omega_3^2 I_T + \omega_4^2 I_V} \quad (9.21)$$

With the mass and stiffness parameters now known, selection of damping coefficients can be performed. Using the damping ratios presented in Table 9.1, in conjunction with the defined parameters, the required damping coefficients can be estimated using inertial components of the 4DOF system in conjunction with the known natural frequencies and stiffnesses, this results in coefficients of C_D and C_T. The resulting model parameters are in Table 9.2:

Table 9.2: Estimated system parameters for a 3rd to 4th gear upshift

	Inertia (kg.m²)		*Stiffness (Nm/rad)*
I_E	0.6	**K_D**	77000
I_D	0.2	**K_T**	16000
I_T	0.28		**Damping (Nm.s/rad)**
I_V	68.82	**C_D**	1.76
-	-	**C_T**	0.12

9.3.3 Free vibration analysis

Undamped free vibration analysis is applied here to compare the simplified 4DOF model to the original 15DOF powertrain model. It is assumed that there is no damping in the system and the system matrix for each state in both powertrain models is formed from equations 1 to 4. The system natural frequencies and modal shapes are then determined through the solution to the Eigenvalue problem, with modal shapes represented by Eigenvectors and squared natural frequency by the Eigenvalues.

Table 9.3: 4DOF and 15DOF system natural frequencies

Model	State (3^{rd} and 4^{th} gears)	Natural frequencies (Hz)					
		1	*2*	*3*	*4*	*5*	*6*
4DOF	Open clutches	0	0	38	114	-	-
	CL1 closed	-	0	7	110	-	-
	CL2 closed	-	0	6	112	-	-
15DOF	Open clutches	0	0	17.8	39.9	102	230.5
	3^{rd} gear	-	0	5.5	34.2	97.7	225.2
	4^{th} gear	-	0	6.9	34.4	94.9	220.2

The natural frequencies for the 4DOF and 15DOF models and the natural frequencies for both open clutch models are reasonably similar in both clutch closed cases. See Table 9.4 for undamped natural frequencies of both systems. With clutches closed the lowest natural frequencies are almost identical, however the second non-rigid frequency is not present in the 4DOF model from the 15DOF powertrain model. This is a consequence of using the open clutch state for solving for spring stiffness. By using either of the other two states to define the stiffnesses will produce accurate modal parameters at only that state. Similarly for the open clutch state only one of the two frequencies can be identified for each decoupled stiffness and inertia group, with the 3^{rd} and 4^{th} open clutch natural frequencies corresponding to the 4^{th} and 5^{th} natural frequencies in the open clutch 15DOF model, a result of the application of four non-zero frequencies in ascending order. As such the lower of each natural frequency is identified in the model.

Table 9.4 presents the 4DOF model natural frequencies and corresponding normalised modal shapes for the simplified powertrain in 3^{rd} gear and Table 9.5 presents the natural

frequencies and corresponding normalised modal shapes for the 15DOF model engaged in 3rd gear. Initially, it may be assumed that the modal shapes of the two powertrain models are significantly different, with the 15DOF modal shapes containing significantly more detail with additional degrees of freedom. However, highlighted in bold in Table 9.6 are the equivalent stations to the 4DOF model in Table 9.5. Corresponding elements are both engine and vehicle stations, with the transmission in the 4DOF model corresponding to the final drive in the 15DOF model, this is selected based on the 5.5Hz modal shape suggesting that the final drive (I_{FD}) element is an accurate choice. This use of the final drive element is critical to the compatibility of the two models as a result of the structure of powertrain models in Appendix C and equations 9.1 to 9.7.

Evaluation of the modal shapes for each model indicates consistencies for these shapes at each of the natural frequencies, with 1st, 2nd, and 3rd natural frequencies in Table 9.4 corresponding with the 1st, 2nd, and 4th natural frequencies in Table 9.5. While in the rigid body and engine modes, ω_{n1} and ω_{n2}, indicate minor variation between stations for the final drive modes, with modal amplitudes being consistent with the final drive modes in the 15DOF model. This indicates that there consistency between lower and higher order models. The last corresponding natural frequency the amplitude results are also completely out of phase this is a result of using different elements for normalising the modal shapes, I_E in the 4DOF and $I_{G1+P1+S1}$ in the higher order model. The overall conclusion is that the simpler 4DOF system can provide a reasonable representation of a more detailed lumped mass model, but some variation in the response of the two systems must be expected.

Table 9.4: Normalised modal shapes and natural frequencies of 4DOF model engaged in 3rd gear

System state	Natural frequency (Hz)	Normalised modal shapes		
		I_E	I_{T+D}	I_V
1 Vehicle rigid body	0	1	0.22	0.22
2 Engine	6	1	0.22	-0.05
3 Transmission	112	1	-0.6	0

Table 9.5: First four normalised modal shapes and natural frequencies of the 15DOF system engages in 3rd gear

System state	ω_n (Hz)	Normalised modal shapes													
		I_e	I_F	I_{D+C1}	$I_{G1+P1+S1}$	I_{C2}	$I_{G2+P2+S2}$	I_{FD}	I_{SH1}	I_{SH2}	I_{SH3}	I_{SH4}	I_{Diff}	I_H	I_V
1 Vehicle RB	0	**1.00**	1.00	**1.00**	1.00	0.74	0.74	0.22	0.22	0.22	0.22	0.22	0.22	0.22	**0.22**
2 Engine & flywheel	5.5	**1.00**	0.99	**0.99**	0.99	0.73	0.73	0.22	0.19	0.16	0.13	0.10	0.08	0.06	**-0.06**
3 Hub & diff	34	**-0.20**	-0.16	**-0.14**	-0.11	-0.06	-0.06	-0.02	0.17	0.35	0.54	0.73	0.91	1.00	**-0.01**
4 Clutch drum & transmission	98	**-0.83**	0.49	**0.93**	1.00	0.79	0.79	0.23	0.18	0.14	0.10	0.06	0.01	-0.02	**0.00**

9.4 TORQUE BASED CONTROLLER DEVELOPMENT FOR THE DCT

Conceptually, the development of transients during clutch-to-clutch shifts is derived from three sources. A step change in any of these parameters results in the development of a transient vibration. The three parameters that change during a shift are:

1. System torques generated at the clutches, engine, and wheels
2. Slip speed between clutch plates and absolute speed of the engine, and
3. Transmission inertia resulting from the stepped ratio transmission.

Figure 9.6 presents the logic for realising torque based shift control of the DCT powertrain. Inputs of engine and clutch slip speeds, clutch pressures, and engine torque are used to control the engagement of the transmission with the estimated torque.

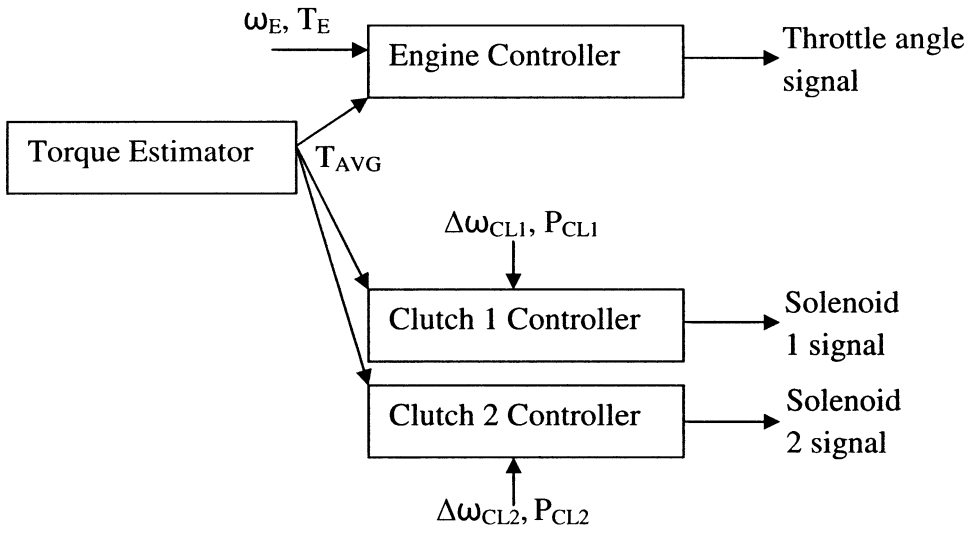

Figure 9.6: Powertrain control logic

Potentially the most important consideration for torque based control is the average torque present in the clutches prior to and post shifting. This torque is estimated for the target torque to release the off going clutch and engage the ongoing clutch. However, as a result of the stepped impact of gear ratios of the DCT and AT, this torque is not identical at these two stages of release and lockup. This torque, T_{AVG}, is determined using equations 9.9 to 9.11 and should be considered as the torque required at the clutch to ensure the continued acceleration of the vehicle at the current rate. Significant aspects to consider are the application of appropriate torque estimations to different clutches and the inclusion of the engine in torque control of the powertrain.

9.4.1 Sensitivity of controller to estimated torque

To evaluate the response of the hydraulic system to inaccuracy of torque estimation, sensitivity analysis of the clutch pressure to variation in the estimated average torque is conducted. To do so the hydraulic system is isolated from the powertrain model and two average torques are assumed, at 200 and 350 Nm. Additionally a ±10% variance is applied to each of these torques and at 1% increments, simulations of the pressure response is carried out to determine the response to this pressure variation.

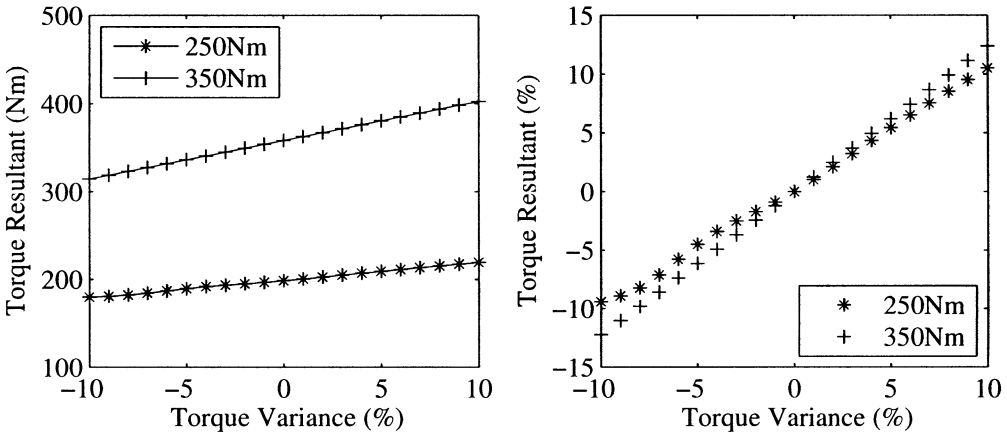

Figure 9.7: Sensitivity study of clutch torque response to variation in estimated torque

The sensitivity study results are presented in Figure 9.7, where, for both plots, the torque variance represents the variation in average torque estimation in from the nominal torques in the legend, while the torque resultant refers to the actual torque generated in the clutch using the hydraulic control system. For each case the torque curves are reasonably linear. This type of result can be expected with hydraulic control systems which are considered to be highly nonlinear systems. The lower average torque of 250 Nm provides fairly accurate clutch torques in response to the average torque variance. However at the higher torque of 350Nm the accuracy is reduced significantly, with the variation from ideal torque at the extremities of ±10% being 2.5% from the nominal value.

9.4.2 Torque orientated clutch control

Shift control of complex vehicle powertrains such as the DCT requires the combined control of engine and clutch to ensure the minimising of shifting transients. Estimation of the required torque becomes very important for minimising shift transients. Dourra

& Kwapis [146] provide an example of torque estimation for automatic transmission systems, with multiple clutches and brake bands involved in shifting. For the DCT torque estimation is simpler, where an accurate estimation of the torque required for maintaining vehicle acceleration is used as the target torque.

It is important in clutch control in particular to simulate both the pre-shift processes, and torque and inertia phase control when studying the interaction of the hydraulic system and the powertrain. In Figure 9.8 the typical combined clutch torques as experienced by the transmission is demonstrated. The solid line represents the locked transmission, and the dashed line represents clutches energised and slipping during the shift transient. Significant characteristics present include the torque hole that results from the handover of torque between releasing and engaging clutches, and the step change of torque upon lockup of the engaged clutch as torque transits from energised clutch torque to average lockup torque. Both these discontinuities can introduce transients into the system.

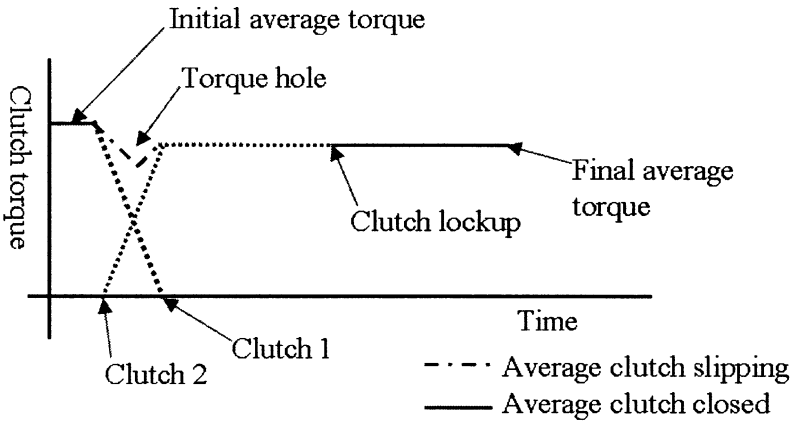

Figure 9.8: Typical torque profiles of both clutches during shifting

Upon detecting the shift requirement, the releasing clutch, in this case clutch 1, has the cylinder pressure reduced to near slip threshold, as defined from the average torque. The target clutch, clutch 2, is prefilled, this pushes the clutch plates just below the point of contact, and the transmission is now ready to shift. The shift itself is separated into the torque and inertia phases. During the torque phase the handover of torque between clutches occurs. Clutch 2 pressure is increased until the dynamic friction torque meets the target torque, simultaneously clutch 1 is reduced in pressure to zero. There is then dynamic friction from clutch 1 and 2 acting on the system. These torques are managed such that the sum of the two equals to target average torque, minimising the loss of tractive load to the road. This is represented in Figure 9.8 as the torque hole. At the

completion of the torque phase clutch 2 torque matches the target output torque, and clutch 1 is completely released. In the inertia phase of engagement clutch 2 alone is maintained at constant pressure until speeds are matched and the transmission locks up. Thus the vehicle transmission is used to match the desired vehicle torque throughout the shifting process.

9.4.2.1 Preshift control

Preshift control is the relatively simple process of preparing the two clutches for shifting. For the target clutch preshift control requires the filling of the clutch cylinder such that friction plates come to near contact, and for the releasing clutch the pressure must be reduced to the point of slip. This is where the static friction in the clutch is equal to the average clutch torque.

To achieve prefill of the target clutch a step input at the maximum of 2 amps is sent for a period of 95ms. During this period the clutch pressure has a minimal increase as the piston moves forward, resisted only by the clutch return spring. Similarly for pressure reduction of the engaged gear the pressure is released from the holding pressure to the slip limit, performed simultaneously with the prefill functions.

9.4.2.2 Torque phase control

The purpose of the torque phase is to seamlessly hand dynamic friction torque from the originally engaged clutch to the clutch that is the target for engagement. To that end the torque phase control must perform three tasks:

1. Determine the target torque at which the releasing clutch will transit from stick to slip states,
2. Determine the required torque at the engaging clutch required to maintain the acceleration of the vehicle with minimum loss of tractive load, and
3. Transfer the torque from the releasing clutch to the engaging clutch in a manner that minimises vehicle transients.

Steps one and two are realised through the application of equations 9.9 to 9.11, used to estimate the average torque in the clutch. Step 3 is performed using simple PI controllers to release and energise the two clutches.

9.4.2.3 Inertia phase control

For the adoption of a torque orientated control strategy in DCT control, the inertia phase control requires that the clutch torque is maintained at a constant torque that is equivalent to the vehicle angular acceleration and any resistance torque. Though it is possible to use higher torques to reduce the shift times, this is likely to result in surging [27] or more significant powertrain transients than is desirable during shifting in lightly damped powertrains. The inertia phase begins once the target torque has been met during the torque phase. Control then proceeds as follows:

1. Determine the target torque for the engaging clutch,
2. Hold pressure at desired torque, and
3. When speeds are matched, set pressure to maximum and lock the clutch.

This process is realised using the torque determined in the torque phase of engagement for the target clutch, with the torque processed into a pressure value based on the clutch friction model. The pressure is fed into a look up table for the control valve and the appropriate signal current is determined and applied to maintain a constant input pressure. With zero slip, pressure is set to maximum and inertia phase is complete.

9.4.3 Alternate engine control methods

Engine control is a significant aspect of DCT, improving shift transient control as both engine speed and torque are required to successfully balance the powertrain during shifting. The engine controls the speed and acceleration of the system through input of torque. Thus, to ensure that the engagement proceeds as desired, torque and speed discontinuities in the engine must be minimised. That is to say, if engine power is balanced with vehicle demand at lockup, then shift transients can be minimised.

Consider the requirements on the engine during a shift. During the torque phase, with both clutches slipping, torque handover between these two clutches is performed. The engine supplies power to the transmission so that the torque handover does not absorb

energy from the drivetrain, increasing the torque hole. At the beginning of the inertia phase, the engine must either accelerate or decelerate as rapidly as possible to the target speed of the transmission. This minimises the transient shift period, reducing torque hole and friction energy generated in clutches. At the end of the shift, the engine must have the same speed and torques as the engaging clutch to minimise transients resulting from imbalances. To assess the impact of engine torque imbalances on shift response two alternate engine control strategies are suggested.

Speed based control proceeds as follows, referring to Figure 9.9:

- Detect shift and completion of clutch pre-fill and gear synchronisation,
- Torque phase control, maintain engine speed until torque handover complete.
- Once releasing clutch pressure at minimum stage is complete begin inertia phase control.
- Control engine speed using throttle angle to synchronise ongoing clutch. and,
- Once clutch locked return engine to driver control.

Torque based control proceeds similarly to speed control during prefill and torque phases. On the completion of torque phase the process is as follows:

- Once releasing clutch pressure at minimum stage is complete. Begin inertia phase control.
- Control engine speed using throttle angle to synchronise ongoing clutch.
- When slip speed is less than 5% of the initial slip speed begin engine torque match. Modify throttle angle to match engine required torque output at the point of clutch lockup, and,
- When clutch is locked, return engine to driver control.

For torque matching, an engine map, based on the throttle angle and engine speed is used in reverse to identify the desired engine torque and required throttle angle. For this the target torque is determined as the average target clutch torque prior to shift, and the engine speed is tracked. As the clutch speed approaches lockup the throttle angle is matched through the engine map to the required torque at a specific speed and ramped up to locking. This is a simple but effective way to determine torque required for engine control, but again ignores the influence of harmonics present in internal combustions engines.

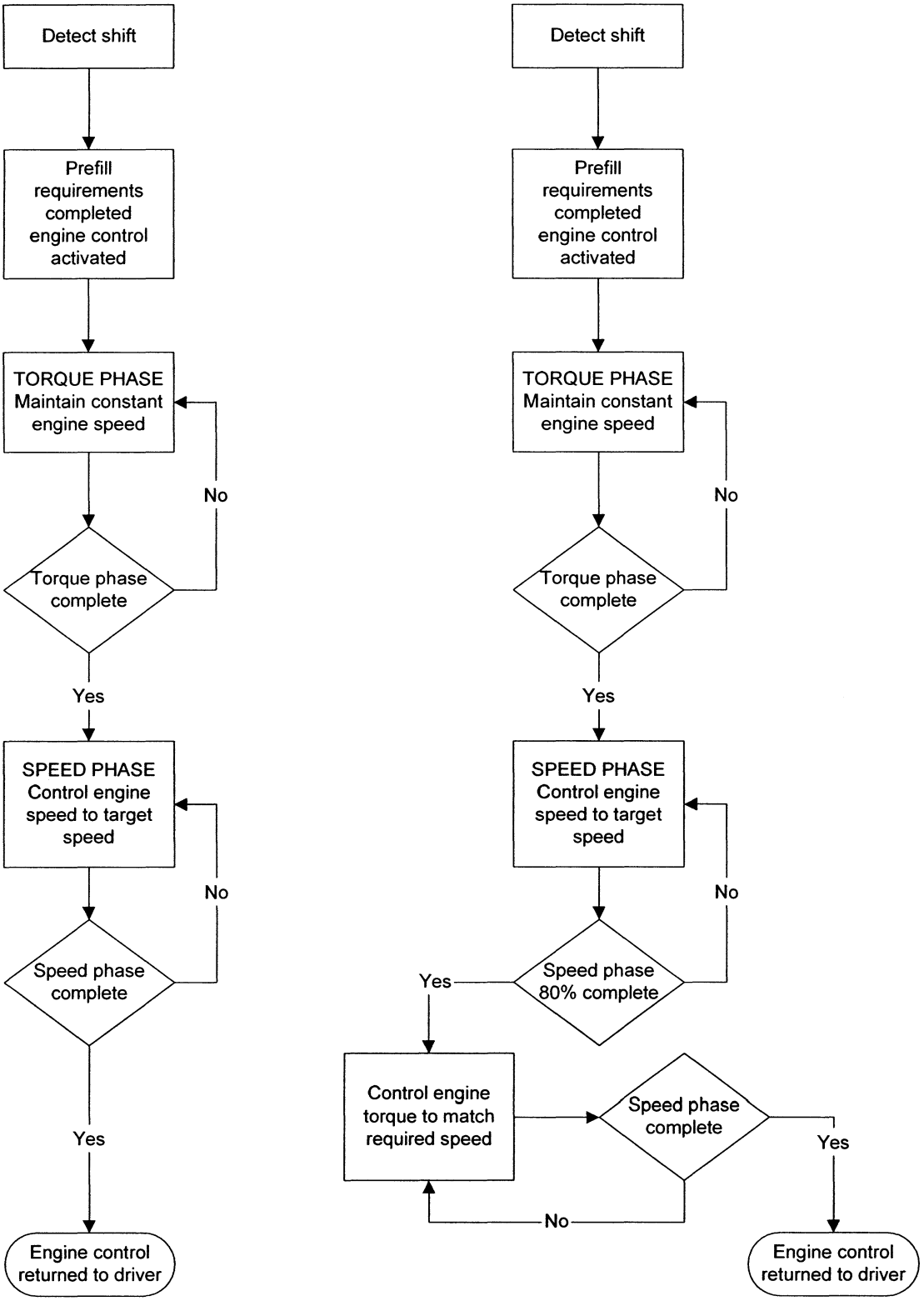

Figure 9.9: Engine control methods. Showing both speed control (left) and torque control (right)

9.5 GENERAL SIMULATION CONTROL SIGNAL RESULTS

For the initial study of shifting in the DCT, consideration must be given to how the control processes reflect on the actuation of clutches and control of the engine. As such a demonstrative simulation is presented here for a third to fourth upshift in the transmission. The vehicle model is accelerated from 70 rad/s and, once a steady acceleration is achieved, the above described shifting process is employed. The simulation results presented at this point are to demonstrate the clutch and engine control only; other aspects will be shown in the following sections.

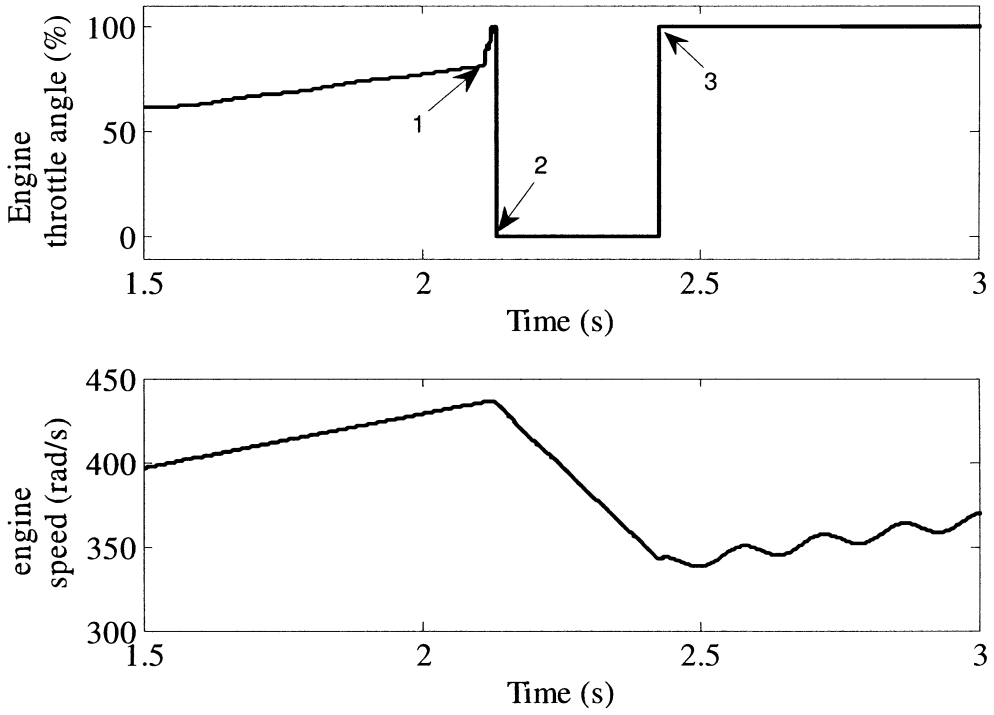

Figure 9.10: Engine control responses from simulation showing throttle angle (above) and engine speed (below)

Figure 9.10 presents the simulation throttle angle and engine speed results for a typical upshift. As described in the engine control method presented previously in this chapter the indicated point 1 of Figure 9.10 represents the beginning of torque phase where the throttle is manipulated to maintain engine speed. Point 2 indicates the beginning of the inertia phase, engine throttle angle is reduced to zero and held until the clutch locks up, signified by point 3 to minimise engine torque. Post lockup the engine throttle is sustained at 100% throttle angle to ensure that ongoing engine control does not interfere with the transient vehicle response.

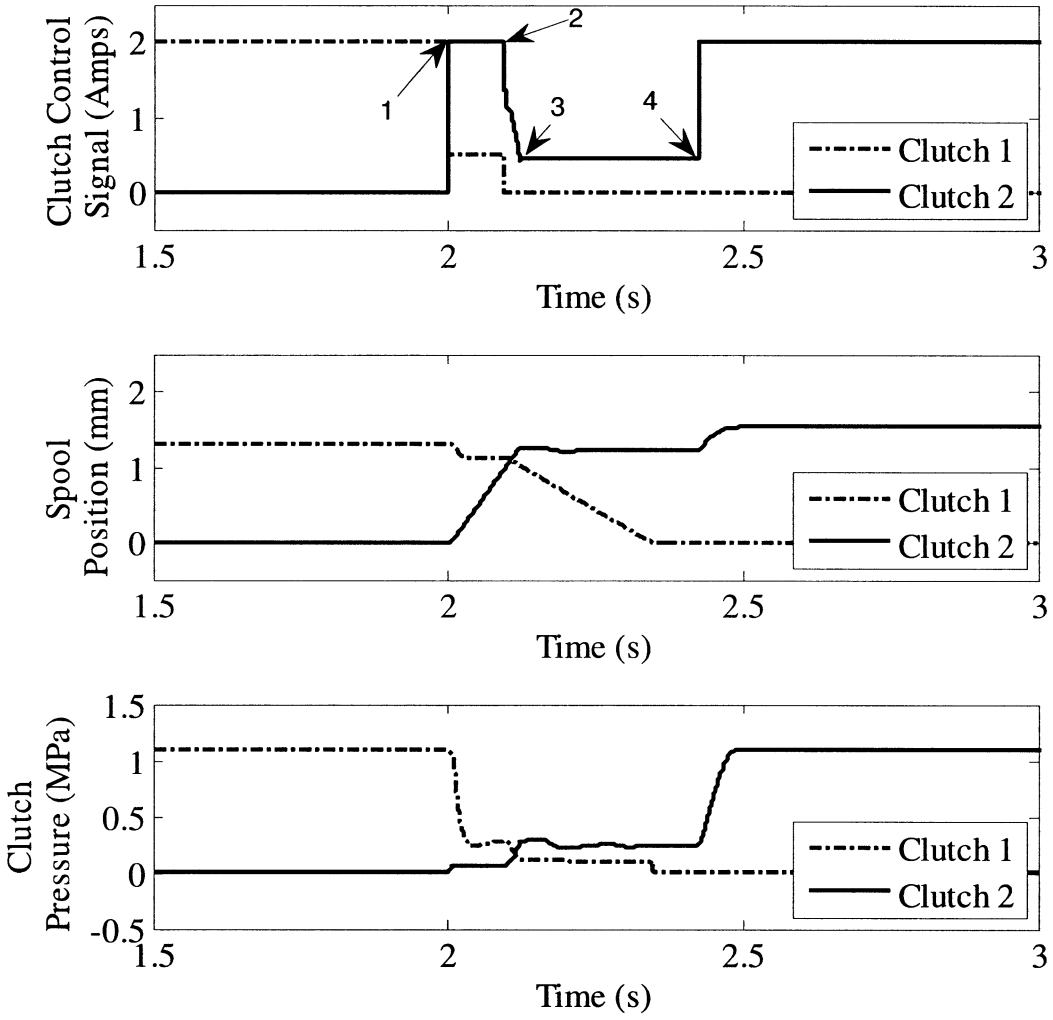

Figure 9.11: Clutch control responses, showing control signal (top), spool position (middle), and clutch pressure (bottom)

The clutch control responses presented in Figure 9.11 focus on the control signal, spool (piston) position, and clutch pressure. Point 1 presents the beginning of the preshift clutch preparation. At this point clutch 2 signal is set to maximum to fill the engaging piston, shown by clutch 2 moving forward, with a pressure increase resulting from the resistance of the clutch return spring. Clutch 1 signal is set based on the friction limit of the clutch. As pressure reduces the piston moves backwards and the chamber reduces in pressure, shown as stabilising at the intermediate pressure in the figure.

At 2, torque phase begins, the control signal for clutch 2 decreases from the maximum to the target pressure signal. This results in the pressure ramping up to the target limit, with some overshoot resulting from the solenoid spool. At this point clutch 1 signal reduces to zero as the pressure is released. It is important to realise here that the control signal does not actively release clutch 1 as a result of the time delay present in the

system preventing control application. The torque phase in particular suggests that time delay may be an issue in the engagement of the powertrain.

Point 3 signifies the beginning of the inertia phase of engagement. During this phase clutch 1 contact between clutch plates is released as the return spring pushes the piston back. At the same time clutch 2 stabilises at the target pressure indicated by the control. The engaging clutch synchronises through friction torque and at point 4 the powertrain locks the target clutch with clutch 2 set at maximum pressure.

9.6 BASIC TORQUE ORIENTATED SHIFTING

For the simulations presented in this paper a general third to fourth gear up shift will be employed. Third gear ratio is 4.443 and fourth gear is 3.3912, this includes the transmission reduction gear and final drive gears. The initial vehicle speed is approximately 70 rad/s, equivalent to about 80km/h, resulting in initial engine speeds near 2800RPM. The final clutch torque is estimated using the average torque in Clutch 2 at the point of slip, as presented in equation 9.9.

9.6.1 Simulations with ideal actuators

For this simulation the hydraulic control system is replaced by ideal input torques for the clutches, demonstrating the ideal response of the system. Assuming ideal actuators to exclude the influence of the hydraulic control system on shifting and use the average torque to minimise torque hole, the hydraulic control system is replaced with ideal clutch torques representing clutch closed, torque and inertia phases. In doing so the clutch 1 torque is ramped down to zero during the torque phase, whilst clutch 2 torque increases to the target torque and is held constant during the inertia phase. When either clutch is locked, its respective torque is held at 1000Nm, representing the maximum static friction in the clutch.

The simulation results presented in Figure 9.12 demonstrate the shift control of the DCT using the assumed ideal actuators. Torques in Figure 9.12 (c) represents the control signals to clutches. The torque phase is assumed to take 50ms and a target torque of 300Nm is used for the maximum clutch 2 torque, and the overall duration of the transient is 350ms. The clutch 2 and drum speeds in Figure 9.13 (a) are maintained

during the torque phase as the torque on clutch 2 increases and clutch 1 is released. During the inertia phase the clutch speed oscillates significantly with the end of torque phase, whilst post clutch lock up oscillations are present, resulting from imbalance of engine torques and the unsteady transient slip speed generated in the clutch. Vehicle acceleration in Figure 9.13 (b) demonstrates a small drop in acceleration in the torque phase, representing the torque hole, and peak-to-peak post lockup oscillations are approximately $10rads^{-2}$, or with a wheel radius of 0.32m, a peak-to-peak variation of linear acceleration of $3.2ms^{-2}$; a reasonable variation in acceleration given the simplification to a lumped mass model. The significance of light damping in the DCT is also obvious with the damping of post lockup oscillations being minimal.

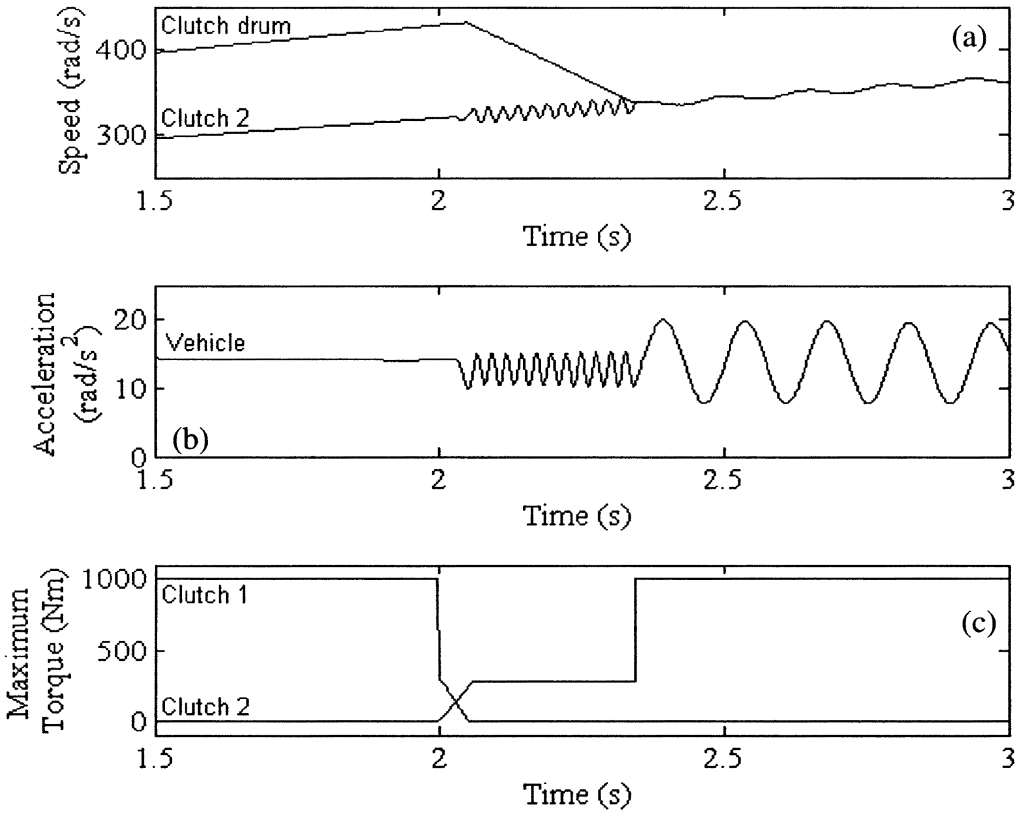

Figure 9.12: Simulation results for a 3-4 up-shift showing speeds for (a) Clutch drum and clutch 2, (b) vehicle acceleration, and (c) clutch pressures during shifting using ideal clutch torques

9.6.2 Simulations with basic control methodology

The second set results are presented for a shift with identical initial conditions to the one detailed above, including torque control technique. To minimise the torque phase in this simulation using the detailed hydraulic system model the controlled torque phase is replaced by a step input for the target torque, minimising delay of the hydraulic system. Results for clutch engagement and vehicle acceleration are shown below:

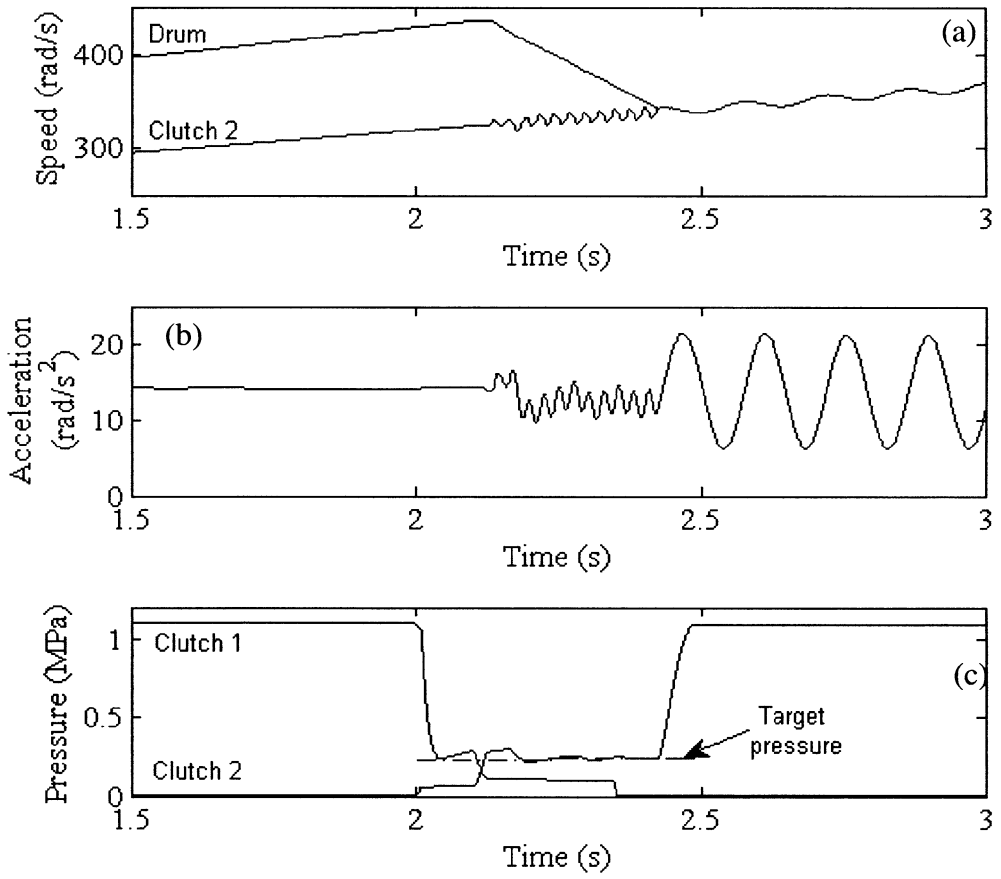

Figure 9.13: Simulation results for a 3-4 up-shift with minimised time delay showing speeds for (a) clutch drum and clutch 2, (b) vehicle acceleration, and (c) clutch pressures during shifting using engine speed control and Clutch 2 average torque estimation

Figure 9.13 presents the transient results for the powertrain model using the average torque from Clutch 2 as the target torque for clutch engagement. With the modelled hydraulic controller, simple engine control is used to aid speed matching between clutch and drum. Unlike with ideal controllers, before shifting is initiated, at 2s preparation must precedes the shift. This is represented in the clutch pressure profile in Figure 9.13 (c), at 2s clutch 1 pressure drops markedly to the target pressure in preparation for the initiation of slip, and there is a small increase in clutch 2 pressure signifying pre-filling of the piston. In accordance with the piecewise clutch model, there is no contact in the

friction plates and no friction torque is produced. Preparation takes approximately 100ms before the torque phase begins with rapid handover between the two clutches, lasting less than 50ms. Similar to the ideal results, the shift transient period is approximately 350ms if shift preparation is excluded. The short torque phase and transition to constant torque in the inertia phase results in the clutch pressure overshooting the target torque before settling to just below the target pressure.

Similar transient vibration in clutch and drum speed synchronisation is generated during the inertia phase in comparing Figure 9.13 to Figure 9.12. However, in place of the small torque hole generated using ideal results, overlap of clutch slip generates a brief increase in vehicle acceleration in Figure 9.13. This is a result of time delay between control signal and the release of clutch 1, with clutch 2 pressure increasing rapidly in attempt to minimise the torque hole.

As the clutch pressure settles, additional variation in the vehicle acceleration during the inertia phase is produced in addition to periodic oscillations. The results demonstrate transients generated in the transmission speed during shifting as a result of releasing the clutch, and transmission and clutch speeds upon lockup of the transmission. The post lock up vibration experienced in the transmission, (a), is also reflected in the vehicle acceleration response, (b), during the post shift steady state. This is increased in comparison to transients in Figure 9.12, resulting from error between clutch actual pressure and target pressure.

9.6.3 Simulations with addition of engine torque control

Using the same simulation parameters as used in the two previous cases, this next simulation utilises torque based clutch control to perform shifting combined with torque balancing of the engine to target torque in the final stages of the inertia phase.

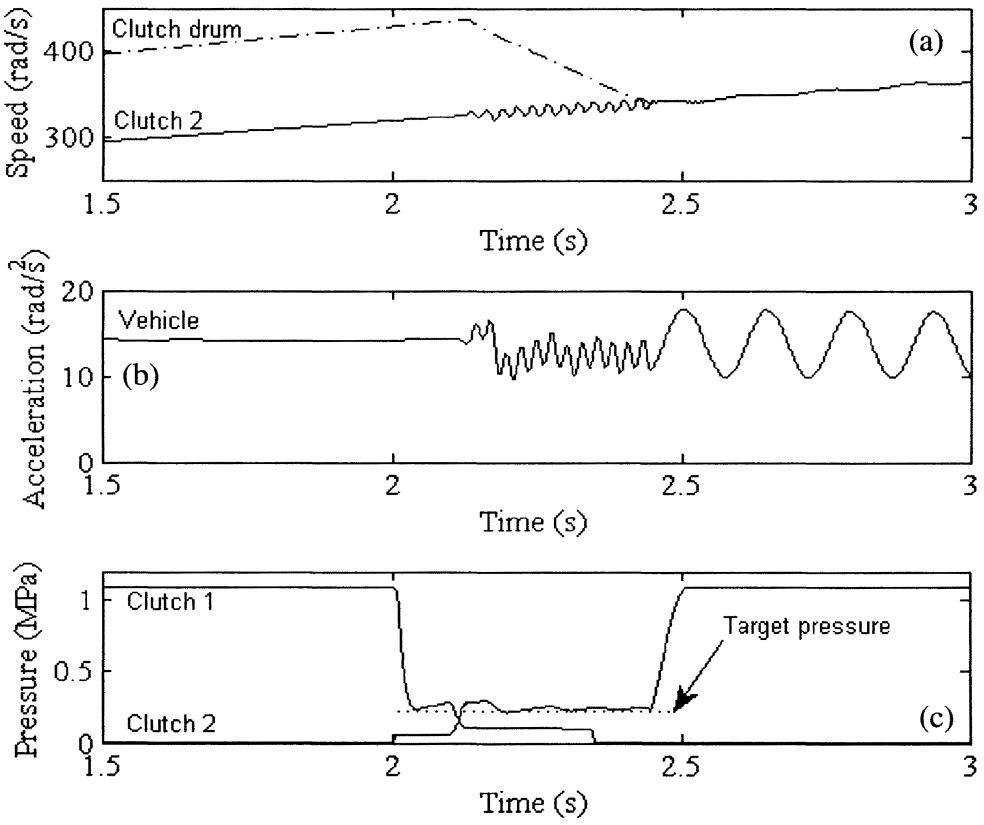

Figure 9.14: Simulation results for a 3-4 up-shift showing speeds for (a) clutch drum and clutch, (b) vehicle acceleration and (c) clutch pressures during shifting using engine speed and torque control, and clutch 2 average torque estimation

The results shown in Figure 9.14 are reasonably similar to those of Figure 9.13 in terms of overall dynamics. The use of engine torque control at the end of engagement increases the duration of the inertia phase as additional energy is applied to the system, resisting the clutch engagement. In Figure 9.14 (a) the synchronisation is slowed in the final stages of the inertia phases as increased energy is imparted on the system. However, the resulting post shift transients in the closed clutch is significantly reduced from Figure 9.13. The vehicle acceleration in graphic (b) of Figure 9.14 supports the improved post shift transient vibration, with peak-to-peak vibrations smaller than those present in all previous simulations. Again there is evidence of clutch overlap in the torque phase during shifting. From part (c), the pre-shift clutch release and pre-fill is identical to the previous simulation. The torque phase is the same, but the inertia phase

is extended as a result of employing the engine torque control. The overall shift transient period, shown in part (c) is extended, taking over 400ms, also a result of the new engine control method. The vehicle speed, as shown in part (b), demonstrates minimal loss in acceleration and tractive load to the road resulting from the clutch-to-clutch shifting. In particular, transients developed in the transmission and vehicle responses are significantly reduced in comparison to Figure 9.13. With the only change to the control algorithm being the torque balancing in the engine in the final stages of the inertia phase, it is reasonable to conclude that significant improvements can be made by balancing system torques prior or at the completion of clutch lockup to minimise discontinuities in the system torques.

9.6.4 Simulations of the influence of error in torque estimation

To further demonstrate the results of inaccurate estimation of the target torque and impact on gear shifting clutch 2, the average torque is increased to 110% of the ideal torque.

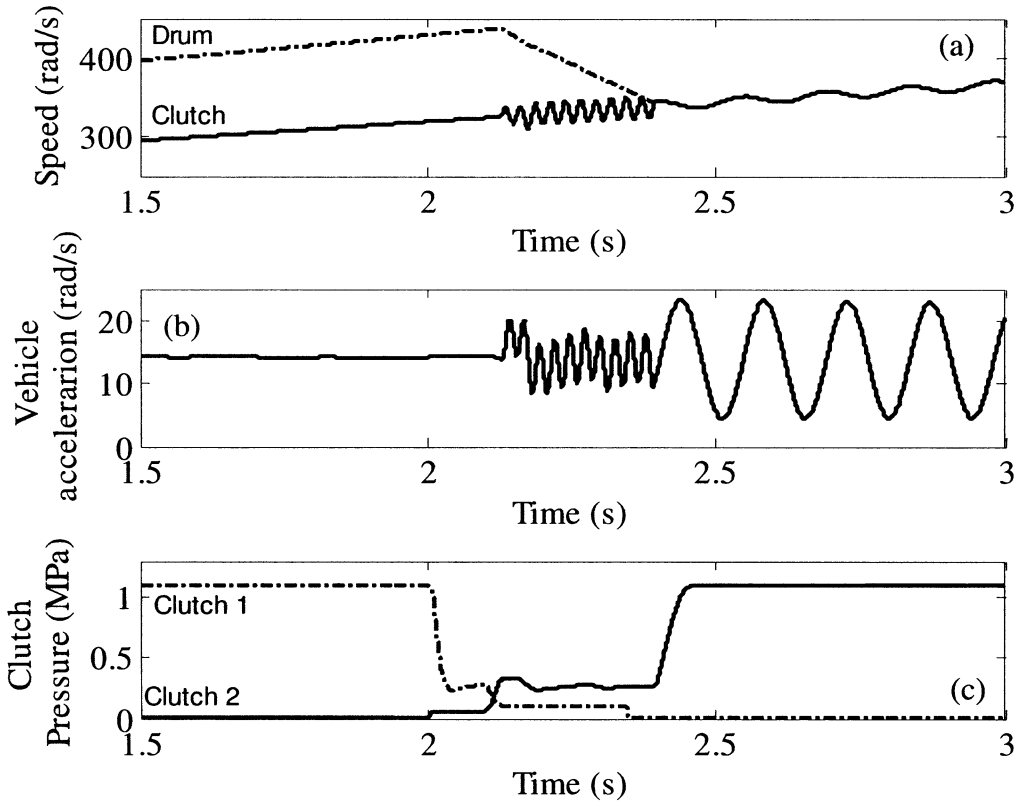

Figure 9.15: Simulation results for a 3-4 up-shift with variance in estimated torque for controller input showing speeds for (a) clutch drum and clutch, (b) vehicle acceleration, and (c) clutch pressures

Immediately the results in Figure 9.15 show degradation of performance in comparison to both Figures 9.13 and 9.14. Figure 9.15 (a) indicates increased vibration during the inertia phase as well as amplified amplitudes during post shift vibration. Additionally, Figure 9.15 (b) indicates increased torque overlap during the torque phase, noting that slip begins at approximately the same time in each of the simulations, and vehicle acceleration oscillations is also significantly increased. Thus the detrimental effects of inaccurate torque estimation are clearly demonstrated in the simulations.

9.6.5 Shift transient simulations with transient engine model

A significant assumption made in the development of this model, and the development of similar models by many other authors, is that mean engine torque models are sufficient for defining the engine torque acting on the powertrain. In Section 8.7.4, a 5 degree of freedom transient engine model was presented, and by making several assumptions and with limited data, a proposed control technique was introduced. This model is sufficient for transient simulations in that both mean torque and peak-to-peak torques vary with control of throttle angle, but is limited in applicability to actual systems. To further evaluate the effect of transient engine torque on the shift process this model is developed in the Simulink environment of Matlab and shift transient simulations performed in line with the standard shift process with engine speed control (see Section 9.3). The following simulation is performed with initial conditions for engine speed of 235 rad/s, corresponding to a wheel speed of 51.2 rad/s, operating at wide open throttle and 3^{rd} to 4^{th} gear upshift. To reduce torque overlap present in previous simulations, the clutch release signal is modified to prevent average torque undercutting the friction limit during release. A longer hold of the clutch pressure will be used to identify any interactions between engine harmonic torques and reduced clutch average pressure.

Inspection of Figure 9.16 suggests that the results of introducing the transient engine torque model is not that significant. Higher frequency vibrations are present, but there is little impact on transient control in comparison to Figure 9.13. Notice that there is stick-slip initiated in clutch 1 at the beginning of the torque phase as high torque pulses in the engine interact with stick-slip algorithm. This results from the extended low pressure period in clutch 1 (Figure 9.16 (c)). Resulting in increase of torque hole during

the torque phase as energy is dissipated during repeated stick-release events and release of clutch 1 is initiated earlier. However vehicle acceleration is reasonably well maintained, Figure 9.16 (b) demonstrates post lockup acceleration higher than those in Figure 9.13 (b), the is likely a result of engine vibrations negatively impacting on the estimation of mean clutch torque. High frequency responses are more dominant in Figure 9.16 (a), with local engine resonances present in the response. Nevertheless these higher frequencies in the clutch speeds have minimal impact in successfully performing shift control, consistent with Goetz, Levesley & Crolla [21] evaluation of the impact of low amplitude, high frequency white noise interfering with control signals.

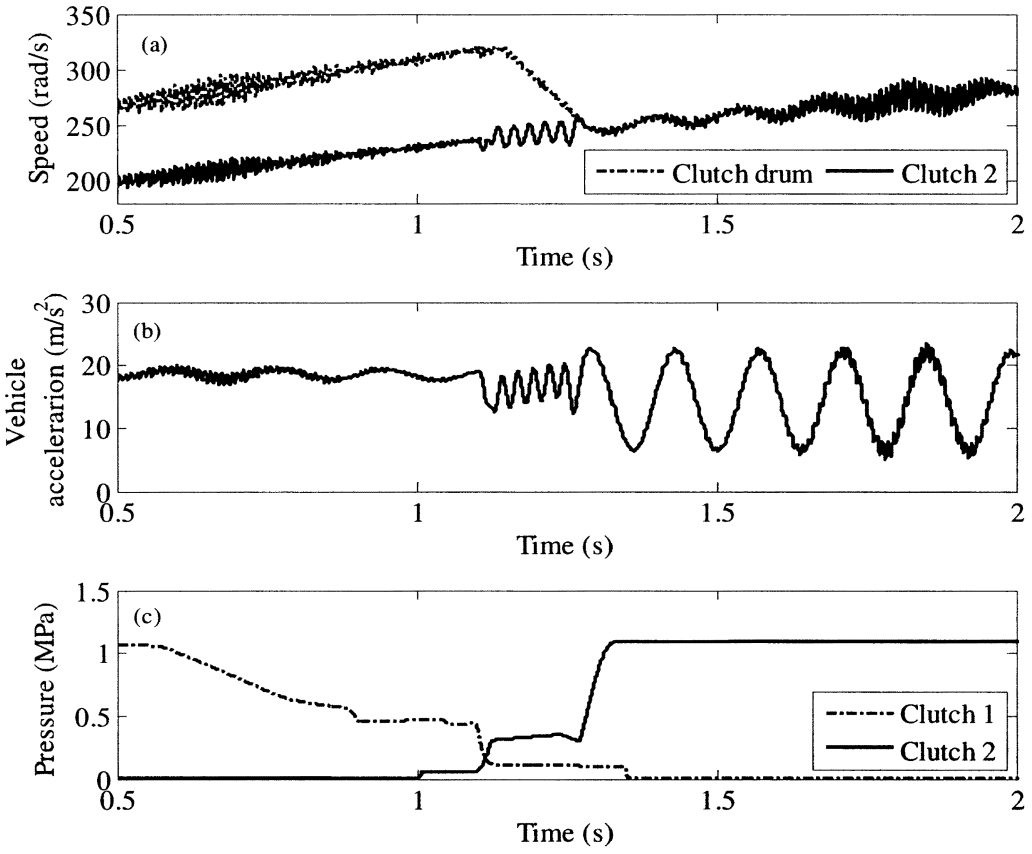

Figure 9.16: Gear shift simulation results for 3rd to 4th upshift using 4DOF model with transient engine torque, (a) clutch drum and hub speeds, and (b) clutch 2 output and total vehicle torques

9.7 COMPENSATION FOR TIME DELAY IN HYDRAULIC CONTROL SYSTEM

Time delay is a well established issue in hydraulic systems, demonstrated in this thesis with the step response rising and settling times in Chapter 3, section 3.5. Simulated results indicate that the delay is a complex response of a combination of factors such as spool proximity to orifice openings, magneto motive load on the spool, and interactions of different feedback pressures. This is reflected in Figure 9.13, where release of clutch 1 during the handover to clutch 2 in the torque phase results in a small degree of clutch overlap. This can be compensated for through application of a simple time delay to the hydraulic system. Equations 8.2 and 8.3 can be redefined to include time delay in the torque as follows:

$$I_D\ddot{\theta}_D + K_D(\theta_D - \theta_E) + C_D(\dot{\theta}_D - \dot{\theta}_E) = U_{C1}(t+\tau) + U_{C2}(t+\tau) \tag{9.20}$$

$$I_T\ddot{\theta}_T + K_T(\theta_V - \theta_T) + C_T(\dot{\theta}_V - \dot{\theta}_T) = -\gamma_1 U_{C1}(t+\tau) - \gamma_2 U_{C2}(t+\tau) \tag{9.21}$$

Here U_{C1} and U_{C2} are the time dependent torque loads for the system, t is time, and τ represents time delay inherent to the system. If the delay in release clutch 1 pressure is considered the primary issue within overlap and therefore torque phase response of the powertrain, the control signal in clutch 2 can be modified to include a transport delay to compensate for the delay of clutch 1. Simulations are performed as per Section 9.6.

The introduction of time delay into the control algorithm has successfully reduced the torque overlap in the powertrain, with the acceleration peak at 1.15 seconds resulting from overshoot of clutch 2 pressure. As can be observed in the comparison between Figure 9.13 and Figure 9.17, post lockup vehicle response is also significantly improved between these simulations. This results from the delay allowing clutch 2 pressure to rise slowly and more rapidly stabilise pressure, minimising any offset imbalance in the powertrain.

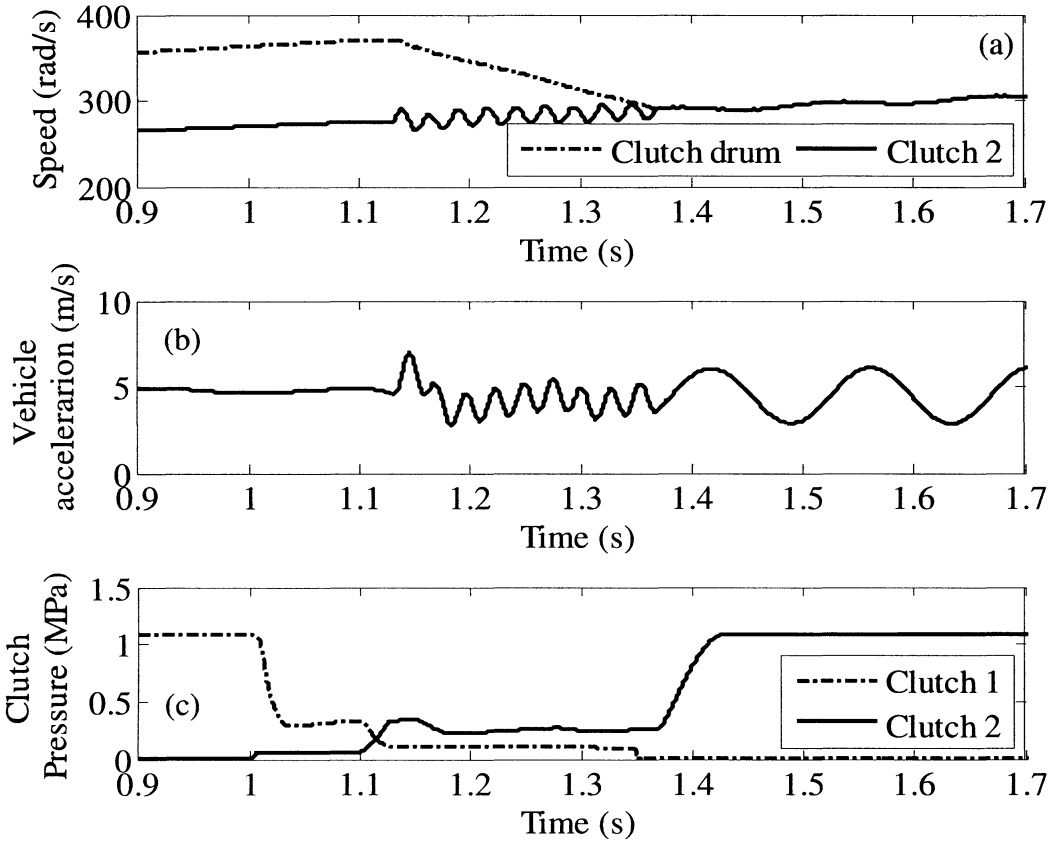

Figure 9.17: Gear shift simulation results for 3rd to 4th upshift using 4DOF model with transient engine torque, (a) clutch drum and hub speeds, and (b) clutch 2 output and total vehicle torques

9.8 CONCLUSIONS

This chapter investigates the impact of various nonlinearities and uncertainties on performance of high quality shifts in DCTs. This is achieved by proposing a 4DOF powertrain model using a simple model reduction of 15DOF powertrain model presented in Chapter 8. Free vibration analysis of natural frequencies and modal shapes was used to compare 4 and 15 DOF models and demonstrate a reasonable degree of consistency between the two models. The model is then integrated with the hydraulic system model introduced in Chapter 3 for clutch control of the DCT, with the focus being the evaluation of the highly nonlinear hydraulic system on shift performance.

A simple control method is used in the powertrain model to provide clutch and engine control through balancing torques at engine and clutches with vehicle acceleration and resistance torque. The principle is that this balances torque through the transient and reduces response in the powertrain as a result of torque discontinuities. This was

demonstrated through the use of predicted torque control of the engine to minimise these discontinuities. Two engine models, presented in Chapter 8, are employed to investigate the impact of torque pulses from the engine on shift quality, and finally a simple representation of time delay is evaluated for the impact on shift control.

Simulations covered four variations in the control process, control using ideal torques, standard clutch and engine control, clutch control with predicted engine torque control, and clutch control with uncertainty in predicted torque. Using ideal torque control as a reference, it was demonstrated that: (1) standard control introduces some clutch overlap resulting from delay in the hydraulic system in an effort to minimise torque hole., (2) the introduction of engine torque control significantly reduces the post clutch lockup transient response, and (3) uncertainty in the mean torque estimated for control was also demonstrated to be a significant contributor to reduction in shift quality. This suggests that the prediction of mean torque of clutches under a range of variables, such as road incline, is required to provide optimum shift quality in DCTs.

The inclusion of harmonic engine torque models on control investigates the impact on shift performance. It was demonstrated to have little impact on controller performance, however torque pulses impacted on clutch release and torque phase, and observed that torque pulses will initiate stick-slip response in the engaged clutch as pressure is reduced in preparation for shifting. Low pressure reduces the maximum static torque, with peak torque pulses from the engine initiating slip in the clutch, increasing the torque hole during torque phase, and reducing performance prior to shifting.

Using simple transport time delay in the controller it was possible to modify the response of clutch 2 to compensate for the delay in release of clutch 1 during the initiation of the torque phase in the controller. Results of simulations here suggest that the detailed study of delay compensation through the application of robust control techniques, such as H-infinity, for clutches and potentially engine will significantly improve the quality of shift responses in the DCT. Though the methods chosen for investigation into time delay issues in the clutch and engine systems are relatively simple, the results here suggest that significant advancement in shift response and quality can be achieved with detailed investigation.

9.8.1 Summary of Contributions

Significant contributions to research in this chapter are:

- Current research into DCT powertrains has ignored the integration of complex hydraulic systems during model development. Commonly simplified models replace the hydraulic system. A significant component of this research therefore has been to combine hydraulics and powertrain in DCT studies. There are however examples of this for different transmissions such as refs [32, 34].
- Engine control method was proposed that manipulated the engine torque prior to clutch lockup and reduce transient response
- This chapter has also investigated the implication of transient torque engine models on shift control in a more extensive method than previously presented, where no torque variation was included [1].
- Introduced time delay into the clutch control algorithm to compensate for release of clutch 1 was employed with reasonable success.

CHAPTER 10: SHIFT TRANSIENT STUDY OF DCT EQUIPPED POWERTRAINS

10.1 INTRODUCTION

Previously a rigid body model of the synchroniser mechanism (Chapter 4) and clutch shift control (Chapter 9) have been developed and studied as well as lumped inertia model for the powertrain (Chapter 8). These are the foundations for transient investigations of synchroniser engagement and shift transient studies of the DCT equipped powertrain using thepresented synchroniser, clutch and engine models.

This chapter is divided into three sections, initially the synchroniser mechanism is investigated using the multi-body model. The modified rigid body model in Chapter 8 is applied to the powertrain, and engagement studies are performed with mean and harmonic engine torque models. The second section uses the pressure and throttle signals from simulations in Chapter 9 to perform transient investigations of shifting with different engine and flywheel configurations. Finally the synchroniser and shift transient studies are combined to investigate any coupling between these two processes.

10.2 DYNAMICS OF SYNCHRONISER ENGAGEMENT IN A DCT POWERTRAIN

Modelling of the synchroniser engagement as part of a lumped inertia DCT powertrain model deploys the models formulated in Chapter 8 identified for state 3 or 4 with one clutch engaged and one synchroniser open before and during gear synchronisation, and states 5 or 6 for clutch engaged and both synchronisers closed. The synchroniser torque has been identified as a highly nonlinear torque dependent on multiple variables, such as sleeve position and clutch speed, and torque inequalities to define the torque acting in the synchroniser. To use the output torque from the rigid boy model will therefore be inappropriate for capturing the response of the synchroniser and powertrain accurately. Rather the modified synchroniser model in section 8.7.3 is used.

Investigation of synchroniser engagement focuses on two separate model arrangements resulting from different applicable engine models. The first simulation is conducted with the mean engine torque model for the purpose of identifying the response resulting from synchroniser engagement, with the second applying the transient engine torque model to demonstrate the impact of forced engine vibrations on synchroniser engagement. This is particularly important as synchroniser engagement with the clutch engaged opens up a path of transmission for engine harmonics to the sleeve. The first simulation, though, will provide a comparison of the rigid body engagement with the lumped inertia model simulations.

10.2.1 Modified synchroniser model

To simulate synchroniser engagement, the rigid body model developed in Chapter 4 must be reformed to be applicable to the lumped inertia model. The first variation occurs in the lumped inertia model developed in Chapter 8. Drag torques are linearised to a damping coefficient coupling clutches and grounded damping element at each gear (see Chapter 5). The second modification is to ignore the synchroniser ring. With low inertia and high applied torque it is more convenient to replace the load with a series of inequalities that can be used to evaluate success of engagement.

Consider also the impact of utilising a detailed hydraulic model. Even under idle conditions high stiffness requires very small time increments to accurately predict response numerically. This impact is reduced by embedding a constant time step Runge-Kutta solver for the sleeve and hydraulic dynamic response in the ODE solver during synchroniser engagement. With a step size of 10^{-7} compared to 10^{-5} for the ODE solver, the embedded hydraulic solver significantly reduced numerical calculations during steady state conditions.

10.2.2 Comparison of rigid body and lumped mass models for analysis

The first test for the synchroniser model is if it can provide simulation results that are consistent with the rigid body model. Simulations are performed with identical initial conditions for both models. Initial vehicle speed is 40 rad/s, and 4^{th} gear is synchronised with 3^{rd} gear engaged in the transmission.

Deviations arise in the two synchroniser engagements in Figure 10.1 at four separate points.

1. Initial displacement to contact
2. Speed synchronisation
3. Ring unblocking
4. Hub indexing

For point (1) the rigid body model is allowed to stabilise before actuation, and pressures vary slightly in comparison to the lumped inertia model which is activated without stabilisation of the fluid pressure. Deviations in (2) and (3) arise from the same issue: with linearising of drag torque for damping coefficients the actual drag will be affected. This has two results. The initial slip speed of the cone is altered, resulting in the extended synchroniser engagement for (2), and the resistance torque to blocking increases, resulting in slower unblocking in (3). While (4) is reasonably similar for both rigid and lumped inertia models, the lumped inertia model fails to maintain cone lock as the ring is released from blocking, generating higher slip between chamfers at the sleeve and hub, and increasing the rate of re-alignment. Overall consideration of these results suggests that the most significant assumption, linearising drag torque, has resulted in variation between the two synchroniser models. This has delayed the engagement of the mechanism, increasing process time by approximately 25%.

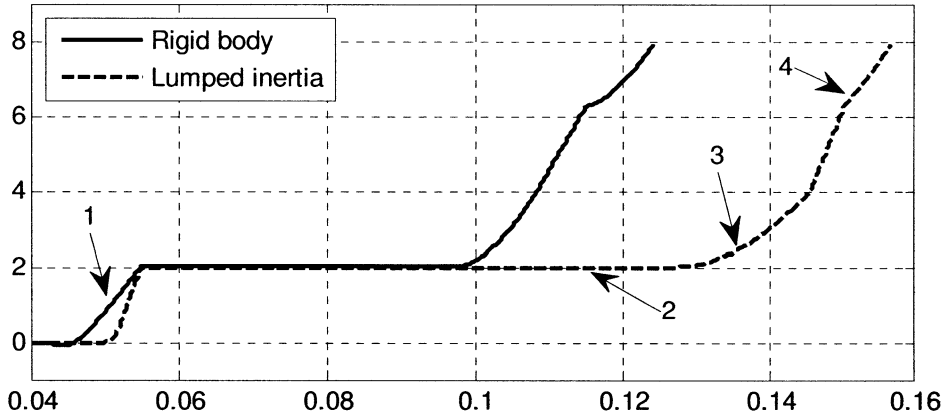

Figure 10.1: Synchroniser sleeve displacement for rigid body model and lumped mass model engagement simulations

10.2.3 Transient simulations with ideal engine torque model

The first series of simulations use the ideal engine model to simulate the mechanism engagement without interference from engine harmonics. For initial simulations, a general shift case for a fourth gear synchronisation with third gear engaged is considered. For these conditions the initial wheel speed is set to 40 rad/s with a corresponding engine speed of 182 rad/s, and throttle angle at 50%.

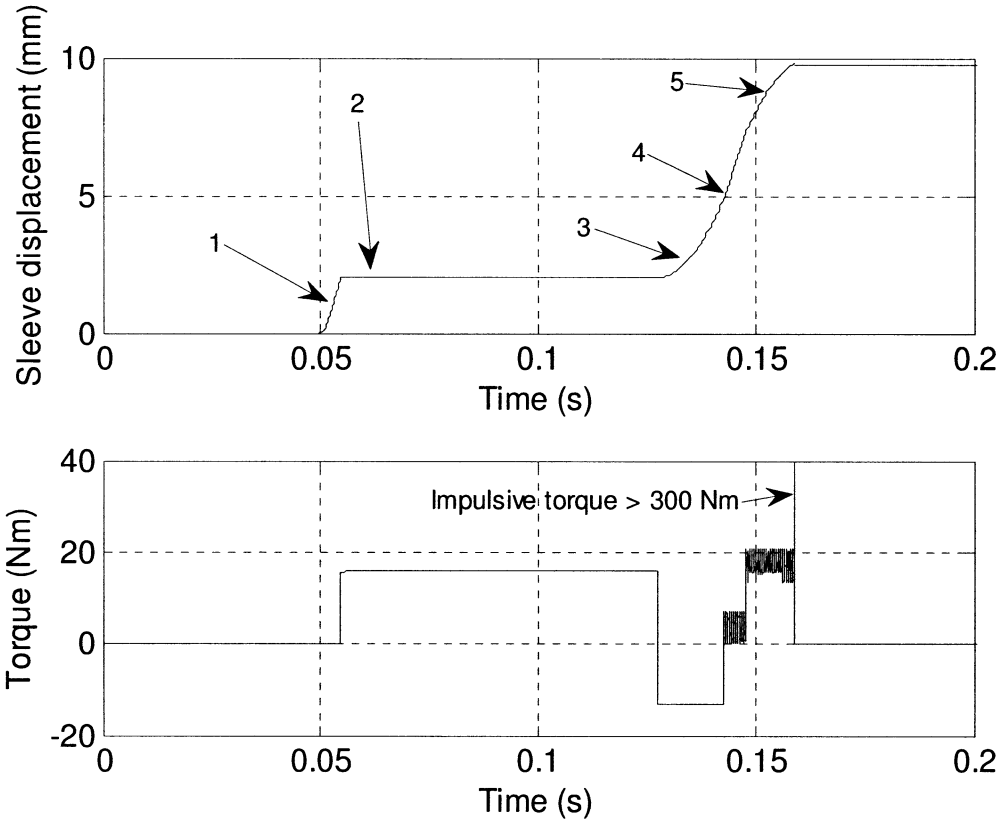

Figure 10.2: Synchroniser engagement responses, showing (top) sleeve displacement during engagement and, (bottom) effective synchroniser torque

Figure 10.2 presents sleeve displacement and synchroniser torque during the mechanism engagement. At 50ms the synchroniser is actuated and moves forward rapidly as hydraulic pressure increases, with the initial displacement taking less than 5ms, indicated by arrow 1. During the next stationary period, arrow 2, speed synchronisation is performed and a constant positive torque is developed in the synchroniser. With the components synchronised, the sleeve moves forward again and the torque rapidly changes direction as blocking chamfers now take up the primary torque role at arrow 3, with the reversal of torque demonstrating the required torque balance of the mechanism during synchronisation. The sleeve pushes forward until it breaches the blocking

chamfers, the cone is released at approximately 140ms and the sleeve moves forward freely (see arrow 4). The unsteady torque here results from vibration in sleeve and gear generating an unsteady friction load on the cone clutch as the sleeve rapidly moves forward. There is then the final chamfer torque as the hub is indexed with the sleeve and interlocks the mechanism at arrow 5. This engagement is slowed by resistances acting against the chamfer torque with vibration of the sleeve again causing oscillations in the chamfer torque at frequency 1788Hz, the local natural frequency for the freewheeling components prior to lockup of the synchroniser.

As the sleeve completes the engagement there is still a relative speed between the two elements. With lockup a torque impulse is generated in the sleeve as a restitution load to halt any remaining relative motion. Though over 300Nm, this torque is developed numerically and is heavily dependent on the time step used during the simulation. Overall the synchroniser torque can be characterised as being highly nonlinear and heavily dependent on sleeve position and relative speed between hub and sleeve.

In Figure 10.3 the absolute and slip speed results for sleeve and hub of the target gear are presented for the duration of the process. With high viscous drag in the wet clutch, the speed of the target gear is actually higher than that of the sleeve when synchronising a higher gear. At end of blocking, the impulse created through realignment of the ring as it is captured by the sleeve releases the cone clutch and significant slip speed is introduced to the mechanism before indexing of the mechanism. This can be an issue as high slip speeds during chamfer contact at hub indexing can also lead to impact damage with chamfer teeth. This results in increased vibration during indexing of the hub and target gear that is not experienced during unblocking of the ring. These are similar processes but the ring unblocking begins with a zero relative velocity. At end of indexing the trapping of hub inside sleeve produces a step speed change consistent with the lockup shock torque discussed previously. This step change, in conjunction with the inertia change, is the primary reasons behind significant post lockup vibration of the mechanism.

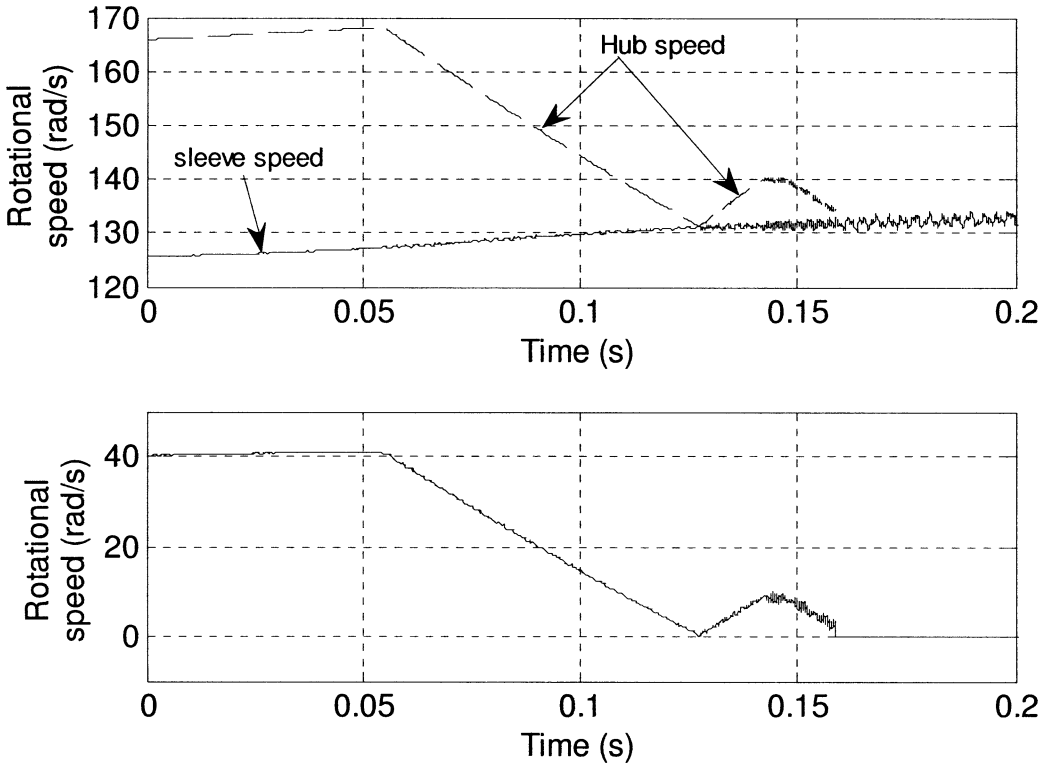

Figure 10.3: Synchroniser hub and sleeve speeds (top), and synchroniser relative speed (bottom)

Another critical aspect of this simulation is the identification of stick-slip in cone clutch at end of synchronisation and before unblocking of the ring. Figure 10.4 provides evidentiary demonstration of minimal stick-slip upon lockup of the cone clutch. Unblocking of the ring then commences rapidly. This provides minimal delay to the process of engagement at the beginning of unblocking the ring.

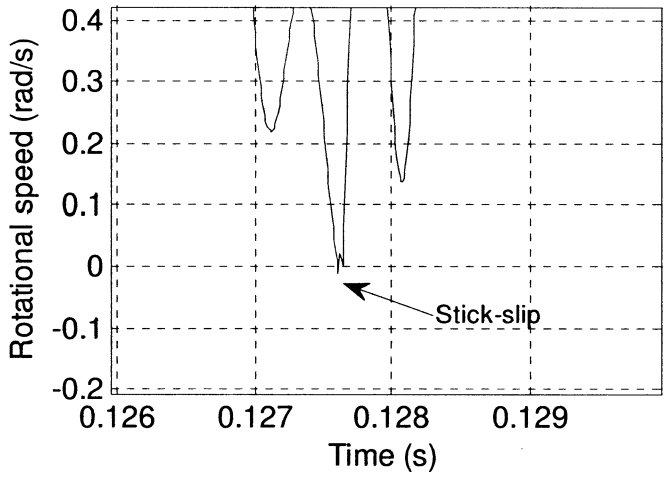

Figure 10.4: Cone slip speed demonstrating stick - slip during final stages of speed synchronisation

10.2.4 Transient simulations with unsteady engine model

So far simulations have demonstrated clearly the actuation of the synchroniser in the ideal case, with no external vibration during engagement. These simulations ignore the input of engine torque harmonics during the synchroniser engagement. In this section, engine torque harmonic model replaces the mean engine torque model for the duration of the simulation. Otherwise the following results are generated using identical parameters to those in the Section 10.2.3.

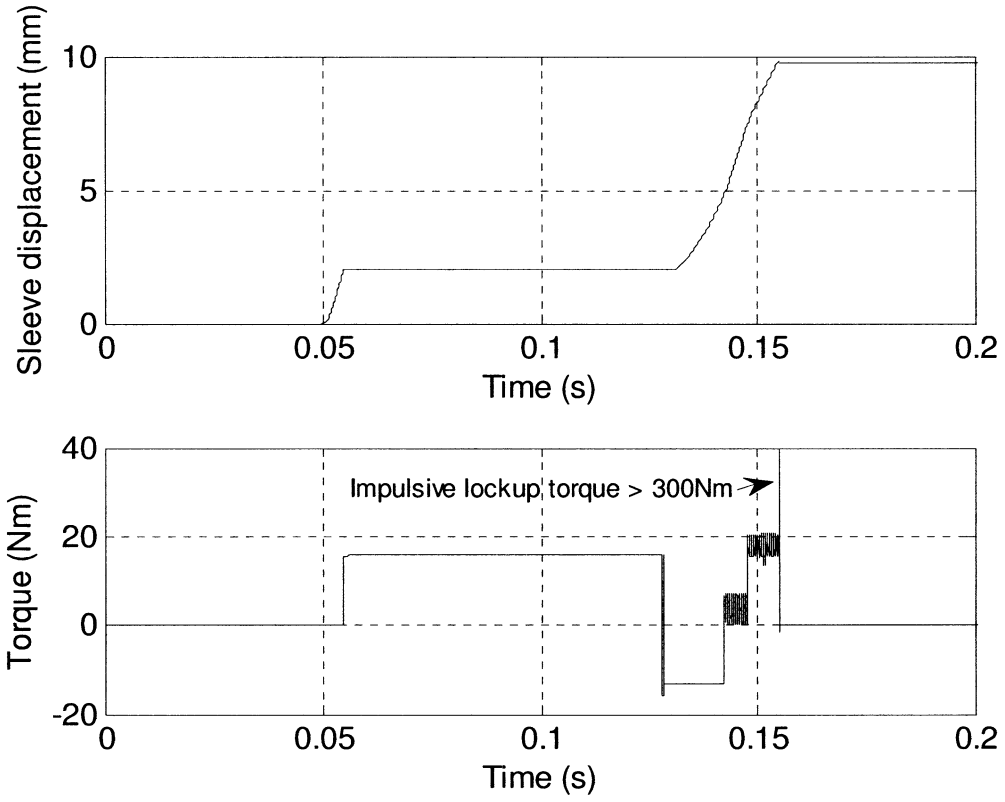

Figure 10.5: Synchroniser engagement responses using dynamic engine model, showing (top) sleeve displacement during engagement and, (bottom) effective synchroniser torque

Comparing results for Figures 10.2 and 10.5 are very similar. However at the end of synchronisation there is evidence of stick-slip phenomena in the cone clutch. Sleeve displacements are consistent, and the duration of engagement does not change significantly. The fluctuation of chamfer torque during indexing is again present, being associated with the directional change of relative chamfer motion during indexing. Such vibrations may contribute to increased wear on chamfer contact surfaces, reducing effectiveness of the chamfer engagement during the indexing of the mechanism.

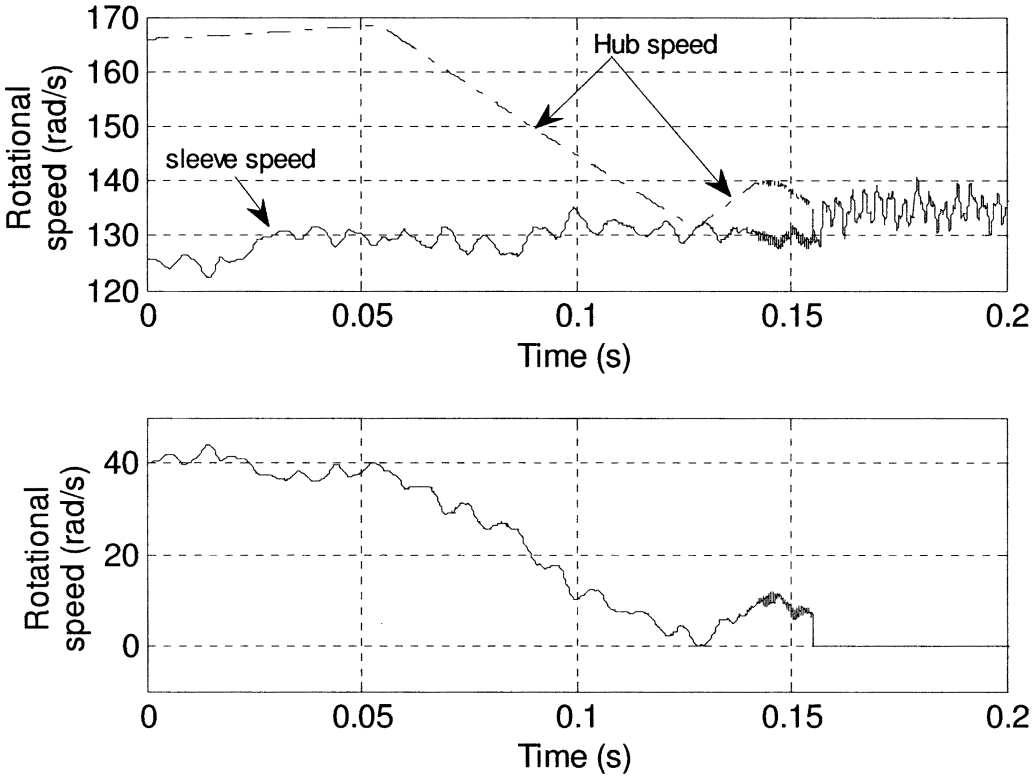

Figure 10.6: Synchroniser hub and sleeve speeds (top), and synchroniser relative speed (bottom) using dynamic engine model

The effects of introducing an harmonic engine torque model onto the powertrain are significantly more pronounced in the synchroniser sleeve and hub rotational speeds. During the initial steady state, sleeve vibration has increased considerably, reflected in the cone slip speed. However, with the exception of indexing, the engagement process is reasonably similar to Figure 10.3, including synchronisation duration and unblocking of the mechanism. During indexing there is increased vibration of the sleeve in particular. This is considered a negative influence of engine torque harmonics on the engagement of the mechanism, and again is likely to contribute to increased wear of chamfer contact surfaces. Stick slip periods are present in the mechanism after speed synchronisation and are significantly pronounced. As shown in Figure 10.7. In Figure 10.4 there is only minor evidence of stick-slip occurring. However, with engine vibration, there is increased stick slip that restricts initiation of unblocking of the synchroniser mechanism (Figure 10.7).

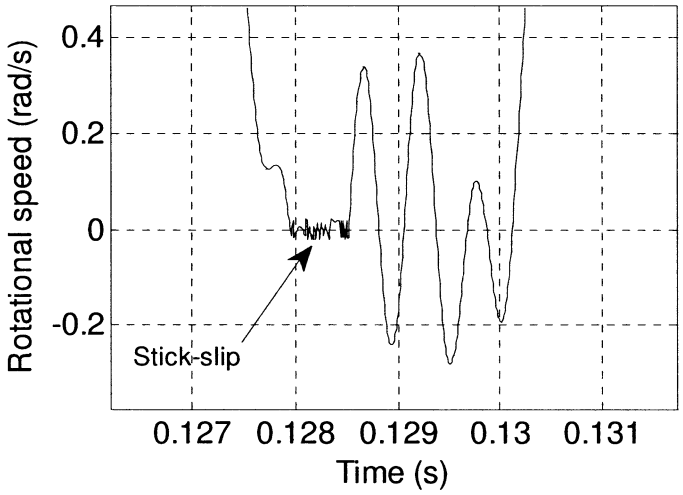

Figure 10.7: Demonstration of stick-slip phenomena using a dynamic engine model

10.2.5 Comparison of responses during synchronisation for steady and unsteady engine models

To further investigate vibration of the mechanism through the introduction of an harmonic engine torque model, comparison of sleeve relative vibration during both synchronisation and indexing of the mechanism is performed with both versions of the engine model. The results are presented in Figure 10.8, and Fast Fourier Transforms of a discrete system is performed for the synchroniser engagement period to identify the introduction of forced engine vibrations. Given the torques acting on the synchroniser sleeve in Figures 10.2 and 10.5 are positive, negative amplitude vibrations are more likely to contribute to the early unblocking of the mechanism as negative vibrations are likely to aid release of chamfers.

Figure 10.8 demonstrates the relative vibration amplitudes of the synchroniser sleeve during different stages of engagement. During synchronisation, Figure 10.8 (a) and (c), vibrations are reasonably consistent with similar vibration amplitudes but a low order frequency can be observed in the harmonic engine model. The results for engine vibrations suggests the possibility for negative vibrations, however this is only for small periods. Thus, while there are negative vibrations present these are unlikely to be sufficient to cause early unblocking of the synchroniser ring.

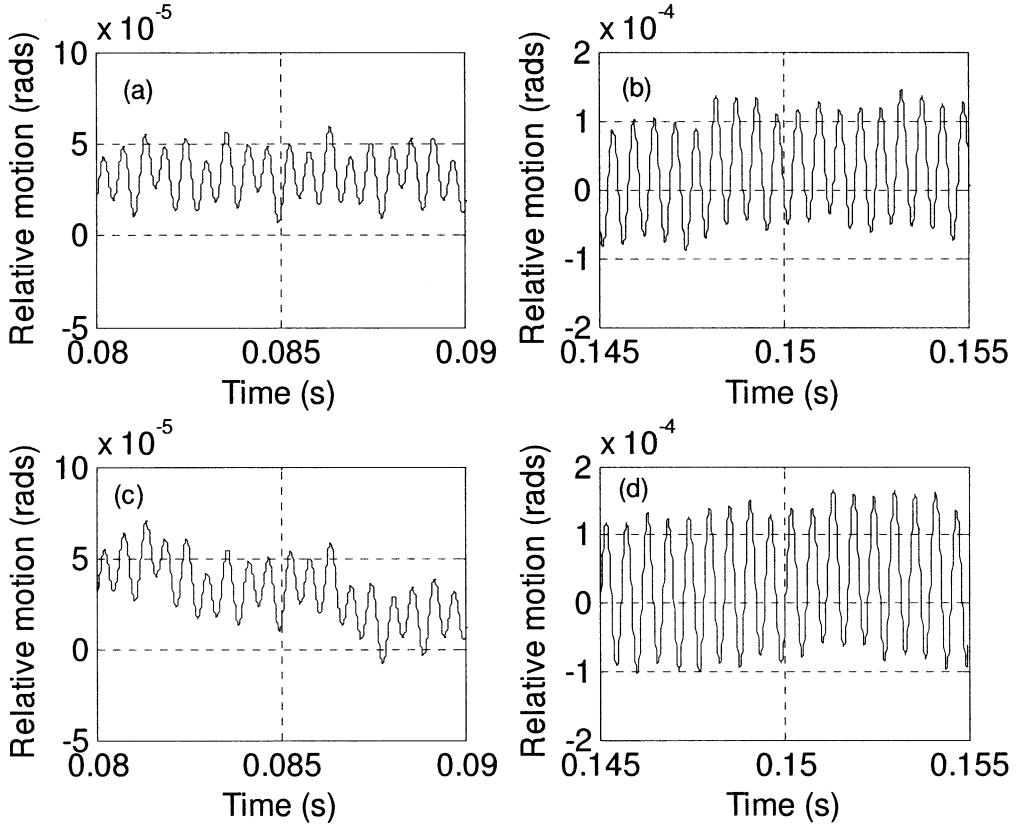

Figure 10.8: Relative vibration synchroniser sleeve during actuation of the synchroniser mechanism. For the ideal engine models (a) during synchronisation and (b) during indexing, and using the unsteady engine model (c) during synchronisation and (d) during indexing

In the Figure 10.8 (b) and (d) there is a significant increase of vibration. In the response during indexing with engine vibration included, a significant increase in vibration amplitudes is observed. This is consistent with earlier demonstrated results, in that the introduction of the engine model contributes to increased vibration of synchroniser components during indexing in particular, suggesting that there is the likelihood of increased wear on the friction contact surfaces.

A more extensive result of the influence of engine vibration can be observed using Fast Fourier Transforms of the sleeve relative vibration during synchroniser engagement. With no engine vibration the influence of system natural frequencies is much more dominant, with peaks corresponding to ω_{n8}, ω_{n9}, and ω_{n11}. These natural frequencies are also observed to a lesser extend in the FFT results for simulations with engine harmonics. However at low frequencies, those below 500Hz, much of these results are hidden by noise generated by numerical error associated with using Fourier transforms on a discrete data set. Figure 10.10 provides a scaled up view of the low frequency responses; the peaks indicated by arrow 1 show the frequency responses introduced

from engine harmonics. It is noted that these harmonics are dependent on engine speed, therefore frequencies will change as the engine speed changes. The introduced forced vibration is observed in Figure 10.6 with external oscillations superimposed over the synchroniser response in Figure 10.3, with only a mean torque engine model applied.

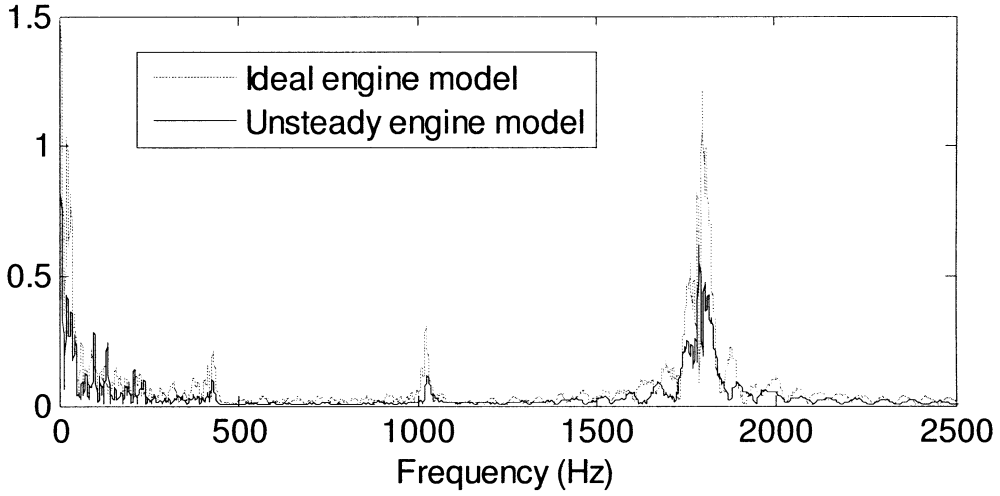

Figure 10.9: Fast Fourier Transforms of sleeve relative vibration during synchronisation

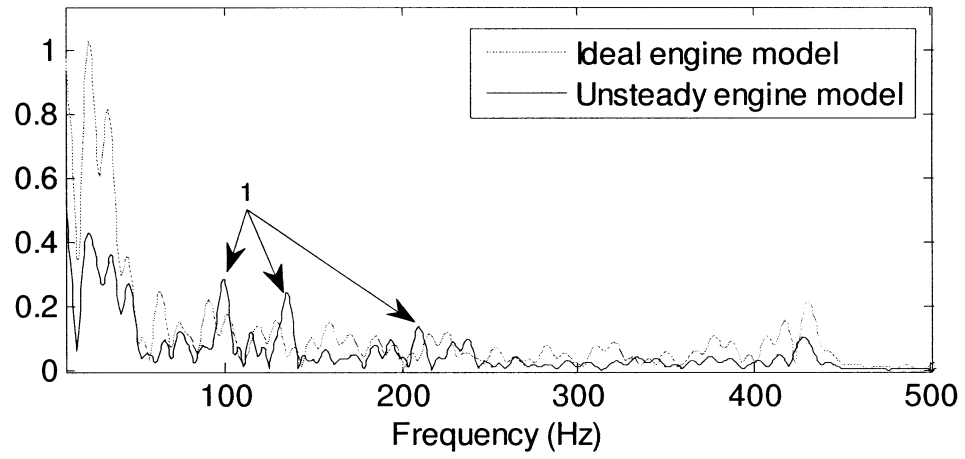

Figure 10.10: Enlarged view of FFT results in figure 10.9, focus on frequencies less than 500Hz

10.3 DYNAMICS OF POWER-ON CLUTCH-TO-CLUTCH SHIFTS IN A DCT POWERTRAIN

Focus now shifts to the shift transient simulations making use of the 15DOF model developed in chapter 8. Lumped inertia models are now used for state 5, engaged in 3rd gear, state 7 during the shift transient, and state 6 for engaged in 4th gear. This study covers a range of powertrain configurations. Simulations are preformed for a typical

shift, including comparison to 4DOF control model to compare performance responses of the two powertrain models, followed by simulations of shifting with the inclusion of a harmonic engine torque model in the powertrain, and the impact of applying a dual mass fly wheel to the powertrain. Torques are now defined from the output pressure and throttle signals derived from the 4DOF shift model in Chapter 9.

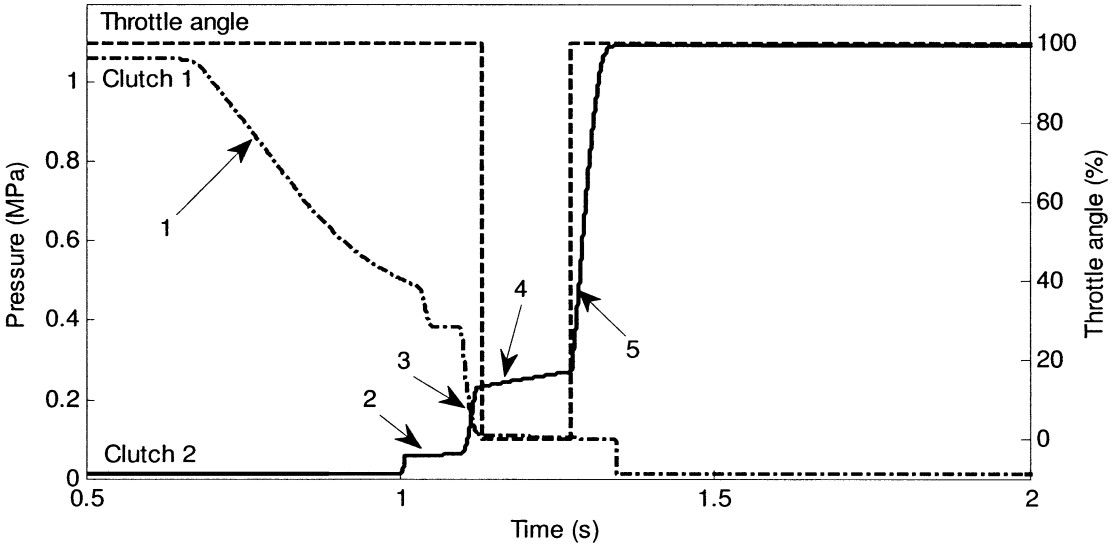

Figure 10.11: Clutch 1, clutch 2, and throttle angle control signals (arrows used to indicate different steps of the shift process)

The clutch pressure and throttle angle signals in Figure 10.11 are generated using the torque estimation equation derived in equations 8.45 to 8.48. It should be noted that these profiles are dependent on the initial speeds of the powertrain and must change as required. The arrows indicate important steps in the clutch shift process, as follows:

1. Clutch 1 release, where clutch 1 pressure is ramped down to the slipping point in preparation for shifting. Ramping is used over a step down to prevent undercutting of the static friction limit that would prematurely initiate slip.
2. Pre-fill of engaged clutch, with the solenoid activated at maximum flow, the clutch is rapidly filled, the increase in pressure represents resistance of the return spring, no torque is transmitted through the clutch.
3. Torque phase, with clutch 2 pressure increased and clutch 1 simultaneously released, torque is transferred from clutch 1 to clutch 2. During this stage throttle angle is maintained to ensure proper release of clutches.

4. Inertia phase, clutch 1 is released and clutch 2 is at the ideal torque, with some transients as pressure stabilises, the clutch drum and engine speeds are reduced to match clutch 2 speeds. Thus engine throttle is set to zero to minimise torque.
5. Lockup detection, with clutch 2 pressure reset to maximum there is some delay as peak pressure is reached. Engine throttle is reset to maximum.

10.3.1 Comparison of 4DOF and 15DOF models

A significant assumption made in developing the control model for the powertrain is that the 4DOF model presented in Chapter 9 is a reasonable approximation of the 15DOF powertrain model developed in Chapter 8. Shift transient simulations have been demonstrated with both models, and indeed the clutch and engine control signals derived from the 4DOF model are applied to the 15DOF model for transient studies.

In the first series of simulations the 4DOF and 15DOF mean torque models are studied. Figure 10.12 presents the 4DOF model results, with (a) presenting the clutch and drum speeds during the transient period, and (b) clutch 2 and net vehicle torques, this is determined as $T_{net}=(T_V+J_V\ddot{\theta}_V).\gamma_{G2}.\gamma_{FD}$. The shift transient is initiated at 1.1 seconds after clutch preparation is completed in accordance with the description in Section 5.3. The torque phase lasts about 20ms, with clutch slip simulations indicating that there is some initial stick slip as the torque is handed over between the two clutches, resulting in a small drop in the vehicle net torque. Also note that during the inertia phase, torques track reasonably well, with net torque vibrations resulting from the release of clutch 1. It is also shown that with no losses modelled in the powertrain, post shift torque vibrations are identical for both clutch 2 and net vehicle torques.

The comparative results are presented in Figure 10.13 for the 15DOF model. Comparing this result to Figure 10.12 (a), transient periods are very similar with the overall engagement reduced by 10 ms, owing primarily to the different responses under transient conditions. The impact of using more detailed models is further revealed with peak to peak amplitudes of vibration significantly reduced in the 15DOF results, and higher frequency responses are also introduced. Again stick-slip of clutch 1 is present, but both amplitude and duration is reduced. The clutch and vehicle torques in Fig 12 (b) and 13 (b) are markedly different, post lockup vibrations in the clutch are significantly affected by higher frequencies. The results show that the vehicle torque is now offset

from the clutch torque as a result of losses introduced in the 15DOF model, and the superposition of multiple vibration frequencies is now present in the vehicle torque. The introduction of more degrees of freedom significantly impacts on the post lockup vehicle torque, and is potentially the most significant result. Peak to peak torques are now reduced to 100Nm variations, significantly lower than the 400Nm peak-to-peak amplitudes resulting from the 4DOF model. This suggests that the driver observed response may vary significantly between the two example models.

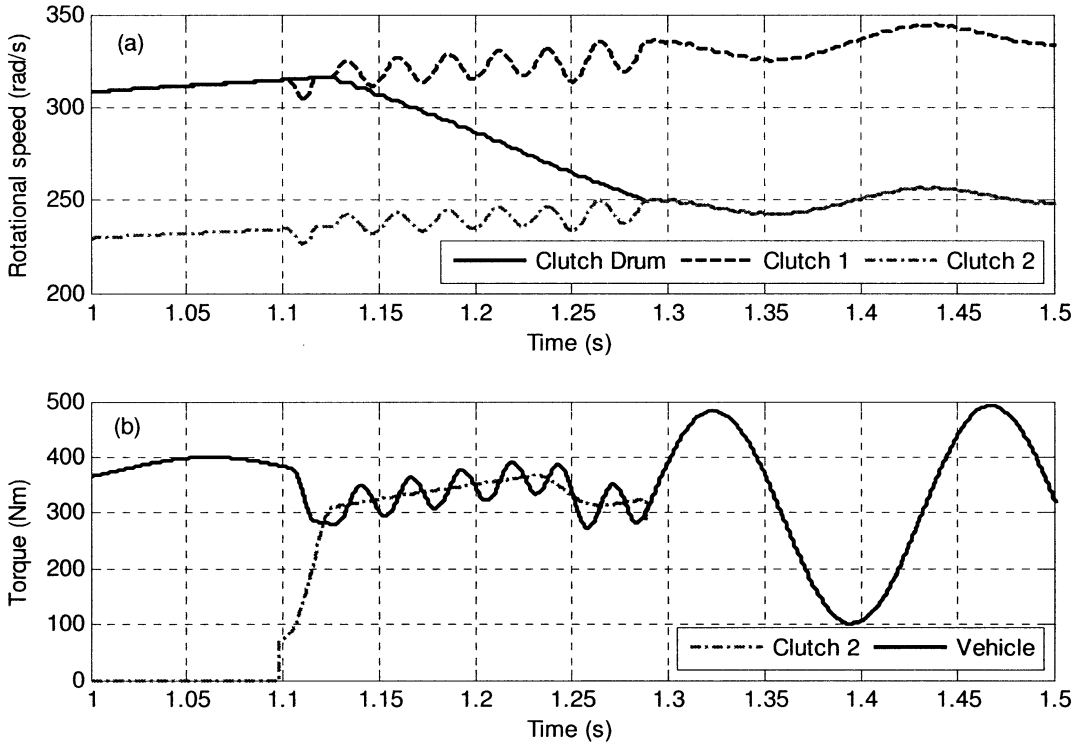

Figure 10.12: Gear shift simulation results for 3rd to 4th upshift using 4DOF model with mean engine torque, (a) clutch drum and hub speeds, and (b) clutch 2 and vehicle torques

Through the evaluation of two different suggested methods for modelling the DCT powertrain, results suggest that increasingly more detailed models are required to evaluate results of transient control studies. It is observed from moving between a 4DOF and 15DOF powertrain model with mean engine torques that the response of the system changes significantly. Output torques vary significantly in terms of amplitude of vibration, suggesting significant differences in observed response. Resulting from the inclusion of power loss elements there is now offset between clutch and vehicle torques, suggesting that the torque estimation methods using clutch 2 average torque may not be sufficiently accurate; loss factors must be included. Furthermore the post lockup torque

response in the 15DOF model significantly improves over the 4DOF model; results suggest that a 4DOF model may be inadequate for DCT applications.

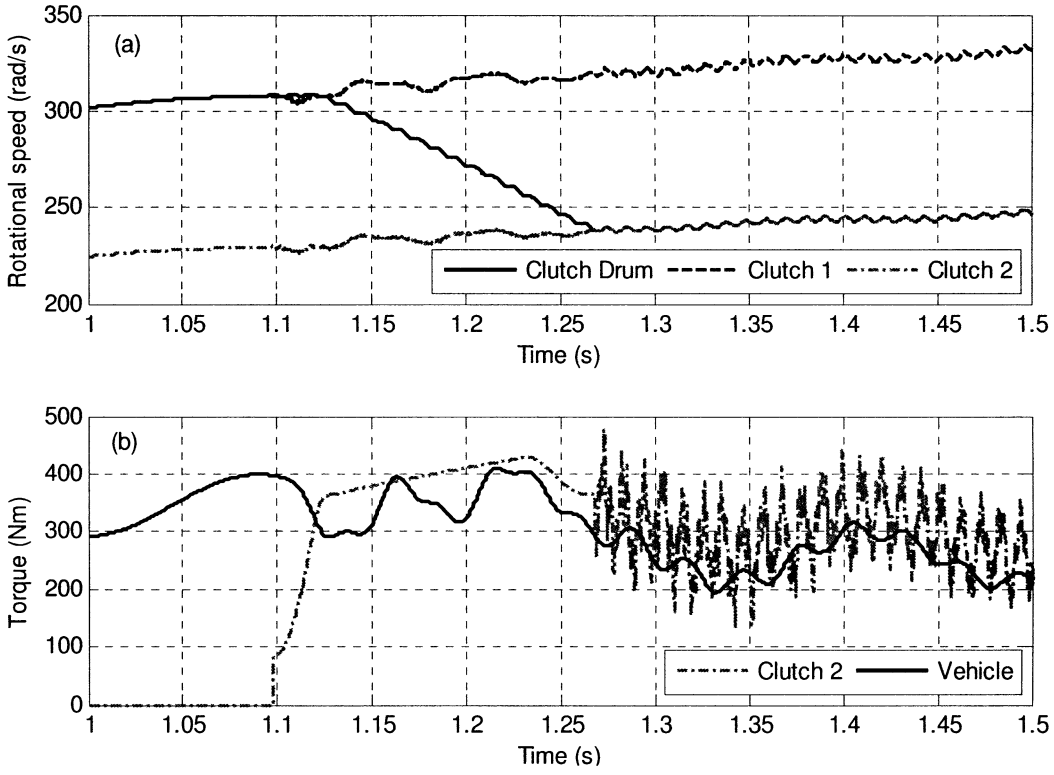

Figure 10.13: Gear shift simulation results for 3rd to 4th upshift using 15DOF model with mean engine torque, (a) clutch drum and hub speeds, and (b) clutch 2 and vehicle torques

10.3.2 Application of transient engine torque model

The following simulation introduces the harmonic torque engine model to the 15 DOF powertrain model. Application of harmonic engine torques introduces higher frequency forced vibrations into the powertrain and can impact on various aspects of shift quality and vehicle performance. Thus it was previously postulated that the use of mean torque models introduces limitations into studying shift transient control of DCT powertrains.

The results in Figure 10.14 provide a detailed evaluation of the impact of applying transient torque engine models to the powertrain. Focusing particularly on Figure 10.14 (b), the vehicle torque starts dropping from 1.05 s as a result of the repeated stick slip generated in clutch 1. This phenomenon is illustrated in Figure 10.15, with multiple stick and slip periods occurring over 50ms time range before shifting, resulting from the engine torque pulses interacting with low pressure and therefore static friction torque in

clutch 1. Ultimately, prior to the initiation of shifting this phenomenon further exacerbates the torque hole during the shift. As the target torque during shifting is estimated from the clutch 2 average torque, the post lockup transient response of clutch 2 in Figure 10.14 (b) indicates that there will be increased uncertainty at which the mean torque value can be readily estimated with the forced vibrations significantly increasing clutch 2 average torque vibrations present in comparison to Figure 10.13 (b).

Comparison of both engine models indicates that the mean torque engine model provides lower transients in resulting vehicle and clutch torques and clutch speeds. The harmonic torque engine model can detrimentally affect the torque phase of shifting through initiation of stick-slip, but has little effect on the inertia phase. It may also impact on torque estimation, affecting the duration of shifting and reduce tractive load during the transient periods, degrading shift performance. It can be considered that with mean torque models the torque output is a steady state average torque, applicable to AT shift control with fluid coupling isolating the drivetrain from forced vibration. As the engine directly drives the powertrain in DCT equipped vehicles there must be consideration for the impact of these engine transients on the vehicle.

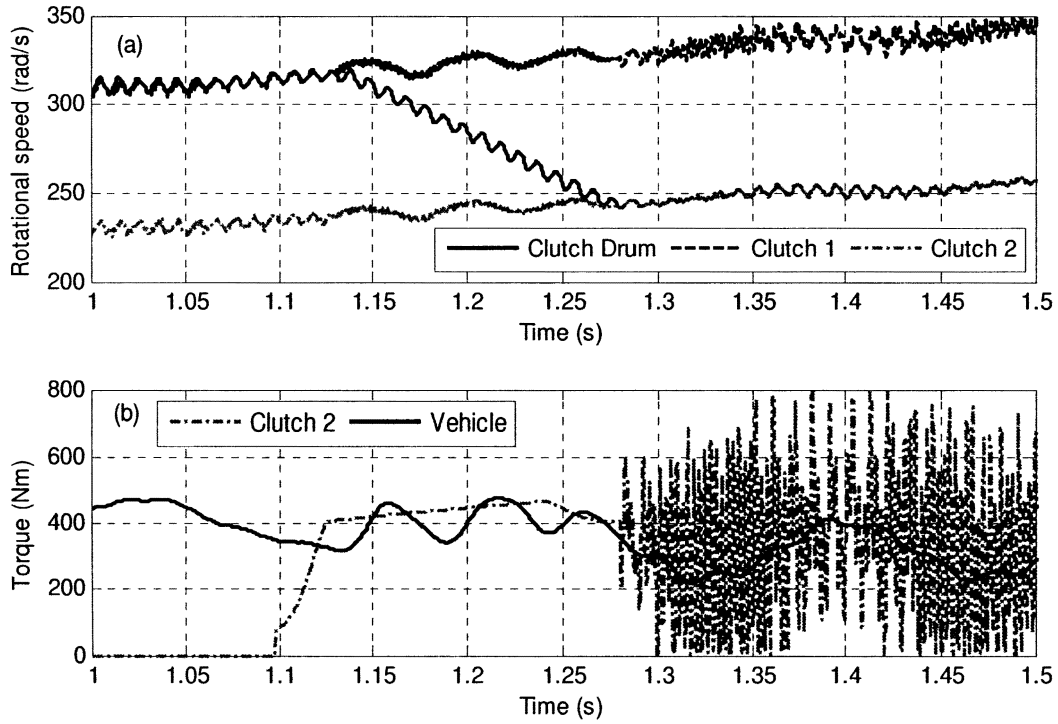

Figure 10.14: Gear shift simulation results for 3rd to 4th upshift using 15DOF model with transient engine torque, (a) clutch drum and hub speeds, and (b) clutch 2 and vehicle torques

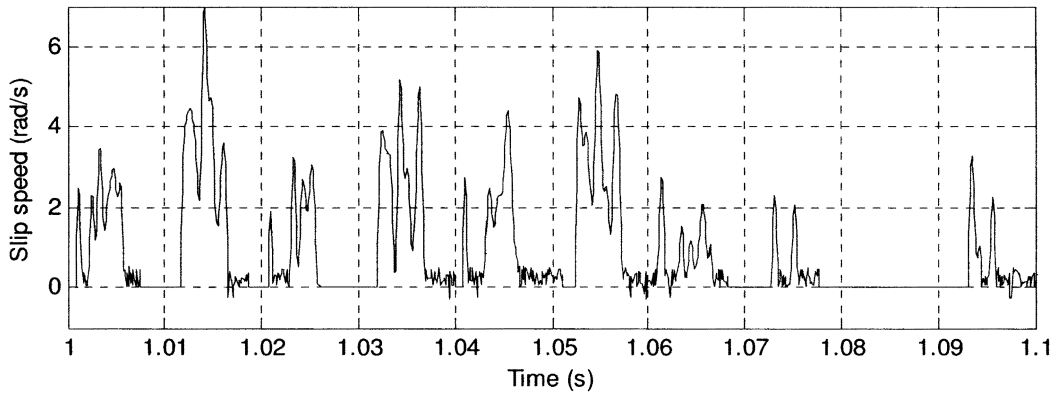

Figure 10.15: Clutch 1 slip speed showing stick slip introduced during pre-shift period in the 15DOF powertrain with transient torque model

10.3.3 Inclusion of DMFW

The final simulation applies the DMFW model identified in Chapter 8, Section 8.4.2 to the 15DOF model to demonstrate the significance of isolating the drivetrain from the engine. Higher damping in the DMFW impacts significantly on the transient response of the system. Stick-slip observed in Figure 10.15 has been completely eliminated, as are the higher frequency vibrations in the clutches and clutch drum. During the torque phase in Figure 10.16 (a) a drop in drum speed is briefly observed before clutch 1 is released. However the torque hole is reduced perceptibly.

The inertia phase is largely unchanged from Figure 10.14 (a) and (b). However vehicle and clutch torque vibrations increase significantly as a result of the higher rotation required for Clutch 1 release. There is some indication that there are difficulties arising in the clutch lockup as the clutch slips at very low speed, a result of hysteresis and lead-lag in the DMFW impeding the engagement. At clutch lockup the drum speed dips with the drop of clutch 2 and vehicle torques that results from DMFW oscillation from lag to lead conditions as the engine again drives the vehicle. In Figure 10.16 (b) Post lockup vibrations of vehicle torque, however, are rapidly suppressed through DMFW damping, and the transmission of engine forced vibrations through the powertrain is attenuated, indicating that the DMFW has capacity to isolate engine harmonics from the remainder of powertrain and reduce the severity of post lockup transients in the clutch. However there continues to be vibration in clutch 2 torques indicating there is still uncertainty in the estimation of mean torque values.

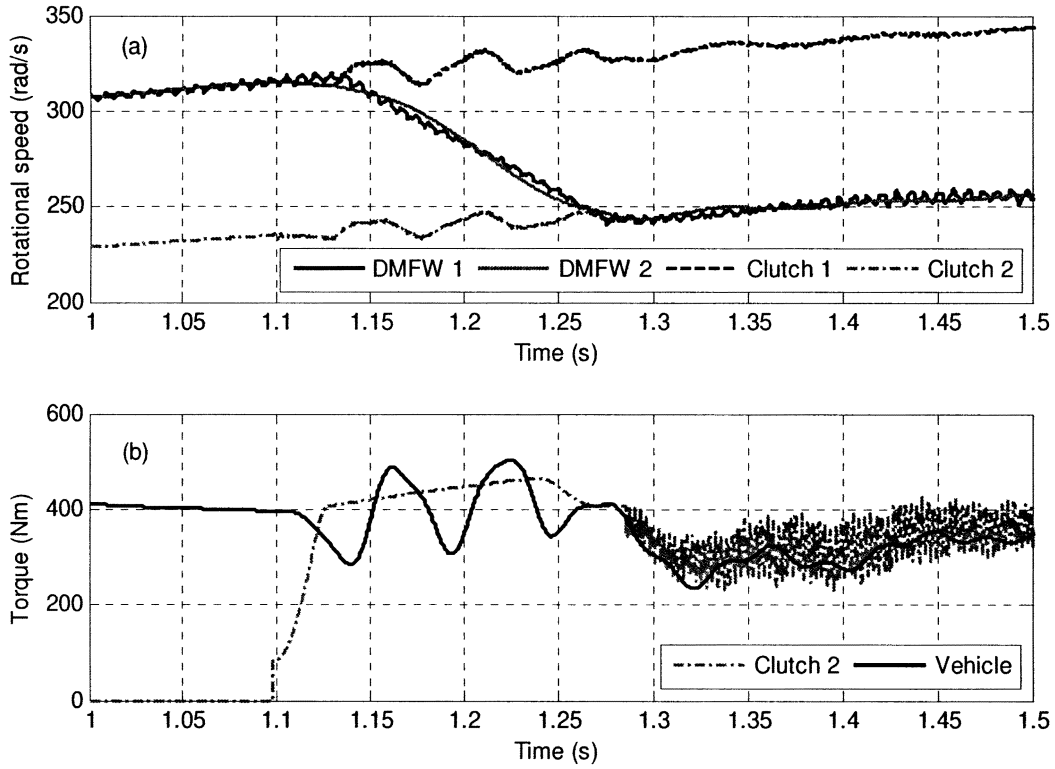

Figure 10.16: Gear shift simulation results for 3rd to 4th upshift using 15DOF model with transient engine torque and linearised DMFW, (a) clutch drum and hub speeds, and (b) clutch 2 and vehicle torques

10.4 THE COMBINED SYNCHRONISER ENGAGEMENT AND SHIFTING IN A DCT POWERTRAIN

Consistently it has been assumed in dual clutch transmission shift control research that synchroniser engagement has no impact on the shift performance. However evaluation of synchroniser engagement was demonstrated to introduce transient vibration post lockup of the synchroniser. Issues can therefore arise in clutch release via stick-slip and torque estimation, suggesting that studies of the interaction of these to processes is pertinent.

Integration of the two models is relatively simple. Process constraints dictate that the synchroniser engagement is a precursor to gearshift. The process of shifting must be defined as a series of events that cannot be realistically run in parallel, see Figure 10.17.

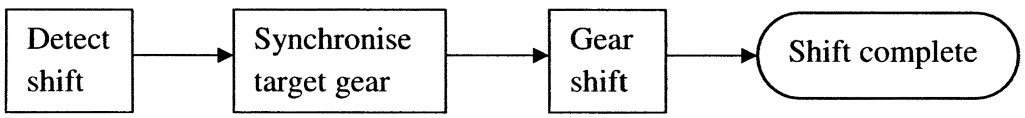

Figure 10.17: Linear shift process in DCTs

The described gear shift process, including synchronisation in the figure above, indicates the relative simplicity required for implementing a combined engagement strategy; the synchroniser model developed for section 10.2 of this chapter is integrated with the preceding shift transient model.

Combined simulations are preformed using a 3rd to 4th gear upshift, with initial vehicle speed of 52 rad/s, equating to an engine speed of 304 rad/s. Synchroniser parameters for cone and chamfers are cone angle 7°, friction coefficient 0.12, chamfer angle 65° and friction coefficient 0.04. Synchronisation is initiated at 0.8s and shift torque phase at 1.095s, with the shift preparation performed at t=1s. The control signal for shifting is presented in Figure 10.18, with throttle angle (%) and clutch 1 and 2 pressures (MPa) shown, here Clutch 1 pressure is ramped down to avoid undercutting of the minimum pressure with the static friction limit. This has a secondary effect of reducing the locked clutch to lower friction limits, and exposing it to transients induced during synchroniser engagement. Also note that the higher initial speed increases the speed differential in clutch and synchroniser, extending both engagement processes.

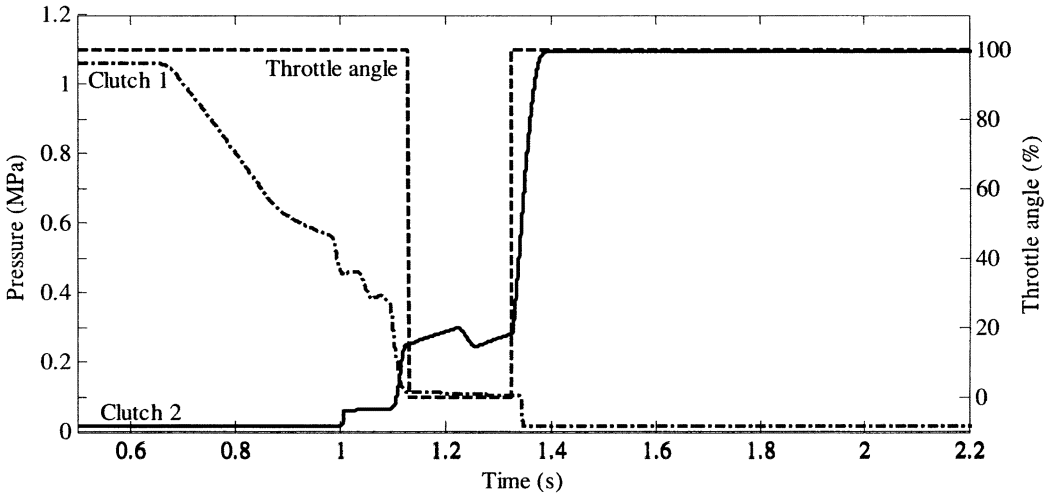

Figure 10.18: combined shift transient engine and clutch 1 and 2 control signals

Shift transient simulation results for the combined synchronisation and gear shift for a 3rd to 4th gear upshift are presented in Figure 10.19 for both clutch 1 and 2, clutch drum, and synchroniser gear hub and sleeve speeds. Results are indicative of previous independent simulations presented in this chapter, such as Figure 10.3 and Figure 10.13 for synchroniser and gear shift, respectively. Synchronisation begins at 0.8 seconds and proceeds nominally though all phases. The higher initial speed extends the gear shift period, and fluctuation of clutch 2 pressure signals gives the impression of instability of

clutch 2 response during shifting. Comparison of Figure 10.19 to 20 corroborates this result with the minimum pressure and subsequent increase during the inertial phase, between 1.2 and 1.3 seconds, corresponding to the increasing amplitudes of clutch 1 and 2 vibrations in the same period.

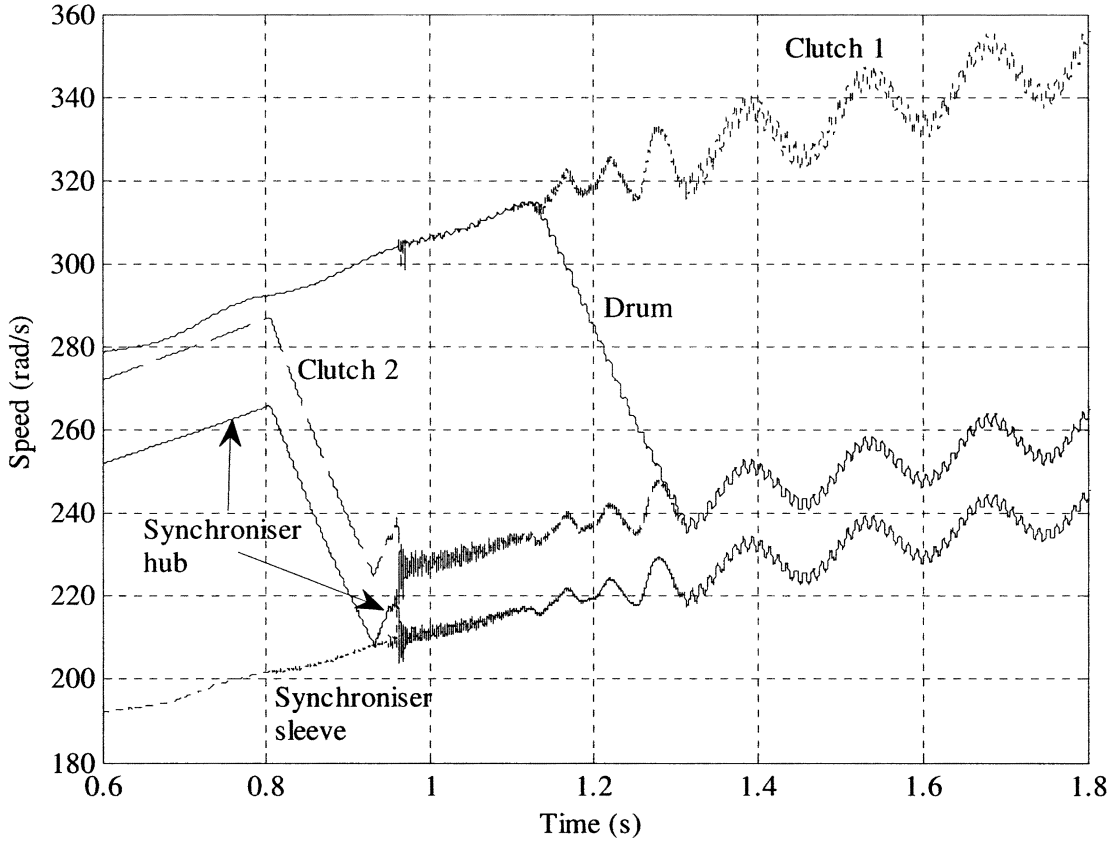

Figure 10.19: combined 4th gear synchronisation and upshift from 3rd to 4th gear simulation

Between the completion of synchronisation and the initiation of gearshift is where the most significant issues are identified. As clutch 1 pressure drops according to Figure 10.18 and the synchroniser lockup introduces an impulsive response, vibrations are introduced to the transmission and shock in the clutch drum may initiate stick-slip response, Figure 10.20 shows this in greater detail. Shock induced vibrations, consistent with studies of synchroniser engagement in this Chapter are in the main suppressed, but higher frequency vibrations remain throughout the shift process, these vibrations being initiated during indexing.

The major frequencies present in the post clutch 2 lockup response of the powertrain are the 6Hz global shuffle mode of the powertrain, and the 98Hz local flywheel mode, similar to 10.13 where the 30Hz model is not excited. Not easily observed from these

results is the excitation of higher frequency modes from synchroniser engagement, above 1000Hz. These result from the lockup impulse and suggest the possibility of clonk response in the powertrain.

Figure 10.20 (a) presents a close up of Figure 10.18 for the clutch drum speed between 0.9 and 1.15 seconds, covering the completion of synchronisation and the initiation of gear shift. Results demonstrate that the lockup torque generated at the end of synchronisation results in a vibration transmitted to clutch 1 and clutch drum, after 0.95 seconds. The transient is rapidly suppressed, and shifting begins normally at 1.1 seconds. During the torque phase from approximately 1.1s, high frequency vibrations are present as clutch 1 moves in and out of slip and engine torque minimises the torque hole. Supported by Figure 10.21 (b), here clutch 1 slip speed results are presented for the same period, the abrupt drum response at the completion of synchronisation initiates brief slip response as the clutch 1 pressure is reduced and impulsive torque is generated as the synchroniser is locked up. This is a result of lock clutch 1 pressure at this time and the numerically determined lockup impulse in the synchroniser.

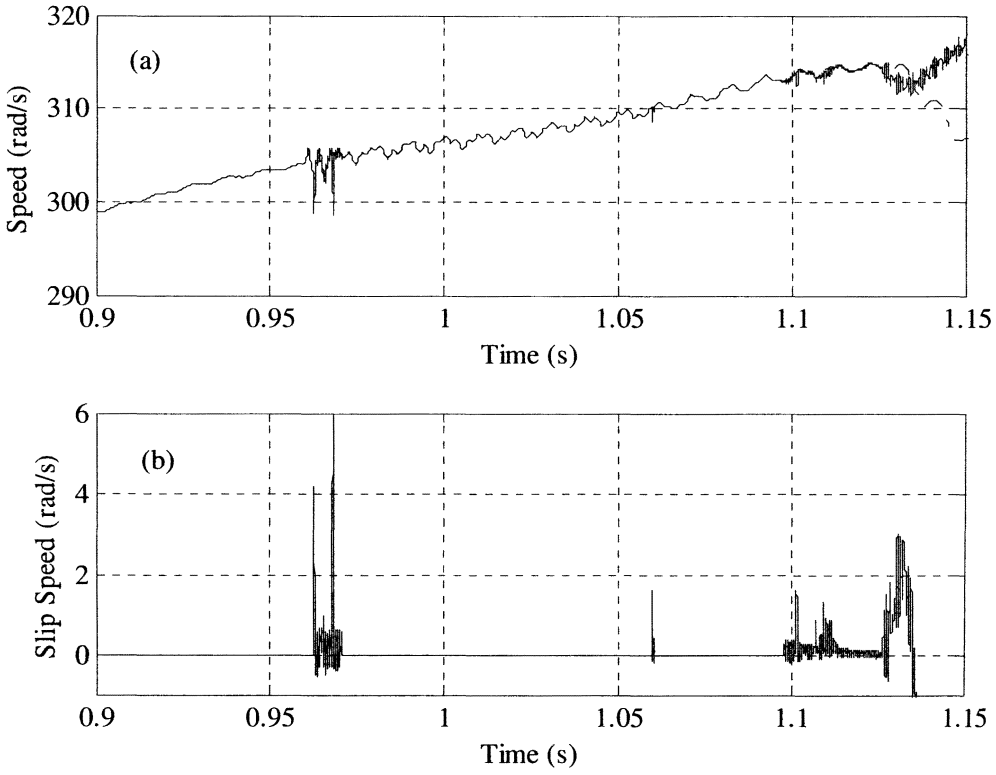

Figure 10.20: Stick-slip simulations (a) drum speed, (b) clutch 1 stick-slip

During speed synchronisation (Figure 10.21 (a)) vibration is dominated by local high frequencies of 1965Hz, the free vibration natural frequency associated with the

freewheeling component during synchronisation. In Figure 10.21 (b) the vibration response after synchronisation is completed in its entirety as shown. The dominant frequencies are 325Hz and 2040Hz, both of which are local natural frequencies of transmission components (see Table 8.4 in Chapter 8). At the initiation of shifting, Figure 10.21 (c) lower frequencies are suppressed and only high natural frequency remains, i.e. 2040Hz. This frequency is also present at clutch 2 lock up, Figure 10.21 (d), which has a second frequency of 98 Hz present. The presence of k Hz frequencies response during all transient states indicates that there is significant vibration transmission at high frequencies, with little capability of suppressing the transient response. Where other lower frequencies are damped out through either traditional damping or the introduction of slipping in the transmission, higher frequencies remain an issue, and are consistent with the possibility of clonk response during most transient states.

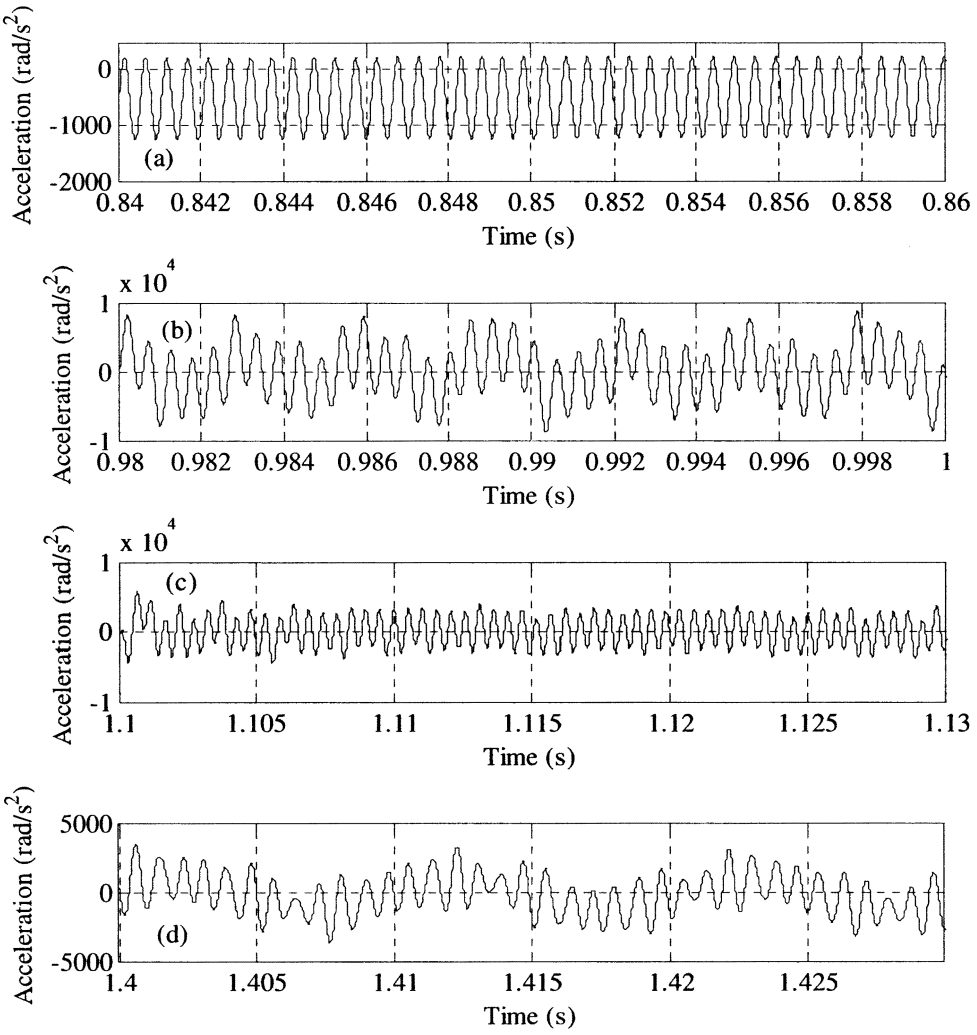

Figure 10.21: acceleration of clutch 2 hub at different stages of synchronisation and gearshift (a) during speed synchronisation, (b) completion of synchronisation, (c) during clutch-to-clutch shift, and (d) after lockup

10.5 CONCLUSIONS

This chapter combines the work of Chapter 4 on synchroniser engagement, Chapter 8 mathematical models of the DCT powertrain, and Chapter 9 clutch shift control to study the simulation of synchronisation and gearshift in a DCT equipped powertrain. In doing so it is divided into three components, investigating synchroniser dynamics, shift dynamics, and combined synchronisation and gearshifts using models presented in Chapter 8.

10.5.1 Simulations of synchroniser engagement

The study of synchroniser engagements using a lumped spring-inertia model with mean and harmonic engine models was used to investigate the engagement dynamics of the synchroniser mechanism in the DCT and identify new issues arising from its use in the DCT. Speed synchronisation, ring unblocking and indexing of the mechanism were all demonstrated to be effective using the mean torque engine model. It was shown that the release of the cone clutch upon completion of ring unblocking results in a relative speed between sleeve and hub chamfers before indexing, which is exacerbated with high drag torque, and is likely to cause some form of impact damage on chamfer contact surfaces, also evidenced by high vibration during indexing.

The introduction of harmonic engine torques to the system was performed to demonstrate the transmissibility of vibrations to the synchroniser and its influence on engagement. The development of stick-slip in the cone prior to unblocking was identified in the later stages of speed synchronisation, resulting from the higher torsional vibration in the system. Vibration during indexing was more substantial that in the mean torque simulations, indicating increased wear on chamfer surfaces.

Results were expanded to include the study of relative motion on the sleeve, and its potential increase with the harmonic engine torque. Overall these results have demonstrated that engine vibrations amplifies vibration in the synchroniser mechanism, which is likely to increase wear on the mechanism, most notably on indexing chamfers where degradation of contact surfaces are likely to inhibit the correct actuation and engagement of the synchroniser. Additionally, there is also the presence of small negative torques in the sleeve as a result of higher vibrations during speed synchronisation. Though present, these are not sufficient to cause early unblocking of

the ring for the conditions present in this simulation, but must be considered important if detrimental engagement conditions are present, such as poor oil wiping of cone friction surfaces or excessive drag.

10.5.2 Simulations of Shift transient

Shift transient studies focused on the evaluation of different powertrain model configurations whilst under shift transients, with particular focus on the impact of harmonic torque engine models on the powertrain and the application of a DMFW model for isolating the drivetrain from these torques.

With the primary goal of this research being the evaluation of different model formations, several conclusions can be drawn. Fundamentally, by increasing the degrees of freedom from 4 (Chapter 9) to 15 in this chapter, the output torque response is modified significantly after gear shift is completed, impacting appreciably on how the powertrain response is evaluated as a result of the shift transient.

Through the introduction of harmonic engine torque models the quality of shifting is reduced, suggesting that the use of mean torque or empirical torque models does not accurately replicate the physical response of a powertrain throughout the shift process. The forced vibrations of the engine model introduces uncertainty into the estimation of average torques for shift controls and initiates stick-slip at the beginning of the transient period, this again signifies that there are some limitations to the application of mean torque models.

Finally, application of a dual mass flywheel model to investigate the impact on transient response of the powertrain. With results indicating a significant improvement of shift quality results when using transient engine torque model, but average torque variations are not completely eliminated for clutch 2. The DMFW response also impacts on clutch lockup and release with high angular displacements required at beginning and end of shift, this increases vehicle oscillations during shift transient period. One limitation of this study that must be acknowledged is that these results will be further enhanced with experimental validation.

10.5.3 Simulations of combined synchronisation and gear shift

The combined synchronisation and gear shift simulations have also been performed to investigate the interrelation of synchronisation and gear shift. This was performed by combining the two models used previously in this chapter for a single transient simulation. Results demonstrate that there is some impact of synchroniser lock up on the transient response of the powertrain. This is particularly critical to the release of clutch 1, with any pressure reduction prior to synchronisation providing the source for the introduction of transients in the transmission. Local transmission vibration response was not significantly suppressed in the powertrain after synchronisation and is present throughout the shift process. These results indicate that audible clonk response may result under certain conditions, particularly during synchroniser engagement. The overall result of combined synchronisation and shift simulation demonstrated however that the control of gearshift is not significantly affected by synchroniser engagement. However provision must be made for highly variable delay in synchroniser engagements, as was demonstrated in Chapter 4.

10.5.4 Summary of contributions

Significant and novel contributions of this chapter include:

- Simulations of synchroniser engagement in a DCT powertrain model using both mean and harmonic torque engine models,
- Shift transient simulations using a number of configurations, including transient torque engine models and dual mass flywheel,
- Demonstration of the impact of DMFW on shift transient response, and
- Transient simulations demonstrating the combined synchronisation and gearshift a DCT equipped powertrain.

CHAPTER 11: TRANSIENT SIMULATIONS WITH BACKLASH IN GEARS AND SYNCHRONISER

11.1 INTRODUCTION

This chapter deals specifically with the transient response in DCT equipped powertrains with the inclusion of gear and synchroniser backlash. It builds on modelling in chapter 8 and simulations of chapter 10 by ignoring the assumption of no backlash in gears and synchronisers, expanding models to include extra degrees of freedom, and evaluating the vibro-impact problem in meshing components. Modelling the mesh nonlinearity introduces gear tooth stiffness with coupling of bearing stiffness and linear displacements for gear pairs or spline stiffness for engaged synchronisers for a purely torsional mesh regime. This results in the pinion, with backlash contact with gear and synchroniser, having an unconstrained motion zone where it can be potentially out of contact with both gear and synchroniser simultaneously.

Backlash excitation is generally initiated with the reversal of torque load, either through manipulation of vehicle torque or local transient response, or excitation in the shuffle mode [45]. For this model, backlash is used for engaged and idling gears and synchronisers only; backlash models for final drive and differential are ignored such that the investigation of transmission gearing only is investigated.

This chapter is then broken into four sections; background information is provided for mesh nonlinear investigations and clonk phenomenon. The nonlinear contact model is then introduced, covering derivation of equations, explanation of the tooth stiffness backlash model, and model parameters used in the transient study. Simulations using backlash models are carried out for synchroniser engagement, shift transients, and engine throttle tip-in/tip-out studies using both mean and harmonic engine torque models. Finally conclusions are drawn.

11.2 MESH NONLINEARITIES

Gear mesh nonlinearities are generally divided into gear tooth stiffness variation or gear tooth backlash problems, and are discussed extensively along with many applications in [130]. Here the variations of different modelling techniques are identified and discussed, ranging from linear time invariant models through to nonlinear time varying models, covering different applications of both backlash and tooth stiffness.

Crowther, *et al,* [43] presents a purely torsional gear and spline mesh model to evaluate mesh response to a range of excitation torques, such as road profile, braking, or engine manipulation. This model is consistent with the neutral gear rattle model in Singh, *et al,* [46]. However, more extensive models that include line-of-action bearing stiffness are frequently employed (e.g. Kahraman & Singh [147]) for a more detailed investigation of the point contact meshing of gears. Some form of these models are applied for investigation of gear rattle (e.g. Dion, *et al,* [148]) and nonlinear dynamics (e.g. Baguet & Jacquenot [149] Kim, Yoo & Chung [150]). Such models are particularly useful for investigation both gear rattle, and also clonk phenomenon in transmission dynamics, however prevalent investigation methods still investigate a single lash contact, where lash is defined as a contact with zero stiffness region in which two components have free motion relative to one another. The chosen clearance in lash zones tends to be quite broad, Crowther, *et al,* [43] uses a lash of 10^{-3}, while Dion, *et al,* [148] is much lower at 10^{-5}, though Crowther, *et al,* [43] demonstrates that the clearance itself has an impact on repetitions in lash zones. Thus the chosen values are particularly significant.

11.2.1 Clonk

The most frequently studied impact of nonlinear gear mesh contact is the presence of clonk in the powertrain response. Gnanakumarr, *et al,* [134] describes clonk as *"a short duration audible high-frequency elasto-acoustic phenomenon, which occurs at load reversal in the presence of lashes in the driveline"*. Clonk frequencies occur in the 300-5000 Hz range [134], with audible response resulting from acoustic modes excited in the driveshafts. In refs [45, 133] identified sources of clonk are expanded to include rapid changes in engine torque and as being observed in the first cycle of the shuffle mode, 2-10Hz. Investigations into clonk phenomenon focus on the impact of gear mesh nonlinearities, [45, 134], nonlinearities in valve train [133], and resulting from clutch

engagement [118]. Excitation methods include the aforementioned clutch engagement and rapid variation in throttle response [151]. There is also a heavy reliance on experimental evaluation of clonk, examples include refs [152, 153].

11.3 MODIFICATIONS TO LUMPED INERTIA MODEL

The introduction of backlash nonlinearities in the synchroniser and reduction gears requires modification to the lumped inertia models presented in chapter 7, particularly the reduction gear pairs and synchronisers. The assumption of no backlash is now removed and gear pairs cannot be lumped as single inertia, gear tooth stiffnesses must be introduced and a torsional nonlinear stiffness must be included in the synchroniser once it is engaged. Figures 11.1, 11.2 and 11.3 can be used to identify modification to the previous powertrain models.

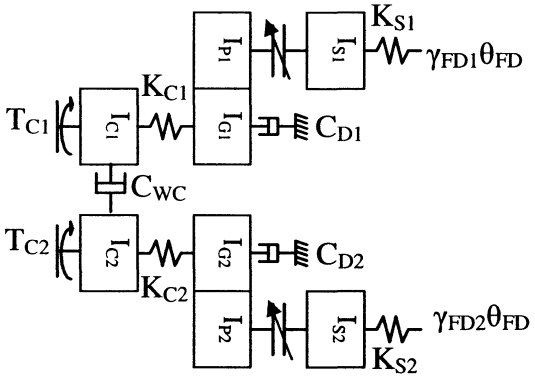

Figure 11.1: Transmission lumped inertia model

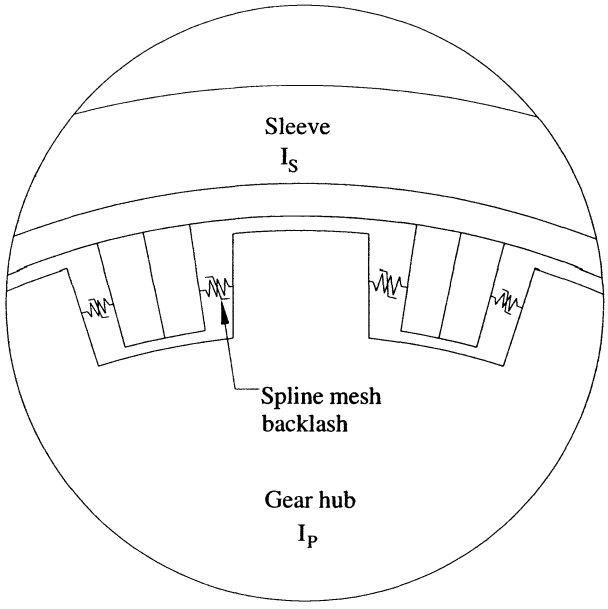

Figure 11.2: mesh contact model for synchroniser splines

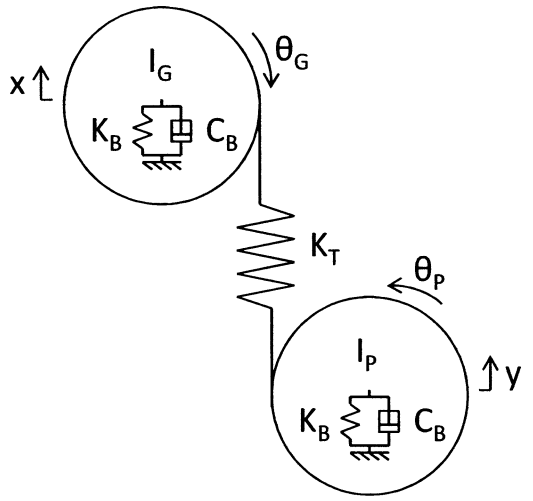

Figure 11.3: Mesh contact model for gear pair

The equations of motion are now modified for the closed synchroniser model as:

$$I_{G1}\ddot{\theta}_{G1}+K_{C1}(\theta_{G1}-\theta_{C1})-C_{D1}\dot{\theta}_{G1}-r_{G1}K_T(\theta_{G1}r_{G1}+x_1-\theta_{P1}r_{P1}-y_1)=0 \quad (11.1)$$

$$I_{P1}\ddot{\theta}_{P1}+r_{P1}K_T(\theta_{G1}r_{G1}+x_1-\theta_{P1}r_{P1}-y_1)-r_{S1}K_S(\theta_{P1}r_{S1}-\theta_{S1}r_{S1})=0 \quad (11.2)$$

$$I_{S1}\ddot{\theta}_{S1}-K_S(\gamma_{FD1}\theta_{FD3}-\theta_{S1})+r_{S1}K_S(\theta_{P1}r_{S1}-\theta_{S1}r_{S1})=0 \quad (11.3)$$

$$M_G\ddot{x}_1-K_{B1}x_1-C_{B1}\dot{x}_1-K_T(\theta_{G1}r_{G1}+x_1-\theta_{P1}r_{P1}-y_1)=0 \quad (11.4)$$

$$M_P\ddot{y}_1-K_{B1}y_1-C_{B1}\dot{y}_1+K_T(\theta_{G1}r_{G1}+x_1-\theta_{P1}r_{P1}-y_1)=0 \quad (11.5)$$

$$I_{G2}\ddot{\theta}_{G2}+K_{C2}(\theta_{G2}-\theta_{C2})-C_{D2}\dot{\theta}_{G2}-r_{G2}K_T(\theta_{G2}r_{G2}+x_2-\theta_{P2}r_{P2}-y_2)=0 \quad (11.6)$$

$$I_{P2}\ddot{\theta}_{P2}+r_{P2}K_T(\theta_{G2}r_{G2}+x_2-\theta_{P2}r_{P2}-y_2)-r_{S2}K_S(\theta_{P2}r_{S2}-\theta_{S2}r_{S2})=0 \quad (11.7)$$

$$I_{S2}\ddot{\theta}_{S2}-K_S(\gamma_{FD2}\theta_{FD3}-\theta_{S2})+r_{S2}K_S(\theta_{P2}r_{S2}-\theta_{S2}r_{S2})=0 \quad (11.8)$$

$$M_G\ddot{x}_2-K_{B2}x_2-C_{B2}\dot{x}_2-K_T(\theta_{G2}r_{G2}+x_2-\theta_{P2}r_{P2}-y_2)=0 \quad (11.9)$$

$$M_P\ddot{y}_2-K_{B2}y_2-C_{B2}\dot{y}_2+K_T(\theta_{G2}r_{G2}+x_2-\theta_{P2}r_{P2}-y_1)=0 \quad (11.10)$$

If the same model is considered with synchroniser 2 open then equations 11.7 and 11.8 are modified to:

$$I_{P2}\ddot{\theta}_{P2}+r_{P2}K_T(\theta_{G2}r_{G2}+x_2-\theta_{P2}r_{P2}-y_2)=0 \tag{11.11}$$

$$I_{S2}\ddot{\theta}_{S2}-K_{S2}(\gamma_{FD2}\theta_{FD3}-\theta_{S2})=T_{S2} \tag{11.12}$$

where r is radius, x is gear linear motion, y is pinion linear motion, and subscript b refers to bearing. The matrix models of the powertrain are then extensively modified, adding eight degrees of freedom for each state. The shifting state (state 7 in Chapter 8) is increased from 15DOF to 23DOF for example. This computational demand is conceived as a significant limitation for transient simulations of numerically stiff models. Continued development of computer processing power means it is possible to apply full level powertrain models with high stiffness and expect a reasonable duration for simulations. For example simulations in this chapter for a 2 second transient simulation with 23DOF and with the ODE15s variable time step solver and a time step of $1x10^{-6}$ s can be reasonably expected to take <2hours, at $1x10^{-7}$ s it is up to 30 hours.

11.3.1 Backlash model

Stiffness terms K_T and K_S represent the nonlinear stiffness in gear mesh and synchroniser splines, respectively. Backlash nonlinearity is defined by a zero stiffness region resulting from clearance in the gear through manufacturing tolerances, design clearances, wear, *et cetera*. In the backlash region, $x < |x_C|$, stiffness is zero, with constant stiffness used for the contact region. These are graphically presented in Figure 11.4 as:

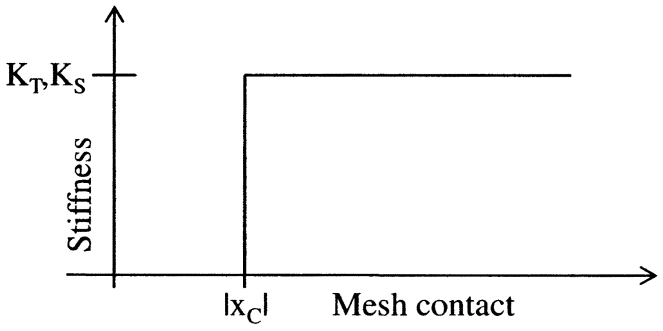

Figure 11.4: Mesh stiffness model for gear and synchroniser contact nonlinearity

The mesh contact stiffness are:

$$K_T = \begin{cases} 0 & |\theta_G r_G + x - \theta_P r_P - y| < x_C/2 \\ 10^8 & |\theta_G r_G + x - \theta_P r_P - y| \geq x_C/2 \end{cases} \tag{11.13}$$

$$K_S = \begin{cases} 0 & |\theta_P - \theta_S| < \theta_C/2 \\ 10^8 & |\theta_P - \theta_S| \geq \theta_C/2 \end{cases} \tag{11.14}$$

where θ_C is contact displacement rotation, X_C is contact displacement length. The mesh backlash models are similar for both synchroniser and gear contact nonlinearities, with X_C representing half the backlash noncontact length. Offset torques are required for gears and pinions to counterbalance the zero contact region. The offset torques are as follows for synchroniser, gear and pinion, respectively:

$$T_{SM} = sign(\theta_P - \theta_S) \times K_S \times |X_{C,S}| \tag{11.15}$$

$$T_{GM} = sign(r_G\theta_G + x - r_P\theta_P - y) \times K_T \times |X_{C,G}| \times r_G \tag{11.16}$$

$$T_{PM} = sign(-r_G\theta_G - x + r_P\theta_P + y) \times K_T \times |X_{C,G}| \times r_P \tag{11.17}$$

The torque vector for open clutches, state 7, is then redefined as:

$$T = \{T_e \;\; 0 \;\; (-T_{C1} - T_{C2}) \;\; T_{C1} \;\; -T_{PM1} \;\; (T_{GM1} - T_{SM1}) \;\; T_{SM1} \;\; T_{C2} \;\; T_{PM2} \;\; (T_{GM2} - T_{SM2}) \;\; T_{SM2} \;\; 0 \;\; 0 \;\; 0 \;\; 0 \;\; 0 \;\; 0 \;\; 0 \;\; -T_V\}^T \tag{11.18}$$

11.3.2 Model parameters

Parameters provided in Table 11.1 are consistent for the 3rd and 4th gears in the powertrain model. Pitch radii will change depending on the gear state chosen, however other parameters are consistent. Some estimation of model parameters has been required for analysis of the system, making use of available literature where possible. Mesh stiffness models produced by He, *et al,* [131, 132] for nonlinear stiffness suggest that a time averaged stiffness of 1×10^8 N/m is reasonable for gears, and a similar torsional equivalent stiffness is used for the synchroniser splines. Methods for determining bearing stiffnesses require detailed bearing information for roller and ball bearings such as preload [154], which is not known for this study, and does not incorporate deflection of shaft in the calculation, with gears some distance from the bearing components. Thus the bearing stiffness is also estimated for the purpose of this

research. Gear and pinion masses are estimated to incorporate shaft, synchroniser, idler gears, etc, and an approximate value is provided.

Table 11.1: Nonlinear contact model parameters

Parameter	*Radius (mm)*	*Parameter*	*Stiffness (N/m)*
r_{G1}	32.9	K_T	$1x10^8$
r_{P1}	47.8	K_S	$1x10^8$
r_{G2}	38.7	K_B	$1x10^6$
r_{P2}	41.8	**Parameter**	**Damping (Nm/s)**
Parameter	**Mass (Kg)**	C_B	0.1
M_G	5	X_C	$5x10^{-6}$ mm
M_P	5	θ_C	$1.4x10^{-5}$ rad

11.4 SIMULATIONS

Studies of excitations with gear backlash consider response under transient conditions, via gear synchronisation and shift transient simulations, and excitation through transient engine torques under steady state conditions and though excitation induced in the throttle angle. Synchroniser parameters for cone and chamfers are cone angle 7°, friction coefficient 0.12, chamfer angle 65° and friction coefficient 0.04. The initial vehicle speed for synchronisation simulations is 35rad/s.

Shift transient simulations are preformed using a 3^{rd} to 4^{th} gear upshift. The shift torque phase is initiated at 1.095s, with the shift preparation performed at 0.7s for clutch 1 release and 1s for clutch 2 fill. The control signals for shifting are presented in Figure 11.5 below, with throttle angle (%) and clutch 1 and 2 pressures (MPa) shown. Tip-in/tip-out simulations are performed for the DCT with both the ideal engine model and the harmonic torque engine model, using the bump function for throttle control.

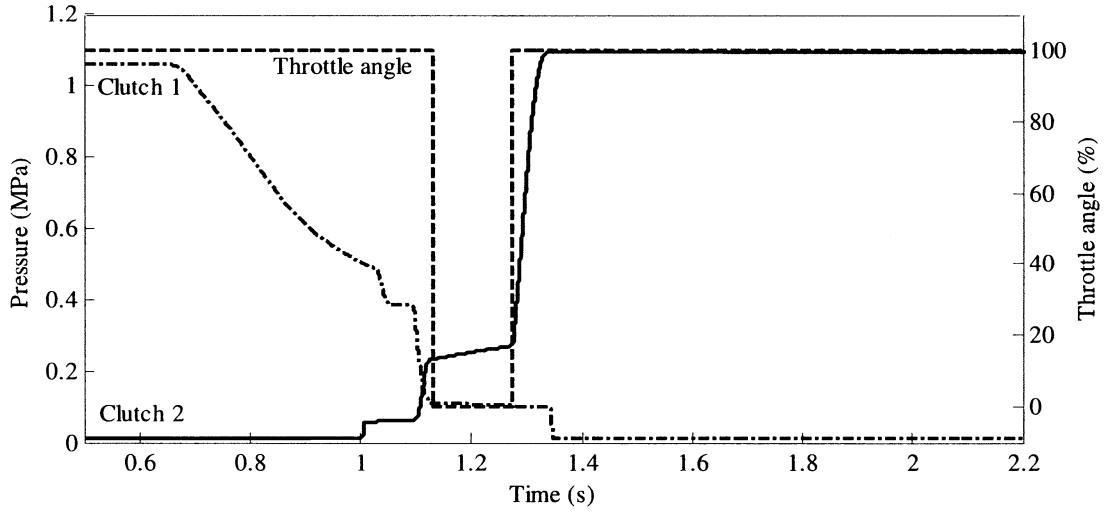

Figure 11.5: Shift control signals for transient simulations

11.4.1 Synchroniser Engagement

Gear synchronisation simulation results with gear mesh backlash are presented in Figure11.6 for sleeve displacement (top) and synchroniser torques (bottom), and results are presented in Figure 11.7 for gear hub and sleeve speeds (top) and slip speed results (bottom). Sleeve displacement results are typical to previous simulations in Chapter 10, and are indicative of successful engagement. Though speed synchronisation is unaffected by the inclusion of this nonlinearity, ring unblocking and, to a lesser extent, indexing are affected, with restriction of sleeve unblocking. Figure 11.7 results do not provide significant indication of negative impact of mesh contact. High frequency vibrations are introduced once engagement is initiated, and are present through the entire engagement process. Vibration amplitudes during engagement far exceed the high frequency vibration identified in Chapter 10 (Figures 10.3 and 10.6) a result of high stiffness in the gear mesh and repeated lash impacts during speed synchronisation. More significant to the engagement response are the lockup vibrations, resulting from different chamfer alignment than used in Chapter 10. The relative speed at completion of indexing is much higher, with the resulting lockup impulse increasing amplitude response, this is also affected by the rattle of gears in lash zones. Results show frequency response as a consequence of the lockup impulse, the frequency of 34Hz is the lowest frequency present. Table 8.4 of Chapter 8 demonstrates that this frequency is dominant at the differential and transmission elements.

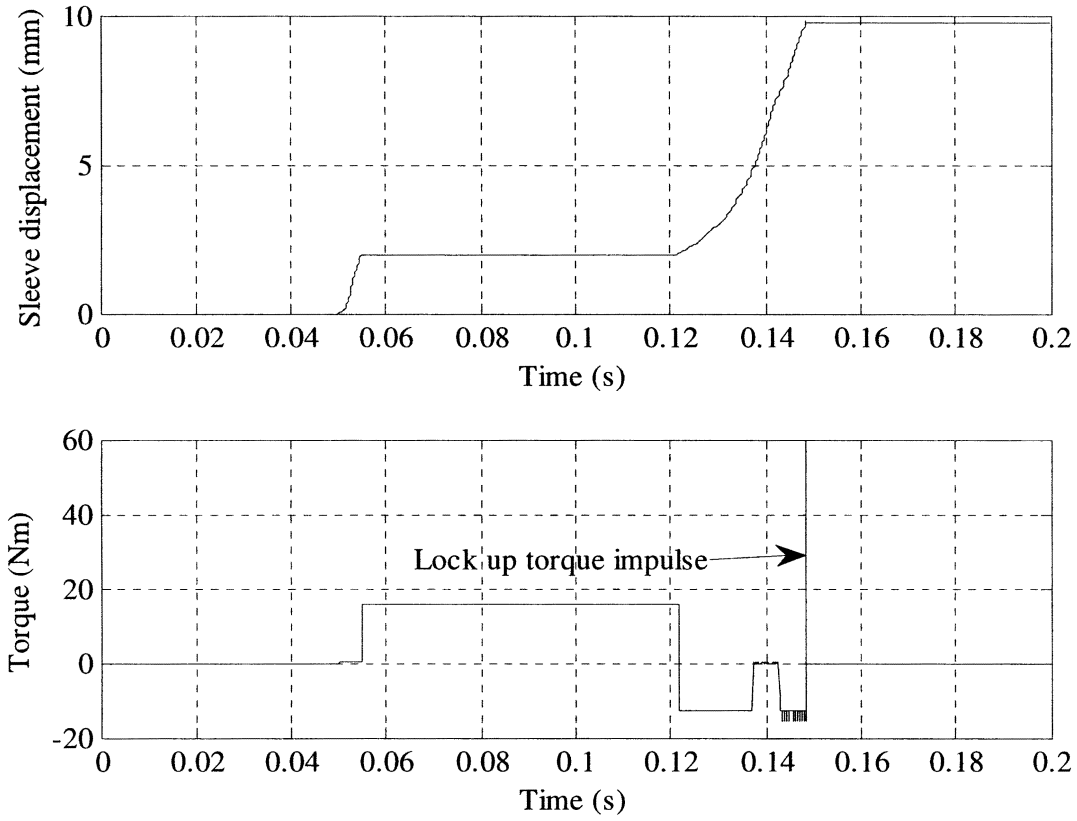

Figure 11.6: Synchroniser sleeve displacement (top) and engagement torque (bottom)

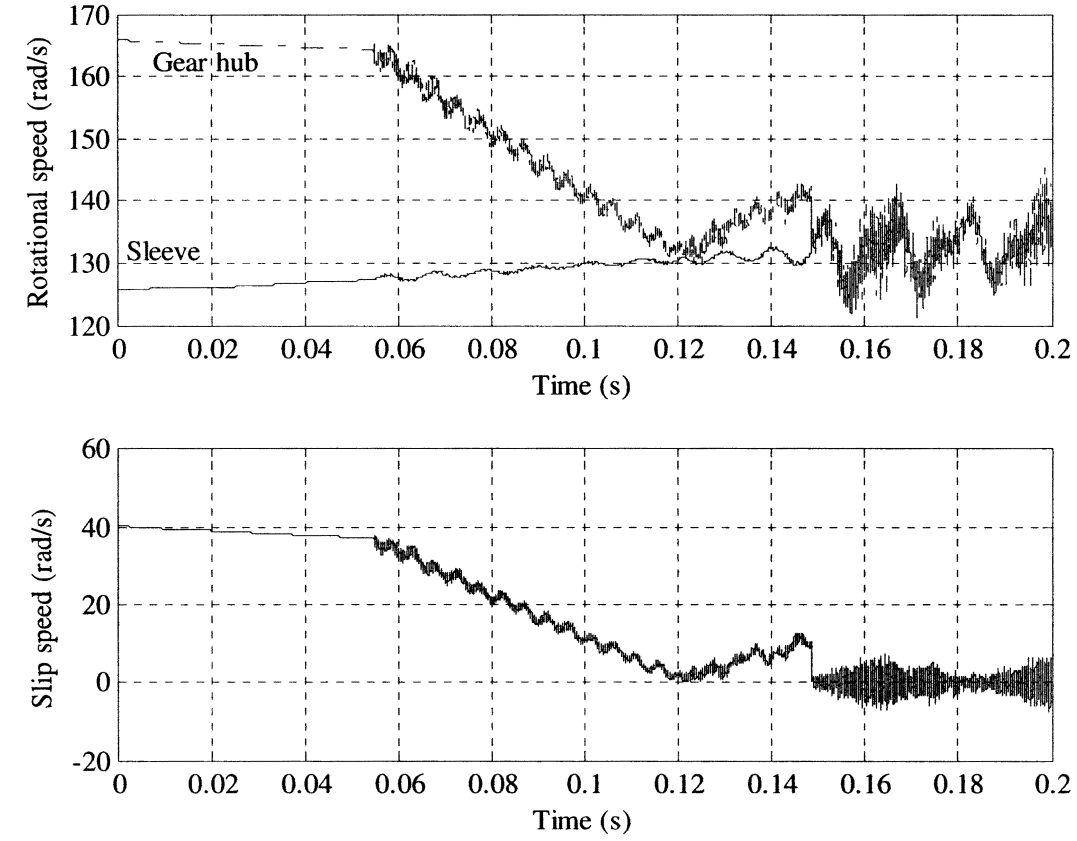

Figure 11.7: Synchroniser hub and sleeve speeds (top), and synchroniser relative speed (bottom)

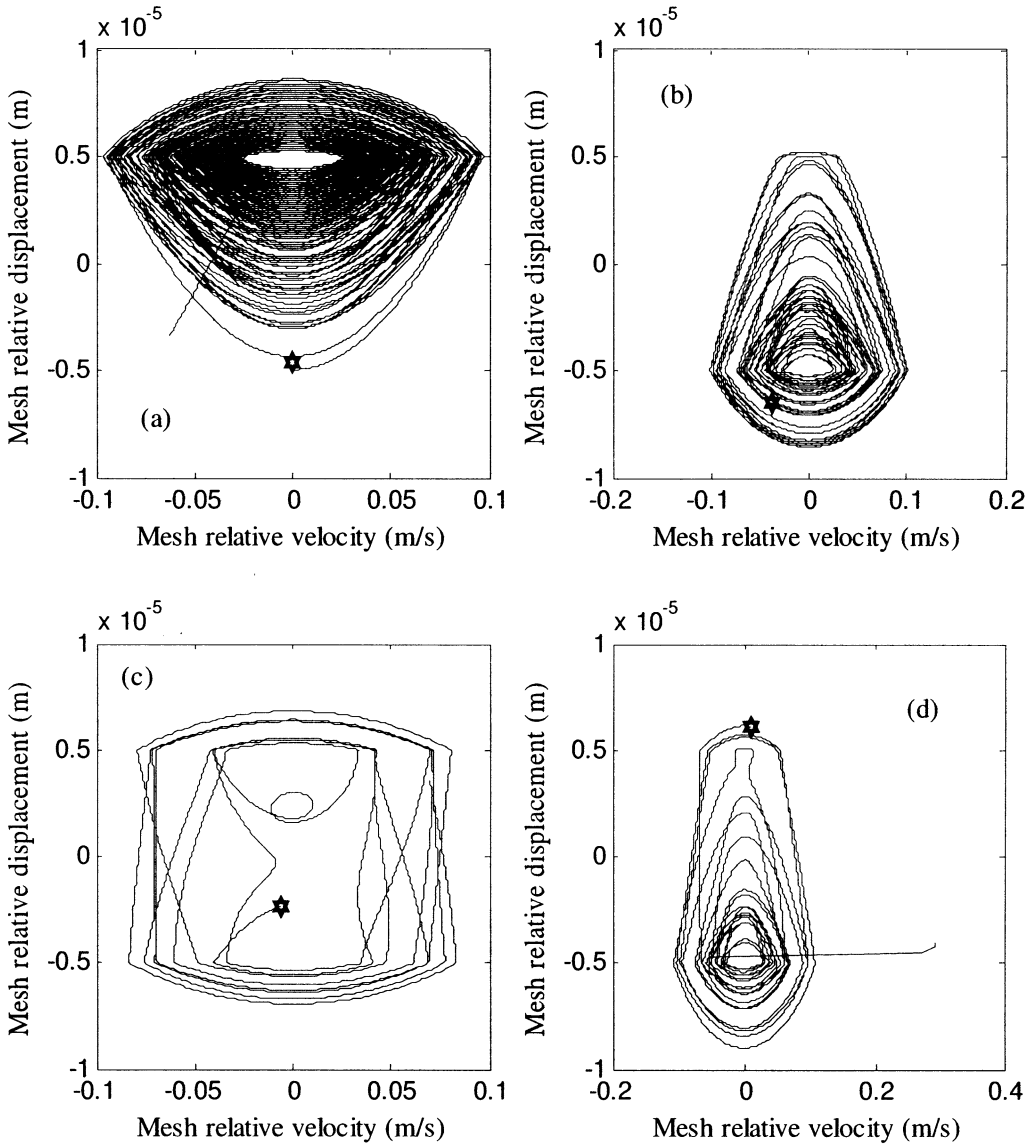

Figure 11.8: Phase plots of target gear mesh during different stages of synchronisation. (a) during speed synchronisation, (b) during ring unblocking, (c) during second displacement, and (d) during indexing. The hexagram indicates the starting point.

The phase plots in Figure 11.8 provide a clearer indication of the effect of the gear mesh elastic model to synchroniser engagement. Figure 11.8 (a) demonstrates steady state initialisation in the negative contact region for the gear. Once synchronisation is initiated, lash is taken up and primary contact moves to the positive contact zone, decaying over the duration of synchronisation. As synchronisation completes and unblocking begins the direction of applied synchroniser torque transits from positive to negative (Figure 11.6 (bottom)) and the resulting gear contact moves from positive to negative contact regions (Figure 11.8 (b)). The abrupt change increases vibration amplitude and several transitions from negative to positive contact zones results,

impeding the unblocking progress. During second displacement (Figure 11.8 (c)) minimal load is present on the gear and rattle is perceived, with both contact regions engaged in roughly equal portions. Figure 11.8 (d) shows the phase plot for indexing, similar to the unblocking portion of engagement results present (Figure 11.8 (b)). However positive mesh contact is more significant.

11.5 SHIFT TRANSIENT WITH GEAR AND SYNCHRONISER BACKLASH

shift transient simulation applies the control signals in Figure 11.5 with the clutch stick-slip model developed in Chapter 8. This is similar to the method in Chapter 10 for shifting, however the original powertrain models are integrated with the nonlinear gear mesh model to investigate vibration induced in the transmission resulting from gear nonlinearities. The initial wheel speed is 35rad/s in 3rd gear, for a 4th gear upshift.

Figure 11.9 presents the shift transient results for clutch drum, and clutch 1 and 2 hubs. The torque results of Figure 11.9 (b) present successful shift transient response of clutch 2 and the net vehicle torque reflected at the gear, torque amplitudes during the inertia phase are somewhat higher than those presented in Chapter 10 (Figure 11.13 (b)) owing to poor release of Clutch 1, and the stick-slip events introduced to the transmission. Clutch 2 torque after clutch lockup combines high frequencies of the mesh contact with lower frequency response of the powertrain. Shuffle mode excitations after clutch lockup show higher frequency excitations in clutch 2 torque response, indicative of shuffle induced clonk in the powertrain.

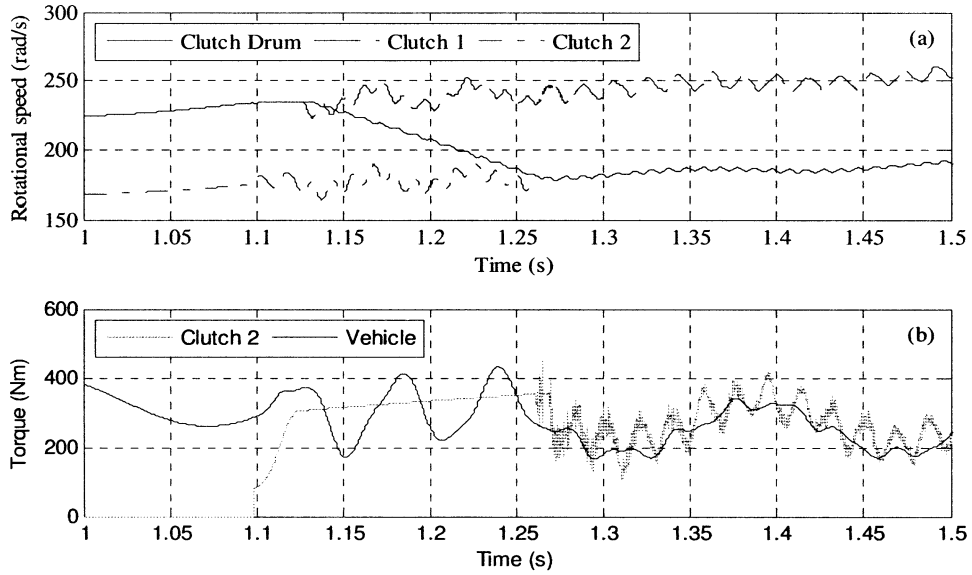

Figure 11.9: Shift transient simulations with nonlinear gear and synchroniser mesh, clutch hub and drum speeds (a), and clutch 2 and net vehicle torque (b)

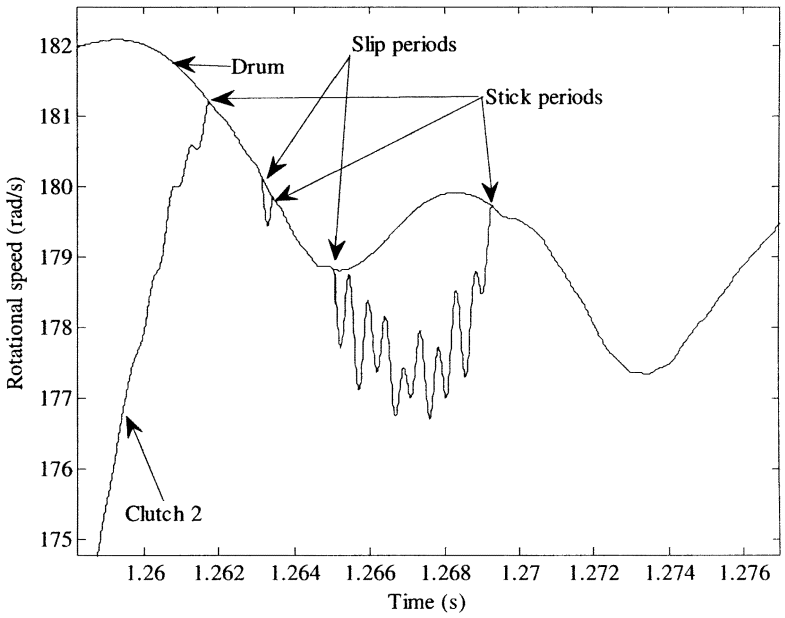

Figure 11.10: Stick slip present in clutch 2 at lockup

Considering the torque phase, inertia phase, and clutch lockup phases of shifting individually, the results in Figure 11.9 (a) show the increasing clutch 2 torque excites the contact at the beginning of the torque phase (1.1s). Stick-slip is initiated in the releasing clutch, clutch 1. The inertia phase proceeds in a manner consistent with results of Chapter 10. However, at lockup stick-slip is initiated in clutch 2 as the clutch pressure increases to maximum. The duration of the slip period is brief (<5ms) (see Figure 11.10) and as such there is no transition into lash (see Figure 11.11). However, these stick-slip events initiate excitations in the now idling 3rd gear and synchroniser.

Figures 11.11 and 11.12 show the mesh contact for both gear and synchroniser. Gear 2 and synchroniser 2 both maintain contact in the positive mesh region for the majority of engagement, with brief excursions into the lash region during the torque phase during stick-slip events. This is particularly important to the lockup of clutch 2 as the corresponding gear and synchroniser do not transit into the lash region. Thus, gear rattle transients are not introduced in the active gear during shift events, only in gear 1 and synchroniser 1 after torque reduces during the inertia phase.

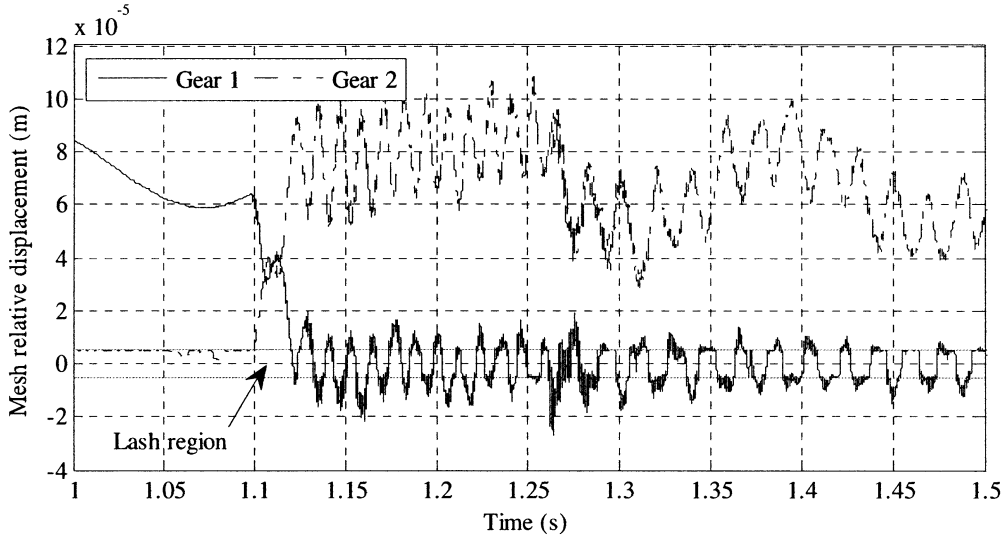

Figure 11.11: Mesh relative displacement plots of both gears during shift transients

Gear 1 and synchroniser 1 release results in rattle between mesh zones as low load and damping combine with rapid release to excite the idling gear. At the clutch 2 lockup stick-slip event (see Figure 11.10) mesh response increases, particularly for the synchroniser. This is a result of releasing of clutch 2 and the transmitted excitation through the transmission.

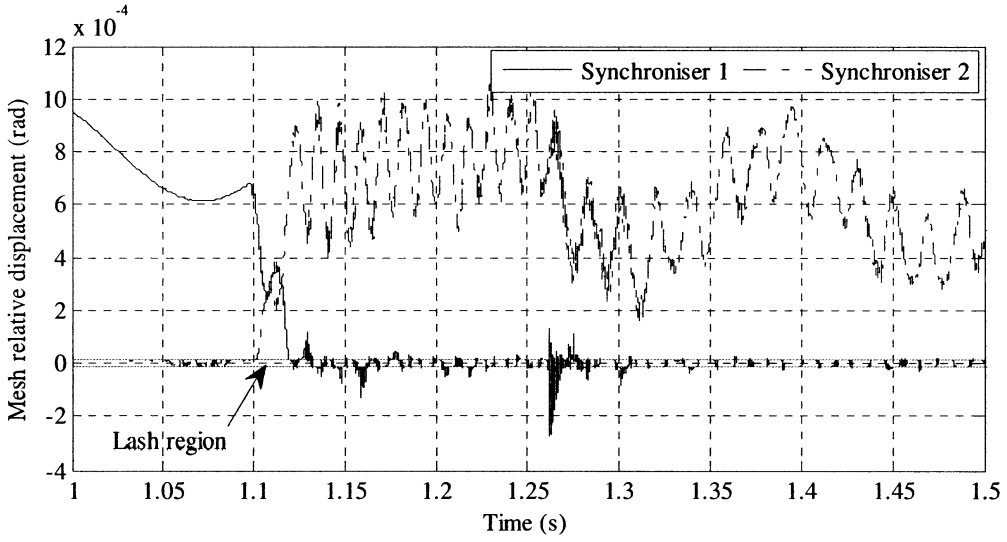

Figure 11.12: Mesh relative displacement plots of both synchronisers during shift transients

11.6 TIP-IN TIP-OUT OF THROTTLE

The response of backlash components to abrupt reductions in acceleration is demonstrated using tip-in/tip-out simulations. With a single clutch continuously

engaged, the engine throttle is decreased from a constant throttle angle condition to minimum before again increasing the throttle. Such manipulation initiates release of the meshed gear to the lash condition as torque load drops and is re-applied. Simulations are performed using this approach with both the original mean torque powertrain model presented in Chapter 8 with backlash, and the transient torque engine model with integrated dual mass flywheel. This will enable the identification of transient responses resulting from the throttle manipulation and responses resulting from the introduced engine vibration.

11.6.1 Throttle tip-in/tip-out modelling

Throttle tip-in tip-out is used to excite the backlash model through variation in applied engine torque to the system. Achieved through the application of a bump function, defined as smooth, with continuous derivatives of all orders, and compactly supported, such that is reaches a zero point rather than asymptotically tending to zero. Such functions do not present discontinuous changes during transition to different regions of the piecewise function (see equation 11.19 below) and therefore are not likely to cause numerical transient response through application. Rather the change in torque will perform this role. The throttle angle variation is modelled using an exponential bump function of three components that define different regions of throttle application, and are normalised to the throttle range of 0 to 100%. The function, graphed in Figure 11.13, is as follows:

$$TA(t) = \begin{cases} 271.8282e^{\frac{1}{1-(4t)^2}}, & t \leq 0.25 \\ 271.8282e^{\frac{1}{1-(2(t-0.75))^2}}, & 0.75 < t \leq 1 \\ 100, & t > 1 \end{cases} \quad (11.19)$$

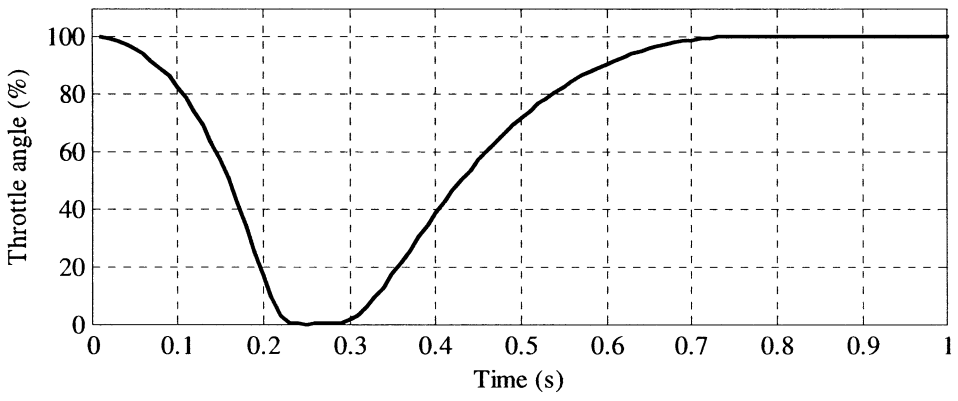

Figure 11.13: Throttle angle tip-in/tip-out according to equation 11.19

11.6.2 Mean torque model simulations

Transient simulations integrating the tip-out/tip-in throttle manipulation with the powertrain are preformed using the powertrain model with 3rd gear and clutch 1 engaged, and 4th gear engaged in the synchroniser; the initial vehicle speed is set to 35 rad/s. Figure 11.14 demonstrates the powertrain response to the applied throttle angle manipulation, with clear demonstration of the reapplication of throttle instigating shuffle mode response in the powertrain. Higher frequencies are present in Gear 2 and Synchroniser 2 indicating a fair degree of rattle present in the transient response, resulting from the lack of damping present in the free pinion.

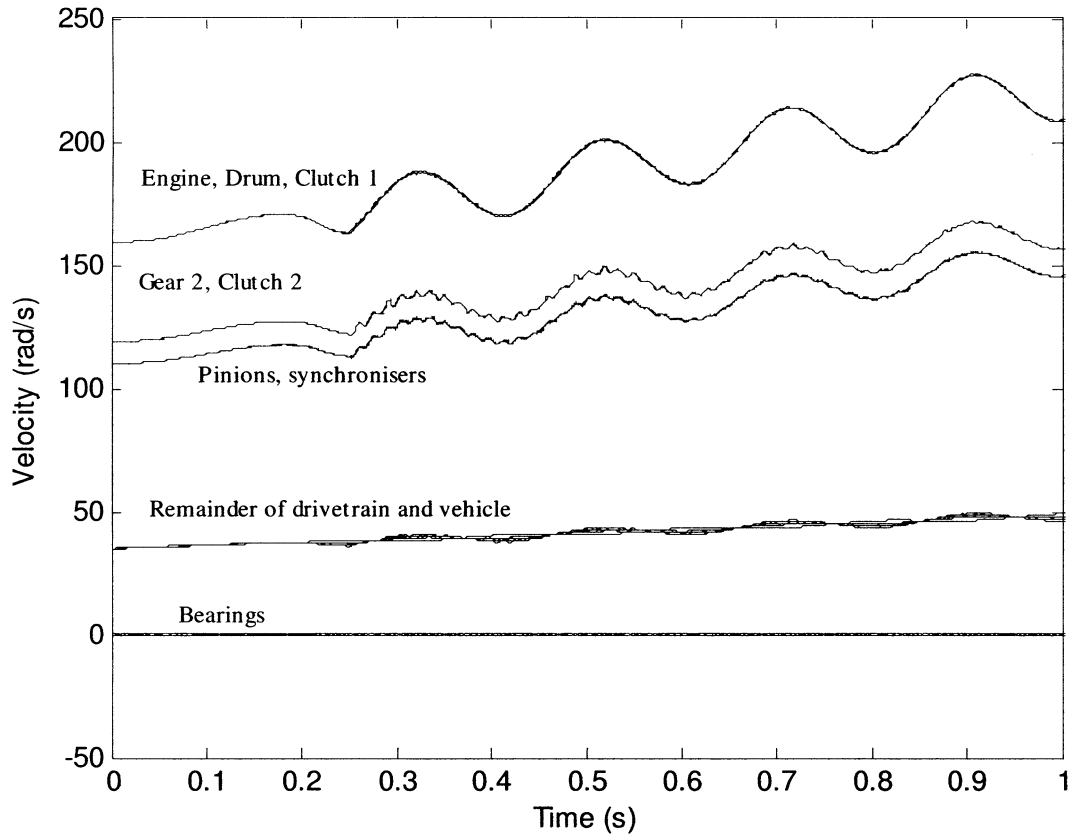

Figure 11.14: Time history of tip-in/tip-out simulation with mean engine torque model

The results of this simulation are shown in Figure 11.15, with time histories of mesh relative displacements in gear and synchroniser, and Figure 11.16, with phase plots for the lash period presented. For both figures grey lines represent the transition from mesh contact to non contact regions. Reasonably similar results are shown at both mesh contacts while under lash, with engine torque minimum at 0.25s both contacts move from positive to negative lash as the load is released, reversing direction again when torque is re-applied to the system. Over the simulation period beyond 0.4s, with

reasonably fine backlash zone, the gear repeatedly enters the lash zone as a result of transient vibration introduced by the torque change. With lower system damping in DCT powertrains this is to be expected. The phase plot in Figure 11.16 shows clean transition of the gear between contact zones, however the larger lash region for the synchroniser results in extended duration in lash.

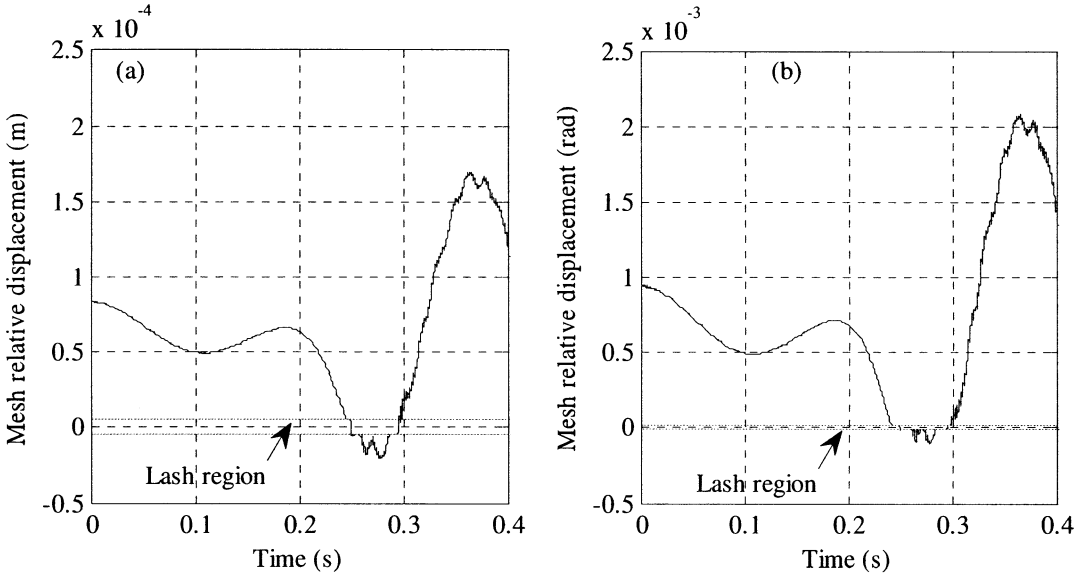

Figure 11.15: Relative displacement plots of (a) Gear 1 and (b) synchroniser 1 during throttle manipulation for tip-in/tip-out simulations with mean engine torque model

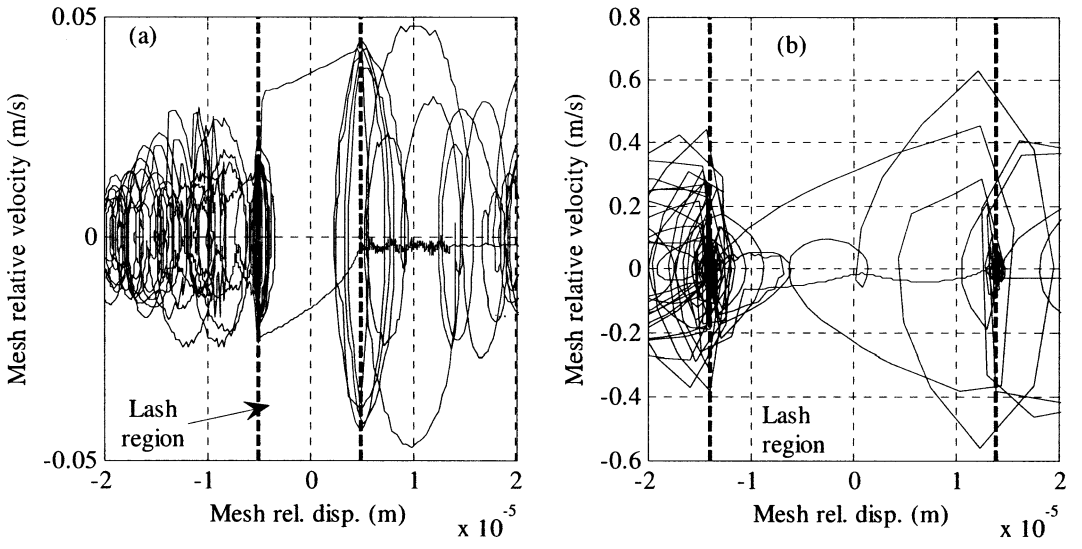

Figure 11.16: Relative velocity-displacement phase plots of (a) Gear 1 and (b) Synchroniser 1 during the lash period with the mean engine torque model

11.6.3 Transient engine vibration and DMFW

As has been previously discussed, the impact of engine vibration must be considered in any DCT powertrain model. Further, Gaillard & Singh [116] and Crowther, *et al,* [43] highlight periodic vibrations, such as engine harmonics, as a potential issue in gear mesh contact studies. To purposefully model the response of the nonlinear mesh model to excitation from engine harmonics, the transient engine model with DMFW is integrated in to the powertrain model. The modified powertrain model with 3rd gear and clutch 1 engaged, and 4th gear engaged in the synchroniser is used here and the gear lash model is integrated to carry out simulations. Again the initial vehicle speed is set to 10 rad/s, and the simulations is permitted to run for 1s in steady state to ensure that the response is stable with no windup error before manipulating engine throttle angle.

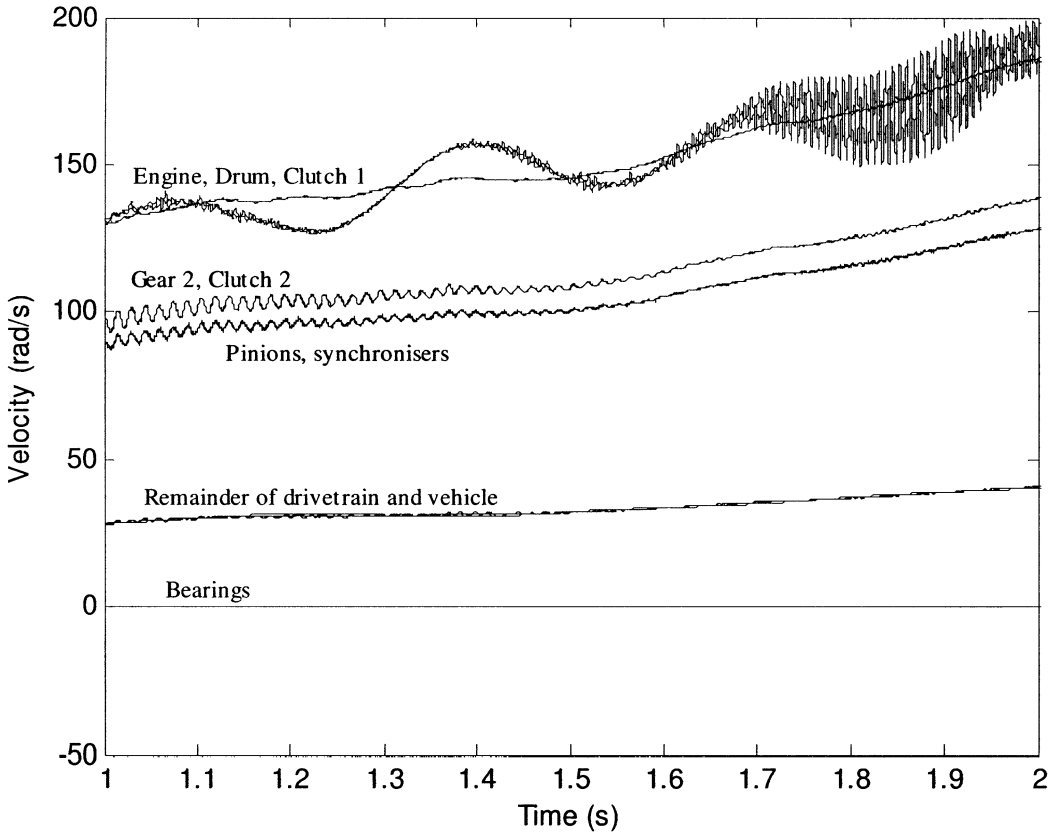

Figure 11.17: Time history of tip-in/tip-out simulation with harmonic engine torque model

In Figure 11.17 the time history shows how significant the inclusion of DMFW is in the reduction of shuffle resulting from the tip-in/tip-out response, with the most significant oscillations restricted to the engine and flywheel inertias. Pinion 2 rattle is still present in a manner largely unchanged from that present in Figure 11.14. The increased

damping present in the powertrain thus has the effect of reducing lash events in the gear mesh as shuffle response is suppressed.

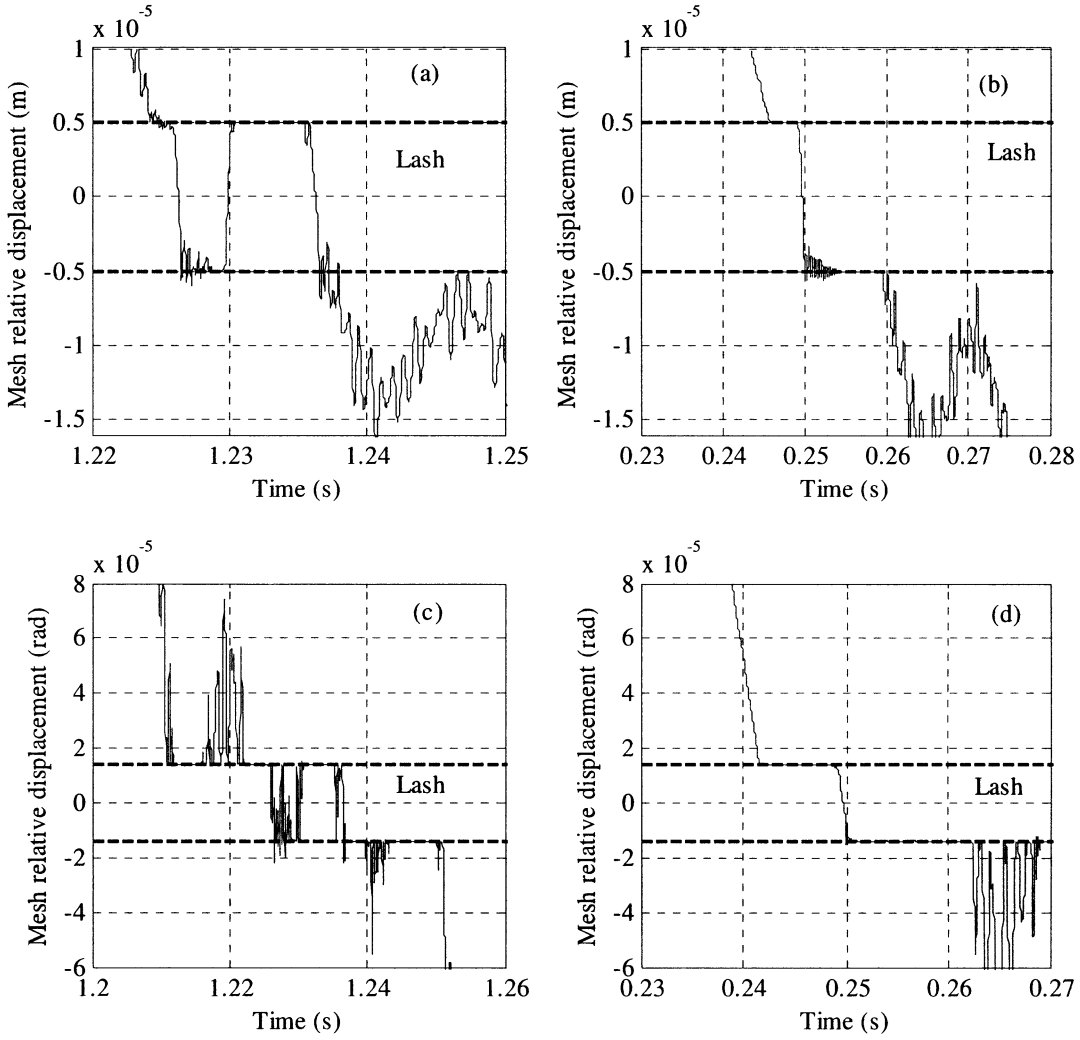

Figure 11.18: First lash transitions for (a) gear 1 with harmonic engine model, (b) gear 1 with mean engine model, (c) synchroniser 1 with harmonic engine model, and (d) synchroniser 1 with mean engine model

The result of introducing engine harmonics is shown through the comparison of results in Figure 11.18. Engine harmonics torques are present in Figure 11.18 (a) for Gear 1 and Figure 11.18 (c) for synchroniser 1 and mean engine torque in Figure 11.18 (b) for Gear 1 and Figure 11.18 (d) for synchroniser 1. In Figure 11.18 (b) and Figure 11.18 (d) the transition from positive to negative lash occurs in distinct phases. With the mesh contact at the interfacial points immediately before and after the minimum throttle angle at 0.25s, torque windup then displaces the contact in mesh regions. However, for the harmonic torque results, the gear moves through the lash before the minimum engine

torque, as the harmonic torque reduces earlier. Furthermore, with increased vibration from the engine torque there is a tendency for both gear and synchroniser to rattle freely under low load conditions.

11.7 CONCLUSIONS

In the previous Chapters 8, 9 and 10, nonlinear NDOF powertrain models have been developed for DCT equipped powertrain and used to investigate the transient response to synchroniser engagement and shift transients. This has combined a variety of powertrain configurations depending on both the transmission state and the inclusion of harmonic torque engine models and dual mass flywheels. This chapter has built on this work to study the performance of similar powertrain configurations with the inclusion of nonlinear gear and synchroniser mesh models, with individual degrees of freedom added to the powertrain to account for gears, pinions, and synchronisers in the transmission. Four transient conditions were studied using four powertrain configurations. These were: (1) synchroniser engagement, (2) shift transients, (3) throttle tip-out/tip-in with mean engine torque models, and (4) throttle tip-out/tip-in with harmonic engine torque model.

Gear rattle is prevalent in results of each of the simulations in this chapter for the idle gear set, with the low load on idle gearing combining with rapid torque variations, such as synchroniser lockup or clutch release, contributing to excitations. Typical rattle response shows the idle gear vibration moving between contact zones periodically, with the lack of significant damping, particularly on the free pinion, and small clearance value both contributing to repetitious engagements. Simulations of tip-in/tip-out indicated that engine harmonic torques in particular reduced the clear transitions between contact zones, with harmonic torque variations increasing frequency of transitions between lash and contact zones. The use of the DMFW in particular was successful in suppressing shuffle response and reducing gear rattle in this simulation.

Clonk response requires combined transmission models and detailed driveshaft models, with ref [134] making use of 247 DOF in the driveshaft for simulations. This provides a broad spectrum of excitation frequencies in the driveshaft for excitation under mesh contacts. Again it has been demonstrated in these simulations that high frequency responses develop in the transmission as a result of transient engagements. However

the application of a simplistic shaft model, only 4 DOF, prevents the coupling of excitations in the mesh with modes in the driveshaft. Results demonstrate that excitations from both abrupt torque changes, synchroniser engagement or tip-in/tip-out, and shuffle mode excitations post shift lockup, all contribute to high frequency excitations of the transmission and powertrain, indicating possibility of *clonk* response.

11.7.1 Summary of contributions

This chapter investigates the contribution of mesh nonlinearities to NVH developments in the DCT powertrain. This included modelling the nonlinear gear mesh and synchroniser splines. Specific novel contributions are:

- Modelling of backlash nonlinearities in a DCT powertrain
- Modelling of synchroniser mesh as a lash nonlinearity
- Investigation of lash effects on synchroniser engagement
- Identification of contributions of backlash nonlinearities to NVH issues of both gear rattle and clonk.

CHAPTER 12: THESIS CONCLUSIONS AND RECOMMENDATIONS

12.1 SUMMARY OF THESIS

The dynamics of a dual clutch transmission equipped powertrain and its components have been investigated in this thesis, including studies into synchroniser dynamic characterisation and control, clutch hydraulics and control, and powertrain transients with the inclusion of multiple nonlinearities. Initially extensive literature research identified major components of DCT powertrains in addition to methods available for modelling and the extent at which modelling and analysis has been performed. The majority of this thesis has then been devoted to the modelling, simulation, and analysis of these components and the DCT powertrain as a complete system.

To study the synchroniser mechanism, a rigid body model was developed incorporating a hydraulic control system (Chapter 3), the mechanism itself (Chapter 4), and drag torque (Chapter 5) models. Extensive simulations carried out on the synchroniser model demonstrated the impact of both design and environmental variables. Significant results include the incapacity to maintain synchronisation after ring unblocking, a result of low cone clutch load and high drag, and the impact of chamfer alignment on duration of engagement (Chapter 4). Characterisation of the impact of drag torque is significant, where it is maximised at the completion of speed synchronisation as a result of high drag in the wet clutch. It is also now bi-directional, being dependent on up or down shifting (Chapter 5). Alternate synchroniser mechanism control methods and designs were evaluated to overcome detrimental alignments and improve the synchroniser performance through increased torque capacity (Chapters 6 & 7).

Clutch control strategies investigated the impact of the hydraulic control system and engine control and dynamics on the shift process. To do so a detailed hydraulic system model is developed through the implementation of fluid dynamics and mechanics theories (Chapter 3), while engine models included both mean torque and harmonic torque models (Chapter 8). To reduce the complexity of the powertrain model a 4 degree of freedom model was developed. Comparison to the 15DOF model using free

vibration analysis demonstrates reasonable compatibility (Chapter 9). The suggested control strategy used balances torques at engine and clutches to reduce the transient response during and after shifting. Shift control simulations were then carried out for gear shifts considering a range of variables, studying the impact on post clutch lockup performance. Consideration of time delay in the engine model and clutch hydraulics, as well as accuracy of torque estimation is shown to be critical to maximising shift quality (Chapter 9).

Transient investigations of the powertrain were then performed making use of powertrain model variations, including different engine models, dual mass flywheel, and backlash models for gears and synchronisers Lumped spring-inertia models were developed for different powertrain states to investigate synchroniser engagement and power-on gear shifts as the primary simulations, with tip-in/tip-out simulations for backlash models also performed (Chapters 8, 10 & 11). Results focused on the powertrain transient response to typical simulations, but also assessed the impact of harmonic torque engine modes of shifting and synchroniser engagements. The results, with or without the dual mass flywheel, indicate that torque variation in the engine as a results of cylinder firings has a significant result on both synchroniser engagements and shift transient response, with dual mass flywheels significantly affecting the transient response, changing the lockup and release of clutches and drum response in particular (Chapter 10). Finally, backlash studies for gear pairs and synchronisers demonstrate gear rattle in idle gears and high frequency response consistent with clonk in post transient states (Chapter 11).

12.2 SUMMARY OF FINDINGS AND CONTRIBUTIONS

The objectives of this project identified in the introduction are repeated here along with the primary findings and contributions that have resulted from this investigation:

1. *Model the main components of a DCT and integrate them into a vehicle powertrain model for predicting the transient characteristics during gear shifting,*

The major components of a DCT equipped powertrain have been modelled in Chapter 3 for the hydraulic system model, Chapter 4 and 5 for synchroniser and drag torque, Chapter 8 contains the full powertrain model for each identified powertrain state with variants including different engine configurations and flywheels, while in Chapter 9 a

reduced order powertrain model was developed and integrated with the hydraulic system to develop and study a shift control methodology. Integration of all models was performed in Chapters 8 and 9.

2. *Modelling of the fast acting synchroniser mechanism for determining dynamic characteristics of the synchronisation process,*

Modelling of the synchroniser mechanism itself was achieved in Chapter 4 as a rigid body mechanism with the powertrain excluded from simulations, and in Chapter 9 using a modified rigid body model for studying powertrain transients. Additionally the hydraulic system model in section 3.6 and the drag torque model in Chapter 5 both make up significant components of the mechanism models. Major outcomes from both models are:

1. Identification of the double bump phenomenon cited by ref [63, 64] using the pressure response, indicating that this is a result of contact events between sleeve and ring chamfers and sleeve and gear hub chamfers with abrupt load change instead of peak load (Chapter 4).
2. Engagement simulations considering both design and environmental factors (Chapter 4), the most significant results demonstrating that regeneration of cone slip in second displacement, and its combination with chamfer alignment to cause variation in the engagement time.
3. The development of dimensionless torques for analysing the synchroniser mechanism model, with results verified using parameter variation (Chapter 4).
4. Demonstration of the influence of drag torque on synchroniser engagement, particularly how variation in drag torque affects synchroniser engagement in DCTs (Chapter 5)
5. Studies of engagement simulations using the powertrain model to compare the response with mean engine torque models to harmonic engine torques (Chapter 10).

3. Identify and study possible solutions to improve the engagement of the synchroniser mechanism as used in the DCT,

Two considerations were made for solutions to improve synchroniser engagements. Firstly, control methods were studied in Chapter 6 to reduce the impact of poor chamfer alignments, and alternate mechanisms were identified that reduce the engagement delay shown in closed loop control, with simulations expanded to include a dry clutch DCT model through the elimination of wet clutch drag. Secondly, alternate synchroniser design was presented in Chapter 7 to increase the cone clutch torque without increasing the design envelop of the mechanism. Major outcomes include:

1. Demonstration that the closed loop control method increases the engagement time significantly (Chapter 6).
2. Use of two excitation tools to reduce engagements over closed loop control, but with limited success (Chapter 6).
3. Modification to thrust piece to provide partial cone clutch activation during second displacement and reduce regeneration of slip in the cone clutch (Chapter 6).
4. Externally mounted synchroniser cone clutch for increased torque, also allowing the ability to increase chamfer torque, reducing mechanism engagement times and improving mechanism resistance to drag torque (Chapter 7).

4. Develop numerical solutions for DCT equipped powertrains to investigate dynamic coupling between multiple nonlinearities for accurate assessment of NVH characteristics.

Numerical studies were carried out in Chapter 9 for clutch shift control and studies with detailed hydraulic system models, in Chapter 10 for general simulations of synchroniser engagement and clutch shift control transients, and in Chapter 11 for backlash studies. The major results are as follows:

1. Transient studies of the combined hydraulic system and powertrain model (Chapter 9) used novel combination of hydraulic system and powertrain for studying DCT shifting with both mean and harmonic engine torque modes, showing that:

   a. precise control of clutch torque and time delay compensation for engine and is necessary to minimise transient response and improve shift quality,
   b. increasing engine torque prior to clutch lockup to balance system torques can reduce post lockup transient response
   c. engine torque harmonics influence the stick-slip release at the beginning of shifting, and
2. The synchroniser mechanism powertrain model investigated with both engine torque models (Chapter 10) is an original investigation into synchroniser mechanism engagements and was used to demonstrate that:
   a. the synchronisation process is successful and simulation results using the mean engine torque model are qualitatively consistent with the rigid body model,
   b. at the beginning of indexing there is an increase in the vibration response resulting from the initial contact and subsequent torque change on the mechanism, suggesting increased wear on indexing chamfers, and
   c. engine torque harmonics negatively impact on the engagement of synchronisers.
3. Shift transient studies of the DCT powertrain findings (Chapter 10) present results that:
   a. forced vibrations from engine harmonics introduce uncertainty in torque estimation, a significant issue in Chapter 9, and can introduce clutch stick-slip at the beginning of the torque phase resulting from torque variations, and
   b. the use of dual mass flywheels can successfully suppress a significant portion of engine harmonics, and provides a major source of powertrain damping, rapidly suppressing vibrations in the post lockup response. However inertia phase vibration increases with pull down of the drum before it releases and lead-lag of flywheel inertias resulting from long travel of spring elements affecting release and lockup during shifting.
4. The combined synchronisation and gear shift simulation (Chapter 10) that synchroniser engagements are unlikely to significantly affect shifting in the powertrain. This ignores variable engagement delay in the synchroniser that will influence the initiation of shift transient. However high frequency vibrations are

introduced as a result of mechanism lockup and high impulsive torques at synchroniser lockup may give rise to NVH issues, particularly clonk.

5. Nonlinear backlash model (Chapter 11) presents simulations using an expanded DCT powertrain model with simulations of synchroniser engagement, gear shift, and tip-in/tip-out simulations, showing that:
    a. synchroniser engagement is largely unaffected by lash induced vibrations as a result of the high frequency of vibrations. However clonk may result after mechanism lockup, as a consequence of the impulse torque. With low damping there is also indication of generation of gear rattle in the synchroniser lash zone,
    b. as with synchroniser engagement, the released gear during shifting generates a degree of rattle in response to low load on the open mechanism clutch and respective components,
    c. simulation results suggest that clonk response in the powertrain is possible with synchroniser engagement, gear shift and tip-in/out simulations. However, experimental verification is required, and
    d. Finally, engine harmonic torques tended to increase the rattle during the minimum tip-in throttle angle, it also reduced both the shuffle response and clonk in the response as a result of the inclusion of a DMFW

12.3 LIMITATIONS TO RESEARCH

Three limitations of this thesis are highlighted, particularly as there is only limited capacity to verify results of this work.

1. The most significant limitation to this research has been the lack of capability to undertake any form of validation to the many models introduced in this thesis. While popular and established methods have been used to evaluate a range of issues such as drag torque, hydraulic system or powertrain models, the accuracy of such models is limited. Detailed experimental work would contribute significantly to the improvement of this research, and provides a significant avenue for further work. Validation of part or all of these models will increase the certainty that can be placed on the quality of results. To the extent that these models could be verified using current available information, this was performed. For example, drag torque models are compared to typical data suggested in [47],

while free vibration analysis of powertrain models suggests that these are representative of typical powertrains. With results containing rigid body modes, global shuffle mode between 2 and 10 Hz, local axle mode at around 30 Hz among typical powertrain frequencies, indicate that models presented are reasonable.

2. Generally simulations have been performed with available data, such that the values of parameters used in these simulations are typical to what will be expected in a powertrain. However a lack of accurate and reliable data limits confidence in results. Consider backlash nonlinearities. These are highly dependent on design parameters, shown in [119]. Thus while the simulations in this thesis provide indication of how these nonlinearities will affect the powertrain response, more accurate information is required to provide more than demonstrative simulations on current work. This same issue is extrapolated to other aspects of research, such as synchroniser modelling or drag torques, where accurate data for modelling will increase the confidence in results.
3. Friction coefficients for wet clutches and synchroniser cones are assumed to be constant. However, Crowther, et al, [30] and Lechner & Naunheimer [49] both demonstrate that this is not the case for either clutch type. The use of speed dependent friction coefficients for clutches in particular will contribute further to an understanding of nonlinearities in DCTs.

12.4 FURTHER RESEARCH

Avenues for further research into DCT transients and control include:

1. The limitations to this research in terms of validation and use of actual powertrain parameters provides a significant avenue for experimental research, particularly as at the time of writing this thesis, the author is unaware of any published work pertaining to validation of DCT shift transients at an academic level. One aspect that should be considered is the use of experimentally determined friction coefficients, particularly as these have been shown to alter the behaviour of powertrain response significantly.
2. Time delay in control of gear shift has been demonstrated here to hold promise in continued improvement to DCT control, particularly compensating for delays

in clutch hydraulics and engine torque control. Though simple simulations were shown in Chapter 9 the robustness of controller is questionable without the implementation of a holistic controller design. Methods such as H-infinite control can be suggested here for further research.

3. One of the main drawbacks of applying DCTs more widely in the automobile industry has been the ability to match high quality automatic transmission gearshifts. Figure 12.1, below shows the powertrain response with clutch 2 pressure held constant at the target pressure with friction lockup in the stick-slip algorithm suppressed. It suggests that, in comparison to Figure 10.19 of Chapter 10, dynamic friction in the clutch can be used to suppress vibration in the DCT, with vibrations in the original figure well suppressed. This is an interesting area of further research as the practicalities of continuous slip are limited by thermal load and precise control of pressure is required to ensure that lockup is prevented, as stick-slip can introduce additional transients.

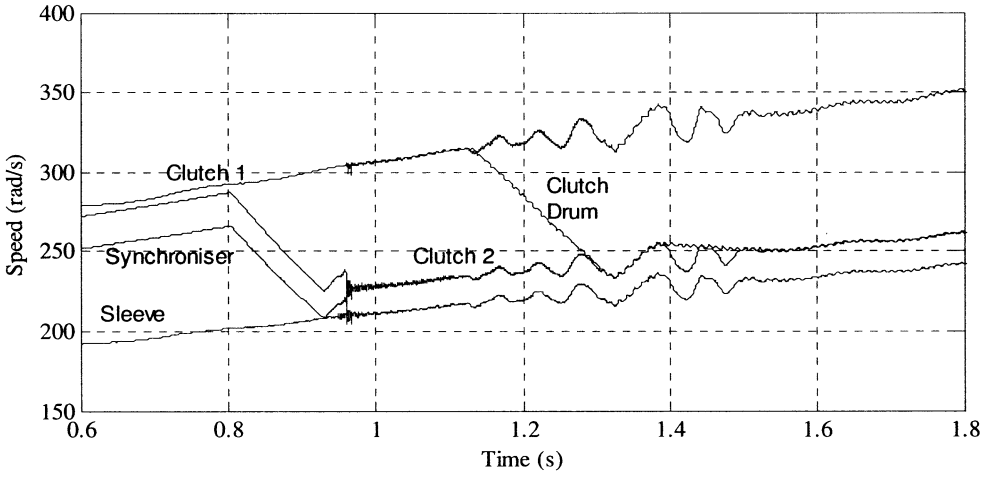

Figure 12.1: Failed simulation of combined synchroniser engagement and gearshift

4. Further investigation into methods for improving synchroniser engagements will also provide an interesting addition to research. Minimising of slip regeneration through the method suggested here or by alternate means will increase repeatability in the shifting process, while very high drag torque in wet clutches is an impediment to rapid and reliable synchronisation before shifting. Modification of synchroniser design and engagement process, such as aiding synchronisation using electric machines, can also reduce the impact of the synchroniser on negative shifting.

5. This thesis has focused mainly on the investigation of powertrain response to nonlinearities. More concise research on how these nonlinearities are excited and to what extent they will impact on powertrain behaviour when excited would provide an interesting area of further research
6. A final area of potential research is the simulation and analysis of powertrain transients with nonlinear damping. It is well established that friction is low speed dependent, while windage is more dominant at high speed. To therefore use full speed and load dependent evaluation of the powertrain system losses presents an interesting proposition for further research into powertrain dynamics.

12.5 CONCLUSION

The principle aims of this thesis were twofold. Study of transient response in DCT equipped powertrains and the investigation into the performance of synchroniser mechanisms. These have been achieved through the development of extensive mathematical models for components and the DCT powertrain, and analysis of the resulting simulations.

The evaluation of DCT equipped powertrains as a lightly damped dynamic system brings to the forefront issues in clutch control, where precise estimation of clutch torques and consideration of engine torque control and influences of time delay are likely to significantly impact on the capability to achieve high quality shifting. While the inclusion of multiple nonlinearities are shown to impact on the quality of shifting. Overall consideration has been given to the advent of stick-slip in either of the two clutches, the onset of clonk-type response, and other forms of powertrain transient response all utilised as qualitative measures of shift performance. Practically speaking, the application of DMFW has provided some clear performance improvements for post lockup suppression of transients, but the long travel of the flywheel is a source of concern during clutch release and lockup.

The dependence of synchroniser performance to a range of design and environmental variables limits the capability to reproduce a consistent engagement time under all operating conditions. Simulations suggest that there is significant variability in the duration of engagement, particularly resulting from environmental variables such as initial speed or operating temperature, and the regeneration of slip in the cone clutch

interacting with the random nature of chamfer alignments. These all suggest that there is considerable need for further development of the mechanism, with two design improvements suggested in this thesis that will provide much of the increased torque requirements, reduce the likelihood of slip regeneration, duration of engagements, and provide positive control of chamfer alignments, thus improving synchroniser repeatability and reliability.

APPENDIX A – UNBLOCKING TIME

This appendix provides a method for calculating the unblocking time for the synchroniser ring by applying basic kinematic and kinetic theories. Assuming that over the realignment period the variation in drag torque is negligible, to determine an approximate unblocking time:

$\delta = \dot{\theta}_S t + 0.5\ddot{\theta}_S t$, which can be arranged as $t = \sqrt{\frac{2\delta}{\ddot{\theta}_S}}$ (A.1 a & b)

Applying Newton's second law, $\sum M = I\alpha$

$I_{FW}\ddot{\theta}_S = T_D + T_B$, or $\ddot{\theta}_S = \frac{T_D + T_B}{I_{FW}}$ (A.2 a & b)

Combining these equations:

$t_B = \sqrt{\frac{2\delta \cdot I_{FW}}{T_D + T_B}}$ (A.3)

APPENDIX B – DISPLACEMENT DERIVATION

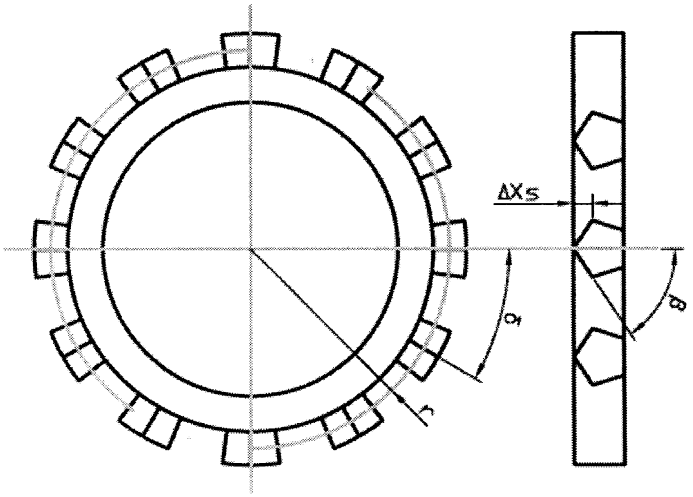

Figure B.1: Typical synchroniser ring layout

To determine the required sleeve displacement to pass chamfers consider the typical synchroniser ring shown below in Figure B.1. The maximum lateral displacement of the sleeve between two consecutive chamfer tips is defined using the term 'y' by the equation $y = r\beta$, which is the equation of the length of an arc. Additionally, the sleeve is constrained by the chamfer angle β. This translates the relative lateral displacement, y, of the ring to the translation of the sleeve, ΔX_S. Using simple trigonometry and considering that for the sleeve to move between two chamfers the ring must be rotated half the length of y we get:

$$\tan\beta = \frac{y/2}{\Delta x_S} \tag{B.1}$$

and by substituting for y:

$$\Delta x_S = \frac{\delta}{2} \cdot \frac{r}{\tan\beta} \tag{B.2}$$

APPENDIX C – MATRIX EQUATIONS OF MOTION FOR POWERTRAIN MODEL

The matrix equations of motion are created from the equations presented in Chapter 8, equation 8.16 To equation 8.41. Equations used in each matrix are dependent on the clutch engaged, summarised as follows:

- State 3 – Clutch 1 and synchroniser 1 are engaged, and synchroniser 2 is disengaged. Relevant equations of motion are: 8.16, 8.17, 8.24-8.27, 8.29, 8.32-8.37, 8.40, 8.41
- State 4 – Clutch 2 and synchroniser 2 are engaged, and synchroniser 1 is disengaged. Relevant equations of motion are: 8.16, 8.17, 8.21-8.23, 8.28, 8.30, 8.32-8.37, 8.40, 8.41
- State 5 – Clutch 1 and synchroniser 1 are engaged, and synchroniser 2 is engaged. Relevant equations of motion are: 8.16, 8.17, 8.23, 8.27, 8.29, 8.30 8.32-8.37, 8.40, 8.41
- State 6 – Clutch 2 and synchroniser 2 are engaged, and synchroniser 1 is engaged. Relevant equations of motion are: 8.16, 8.17, 8.21, 8.28, 8.29, 8.30 8.32-8.37, 8.40, 8.41
- State 7 – Synchroniser 1 and synchroniser 2 are engaged, and both clutches disengaged. Relevant equations of motion are: 8.16-8.18, 8.21, 8.24, 8.29, 8.30 8.32-8.37, 8.40, 8.41

State 3 – Clutch 1 closed, even synchroniser open

State three is the condition where an odd gear in the transmission is engaged with its primary clutch, whilst the even gear is either freewheeling or has the synchroniser energised, but not locked. This results in degrees of freedom for the synchroniser and respective even gear.

$$\boldsymbol{I} = \left\{ I_e \;\; I_F \;\; (I_D + I_{C1}) \;\; \left(\frac{I_{P1} + I_{S1}}{\gamma_1} + I_{G1}\right) \;\; I_{C2} \;\; \left(\frac{I_{P2}}{\gamma_2} + I_{G2}\right) \;\; I_{S2} \;\; \gamma_{FD1}^2 I_{FD1} + \gamma_{FD2}^2 I_{FD2} + I_{FD3} \;\; I_{SH} \;\; I_{SH} \;\; I_{SH} \;\; I_{Diff} \;\; 2I_H \;\; 2I_T \right\}^{diag}$$

$$\boldsymbol{T} = \left\{ T_e \;\; 0 \;\; -T_{C2} \;\; 0 \;\; T_{C2} \;\; -T_{S2}/\gamma_2 \;\; T_{S2} \;\; 0 \;\; 0 \;\; 0 \;\; 0 \;\; 0 \;\; 0 \;\; 0 \;\; T_V \right\}^T$$

$$\boldsymbol{\theta} = \{ \theta_e \;\; \theta_F \;\; \theta_D \;\; \theta_{G1} \;\; \theta_{C2} \;\; \theta_{G2} \;\; \theta_{S2} \;\; \theta_{FD3} \;\; \theta_{SH1} \;\; \theta_{SH2} \;\; \theta_{SH3} \;\; \theta_{SH4} \;\; \theta_{Diff} \;\; \theta_H \;\; \theta_V \}^T$$

$$\boldsymbol{C} = \begin{bmatrix}
0 & & & & & & & & & & & & & & & & \\
 & C_F & -C_F & & & & & & & & & & & & & & \\
 & -C_F & C_F + C_{WC} & -C_{WC} & & & & & & & & & & & & & \\
 & & & C_{G1} & & & & & & & & & & & & & \\
 & & -C_{WC} & & C_{WC} & & & & & & & & & & & & \\
 & & & & & C_{G2} & & & & & & & & & & & \\
 & & & & & & 0 & & & & & & & & & & \\
 & & & & & & & \gamma_{FD1} C_{FD1} + \gamma_{FD2} C_{FD2} + C_{SH} & -C_{SH} & -C_{SH} & -C_{SH} & -C_{SH} & -C_{SH} & -C_{SH} & 2C_H & -2C_H \\
 & & & & & & & -C_{SH} & 2C_{SH} & 2C_{SH} & 2C_{SH} & 2C_{SH} & 2C_{SH} & 2C_{SH} & -2C_H & 2C_H
\end{bmatrix}$$

$$
\boldsymbol{K} = \begin{bmatrix}
K_e & -K_e & & & & & & & & & & & & & \\
-K_e & K_e + K_F & -K_F & & & & & & & & & & & & \\
 & -K_F & K_F+K_{C1} & -K_{C1} & & & & & & & & & & & \\
 & & -K_{C1} & K_{C1} + K_{S1}/\gamma_1^2 & & & & -\gamma_{FD1}K_{S1}/\gamma_1 & & & & & & & \\
 & & & & K_{C2} & -K_{C2} & & & & & & & & & \\
 & & & & -K_{C2} & K_{C2} & & & & & & & & & \\
 & & & & & & K_{S2}/\gamma_2^2 & -\gamma_{FD2}K_{S2}/\gamma_2 & & & & & & & \\
 & & & -\gamma_{FD1}K_{S1}/\gamma_1 & & & -\gamma_{FD2}K_{S2}/\gamma_2 & \gamma_{FD1}^2K_{S1} + \gamma_{FD2}^2K_{S2} + K_{SH} & -K_{SH} & & & & & & \\
 & & & & & & & -K_{SH} & 2K_{SH} & -K_{SH} & & & & & \\
 & & & & & & & & -K_{SH} & 2K_{SH} & -K_{SH} & & & & \\
 & & & & & & & & & -K_{SH} & 2K_{SH} & -K_{SH} & & & \\
 & & & & & & & & & & -K_{SH} & 2K_{SH} & -K_{SH} & & \\
 & & & & & & & & & & & -K_{SH} & K_{SH} + K_{AX} & -K_{AX} & \\
 & & & & & & & & & & & & -K_{AX} & K_{AX} + 2K_H & -2K_H \\
 & & & & & & & & & & & & & -2K_H & 2K_H
\end{bmatrix}
$$

State 4 – Clutch 2 closed, odd synchroniser open

This state is the even counterpart to state 3, with odd gear freewheeling and the vehicle being driven by the even gear.

$$\boldsymbol{I} = \left\{ I_e \;\; I_F \;\; (I_D + I_{C2}) \;\; I_{C1} \;\; \left(\frac{I_{P1}}{\gamma_1} + I_{G1}\right) \;\; I_{S1} \;\; \left(\frac{I_{P2} + I_{S2}}{\gamma_2} + I_{G2}\right) \;\; \gamma_{FD1}^2 I_{FD1} + \gamma_{FD2}^2 I_{FD2} + I_{FD3} \;\; I_{SH} \;\; I_{SH} \;\; I_{SH} \;\; I_{Diff} \;\; 2I_H \;\; 2I_T \right\}^{diag}$$

$$\boldsymbol{T} = \left\{ T_e \;\; 0 \;\; -T_{C1} \;\; T_{C1} \;\; -T_{S1}/\gamma_1 \;\; T_{S1} \;\; 0 \;\; 0 \;\; 0 \;\; 0 \;\; 0 \;\; 0 \;\; 0 \;\; 0 \;\; T_V \right\}^T$$

$$\boldsymbol{\theta} = \{ \theta_e \;\; \theta_F \;\; \theta_D \;\; \theta_{C1} \;\; \theta_{G1} \;\; \theta_{S1} \;\; \theta_{G2} \;\; \theta_{FD3} \;\; \theta_{SH1} \;\; \theta_{SH2} \;\; \theta_{SH3} \;\; \theta_{SH4} \;\; \theta_{Diff} \;\; \theta_H \;\; \theta_V \}^T$$

$$\boldsymbol{C} = \begin{bmatrix}
0 & & & & & & & & & & & & & & \\
 & C_F & -C_F & & & & & & & & & & & & \\
 & -C_F & C_F + C_{WC} & -C_{WC} & & & & & & & & & & & \\
 & & -C_{WC} & C_{WC} & C_{G1} & & & & & & & & & & \\
 & & & & 0 & C_{G2} & & & & & & & & & \\
 & & & & & \gamma_{FD1} C_{FD1} + \gamma_{FD2} C_{FD2} + C_{SH} & -C_{SH} & & & & & & & & \\
 & & & & & -C_{SH} & 2C_{SH} & -C_{SH} & & & & & & & \\
 & & & & & & -C_{SH} & 2C_{SH} & -C_{SH} & & & & & & \\
 & & & & & & & -C_{SH} & 2C_{SH} & -C_{SH} & & & & & \\
 & & & & & & & & -C_{SH} & C_{Diff} + C_{SH} & & & & \\
 & & & & & & & & & & 2C_H & -2C_H & & \\
 & & & & & & & & & & -2C_H & 2C_H & &
\end{bmatrix}$$

$$
\mathbf{K} = \begin{bmatrix}
K_e & -K_e & & & & & & & & & & & & & & & & & & & & & & \\
-K_e & K_e + K_F & -K_F & & & & & & & & & & & & & & & & & & & & & \\
 & -K_F & K_F + K_{C2} & & & -K_{C2} & & & & & & & & & & & & & & & & & & \\
 & & & K_{C1} & -K_{C1} & & & & & & & & & & & & & & & & & & & \\
 & & & -K_{C1} & K_{C1} & & & & & & & & & & & & & & & & & & & \\
 & & -K_{C2} & & & K_{C2} + K_{S2}/\gamma_2^2 & -\gamma_{FD2}K_{S2}/\gamma_2 & & & & & & & & & & & & & & & & & \\
 & & & & & K_{S1}/\gamma_1^2 & -\gamma_{FD1}K_{S1}/\gamma_1 & & & & & & & & & & & & & & & & & \\
 & & & & & -\gamma_{FD1}K_{S1}/\gamma_1 & \gamma_{FD1}^2K_{S1} + \gamma_{FD2}^2K_{S2} + K_{SH} & -K_{SH} & & & & & & & & & & & & & & & \\
 & & & & & & -K_{SH} & 2K_{SH} & -K_{SH} & & & & & & & & & & & & & & \\
 & & & & & & & -K_{SH} & 2K_{SH} & -K_{SH} & & & & & & & & & & & & & \\
 & & & & & & & & -K_{SH} & 2K_{SH} & -K_{SH} & & & & & & & & & & & & \\
 & & & & & & & & & -K_{SH} & K_{SH} + K_{AX} & -K_{AX} & & & & & & & & & & \\
 & & & & & & & & & & -K_{AX} & K_{AX} + 2K_H & -2K_H & & & & & & & & & \\
 & & & & & & & & & & & -2K_H & 2K_H & & & & & & & & & \\
\end{bmatrix}
$$

State 5 – Clutch 1 closed, even synchroniser closed

The fifth state constitutes the powertrain in preparation or after completing a shift to or from the even gearset, respectively. Therefore the odd gear and clutch are engaged, with the even synchroniser closed.

$$\boldsymbol{I} = \left\{ I_e \;\; I_F \;\; (I_D + I_{C1}) \;\; \left(\frac{I_{P1} + I_{S1}}{\gamma_1} + I_{G1}\right) \;\; I_{C2} \;\; \left(\frac{I_{P2} + I_{S2}}{\gamma_2} + I_{G2}\right) \;\; \gamma_{FD1}^2 I_{FD1} + \gamma_{FD2}^2 I_{FD2} + I_{FD3} \;\; I_{SH} \;\; I_{SH} \;\; I_{SH} \;\; I_{Diff} \;\; 2I_H \;\; 2I_T \right\}^{diag}$$

$$\boldsymbol{T} = \{T_e \;\; 0 \;\; -T_{C2} \;\; 0 \;\; T_{C2} \;\; 0 \;\; 0 \;\; 0 \;\; 0 \;\; 0 \;\; 0 \;\; 0 \;\; 0 \;\; T_V\}^T$$

$$\boldsymbol{\theta} = \{\theta_e \;\; \theta_F \;\; \theta_D \;\; \theta_{G1} \;\; \theta_{C2} \;\; \theta_{G2} \;\; \theta_{FD3} \;\; \theta_{SH1} \;\; \theta_{SH2} \;\; \theta_{SH3} \;\; \theta_{SH4} \;\; \theta_{Diff} \;\; \theta_H \;\; \theta_V\}^T$$

$$\boldsymbol{C} = \begin{bmatrix}
0 & & & & & & & & & & & & & & \\
 & C_F & -C_F & & & & & & & & & & & & \\
 & -C_F & C_F + C_{WC} & -C_{WC} & & & & & & & & & & & \\
 & & & C_{G1} & & & & & & & & & & & \\
 & & -C_{WC} & & C_{WC} & & & & & & & & & & \\
 & & & & & C_{G2} & & & & & & & & & \\
 & & & & & & \gamma_{FD1} C_{FD1} + \gamma_{FD2} C_{FD2} + C_{SH} & -C_{SH} & & & & & & & \\
 & & & & & & -C_{SH} & 2C_{SH} & -C_{SH} & & & & & & \\
 & & & & & & & -C_{SH} & 2C_{SH} & -C_{SH} & & & & & \\
 & & & & & & & & -C_{SH} & 2C_{SH} & -C_{SH} & & & & \\
 & & & & & & & & & -C_{SH} & C_{Diff} + C_{SH} & & & & \\
 & & & & & & & & & & & 2C_H & -2C_H & & \\
 & & & & & & & & & & & -2C_H & 2C_H & &
\end{bmatrix}$$

$$
\boldsymbol{K} = \begin{bmatrix}
K_e & -K_e & & & & & & & & & & & & & \\
-K_e & K_e + K_F & -K_F & & & & & & & & & & & & \\
 & -K_F & K_F + K_{C1} & -K_{C1} & & & & & & & & & & & \\
 & & -K_{C1} & K_{C1} + K_{S1}/\gamma_1^2 & & & & -\gamma_{FD1}K_{S1}/\gamma_1 & & & & & & & \\
 & & & & K_{C2} & -K_{C2} & & & & & & & & & \\
 & & & & -K_{C2} & K_{C2} + K_{S2}/\gamma_2^2 & & -\gamma_{FD2}K_{S2}/\gamma_2 & & & & & & & \\
 & & & -\gamma_{FD1}K_{S1}/\gamma_1 & & -\gamma_{FD2}K_{S2}/\gamma_2 & \gamma_{FD1}^2K_{S1} + \gamma_{FD2}^2K_{S2} + K_{SH} & -K_{SH} & & & & & & & \\
 & & & & & & -K_{SH} & 2K_{SH} & -K_{SH} & & & & & & \\
 & & & & & & & -K_{SH} & 2K_{SH} & -K_{SH} & & & & & \\
 & & & & & & & & -K_{SH} & 2K_{SH} & -K_{SH} & & & & \\
 & & & & & & & & & -K_{SH} & 2K_{SH} & -K_{SH} & & & \\
 & & & & & & & & & & -K_{SH} & K_{SH} + K_{AX} & -K_{AX} & & \\
 & & & & & & & & & & & -K_{AX} & K_{AX} + 2K_H & -2K_H & \\
 & & & & & & & & & & & & -2K_H & 2K_H &
\end{bmatrix}
$$

State 6 – Clutch 2 closed, odd synchroniser closed

Again the counterpart of the previous state, the vehicle is driven through the even half of the transmission with the odd gear synchronised.

$$\boldsymbol{I} = \left\{ I_e \;\; I_F \;\; (I_D + I_{G2}) \;\; I_{C1} \;\; \left(\frac{I_{P1} + I_{S1}}{\gamma_1} + I_{G1}\right) \;\; \left(\frac{I_{P2} + I_{S2}}{\gamma_2} + I_{G2}\right) \;\; \gamma_{FD1}^2 I_{FD1} + \gamma_{FD2}^2 I_{FD2} + I_{FD3} \;\; I_{SH} \;\; I_{SH} \;\; I_{SH} \;\; I_{Diff} \;\; 2I_H \;\; 2I_T \right\}^{diag}$$

$$\boldsymbol{T} = \{T_e \;\; 0 \;\; -T_{C1} \;\; T_{C1} \;\; 0 \;\; 0 \;\; 0 \;\; 0 \;\; 0 \;\; 0 \;\; 0 \;\; 0 \;\; 0 \;\; T_V\}^T$$

$$\boldsymbol{\theta} = \{\theta_e \;\; \theta_F \;\; \theta_D \;\; \theta_{C1} \;\; \theta_{G1} \;\; \theta_{G2} \;\; \theta_{FD3} \;\; \theta_{SH1} \;\; \theta_{SH2} \;\; \theta_{SH3} \;\; \theta_{SH4} \;\; \theta_{Diff} \;\; \theta_H \;\; \theta_V\}^T$$

$$\boldsymbol{C} = \begin{bmatrix} 0 & & & & & & & & & & & & & \\ & C_F & -C_F & & & & & & & & & & & \\ & -C_F & C_F + C_{WC} & -C_{WC} & & & & & & & & & & \\ & & -C_{WC} & C_{WC} & & & & & & & & & & \\ & & & & C_{G1} & & & & & & & & & \\ & & & & & C_{G2} & & & & & & & & \\ & & & & & & \gamma_{FD1}C_{FD1} + \gamma_{FD2}C_{FD2} + C_{SH} & -C_{SH} & & & & & & \\ & & & & & & -C_{SH} & 2C_{SH} & -C_{SH} & & & & & \\ & & & & & & & -C_{SH} & 2C_{SH} & -C_{SH} & & & & \\ & & & & & & & & -C_{SH} & 2C_{SH} & -C_{SH} & & & \\ & & & & & & & & & -C_{SH} & C_{Diff} + C_{SH} & & & \\ & & & & & & & & & & & 2C_H & -2C_H & \\ & & & & & & & & & & & -2C_H & 2C_H & \end{bmatrix}$$

$$
\boldsymbol{K} = \begin{bmatrix}
K_e & -K_e & & & & & & & & & & & & \\
-K_e & K_e + K_F & -K_F & & & & & & & & & & & \\
 & -K_F & K_F + K_{C2} & & & -K_{C2} & & & & & & & & \\
 & & & K_{C1} & -K_{C1} & & & & & & & & & \\
 & & & -K_{C1} & K_{C1} + K_{S1}/\gamma_1^2 & & & -\gamma_{FD1}K_{S1}/\gamma_1 & & & & & & \\
 & & -K_{C2} & & & K_{C2} + K_{S2}/\gamma_2^2 & & -\gamma_{FD2}K_{S2}/\gamma_2 & & & & & & \\
 & & & & -\gamma_{FD1}K_{S1}/\gamma_1 & -\gamma_{FD2}K_{S2}/\gamma_2 & \gamma_{FD1}^2K_{S1} + \gamma_{FD2}^2K_{S2} + K_{SH} & -K_{SH} & & & & & & \\
 & & & & & & -K_{SH} & 2K_{SH} & -K_{SH} & & & & & \\
 & & & & & & & -K_{SH} & 2K_{SH} & -K_{SH} & & & & \\
 & & & & & & & & -K_{SH} & 2K_{SH} & -K_{SH} & & & \\
 & & & & & & & & & -K_{SH} & 2K_{SH} & -K_{SH} & & \\
 & & & & & & & & & & -K_{SH} & K_{SH} + K_{AX} & -K_{AX} & \\
 & & & & & & & & & & & -K_{AX} & K_{AX} + 2K_H & -2K_H \\
 & & & & & & & & & & & & -2K_H & 2K_H
\end{bmatrix}
$$

State 7 – Shifting, both clutches open, both synchronisers closed

With the powertrain in the state of shifting, both synchronisers are closed, but the clutches are open and energised.

$$\boldsymbol{I} = \left\{ I_e \;\; I_F \;\; I_D \;\; I_{C1} \;\; \left(\frac{I_{P1}+I_{S1}}{\gamma_1}+I_{G1}\right) \;\; I_{C2} \;\; \left(\frac{I_{P2}+I_{S2}}{\gamma_2}+I_{G2}\right) \;\; \gamma_{FD1}^2 I_{FD1} + \gamma_{FD2}^2 I_{FD2} + I_{FD3} \;\; I_{SH} \;\; I_{SH} \;\; I_{SH} \;\; I_{Diff} \;\; 2I_H \;\; 2I_T \right\}^{diag}$$

$$\boldsymbol{T} = \{T_e \;\; 0 \;\; -T_{C2} - T_{C1} \;\; T_{C1} \;\; 0 \;\; T_{C2} \;\; 0 \;\; 0 \;\; 0 \;\; 0 \;\; 0 \;\; 0 \;\; 0 \;\; 0 \;\; T_V\}^T$$

$$\boldsymbol{\theta} = \{\theta_e \;\; \theta_F \;\; \theta_D \;\; \theta_{C1} \;\; \theta_{G1} \;\; \theta_{C2} \;\; \theta_{G2} \;\; \theta_{FD3} \;\; \theta_{SH1} \;\; \theta_{SH2} \;\; \theta_{SH3} \;\; \theta_{SH4} \;\; \theta_{Diff} \;\; \theta_H \;\; \theta_V\}^T$$

$$\boldsymbol{C} = \begin{bmatrix}
0 & & & & & & & & & & & & & & \\
 & C_F & -C_F & & & & & & & & & & & & \\
 & -C_F & C_F & & & & & & & & & & & & \\
 & & & C_{WC} & -C_{WC} & & & & & & & & & & \\
 & & & -C_{WC} & C_{G1} & -C_{WC} & & & & & & & & & \\
 & & & & & C_{G2} & & & & & & & & & \\
 & & & & & & \gamma_{FD1}C_{FD1} + \gamma_{FD2}C_{FD2} + C_{SH} & -C_{SH} & -C_{SH} & -C_{SH} & -C_{SH} & & & & \\
 & & & & & & -C_{SH} & 2C_{SH} & -C_{SH} & 2C_{SH} & -C_{SH} & & & & \\
 & & & & & & -C_{SH} & -C_{SH} & 2C_{SH} & -C_{SH} & 2C_{SH} & -C_{SH} & & & \\
 & & & & & & -C_{SH} & -C_{SH} & -C_{SH} & 2C_{SH} & -C_{SH} & C_{Diff} + C_{SH} & & & \\
 & & & & & & & & & & & & 2C_H & -2C_H & \\
 & & & & & & & & & & & & -2C_H & 2C_H &
\end{bmatrix}$$

$$
\boldsymbol{K} = \begin{bmatrix}
K_e & -K_e & & & & & & & & & & & & & & & & & & & & & & \\
-K_e & K_e + K_F & -K_F & & & & & & & & & & & & & & & & & & & & & \\
 & -K_F & K_F & & & & & & & & & & & & & & & & & & & & & \\
 & & & K_{C1} & -K_{C1} & & & & & & & & & & & & & & & & & & & \\
 & & & -K_{C1} & K_{C1} + K_{S1}/\gamma_1^2 & & & & & & & & & & & & & & & & & & & \\
 & & & & & K_{C2} & -K_{C2} & & & & & & & & & & & & & & & & & \\
 & & & & & -K_{C2} & K_{C2} + K_{S2}/\gamma_2^2 & & & & & & & & & & & & & & & & & \\
 & & & & & & & & -\gamma_{FD1}K_{S1}/\gamma_1 & & & & & & & & & & & & & & & \\
 & & & & & & & & -\gamma_{FD2}K_{S2}/\gamma_2 & & & & & & & & & & & & & & & \\
 & & & & & & & -\gamma_{FD1}K_{S1}/\gamma_1 & -\gamma_{FD2}K_{S2}/\gamma_2 & \gamma_{FD1}^2K_{S1} + \gamma_{FD2}^2K_{S2} + K_{SH} & -K_{SH} & & & & & & & & & & & & & \\
 & & & & & & & & & -K_{SH} & 2K_{SH} & -K_{SH} & & & & & & & & & & & \\
 & & & & & & & & & & -K_{SH} & 2K_{SH} & -K_{SH} & & & & & & & & & & \\
 & & & & & & & & & & & -K_{SH} & 2K_{SH} & -K_{SH} & & & & & & & & & \\
 & & & & & & & & & & & & -K_{SH} & 2K_{SH} & -K_{SH} & & & & & & & & \\
 & & & & & & & & & & & & & -K_{SH} & K_{SH} + K_{AX} & -K_{AX} & & & & & & & \\
 & & & & & & & & & & & & & & -K_{AX} & K_{AX} + 2K_H & -2K_H & & & & & \\
 & & & & & & & & & & & & & & & -2K_H & 2K_H & & & & & \\
 & & & & & & & & & & & & & & & & & & & & & \\
 & & & & & & & & & & & & & & & & & & & & & \\
 & & & & & & & & & & & & & & & & & & & & & \\
 & & & & & & & & & & & & & & & & & & & & & \\
 & & & & & & & & & & & & & & & & & & & & & \\
 & & & & & & & & & & & & & & & & & & & & &
\end{bmatrix}
$$

REFERENCES

[1] M. Goetz, "Integrated Powertrain control for Twin Clutch Transmissions," Thesis for PhD, University of Leeds, 2005.

[2] G.R. Holmes and R. Tamba, "Solenoid control valve," US 7 082 965 B2, 2006.

[3] R. Berger, R. Meinhard and C. Bunder, "The Parallel Shift Gearbox PSG," LuK Symposium, pp. 197-210, 2002.

[4] U. Wagner, R. Berger, M. Ehrlich and M. Homm, "Electromotoric actuators for double clutch transmissions - best efficiency by itself,", LuK Symposium, pp. 137-153, 2006.

[5] B. Matthes and F. Geunter, "Dual Clutch Transmissions - Lessons Learnt and Future Potential," SAE Technical Paper 2005-01-1021, 2005.

[6] P. Tenberge, "Double Clutch Transmission - Power-shiftable Winding Transmission," VDI-Berichte, vol. 1665, pp. 1033-1050, 2002.

[7] R. Ahlawat, H.K. Fathy, B. Lee, J.L. Stein and D. Jung, "Modelling and simulation of a dual clutch transmission vehicle to analyse the effect of pump selection on fuel economy," Vehicle System Dynamics, pp. 1-18, 2009.

[8] C. Certez, O. Scherf, K. Stutzer, R. Schierhorn and D. Kelly, "Wet or Dry Clutches for Dual Clutch Transmissions," FISITA World Congress, Paper number: F2004F136, 2004.

[9] F. Rudolph, M. Schafer, A. Damm, F.T. Metzner and I. Steinberg, "The Innovative Seven Speed Dual Clutch Gearbox for Volkswagen's Compact Cars," 28th Internationales Wiener Motorensymposium, 2007. Reprinted in Fortschritt Berichte-Vdi Reihe 12 Verkehrstechnik Fahrzeugtechnik, vol .639 (2), pp 242-264, 2007.

[10] G. Wagner, "Application of Transmission systems for Different Driveline Configurations in Passenger Cars," SAE Technical Paper: 2001-01-0882, 2001.

[11] J. Wheals, A. Turner, K. Ramsay, A. O'Neil, J. Bennett and H. Fang, "Double Clutch Transmission (DCT) using Multiplexed Linear Actuation Technology and Dry Clutches for High Efficiency and Low Cost," SAE Technical Paper: 2007-01-1096, 2007.

[12] A.J. Turner, K. Ramsay, R.E. Clark and D. Howe, "Development of high force electromechanical linear actuator for shift-by-wire automated manual transmissions," SAE Technical Paper: 2006-01-0360, 2006.

[13] D. Rolland, A. O'Neill, T. Burchell, R. Robinson, J. Behrenroth, J. Wheals and R. Gordon, "New high performance dual clutch transmission," in FISITA World Congress, Paper number: F2006P005, 2006.

[14] U. Wagner and A. Wagner, "Electric Shift Gearbox (ESG) - Consistent development of the dual clutch transmission to a mild hybrid system," SAE Technical Paper, 2005-01-4182, 2005.

[15] A.S. Joshi, N.P. Shah and C. Mi, "Modelling and simulation of a dual clutch hybrid vehicle powertrain," Vehicle Power and Propulsion Conference, pp. 1666-1673, 2009.

[16] A. Burke and H. Zhao, "Simulations of plug-in hybrid vehicles using advanced lithium batteries and ultra capacitors on various driving cycles," Institute of transportation studies., 2010.

[17] S.W. Zhang G. and S. Zheng, "Study on the engine management strategy of DCT-based series-parallel PHEV," in 2010 International conference on computing, control and industrial engineering, pp. 25-29, 2010.

[18] O. Sundstrom, P. Soltic and L. Guzzella, "A transmission actuated energy management strategy," IEEE Transactions on Vehicular Technology, vol. 59, pp. 84-92, 2009.

[19] M. Goetz, M. Levesley and D. Crolla, "Dynamics and Control of Gearshifts on Twin-Clutch Transmission," Proceedings of the Institution of Mechanical Engineers Part D: Journal Automobile Engineering, vol. 219, pp. 951-963, 2005.

[20] M. Goetz, M. Levesley and D. Crolla, "Dynamic Modelling of a Twin Clutch Transmission for Controller Design," Materials Science Forum, vol. 440-441, pp. 253-261, 2003.

[21] M. Goetz, M. Levesley and D. Crolla, "A Gearshift Controller for Twin Clutch Transmissions," VDI Berichte, vol. 1786, pp. 381-400, 2003.

[22] Y. Zhang, X. Chen, X. Zhang, H. Jiang and W. Tobler, "Dynamic Modelling and Simulation of a Dual-Clutch Automated Lay-Shaft Transmission," Transactions of the American Society of Mechanical Engineers, vol. 127, pp. 302-307, 2005.

[23] M. Kulkarni, T. Shim and Y. Zhang, "Shift Dynamics and Control of Dual-Clutch Transmissions," Mechanism and Machine Theory, vol. 42, pp. 168-182, 2007.

[24] S. Kirschstein, "The Impact of Launch Control on the Vibration Behaviour of a Dual Clutch Transmission Powertrain," VDI Berichte, vol. 1971, pp. 197-217, 2007.

[25] X. Song, J. Liu and D. Smedley, "Simulation Study of Dual Clutch Transmission for Medium Duty Truck Application," SAE Technical Paper: 2005-01-3590, 2005.

[26] Y. Lei, J. Wang and A. Ge, "Research on Control strategies of Double Clutch Transmission Based on System Simulation," FISITA World Congress Paper Number: F2006P041, 2006.

[27] Y. Liu, D. Qin, H. Jiang and Y. Zhang, "A systematic model for dynamics and control of dual clutch transmissions," Transactions of the American Society of Mechanical Engineers, Journal of Mechanical Design, vol. 131, 2009.

[28] G. Xuexun, F. Chang, Y. Jun and Y. Zheng, "Modelling and Simulation Research of Dual Clutch Transmission Based on Fuzzy Logic Control," SAE Technical Paper: 2007-01-3754, 2007.

[29] P. Couderc, J. Callenaere, J. Der Hagopian, G. Ferraris, A. Kassai, Y. Borjesson, L. Verdillon and S. Gaimard, "Vehicle driveline dynamic behaviour: Experimentation and Simulation," Journal of Sound and Vibration, vol. 218, pp. 133-157, 1998.

[30] A. Crowther, N. Zhang, D.K. Liu and J. Jeyakumaran, "Analysis and Simulation of Clutch Engagement Judder and Stick-Slip in Automotive Powertrain Systems," Proceedings of the Institution of Mechanical Engineers Part D: Journal of Automobile Engineering, vol. 218, pp. 1427-1446, 2004.

[31] H. Bartlett and R. Whalley, "Power Transmission System Modelling," Proceedings of the Institution of Mechanical Engineers: Part C: Journal of Mechanical Engineering Science, vol. 212, pp. 497-508, 1998.

[32] J. Jeyakumaran and N. Zhang, "Friction induced Vibration of Clutches in an Automatic Transmission," in Asia Pacific Vibration Conference 2005, pp. 174-179, 2005.

[33] S. Watechagit and K. Srinivasan, "Modelling and Simulation of Shift Hydraulic System for a Stepped Automatic Transmission," SAE Technical Paper: 2003-01-0314, 2003.

[34] G. Lucente, M. Montanari and C. Rossi, "Modelling of an automated manual transmission system," Mechatronics, vol. 17, pp. 73-91, 2007.

[35] M. Pesgens, B. Vroemen, B. Stouten, F. Veldpaus and M. Steinbuch, "Control of a hydraulically actuated continuously variable transmission," Vehicle System Dynamics, vol. 44, pp. 387-406, 2006.

[36] N.D. Manring, Hydraulic control systems, USA: John Wiley & Sons, 2005.

[37] J. Stringer, Hydraulic systems analysis, an introduction, London, UK: Macmillan Press Ltd, 1976.

[38] P. Dransfield, Hydraulic control systems - Design and analysis of their Dynamics, Germany: Springer-Verlag, 1981.

[39] F.D. Norvelle, Electro hydraulic control systems, USA: Prentice Hall, 2000.

[40] J.J. Moskwa and J.K. Hedrick, "Nonlinear algorithms for Automotive Engine Control," IEEE Control Systems Magazine, pp. 88-92, 1990.

[41] U. Kiencke and L. Nielson, Automotive control systems, Germany: Springer, 2005.

[42] J. Zhang, L. Chen and G. Xi, "System Dynamic Modelling and Adaptive Optimal Control for Automatic Clutch Engagement of Vehicles Proceedings of the Institution of Mechanical Engineers Part D: Journal of Automobile Engineering, vol. 216, pp. 983-983-991, 2002.

[43] A.R. Crowther, R. Singh, N. Zhang and C. Chapman, "Impulsive response of an automated transmission system with multiple clearances: formulation, simulation, and experiment," Journal of Sound and Vibration, vol. 306, pp. 444-466, 2007.

[44] J. Fredriksson and J. Karlsson, "Cylinder-by-cylinder engine models vs. mean value engine models for use in powertrain control applications," SAE Technical Paper 1999-01-0906, 1999.

[45] S. Theodossiades, M. Gnanakumarr, H. Rahnejat and M. Menday, "Mode identification in impact-induced high-frequency vehicular driveline vibrations using an elasto-multi-body dynamics approach," Proceedings of the Institution of Mechanical Engineers, Part K: Journal of Multi-Body Dynamics, vol. 218, pp. 81-94, 06. 2004.

[46] R. Singh, H. Xie and R.J. Comparin, "Analysis of automotive neutral gear rattles," Journal of Sound and Vibration, vol. 131, pp. 177-196, 1989.

[47] G. Lechner and H. Naunheimer, Automotive Transmissions - Fundamentals, Selection, Design and Application, Germany: Springer-Verlag, 1999.

[48] Y. Yang, R.C. Lam and T. Fujii, "Prediction of torque response during engagement of wet friction clutch," SAE Technical Paper 981097, 1998.

[49] R.J. Socin and L.K. Walters, "Manual Transmission Synchronizers," SAE Technical Paper, 680008, 1968.

[50] N. Abdel-Halim, D. Barton, D. Crolla and A. Selim, "Performance of Multicone Synchronizers for Manual Transmissions," Proceedings of the Institution of Mechanical Engineers Part D: Journal of Automobile Engineering, pp. 55-65, 2000.

[51] S.T. Razzacki, "Synchroniser Design: A Mathematical and Dimensional Treatise," SAE Technical Paper, 2004-01-1230, 2004.

[52] S.T. Razzacki and J. Hottenstein, "Synchroniser Design and Development for Dual Clutch Transmission (DCT)," SAE Technical Paper, 2007-01-0114, 2007.

[53] E. M'Ewen, "The theory of gear changing," Proceedings of the Institution of Mechanical Engineers, pp. 30-40, 1948.

[54] L. Sykes, "The XJ220 Triple-Cone Synchroniser - A Case Study," Autotech, Institute of Mechanical Engineers pp. 33-47, 1993.

[55] A. Szadkowski, "Shiftability and Shift Quality issues in clutch-transmission systems," SAE Technical Paper, 912697, 1991.

[56] A. Szadkowski and G.J. Mcnerney, "Engineering method for rating shift quality," SAE Technical Paper, 932996, 1993.

[57] D. Kelly and C. Kent, "Gear shift quality improvement in manual transmissions using dynamic modelling," in FISITA world automotive congress, paper number F200A126, 2000.

[58] J. Austen, "Synchromesh Mechanisms," in Drive Line Engineering Conference Institute of Mechanical Engineers, pp. 431-437, 1969.

[59] I. Rosen, S. Kruk, P. Eker and H. Mellgren, "Synchromesh Mechanisms: Experience of Heavy Duty Truck Gearboxes," in Drive Line Engineering Conference Institute of Mechanical Engineers, pp. 439-476, 1969.

[60] Y. Liu and C. Tseng, "Simulation and analysis of synchronisation and engagement on manual transmission gearbox," International Journal of Vehicle Design, vol. 43, pp. 200-220, 2007.

[61] T.M. Manoz Kumar, S. D'mello and V. Pattabiraman, "Optimisation of synchroniser of typical 5-speed manual shift synchromesh transmission using statistics based simulation techniques," SAE Technical Paper, 2006-32-0069, 2006.

[62] G. Matinu, M. Gobbi and C. Miano, "Optimal design of a double cone synchroniser," in Optimal design of complex mechanical systems: with applications to vehicle engineering, Berlin: Springer, 2006, pp. 245-262.

[63] J. Kim, S. Park, C. Seok, H. Song, D. Sung, C. Lim, J. Kim and H. Kim, "Simulation of the shift force for a manual transmission," Proceedings of the Institution of Mechanical Engineers, Part D: Journal of Automobile Engineering, vol. 217, pp. 573-581, 2003.

[64] L. Lovas, D. Play, J. Marialigeti and J. Rigal, "Mechanical Behaviour Simulation for Synchromesh Mechanism Improvements," Proceedings of the Institution of Mechanical Engineers, Part D: Journal of Automobile Engineering, vol. 220, pp. 919-945, 2006.

[65] H. Hoshino, "Analysis on Synchronisation Mechanism of Transmission," SAE Technical Paper, 1999-01-0734, 1999.

[66] B. Paffoni, R. Progri, R. Gras and J. Blouet, "The hydrodynamic phase of Gearbox synchromesh operation: the influence of radial and circumferential grooves," Proceedings of the Institution of Mechanical Engineers: Part J: Journal of Engineering Tribology, vol. 211, pp. 107-116, 1997.

[67] B. Paffoni, R. Progri and R. Gras, "The mixed phase of gearbox synchromesh operation" Proceedings of the Institution of Mechanical Engineers: Part J: Journal of Engineering Tribology, vol. 214, pp. 157:165, 2000.

[68] J.J. Greenbaum, M.A. Kluger and B.E. Westmoreland, "Manual Transmission Efficiency Trends and Characteristics," SAE Technical Paper, 942274, 1994.

[69] N.E. Anderson and S.H. Loewenthal, "Spur Gear System Efficiency at Part and Full Load," NASA Technical Paper 1622, 1980.

[70] N.E. Anderson and S.H. Loewenthal, "Effect of Geometry and Operating Conditions on Spur Gear System Power Loss," 2nd International Power Transmission and Gearing Conference, 1980.

[71] N.E. Anderson, S.H. Loewenthal and J.D. Black, "An analytical method to predict efficiency of aircraft gearboxes," NASA., Tech. Rep. 84-C-8, pp. 1-9, 1984.

[72] P. Heingartner and D. Mba, "Determining Power Losses in Helical Gear Mesh," Gear Technology, pp. 32-37, September/October 2005. 2005.

[73] C. Changenet, X. Oviedo-Marlot and P. Velex, "Power loss predictions in geared transmissions using thermal networks-application to a six speed manual gearbox," Transactions of the American Society of Mechanical Engineers, vol. 128, pp. 618-625, 2006.

[74] Y. Diab, F. Ville and P. Velex, "Investigations on Power Losses in high speed gears," Proceedings of the Institution of Mechanical Engineers: Part J: Journal of Engineering Tribology, vol. 220, pp. 191-198, 2006.

[75] A. Briec and G. Hennequet, "Fuel Consumption Due to Drag Torques in Manual Gearboxes," Autotech '93 Institute of Mechanical Engineers pp. 89-94, 1993.

[76] British Standards Institute, BS ISO/TR 14179-1:2001, "Gears - Thermal Capacity - Part 1: Rating gear drives with thermal equilibrium at 95°C sump temperature," 2001.

[77] T.A. Harris, Rolling Bearing Analysis, USA: John Wiley & Sons, Inc., 1966, .

[78] L.G. Malmer, "SKF Bearing Calculations," vol. 2008, Last accessed JAN 2008 URL: www.skf.com/portal/skf/home/products?maincatalogue=1&lang=en&newlink=1_0_35.

[79] Y. Yuan, E. Liu, J. Hill and Q. Zou, "An Improved Hydrodynamic Model for Open Wet Transmission Clutches," Journal of Fluids Engineering, vol. 129, pp. 333-337, 2007.

[80] J. Deur, J. Petric, J. Asgari and D. Hroval, "Modelling of wet clutch engagement including a thorough experimental validation," SAE Technical Paper 2005-01-0877, 2005.

[81] H. Kitabayashi, C. Yu Li and H. Hiraki, "Analysis of the various factors affecting drag torque in multiple plate wet clutches," JSAE Technical Paper 2003-01-1973, 2003.

[82] Y. Diab, F. Ville and P. Velex, "Prediction of power losses due to tooth friction in gears," Tribology Transactions, vol. 49, pp. 260-270, 2006.

[83] Y. Michlin and V. Myunster, "Determination of Power Losses in Gear Transmissions with rolling and sliding friction incorporated," Mechanism and Machine Theory, vol. 37, pp. 167-174, 2002.

[84] H. Xu, A. Kahraman, N.E. Anderson and D.G. Maddock, "Prediction of mechanical efficiency of parallel-axis gear pairs," Journal of Mechanical Design, vol. 129, pp. 58-68, 2007.

[85] G.H. Benedict and B.W. Kelley, "Instantaneous coefficients of gear tooth friction," American Society of Lubrication Engineers (ASLE) Transactions, vol. 4, pp. 59-70, 1961.

[86] S. He, S. Cho and R. Singh, "Prediction of dynamic friction forces in spur gears using sliding friction formulations," Journal of Sound and Vibration, vol. 309, pp. 843-851, 2008.

[87] B.R. Hohn, K. Michaelis and H.P. Otto, "Influence of immersion depth of dip lubricated gears on power loss, bulk temperature and scuffing load carrying capacity," International Journal of Mechanics and Materials in Design, 2007.

[88] C. Changenet and P. Velex, "A Model for the Prediction of Churning Losses in Geared Transmissions - Preliminary Results," Transactions of the American Society of Mechanical Engineers: Journal of Mechanical Design, vol. 129 (1), pp. 128-133, 2007.

[89] P. Luke and A.V. Olver, "A study of churning losses in dip-lubricated spur gears," Proceedings of the Institution of Mechanical Engineers: Part G Journal of Aerospace Engineering, vol. 213, pp. 337-346, 1999.

[90] J.R. Boness, "Churning losses of discs and gears running partially submerged in oil," in Proceedings of the 1989 International Conference on Power Transmission and Gearing, pp. 355-359, 1989.

[91] A.S. Terekhov, "Basic Problems of Heat Calculation of Gear Reducers," in JSME international conference on motion and power transmissions, Gear Unit Design 2, pp. 490-495, 1991.

[92] P.H. Dawson, "Windage loss in larger high speed gears," Proceedings of the Institution of Mechanical Engineers, vol. 198A, pp. 51-59, 1984.

[93] Y. Diab, F. Ville, P. Velex and C. Changenet, "Windage losses in high speed gears - preliminary experimental and theoretical results," Transactions of the American Society of Mechanical Engineers: Journal of Mechanical Design, vol. 126, pp. 903-908, 2004.

[94] K. Al-Shibl, K. Simmons and C.N. Eastwick, "Modelling windage power loss from an enclosed spur gear," Proceedings of the Institution of Mechanical Engineers: Part A Journal of Power and Energy, vol. 221, pp. 331-341, 2007.

[95] C.N. Eastwick and G. Johnson, "Gear Windage: A Review," Journal of Mechanical Design, vol. 130, 2008.

[96] G. Favennec, B. Sall, M. Lebrun and M. Alirand, "Analysis of a Hydraulic Control Circuit of an Automatic Gearbox," SAE Technical Paper 2003-01-0317, 2003.

[97] Y. Wang, M. Kraska and W. Ortmann, "Dynamic modelling of a variable force solenoid and a clutch for hydraulic control in vehicle transmission system," Proceedings of the American Control Conference, pp. 1789-1793, 2001.

[98] C. Guan and S. Pan, "Adaptive sliding mode control of electro-hydraulic system with nonlinear unknown parameters," Control Engineering Practice, vol. 16, pp. 1275-1284, 2008.

[99] N.D. Vaughan and J.B. Gamble, "The modelling and simulation of a proportional solenoid valve," Transactions of the American Society of Mechanical Engineers, Journal of Dynamic Systems, Measurement, and Control, vol. 118, pp. 120-125, 1996.

[100] J. Pohl, M. Sethson, P. Krus and J. Palmberg, "Modelling and simulation of a fast 2/2 switching valve," Proceedings of the international conference on fluid power, pape number: 310027, 2001.

[101] J.A. Ferreira, F. Gomes Almeida, M.R. Quintas and Estima de Oliveira, J. P., "Hybrid models for hardware in the loop simulation of hydraulic systems, Part 1: theory," Proceedings of the Institution of Mechanical Engineers, Part I: Journal of Systems and Control Engineering, vol. 218, pp. 465-474, 2004.

[102] J.R. Valdes, M.J. Maina, J.L. Nunez and T. Putz, "Reduced order model for estimation of fluid flow and flow forces in hydraulic proportional valves," Energy Conservation and Management, vol. 49, pp. 1517-1529, 2008.

[103] J. Yu, Z. Chen and Y. Lu, "The variation of oil effective bulk modulus with pressure in hydraulic systems," Transactions of the American Society of Mechanical Engineers, Journal of Dynamic Systems, Measurement, and Control, vol. 116, pp. 146-150, 1994.

[104] T. Kajima and Y. Kawamura, "Development of a high-speed solenoid valve: Investigation of solenoids," IEEE Transactions on Industrial Electronics, vol. 42, pp. 1-8, 1995.

[105] E.E. Topcu, Z. Kamis and I. Yuksel, "Simplified numerical solution of electromechanical systems by look-up tables," Mechatronics, vol. 18, pp. 559-565, 2008.

[106] P.R. Crossley and J.A. Cook , "A Nonlinear Engine Model for Drivetrain System Development," IEEE Conference Proceedings, pp. 921-925, 1991.

[107] C.F. Taylor, " Internal combustion engine in theory and practice, Volume 2: Combustion, fuels, materials, and design;" USA: the MIT Press, 1985, .

[108] M. Larmi, "Torsional Vebration analysis of internal combustion engine shafting system," Helsinki University of Technology., Tech. Rep. Me 119, 1996.

[109] F.L. Schulte, "The Dual Mass Flywheel," LuK Technical Paper, April 1986. 1986.

[110] W. Reik, "Clutches, Torque converters and dampers - linking the engine and transmission in new drivetrain concepts," LuK Symposium. 2006.

[111] A. Kooy, A. Gillmann, J. Jackel and M. Bosse, "DMFW - Nothing new?", LuK Symposium pp. 5-14, 2002.

[112] W. Reik, R. Seebacher and A. Kooy, "Dual Mass flywheel," LuK Symposium, pp. 69-93, 1999.

[113] M. Schnurr, "Development of the super long travel dual mass fly wheel," 4th LuK Symposium, pp. 55-79, 1990.

[114] R. Stephenson and E.W. Gaylord, "Natural frequency of the compound centrifugal pendulum," Applied Science Research, vol. 10, pp. 180-184, 1961.

[115] K. Yamamoto, M. Umeyama, H. Ishikawa, T. Otake and K. Kobayashi, "Consideration of a new type two mass flywheel," SAE Technical Paper 911059, pp. 161-166, 1991.

[116] C.L. Gaillard and R. Singh, "Dynamic analysis of automotive clutch dampers," Applied Acoustics, vol. 60, pp. 399-424, 2000.

[117] J. Kim, "Launching performance analysis of a continuously variable transmission vehicle with different torsional couplings," Journal of Mechanical Design, vol. 127, pp. 295-301, 2005.

[118] S. Theodossiades, M. Gnanakumarr, H. Rahnejat and P. Kelly, "Effect of a dual mass flywheel on the impact induced noise in vehicular powertrain systems," Proceedings of the Institution of Mechanical Engineers, Part D: Journal of Automobile Engineering, vol. 220, pp. 747-761, 2006.

[119] A. Crowther and N. Zhang, "Torsional finite elements and nonlinear modelling in vehicle powertrain dynamics," Journal of Sound and Vibration, vol. 184, pp. 825-849, 2005.

[120] A.R. Crowther, "Transient vibration in powertrain systems with automatic transmissions," 2004.

[121] N. Zhang, A. Crowther, D.K. Liu and J. Jeyakumaran, "A Finite Element Method for the Dynamic Analysis of Automatic Transmission Gear Shifting with a Four-Degree-of-Freedom Planetary Gearset Element," Proceedings of the Institution of Mechanical Engineers, Part D: Journal of Automobile Engineering, vol. 217, pp. 461-473, 2003.

[122] A. Serrarens, M. Dassen and M. Steinbuch, "Simulation and Control of an Automotive dry Clutch," Proceedings of the 2004 American Control Conference pp. 4078-4083, 2004.

[123] Z. Sun and K. Hebbale, "Challenges and Opportunities in Automotive Transmission Control," Proceedings of the 2005 American Control Conference pp. 3284-3284-3289, 2005.

[124] A. Haj-Fraj and F. Pfeiffer, "Dynamic modelling and analysis of automatic transmissions," Proceedings of the 1999 IEEE/ASME international conference on advanced intelligent mechatronics, pp. 1026-1031, 1999.

[125] M. Ibamoto, H. Kuroiwa, T. Minowa, K. Sato and T. Tsuchiya, "Development of smooth shift control system with output torque estimation," SAE Technical Paper: 950900, 1995.

[126] K. Adachi, Y. Ochi, S. Segawa and A. Higahimata, "Slip control for a lock-up clutch with a robust control method," Proceedings of the SICE annual conference, pp. 744-749, 2004.

[127] R. Zanasi, A. Visconti, G. Sandoni and R. Morselli, "Dynamic Modelling and Control of a Car Transmission System," IEEE/ASME International Conference on Advance Intelligent Mechatronics, pp. 416-421, 2001.

[128] F. Garofalo, L. Glielmo, L. Iannelli and F. Vasca, "Smooth engagement for automotive dry clutch," Proceedings of the 40th IEEE conference on decision and control, pp. 529-534, 2001.

[129] A. Phillips and S. Bai, "Smooth Launch Control of an Integrated Friction Launch Automatic Transmission," FISITA World congress F2006P035, 2006.

[130] J. Wang, R. Li and X. Peng, "Survey of nonlinear vibration of gear transmission systems," Applied Mechanics Review, vol. 56, pp. 309-329, 2003.

[131] S. He, R. Gunda and R. Singh, "Inclusion of sliding friction in contact dynamics model for helical gears," Transactions of the American Society of Mechanical Engineers: Journal of Mechanical Design, vol. 129, pp. 48-57, 2007.

[132] S. He, T. Rook and R. Singh, "Construction of semi analytical solutions to spur gear dynamics given periodic mesh stiffness and sliding friction functions," Journal of Mechanical Design, vol. 130, pp. Ref. No.: 122601-1, 2008.

[133] M. Teodorescu, S. Theodossiades and H. Rahnejat, "Multi-physics approach to design analysis of powertrain sub-systems," in 12th IFToMM World Congress, 2007.

[134] M. Gnanakumarr, S. Theodossiades, H. Rahnejat and M. Menday, "Impact-induced vibration in vehicular driveline systems: theoretical and experimental investigations," Proceedings of the Institution of Mechanical Engineer: Part K Journal of Multi-Body Dynamics, vol. 219, pp. 1-12, 03. 2005.

[135] S. Theodossiades, M. Gnanakumarr and H. Rahnejat, "Root cause identification and physics of impact-induced driveline noise in vehicular powertrain systems," Proceedings of the Institution of Mechanical Engineers: Part D Journal of Automobile Engineering, vol. 219, pp. 1303-1319, 11. 2005.

[136] W.J. Palm III, Introduction to Matlab 6 for engineers, USA: McGraw-Hill, 2001, .

[137] R.V. Vyrabov, "Friction in a cone clutch and in a friction drive with wedge type bodies," Journal of Tribology, vol. 113, pp. 681-688, 1991.

[138] R.C. Lam, B. Chavdar and T. Newcomb, "New Generation Friction Materials and Technologies," SAE Technical Paper: 2006-01-0150, 2006.

[139] B.J. Hamrock, Fundamentals of Fluid Film Lubrication USA: McGraw-Hill, 1994, pp. 672.

[140] S.P. Kemp and J.L. Linden, "Physical and Chemical Properties of a Typical Automatic Transmission Fluid," 1990.

[141] H. Schlichting, Boundary layer theory, Antigua: McGraw-Hill Classic, 1979, .

[142] C.R. Aphale, J. Cho, W.W. Schultz, S.L. Ceccio, T. Yoshioka and H. Hiraki, "Modelling and Parametric Study of Torque in Open Clutch Plates," Transactions of the American Society of Mechanical Engineers: Journal of Tribology, vol. 128, pp. 422-430, 2006.

[143] A. Stokes, "Manual Gearbox Design," Great Britain: Butterworth-Heinemann Ltd, 1992, pp. 22-26.

[144] S.S. Rao, Mechanical Vibrations, USA: Addison-Wesley Publishing Co., 1986, .

[145] Mathworks, "Stateflow and Stateflow Coder User's Guide," 2010.

[146] H. Dourra and D. Kwapis, "Development of output torque equation for double swap shift control," SAE Technical Paper 2007-01-1308, 2007.

[147] A. Kahraman and R. Singh, "Non-linear dynamics of a geared rotor-bearing system with multiple clearances," Journal of Sound and Vibration, vol. 144, pp. 469-506, 2/8. 1991.

[148] J. Dion, S. Le Moyne, G. Chevallier and H. Sebbah, "Gear impacts and idle gear noise: Experimental study and non-linear dynamic model," Mechanical Systems and Signal Processing, vol. 23, pp. 2608-2628, 11. 2009.

[149] S. Baguet and G. Jacquenot, "Nonlinear couplings in a gear-shaft-bearing system," Mechanism and Machine Theory, vol. 45, pp. 1777-1796, 12. 2010.

[150] W. Kim, H.H. Yoo and J. Chung, "Dynamic analysis for a pair of spur gears with translational motion due to bearing deformation," Journal of Sound and Vibration, vol. 329, pp. 4409-4421, 10/11. 2010.

[151] S. Vafaei, M. Menday and H. Rahnejat, "Transient high-frequency elasto-acoustic response of a vehicular drivetrain to sudden throttle demand," Proceedings of the Institution of Mechanical Engineers: Part K Journal of Multi-Body Dynamics, vol. 215, pp. 35-52, 03/20. 2001.

[152] A. Farshidianfar, M. Ebrahimi, H. Rahnejat and M.T. Menday, "High frequency torsional vibration of vehicular driveline systems in clonk," Heavy Vehicle Systems, International Journal of Vehicle Design, vol. 9, pp. 127-149, 2002.

[153] M.T. Menday, H. Rahnejat and M. Ebrahimi, "Clonk: An Onomatopoeic Response in Torsional Impact of Automotive drivelines," Proceedings of the Institution of Mechanical Engineers: Part D Journal of Automobile Engineering, vol. 213, pp. 349-357, 07/02. 1999.

[154] T.C. Lim and R. Singh, "Vibration transmission through rolling element bearings, part I: Bearing stiffness formulation," Journal of Sound and Vibration, vol. 139, pp. 179-199, 6/8. 1990.